







# **Seismic Risk Assessment of Masonry Walls and Risk Reduction by Means of Prestressing**

**Dissertation**

submitted to and approved by the

Department of Architecture, Civil Engineering and Environmental Sciences  
University of Braunschweig – Institute of Technology  
and the  
Faculty of Engineering  
University of Florence

in candidacy for the degree of a

**Doktor-Ingenieur (Dr.-Ing.) /**

**Dottore di Ricerca in Risk Management on the Built Environment <sup>\*)</sup>**

by

Silvio T. Sperbeck

Born 26.08.1976

from Haldensleben, Germany

Submitted on	23 October 2008
Oral examination on	5 December 2008
Professorial advisors	Prof. Harald Budelmann Prof. Gianni Bartoli

2009

\*) Either the German or the Italian form of the title may be used.



The dissertation is published in an electronic form by the Braunschweig university library at the address

<http://www.biblio.tu-bs.de/>



An ounce of prevention is worth a pound of cure.



## Abstract

The resistance of masonry structures against earthquake action is limited by its low shear strength. Vertical prestressing is mainly considered in order to improve the shear capacity and the ductility of masonry. Experimental tests have already shown the suitability of this method in case of static and static cyclic action. By means of a risk based design, a theoretical investigation is presented that considers dynamic loading.

The basis for the management of seismic risk of masonry, that is considered in the present doctoral thesis, is a developed risk management chain with definitions of its important components as well as introductory statements about different risk types and possibilities to describe and classify them. An important advantage of this risk management concept is the separation of risk into categories. The first includes only physical damage of the structure, while the second category considers the consequences of the physical damage that may be loss of life, economic, historical, social or cultural loss. Generally, the estimation of such losses entails very high effort. Moreover, it can currently not be carried out completely and reasonably, since there is still considerable need for deeper research and further development. Thus, the user of the suggested risk management concept has the possibility to deal only with the risk related to the physical damage, as it is done in the present work. Demandable knowledge about earthquakes, their artificial generation and simulation in transient structural analyses is provided as well as their probabilistic description to take into account their probability of occurrence and scattering, exemplarily demonstrated for the region of Aachen, Germany. Essential basics regarding dynamic structural behaviour and modern demands for aseismic design are explained. Concerning its significance, special attention is given to ductility.

The main focus lies on the analysis of vulnerability of unreinforced and vertical prestressed masonry. Its results are physical damages that are used for the above mentioned risk estimation. In order to carry out such analyses in a profound and pursuable manner, the structural behaviour of unreinforced and prestressed masonry, failure mechanisms, influencing factors and the effect of prestressing are particularly discussed as well as experimental investigations and application examples. The impact of vertical prestressing and its dependency on practical methods of execution on the meaningful ductility is asserted, described and theoretically explained by an interaction between internal prestressing elements (tendons) and the wall itself. Numerical methods and three material laws for masonry are elucidated that are used for the extensive simulations regarding the in-plane behaviour. By means of the experimental tests, the numerical models are calibrated.

The impact of prestressing on the dynamic behaviour is pointed out. Furthermore, influencing factors on the structural behaviour and simulations results are investigated such as wall slenderness, support conditions, position of the tendons and numerical modelling techniques of prestressing. Also sensitivities and correlations are results of extensive probabilistic simulations which include loading as well as resistance uncertainties. However, the evaluation of probability density functions for different damage parameters is the main aim of the probabilistic simulations. As an outcome, vertical prestressing of masonry is only conditionally useful in case of seismic action. It depends on several factors, for instance properties of the structure and earthquake, degree of prestressing or considered damage parameter. In general, the mortar damage is reduced, but the unit damage increased. Thus, further ideas are taken into account and developed to reduce the damage of masonry in case of seismic action. A detailed investigation of such method was neither the purpose nor the intention of this thesis. It closes with the application of the suggested risk management concept to an example. By means of calculated damages and their probabilities, the risk is calculated and compared.

Keywords: Masonry, earthquakes, prestressing, retrofitting, probabilistic, risk management



## Acknowledgements

This doctoral thesis originated within the framework of a joint German-Italian Research Training Group “Risk Management of Natural and Civilization Hazards on Buildings and Infrastructure”, sponsored by the German Research Foundation (Deutsche Forschungsgemeinschaft, DFG).

First of all, thank you to my family, not only for the virtues of hard work and good character they taught me, but also for the understanding and support they showed me throughout the project. During these almost four years I was very often inattentive to my family, and I apologise to them for this.

Going on in chronological sequence, I would like to express a special thanks to my advisor Professor Harald Budelmann from the Technische Universität Braunschweig for the opportunity to join the above mentioned international research team as well as for his encouragement, our interesting discussions and his fatherly supervision. I learnt many important things for future work and life. In the same manner, I would like to acknowledge my tutor Professor Gianni Bartoli from the Università degli Studi di Firenze for the rich discussions, his great professional experience, helpful advice and his kindness. Grazie mille!

My two dear colleagues, Marcel Urban and Timm Pliefke, deserve special thanks. I had a remarkable time, with very interesting, fruitful and enjoyable teamwork. I heartily thank you both for everything!

These results would have been almost impossible to achieve without Professor Sergio Lagomarsino and Dr. Chiara Calderini from the Università degli Studi di Genova. I am sincerely thankful for their permission and support in implementing their material model into my research.

Moreover, I thank all members of the examination committee for their interest in my work and the pleasant atmosphere during the examination.

I would like to express my appreciation to every involved colleague of the iBMB and other research institutes for experimental data, informative advice and interesting discussions.

For their effort to work accurately and with interest, on weekends and in the night, I wish to thank every student involved in this research project during the four years.

The intangible experiences during my time in the International Research Training Group 802 would not have been possible without Professor Udo Peil and Professor Claudio Borri, who founded and lead it. So I thank you.

Etingen, August 2009

Silvio T. Sperbeck



## Contents

<b>1</b>	<b>INTRODUCTION .....</b>	<b>1</b>
1.1	MOTIVATION .....	1
1.2	PROBLEM DEFINITION, LIMITATION AND SOLUTION .....	1
1.3	OVERVIEW OF THE THESIS .....	2
<b>2</b>	<b>RISK MANAGEMENT .....</b>	<b>5</b>
2.1	GENERAL REMARKS .....	5
2.1.1	Catastrophes .....	5
2.1.2	Uncertainties .....	9
2.2	METHODOLOGY FOR MANAGING DISASTER RISK .....	10
2.2.1	Existing definitions of disaster risk .....	11
2.2.2	Risk management concept .....	12
2.2.2.1	Risk identification phase .....	13
2.2.2.2	Risk assessment phase .....	13
2.2.2.3	Risk treatment phase .....	16
2.2.3	Evaluation and integration of most common definitions .....	17
2.3	MEASURING RISK .....	18
2.3.1	General remarks .....	18
2.3.2	Damage parameters .....	19
2.3.3	Loss parameters .....	20
2.4	RISK EVALUATION .....	21
2.5	SUMMARY .....	23
<b>3</b>	<b>EARTHQUAKES AND STRUCTURAL RESPONSE .....</b>	<b>25</b>
3.1	GENERAL REMARKS .....	25
3.2	DESCRIPTION OF EARTHQUAKES .....	27
3.2.1	Magnitudes and seismic moment .....	27
3.2.2	Amplitude parameters .....	28
3.2.3	Duration .....	28
3.2.4	Intensity .....	29
3.2.4.1	Time domain .....	29
3.2.4.2	Damage intensity scales .....	30
3.2.5	Frequency content parameters .....	32
3.3	EARTHQUAKE RECORDS .....	32
3.4	STRUCTURAL DYNAMIC .....	33
3.4.1	Single-degree-of-freedom system .....	33
3.4.2	Damping .....	34
3.5	CORRELATION BETWEEN STRONG MOTION PARAMETERS AND STRUCTURAL DAMAGE .....	35
3.6	PROBABILITY OF EARTHQUAKE LOADING .....	36
3.6.1	General remarks .....	36
3.6.2	Probability assessment for an endangered region and ground motion estimation .....	39
3.7	REQUIREMENTS ON THE SEISMIC PERFORMANCE OF STRUCTURES .....	42
3.7.1	General remarks .....	42
3.7.2	Shear capacity .....	44
3.7.3	Ductility .....	44
3.7.4	Conclusion .....	44
3.8	SUMMARY .....	45
<b>4</b>	<b>MASONRY .....</b>	<b>47</b>
4.1	UNREINFORCED MASONRY .....	47

4.1.1	Mechanical properties of masonry .....	47
4.1.1.1	Material behaviour of units and mortar .....	47
4.1.1.2	Compression behaviour of masonry .....	48
4.1.1.3	Tension behaviour of masonry .....	49
4.1.1.4	Shear behaviour of masonry .....	49
4.1.2	Support conditions of masonry walls .....	52
4.1.3	Failure mechanisms of horizontal in-plane loaded masonry walls .....	52
4.1.4	Influencing parameters on failure mechanisms .....	55
4.1.4.1	Vertical load level, slenderness and support conditions .....	55
4.1.4.2	Material parameters of masonry .....	56
4.1.5	Experimental tests of shear walls .....	57
4.1.5.1	Eindhoven .....	57
4.2	VERTICAL PRESTRESSED MASONRY .....	58
4.2.1	Means to apply vertical prestressing in practice .....	58
4.2.2	Function of prestressing .....	60
4.2.2.1	Shear behaviour .....	60
4.2.2.2	Bending behaviour .....	61
4.2.2.3	Stability .....	62
4.2.2.4	Cracking .....	63
4.2.3	Comparison of historical and modern masonry regarding a reasonable application of vertical prestressing .....	63
4.2.4	Experimental tests of prestressed shear walls .....	65
4.2.4.1	Dortmund .....	65
4.2.4.2	iBMB tests of Braunschweig .....	66
4.2.5	Wall-tendon interaction .....	70
4.2.6	Examples of application .....	71
4.2.6.1	Salvation Army Citadel .....	71
4.2.6.2	Kindergarten Zurich .....	73
4.2.6.3	Factory Regensdorf .....	74
4.2.6.4	Hall 8 iBMB .....	75
4.2.6.5	EMPA-building in Dübendorf .....	77
4.2.6.6	The bell tower in Trignano .....	78
4.3	NUMERICAL MODELLING .....	79
4.3.1	Modelling strategies for masonry .....	79
4.3.2	Basics of plastic theory .....	80
4.3.3	Material models .....	82
4.3.3.1	Interface material model of Delft .....	82
4.3.3.2	Material model of Lagomarsino and Gambarotta .....	83
4.3.3.3	Material model of Schlegel .....	87
4.3.3.4	Discussion of the models for a reasonable application .....	90
4.3.4	Damage parameters .....	90
4.3.4.1	Storey drift .....	90
4.3.4.2	Mortar damage .....	91
4.3.4.3	Unit damage .....	91
4.3.4.4	Plastic strains .....	91
4.3.4.5	Plastic activity .....	92
4.3.4.6	Stresses .....	92
4.3.5	Numerical modelling of prestressed masonry .....	93
4.3.5.1	Means to model vertical prestressing .....	93
4.3.5.2	Reasons to model tendons .....	93
4.4	SUMMARY .....	93

<b>5</b>	<b>IMPACT OF PRESTRESSING ON THE DYNAMIC BEHAVIOUR .....</b>	<b>95</b>
5.1	EXPERIMENTAL RESULTS .....	96
5.1.1	Static shear wall tests .....	96
5.1.2	Static cyclic shear wall tests .....	98
5.1.3	Dynamic shear wall tests .....	98
5.1.4	Dynamic tests of prestressed beams .....	98
5.2	RESULTS OF NON-LINEAR SIMULATIONS .....	99
5.3	SUMMARY .....	99
<b>6</b>	<b>NUMERICAL INVESTIGATION OF NON-PRESTRESSED AND PRESTRESSED MASONRY STRUCTURES .....</b>	<b>101</b>
6.1	EXPERIMENTAL TESTS OF STATIC LOADED SHEAR WALLS .....	101
6.2	CASE STUDIES .....	104
6.2.1	Results of a non-linear static case study .....	104
6.2.1.1	Basics of the case study .....	104
6.2.1.2	Model .....	105
6.2.1.3	Impact on change of prestressing forces in the tendon .....	106
6.2.1.4	Restoring forces due to tendons .....	108
6.2.1.5	Rotation of the top .....	110
6.2.1.6	Shear capacity .....	111
6.2.1.7	Ductility .....	113
6.2.1.8	Summary of unexpected and important results .....	114
6.2.2	Results of a non-linear dynamic case study .....	115
6.2.2.1	Basics of the case study .....	115
6.2.2.2	Results .....	115
6.3	SIMULATION OF THE EXPERIMENTAL TESTS OF PRESTRESSED WALLS .....	119
6.3.1	Static and static cyclic loading .....	119
6.3.2	Earthquake simulation with and without prestressing .....	132
6.3.2.1	Wall 1 .....	132
6.3.2.2	Wall 3 .....	137
6.3.3	Probabilistic earthquake simulation with and without prestressing .....	142
6.3.3.1	Wall 1 .....	143
6.3.3.2	Wall 3 .....	147
6.4	SIMULATION OF HALL 8 IBMB .....	155
6.4.1	Simulation of the existing state .....	156
6.4.2	Simulation without prestressing .....	158
6.5	SUMMARY .....	159
<b>7</b>	<b>FURTHER MEASURES TO ATTAIN A GOOD SEISMIC PERFORMANCE .....</b>	<b>161</b>
7.1	DISCUSSION OF FURTHER MEASURES .....	161
7.1.1	Microscopic level - Reasonable material parameter selection for masonry .....	161
7.1.2	Macroscopic level - Reasonable parameter selection for walls .....	161
7.1.2.1	Wall geometry .....	162
7.1.2.2	Vertical load level .....	162
7.1.2.3	Elastomer bearing .....	162
7.1.2.4	Miscellaneous ideas .....	162
7.2	SIMULATION OF FURTHER MEASURES .....	163
7.2.1	Division in slender walls as non-prestressed and prestressed version .....	163
7.2.2	Unit type, masonry bond and unit size .....	168

- 8 APPLICATION OF THE RISK MANAGEMENT METHODOLOGY TO EVALUATE DIFFERENT MEASURES ..... 171**
  - 8.1 HAZARD ANALYSIS..... 171
  - 8.2 DAMAGE ASSESSMENT ..... 171
  - 8.3 RISK CALCULATION..... 173
  - 8.4 RISK REDUCTION - COMPARISON OF PRESTRESSED AND NON-PRESTRESSED WALLS..... 176
  - 8.5 OPTIMISATION..... 176
  - 8.6 IMPACT OF PRESTRESSING ON THE LOSS ..... 177
  
- 9 SYNOPSIS ..... 179**
  - 9.1 SUMMARY..... 179
  - 9.2 CONCLUSION ..... 181
  - 9.3 OUTLOOK ..... 181
  
- APPENDIX A: RISK MANAGEMENT GLOSSARY ..... 183**
  
- APPENDIX B: DATA OF ARTIFICIAL GENERATED EARTHQUAKE FOR PROBABILISTIC ANALYSES ..... 187**
  
- APPENDIX C: DATA OF ARTIFICIAL GENERATED STRONG MOTION EARTHQUAKE..... 195**
  
- APPENDIX D: ROTATION OF THE WALL FOR SC 2 IN DEPENDENCY ON TENDON POSITION AND SLENDERNESS..... 199**
  
- APPENDIX E: PROBABILISTIC RESULTS FOR WALL 1 AND WALL 3 ..... 201**
  
- APPENDIX F: DESCRIPTION OF THE NORTHRIDGE EARTHQUAKE ..... 211**
  
- APPENDIX G: RISK ESTIMATION ..... 213**
  
- APPENDIX H: MATERIAL PARAMETERS ..... 219**
  
- APPENDIX I: SUGGESTIONS FOR THE PRACTICAL APPLICATION OF PRESTRESSING ON MASONRY ..... 223**
  
- LIST OF ABBREVIATIONS ..... 225**
  
- REFERENCES..... 233**

# 1 Introduction

## 1.1 Motivation

The number of victims as well as loss caused by earthquakes is enormous. Merely, the recent earthquake of 12 May 2008 in the region Sichuan, China (see Fig. 1-1 on the left) caused 87,476 fatalities and a loss of approximately 30,000 Million US\$ [EM-DAT 2008]. This event with a moment magnitude  $M_w$  of 7.9 occurred in a low depth of 19 kilometres [USGS 2008], which usually leads to high damages as demonstrated in Fig. 1-1 on the right. Resulting from a similar earthquake in 1976, approximately 242,000 people lost their lives and a loss of 5,600 Million US\$ has been calculated [EM-DAT 2008].



Fig. 1-1: Earthquake eastern Sichuan, China, 12 May 2008, Left: Location [USGS 2008], Right: Damage [WiCo 2008]

More than 100 years ago Mario Baratta - one of the fathers of modern Italian seismology - noticed: "People are not killed by earthquakes, but by their buildings. Earthquakes cannot be avoided; however buildings can be made earthquake resistant." [Empelmann 2006]. All over the world, a huge amount of historical as well as modern structures is made of masonry, which is usually notorious to have a low earthquake resistance. Moreover, the new version of the European standard for earthquake loading [Eurocode 8] imposes higher seismic loading than previous versions, whereas the resistance of masonry is apparently underestimated by the newest version of the European standard for masonry [Eurocode 6]. Therefore, this thesis is focused on the assessment and the reduction of risk regarding masonry buildings.

## 1.2 Problem definition, limitation and solution

Hazards associated with earthquakes are commonly referred to as seismic hazards, which can be subdivided into ground shaking, structural hazards, liquefaction, landslide, lifeline hazards, tsunamis etc. In the framework of this thesis, ground shaking and structural hazards of masonry are considered. The resistance of masonry structures against earthquake action is limited by its low shear strength. Besides in [Eurocode 6] a very small ductility is assumed for unreinforced masonry. Vertical local prestressing is considered in order to improve the shear capacity and the ductility. Static and static cyclic tests have shown the suitability of this method [Budelmann et al. 2004]. More research for different masonry constructions is desirable. In addition, a detailed investigation of the dynamic behaviour is demandable before using the strengthening method against earthquake action. The large quantity of necessary experimental tests is very expensive, especially with shaking tables. The first goal of this thesis is to provide and verify possibilities, based on numerical methods, to investigate the usefulness of vertical prestressing with particular emphasis on the dynamic behaviour of masonry as well as to estimate the risk probabilistically.

Usually, capacity or performance based design methods are utilized to judge on the design resistance and advantageousness of rehabilitation and strengthening measures. Finally, this work uses a risk based design, which accounts also for several damage stages, in order to assess the benefit of prestressing more in detail. In order to allow a reasonable application of risk management, first of all a clear risk management methodology is demandable. Therefore, important terms are defined and a risk management concept is suggested for disaster risk regarding catastrophes dealing with environmental and engineering purposes only. Financial risk management is not taken into account. The complete risk management chain – presented in Section 2.2 cannot be reasonably processed in a single thesis. Diverse theses are focused on different parts. This work is concentrated on the risk assessment of masonry and risk reduction by means of vertical prestressing and some additional measures. Whereas, the risk assessment with special emphasis on the hazard analysis is investigated in [Urban 2007].

The focus of this study lies on modern masonry. The reasons for this as well as the delineation of historical and modern masonry are discussed elaborately in Section 4.2.3. The huge variety of loadbearing behaviour of masonry structures cannot be reasonably considered in depth. Thus, the work focuses on in-plane behaviour, since it is very important in case of seismic action. Several material models and numerical codes are taken into account, discussed and used to predict the behaviour of masonry. For the main task – transient earthquake simulations, additionally considered in the probabilistic range – a macro-modelling method by means of the material model of Lagomarsino and Gambarotta [Gambarotta, Lagomarsino 1997b] is utilized in combination with the finite element program ANSYS®. This allows a prediction of damage via special damage parameters for units and mortar. Several detected factors which influence masonry behaviour and numerical results are investigated and discussed.

The probabilities of damages can be estimated by means of probabilistic methods. Thereto, Latin Hypercube sampling is applied by means of the advanced program optiSLang®, which is used in combination with ANSYS®, in order to carry out dynamic probabilistic analyses. The damage probabilities – calculated in this way – are utilized to estimate risks and to compare the benefit of vertical prestressing in case of seismic action. A focussing of this work on the structural risk is sufficient to judge on the usefulness of rehabilitation measures and to avoid the integration of inaccuracy, which inheres in loss assessment. The last is caused by the lack of knowledge, the missing of well established accurate methods to determine the losses as well as profound databases. Another reason is the high degree of subjectivity. In the framework of task sharing, the component loss assessment of the risk management chain is precisely investigated in [Plieffe 2010].

### 1.3 Overview of the thesis

Several components like hazard assessment, vulnerability analysis and damage assessment are necessary for a final risk calculation and management. These components are treated separately in their related chapters, where the corresponding partial results are arrived and presented. After all, these components in terms of partial results are compounded in Chap. 8 within the risk calculation. First, the meaning of risk management, a newly developed methodology to manage disaster risk, its basics and useful tools to measure and treat risk are described in Chap. 2 for catastrophes in general. An advantage of the suggested methodology is the subdivision of risk in two main categories. The first accounts only for structural damage (it is referred to as structural risk), while the loss is considered in the total risk (see Section 2.2). Therefore, the user has the possibility to calculate the risk, merely based on structural information, without any further data of financial or other consequences.

The seismic hazard and the parameters for its description are elucidated in Chap. 3 as well as basic knowledge of dynamic structural response and requirements on its seismic performance.

The results of a probabilistic hazard assessment for the region of Aachen, Germany are important for subsequent probabilistic transient simulations in Chap. 6.

Chap. 4 starts with the introduction of unreinforced masonry (normal masonry without any retrofitting, strengthening or rehabilitation measures). Essential theory regarding mechanical properties and failure mechanisms as well as influencing parameters is given, which is the base for a retrofitting of masonry and its numerical modelling. A subsequent subchapter is devoted to vertical prestressing and its impact on the failure mechanisms is described as well as means for the practical application and reasonable application fields. Furthermore, some examples are presented, where vertical prestressing is already used. Experimental tests for non-prestressed and prestressed masonry are described, which are used in Chap. 6 to verify material models and for the calibration of the numerical wall models. After all, the numerical modelling of the complex material behaviour of masonry is explained. Three useful material models are briefly described. Main emphasis lies on the material model of Lagomarsino and Gambarotta [Gambarotta, Lagomarsino 1997b], which is mainly used in Chap. 6 and 7 for the transient simulations as well as for the probabilistic dynamic analyses. Moreover, damage parameters are explained, which are utilised in the numerical models of later chapters to predict the damage and damage probabilities. The impact of prestressing on the dynamic behaviour is investigated and expounded in Chap. 5. Several experimental test results of literature are presented to verify the theoretical assumptions and to derive several effects and mechanisms.

In Chap. 6, the prestressing measure is numerically investigated. Comparisons of prestressed and non-prestressed structures are given. First of all, experimental tests described in Chap. 4 are used in order to verify the material models and to calibrate the material input parameters. Furthermore, case studies are carried out, since experimental tests are expensive and results are often not sufficiently available in literature. In the framework of the shear wall tests of Braunschweig [Budelmann et al. 2004], exclusively prestressed shear walls were investigated. Due to a limited budget, reference walls were not included to compare the behaviour and damages. This gap is closed at least by means of additional numerical simulations referring to such non-prestressed reference walls. Moreover, the dynamic behaviour of prestressed shear walls as well as comparisons to non-prestressed shear walls are of high interest to assess the usefulness of this measure in case of seismic action. However, experimental tests with shaking tables could not be funded. Therefore, dynamic simulations are performed. Especially, the calibrated numerical wall models (of the prestressed shear wall tests of Braunschweig) are subjected to earthquakes. Afterwards, they are extended unto probabilistic simulations, which include the scattering of material parameters, loading and support conditions to find sensitivities and correlations, but also to obtain damage probabilities. In addition, an existing building – Hall 8 of the iBMB/MPA in Braunschweig – is partly investigated to demonstrate the improvement due to prestressing regarding needed shear capacity of bracing walls.

Additionally, further measures – found during this work to improve the seismic performance of masonry – are briefly described and discussed in Chap. 7. On the one hand, measures of the microscopic level are considered as unit sizes, different bonds regarding impacts of overlapping and length/height ratio. On the other hand, measures on macroscopic level are considered. Special emphasis lies on the wall geometry, which has an important impact on failure mechanisms and ductility. Combinations of such measures with vertical prestressing are modelled as well. First numerical investigations show the complexity of a correct judgement concerning the usefulness of the discussed measures in case of seismic action. So far, this chapter may be understood as an extended outlook for further research. The partial results needed for risk estimation are finally compounded in Chap. 8. The most important components are the damage probabilities as a result of the transient probabilistic analyses in Chap. 6. Based on these data, risks are calculated for different damage parameters, for both non-prestressed and prestressed structural elements. Comparisons of the risks exhibit the impact of vertical local prestressing on the damage of seismic loaded masonry.



## 2 Risk management

### 2.1 General remarks

Nowadays, risk management is applied throughout several disciplines as finance, medical science, insurance industry, mechanical engineering as well as disaster management. Also in civil engineering, risk management gains more importance. It is difficult to find the roots. In modern applications the first ideas of risk management may be found in early economic theories around the 1920's [Knight 1921]. These are related to insurance and stock market decision theory. In the middle of the last century the method was introduced into health sciences, where a first definition of risk management was offered. Despite this thesis is focused on seismic risk, in this chapter the risk management subject is treated in general to provide a profound basic knowledge for several fields of application.

#### 2.1.1 Catastrophes

The number of catastrophes increased world wide significantly in the last thirty years as shown in Fig. 2-1. The annual number of disaster events and the annual mortality - using a five-year moving average - is presented. The fact that disaster occurrence has almost doubled between 1995 and 2006 may be influenced by increased access to information and increasing exposure. Nevertheless, it may be amplified due to the number of small climatic hazard events.

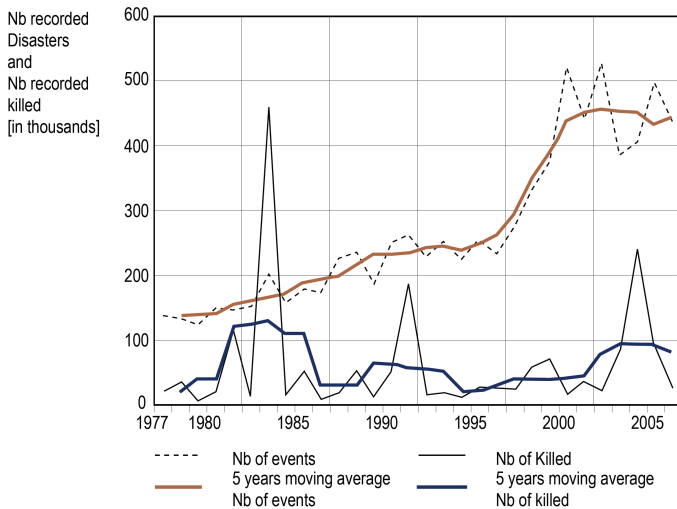


Fig. 2-1: Trends of recorded natural disasters and of numbers of killed, 1977-2006 [ISDR 2007]

Moreover, Fig. 2-2 displays the increase in overall losses and insured losses of great natural catastrophes since 1950 by trend curves. World wide, the increase of exposed people and values (e.g. high developed valuable structures and sensitive businesses) requires methods to handle this problem. Therefore, risk management seems to be the most reasonable tool actually available.

A lot of catastrophe types due to civil, anthropogenic or natural impact have to be distinguished. Natural catastrophes have a very important impact. Events as earthquakes, floods, wind storms, landslides and droughts belong to this category. Regarding data of the Munich Re reinsurance

[Munich Re 2007] (see also Fig. 2-2), the overall losses totalled 1,800bn US\$ in current values, which shows the significance of natural disasters. Therefrom, only the earthquake of 17 January 1995 in the Japanese city of Kobe and the Hurricane Katrina in the United States of 25-30 August 2005 caused 278bn US\$. Another large group are the technical catastrophes, which may be roughly divided into industrial catastrophes and transportation catastrophes. Numerous other causes of death may be mentioned. The most significant types are health conditions, social environment including poverty and violence in all forms, i.e. as well sports activities and wars. Despite these are frequent reasons for fatalities, they are perceived as less important. In opposition to natural or industrial catastrophes, the last group is usually characterised by a much more uniform occurrence in space and time. Thus, it does not lead to numerous fatalities related to a short time event. Moreover, the media report much more about punctual disasters.

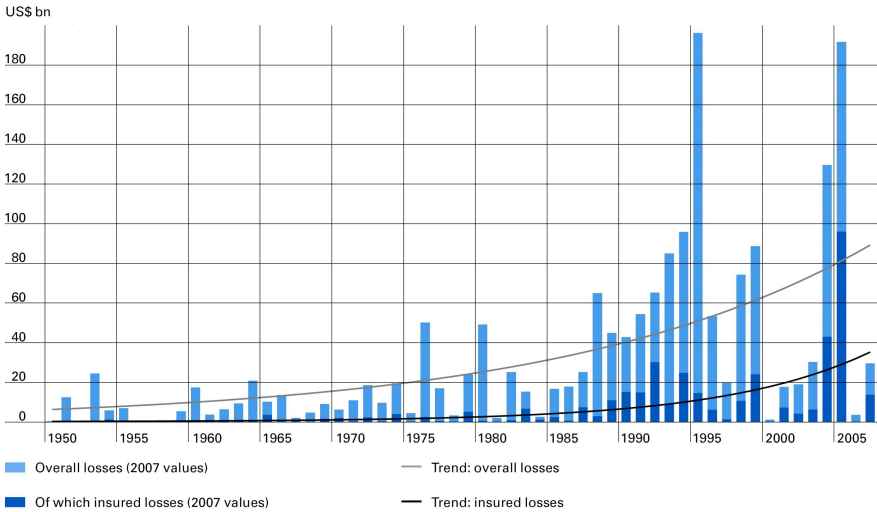


Fig. 2-2: Great natural catastrophes: Overall losses and insured losses – Absolute values and long-term trends [Munich Re 2007]

For Germany, Italy and China the most important natural disasters occurred from 1900 up to the current time as listed in Tab. 2-1, Tab. 2-2 and Tab. 2-3. The data are taken from the Emergency Disasters Data Base [EM-DATA 2008].

Disaster	Date	Killed	Disaster	Date	Affected	Disaster	Date	Damage [Mio US\$]
Extr. temp.	Aug. 03	9,355	Flood	11.08.2002	330,108	Flood	11.08.2002	11,600,000
Storm	Feb. 62	347	Flood	21.12.2993	100,000	Extr. temp.	Aug. 03	1,650,000
Storm	02.01.1976	82	Flood	22.05.1999	100,000	Storm	26.12.1999	1,600,000
Storm	Jan. 90	64	Flood	10.01.1995	30,000	Storm	02.01.1976	1,300,000
Storm	12.11.1972	54	Flood	04.07.1997	15,000	Storm	25.01.1990	1,200,000
Extr. temp.	04.01.1997	30	Flood	26.03.1988	3,500	Storm	25.02.1990	1,200,000
Flood	11.08.2002	27	Earthquake	13.04.1992	1,525	Storm	28.02.1990	1,200,000
Storm	28.02.1990	24	Flood	28.03.2006	1,000	Flood	10.01.1995	1,000,000
Storm	24.12.1999	15	Epidemic	01.02.2002	600	Storm	12.07.1984	1,000,000
Storm	26.10.2002	11	Flood	10.07.2005	450	Storm	12.07.1984	950,000

Tab. 2-1: Top ten natural events in Germany (1900-2008) for fatalities, affected persons and damage [EM-DAT 2008]

To be included into this database the catastrophe has to cause one of the following four criteria: Ten or more reported killed people, hundred reported people affected, and a call for international assistance or the declaration of a state of emergency. The mentioned tables are ranked for killed as well as affected persons and caused damage. For every country different characteristics are easily visible. In Germany storms and extreme temperatures are the main reasons for fatalities and damage. Many people are affected by floods. In Italy, earthquakes lead in all three rankings. It may be said, earthquakes are the most problematic natural catastrophe in Italy. In addition landslides and volcanoes lead to victims. In China as well as in Germany mainly floods affect a lot of people and cause high damages. Regarding killed people, the variety of reasons in China is broad. The main reasons are droughts, floods, earthquakes and an epidemic in 1909.

Disaster	Date	Killed	Disaster	Date	Affected	Disaster	Date	Damage [Mio US\$]
Earthquake	28.12.1908	75,000	Flood	07.10.1970	1,301,650	Earthquake	23.11.1980	20,000,000
Earthquake	13.01.1915	29,980	Flood	03.11.1966	1,300,000	Flood	01.11.1994	9,300,000
Extr. temp.	16.07.2003	20,089	Earthquake	23.11.1980	400,000	Flood	14.10.2000	8,000,000
Earthquake	23.11.1980	4,689	Earthquake	06.05.1976	218,222	Earthquake	26.09.1997	4,524,900
Earthquake	08.09.1905	2,500	Flood	14.11.1951	170,000	Extr. temp.	16.07.2003	4,400,000
Slides	09.10.1963	1,917	Earthquake	28.12.1908	150,000	Earthquake	06.05.1976	3,600,000
Earthquake	23.07.1930	1,883	Earthquake	15.01.1968	55,563	Flood	03.11.1966	2,000,000
Earthquake	06.05.1976	922	Flood	14.10.2000	43,000	Wildfire	Mar. 1990	880,000
Volcano	18.04.1906	700	Earthquake	26.09.1997	38,100	Drought	Apr. 97	800,000
Slides	25.10.1954	297	Earthquake	09.09.1976	32,000	Earthquake	31.10.2002	796,000

Tab. 2-2: Top ten natural events in Italy (1900-2008) for fatalities, affected persons and damage [EM-DAT 2008]

Disaster	Date	Killed	Disaster	Date	Affected	Disaster	Date	Damage [Mio US\$]
Drought	1928	3,000,000	Flood	01.7.1998	238,973,000	Flood	01.7.1998	30,000,000
Flood	Jul. 59	2,000,000	Flood	01.6.1991	210,232,227	Earthq.	12.5.2008	30,000,000
Epidemic	1909	1,500,000	Flood	30.6.1996	154,634,000	Drought	Jan. 94	13,755,200
Drought	1920	500,000	Flood	23.6.2003	150,146,000	Flood	30.6.1996	12,600,000
Flood	Jul. 39	500,000	Flood	15.5.1995	114,470,249	Flood	23.6.1999	8,100,000
Earthq.	27.07.1976	242,000	Flood	15.6.2007	105,004,000	Flood	23.6.2003	7,890,000
Earthq.	22.05.1927	200,000	Flood	23.6.1999	101,024,000	Flood	01.6.1991	7,500,000
Earthq.	16.12.1920	180,000	Flood	14.7.1989	100,010,000	Extr. temp.	10.1.2008	7,500,000
Flood	Jul. 31	145,000	Storm	14.3.2002	100,000,000	Flood	15.5.1995	6,720,000
Flood	1935	142,000	Drought	Jan. 94	82,000,000	Flood	Aug. 96	6,314,500

Tab. 2-3: Top ten natural events in China (1900-2008) for fatalities, affected persons and damage [EM-DAT 2008]

According to International Strategy for Disaster Reduction (ISDR), world wide 118 million people are exposed annually to earthquake with magnitude higher than 5.5 on Richter scale [ISDR 2007]. A comparison of Fig. 2-3 and Fig. 2-4 with the earthquake zones given in Fig. 3-1 exhibits clearly the relation between seismic active zones and resulting fatalities as well as economic loss. As expected, the settlement of such zones is the third important factor leading to risk. Thus, in zones of high seismicity no risk exists, if nothing is exposed. The distribution of mortality risk (see Fig. 2-3) and economic loss risk (see Fig. 2-4) from earthquakes are broadly similar. Small difference exists regarding their quantity. In industrialized countries as USA and New Zealand the economic loss is greater than the mortality. Regarding developing and new industrialized countries as Pakistan, India and Bangladesh the mortality is equal or greater than the economic loss.

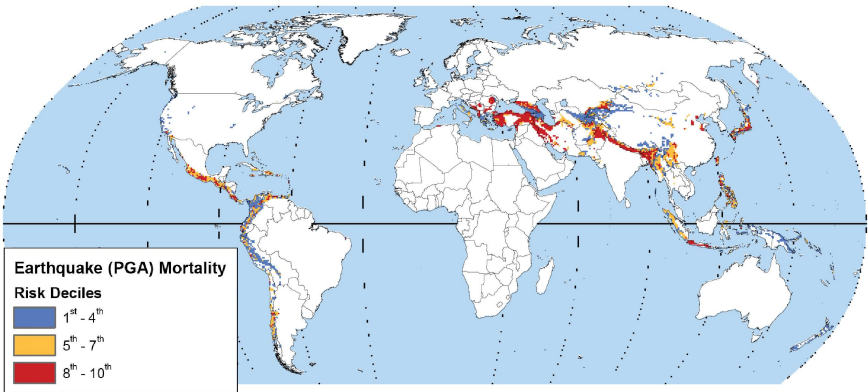


Fig. 2-3: Distribution of mortality from earthquakes [ISDR 2007]

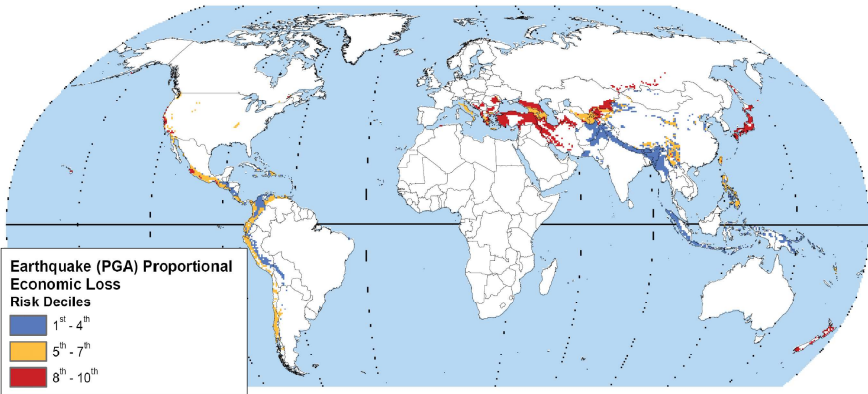


Fig. 2-4: Distribution of proportional economic loss from earthquakes [ISDR 2007]

In Fig. 2-5 the vulnerability of national population for earthquakes is depicted. On the horizontal axis the number of population yearly exposed (in average) to earthquakes is shown, while the vertical axis displays the average number of fatalities expressed in terms of realized mortality from 1980-2000. The ratio killed to exposed provides a proxy for vulnerability. Countries on the top left of the figure are more vulnerable than those on the bottom right. For the interpretation of this graph this difference is important. Countries like Japan and the USA below the trend line may have high levels of hazard exposure, but low levels of vulnerability relative to that exposure. In contrast, a country like Armenia has a high level of vulnerability relative to its level of hazard exposure. The population in Iran is 1,000 times more vulnerable regarding earthquakes than in the USA [ISDR 2007]. This vulnerability of national population is indirectly related to the structural vulnerability. In industrialized countries the structural design is safer than in developing countries. Thus, collapse is often avoided in industrial countries, which reduces the number of fatalities. The value of the structures is usually higher as well as the repairing cost. Therefore, the economic damage in industrial countries is greater. All these show the importance of well designed structures. Desirable is a design which not only avoids collapse, but also limits damage.

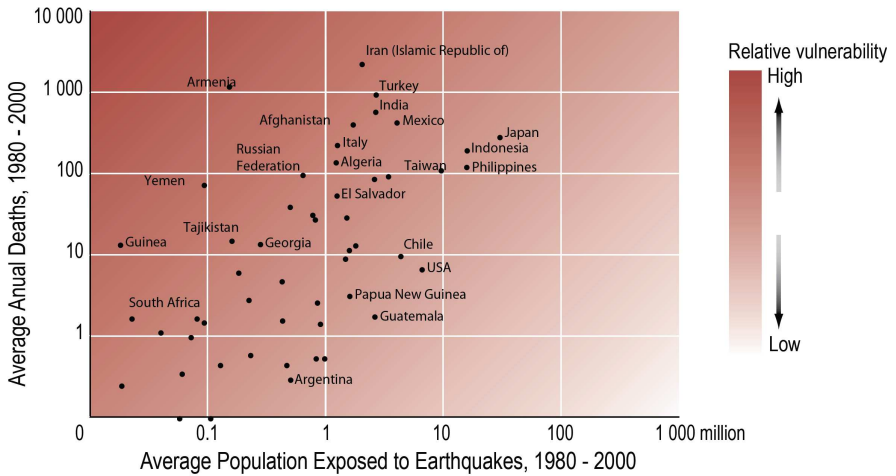


Fig. 2-5: Vulnerability of national population for earthquakes [ISDR 2007]

The last ten earthquakes in China, which caused the most fatalities during the last thirty years, are listed in Tab. 2-4. The people affected and the damage related to each earthquake are given as well. This makes clear the importance of an improvement in structural design also in China.

Dates	Location	Killed	Tot. affected	Est. damages [Mio US\$]
12.05.2008	Wenchuan country	87,476	45,976,596	30,000
06.11.1988	Lancang, Menglian	939	1,270,364	269
03.02.1996	Lishui, Ninglang	309	5,077,795	506
24.02.2003	Jiashi (Payzawat)	268	5,170,000	157
24.01.1981	Sichuan province	150	25,850	
26.04.1990	Qinghai Province	126	34,319	58.35
23.08.1985	Wuqia-Shufu area	67	16,100	
10.01.1998	Hebei province	49	5,980,000	285.5
24.10.1995	Yunnan province	46	20,297	80
11.07.1979	Jiangsu province	41	2,000	
27.08.1979	Wu-Yuan area	41	2,104	

Tab. 2-4: Top ten earthquakes in China (1978-2008) ranked for fatalities as well as related affected persons and damage [EM-DAT 2008]

### 2.1.2 Uncertainties

In the framework of risk management uncertainties have an essential meaning. Thus, some basics regarding uncertainties are given in this section. The term uncertainty is used in numerous different fields as statistics, insurance, finance, philosophy, psychology, engineering, and information science. It applies to predictions of future events, to physical measurements already made, or to the unknown. First of all, a reasonable definition of uncertainty [Hubbard 2007] is provided: "The lack of certainty, a state of having limited knowledge where it is impossible to exactly describe existing state or future outcome, more than one possible outcome." Regarding the measurement of uncertainty, Hubbard points out: "A set of possible states or outcomes where probabilities are assigned to each possible state or outcome - this also includes the application of a probability density function to continuous variables." A huge variety of types of uncertainties exist. They are commonly distinguished into two main groups. The *epistemic uncertainty* is in-

troduced by insufficient modelling of systems. Consequently, this uncertainty type is model dependent and can be eliminated by creating a precise model. It may be expressed as the variability of the results of a repeated experiment. The *aleatory uncertainty* is due to natural and unpredictable variations in the system studied [Urban 2007]. It cannot be reduced, because of the inherently randomness. Hence, it is often named as aleatory variability.

For a procedure which tries to take into account uncertainty due to lack of knowledge – referred to as knowledge uncertainty – of all the causes and effects in a physical or social system, it is possible to distinguish between *process model uncertainty* and *statistical inference uncertainty* as well as *statistical model uncertainty* [Floodrisknet 2008]. All models are a simplification of the reality! Never, they can be considered complete exact. Therefore, they subject to *process model uncertainty*. Measured data versus modelled data comparisons give an insight into the extent of model uncertainty, but do not produce a complete picture [Floodrisknet 2008]. The *statistical inference uncertainty* is a formal quantification of the uncertainty of estimating the population from a sample, and is related to the extent of data and variability of the data that make up the sample [Floodrisknet 2008]. The *statistical model uncertainty* might be described as uncertainty associated with the fitting of a statistical model, which is usually assumed to be proper. However, if two different models fit a set of data equally well but have different extrapolations/interpolations, then this assumption is not valid and there is *statistical model uncertainty* [Floodrisknet 2008]. The reasons responsible to introduce uncertainty in a model might be: The model structure (accuracy of a mathematical model to describe a real system), the initial and boundary conditions (accuracy of information and data for boundary and initial conditions), the numerical approximation (suitability of numerical method to approximate the real system performance), the data for input and model parameters. The goal of uncertainty quantification is to assign an appropriate model to a real-world situation.

### 2.2 Methodology for managing disaster risk

Within the scientific community a great variety of risk management methods and definitions exists, caused by the use of risk management throughout several disciplines and for diverse perils. So far no consistency in the risk management terminology has been achieved as the miscellaneous catastrophes, such as earthquakes, floods, storms or landslides are very different in nature and cause various harms to the affected region. The many existing definitions for similar principles within the risk management processes often result in confusion. Especially when it comes to interdisciplinary co-operations, an inhomogeneous understanding of basal terms might impose problems in communication. Moreover, different definitions as well as ways to estimate and evaluate risk frequently lead to results, which are not comparable as the considered range of consequences, that is included in the calculation, is quite uneven. Therefore, costly risk studies often do not provide sufficient assistance to decision makers and accordingly, huge mistakes can be made. As a result, a unified methodology to define and to calculate risk throughout various disciplines is indispensable for a rational quantification, comparison, and treating of risks. In this way, an effective expenditure of society resources into risk reduction can be guaranteed and thus, an adequate safety level obtained.

This subchapter resulting from a long development process for the Research Training Group 802 is a contribution to approach these tasks and is also published in [Pliefke, Sperbeck, Urban 2006] and [Pliefke et al. 2007]. It provides reasonable definitions which are summed up in Appendix A as well as a standardized language for communicating and managing risk among stakeholders. To do this in a justifiable manner, firstly risk definitions and concepts existing in literature are reviewed and out of these, classes of risk calculation schemes are extracted. Subsequently, a risk management concept is presented that covers the whole risk management chain. The discussion of the risk management workflow is accompanied by delineating the repeated occurring basal

risk terms and illustrating their interrelations graphically. The risk calculation schemes are integrated in the concept and their advantageousness with respect to different application fields is discussed.

### 2.2.1 Existing definitions of disaster risk

Management and analysis of natural disaster risk is a high multidisciplinary field of research. The work of natural scientists is involved to determine the hazard characteristic parameters such as probability of occurrence and intensity of an event for a special location, followed by a profound engineering analysis about the building structure and infrastructural responses due to natural disaster loads. Moreover, investigations of economists are needed to estimate the monetary consequences of the damages and harms to the affected region, resulting in a political discussion about how to handle the peril in order to guarantee an adequate safety level for society. This necessity to consider disaster management from the perspective of a great variety of sciences has led to the development of various quantitative as well as qualitative approaches towards disaster management. Each field is trying to cultivate their own understanding of disaster related terms. As a result, communication within the disaster management community is often accompanied by misunderstandings and confusion due to colliding definitions and concepts. Therefore, a homogeneous understanding of disaster management is crucial for an efficient coordination of the important sub-steps and collaboration throughout the various disciplines. Due to this problematic an extensive literature review has been performed. In the following, exemplary definitions of risk are provided to demonstrate the wide range of definitions existing in literature.

- “A state of uncertainty where some possible outcomes have an undesired effect or significant loss. ... A set of measured uncertainties where some possible outcomes are losses, and the magnitudes of those losses - this also includes loss functions over continuous variables.” [Hubbard 2007]
- “The risk is associated with flood disaster for any region is a product of both the region’s exposure to the hazard (natural event) and the vulnerability of objects (society) to the hazard. It suggests that three main factors contribute to a region’s flood disaster risk: hazard, exposure and vulnerability.” [Hori et al. 2002]
- “Risk is the product of hazard (*H*) and vulnerability (*V*) as they affect a series of elements (*E*) comprising the population, properties, economic activities, public services, and so on, under the threat of disaster in a given area” [Alexander No Date]
- “The probability of harmful consequences, or expected loss of lives, people injured, property, livelihoods, economic activity disrupted (or environment damaged) resulting from interactions between natural and human induced hazards and vulnerable conditions. Risk is conventionally expressed by the equation:  $Risk = Hazard \times Vulnerability$ .” [UNDP 2004]
- “Risk is the probability of an event multiplied by the consequences if the event occurs.” [Einstein 1988]
- “A combination of the probability or frequency of occurrence of a defined hazard and the magnitude of the consequences of the occurrence. More specific, a risk is defined as the probability of harmful consequences, or expected loss (of lives, people, injured, property, livelihoods, economic activity disrupted or environment damaged) resulting from interactions between natural or human induced hazards.” [European Spatial Planning Observation Network 2003]
- Risk is an expression or possible loss over a specific period of time or number of operational cycles. It may be indicated by the probability of an accident times the damage in dollars, lives, or operating units.” [Hammer 1972]

Out of these citations basically five widespread classes of definitions of disaster risks can be extracted and are categorized subsequently:

$Risk = Hazard \cdot Vulnerability \cdot Exposure$  Def. (2-1)

$Risk = Hazard \cdot Vulnerability$  Def. (2-2)

$Risk = Probability \cdot Consequences$  Def. (2-3)

$Risk = Probability \cdot Loss$  Def. (2-4)

$Risk = Probability \cdot Damage$  Def. (2-5)

These risk formulae as well as the exemplary verbal definitions make clear that the different understandings of the term risk are mainly caused by the diverse meanings of the terms hazard, vulnerability, exposure, damage and loss. Obviously, the definition boundaries are blurred and intersecting between the authors' grasps. Therefore, there is the need to clearly clarify what is understood by each term. Furthermore, it is evident throughout the definitions that no clear equation is used to define the risk. Whereas some authors define risk as a product of several terms, others even avoid any mathematical deepness by simply arguing that risk is a function of several expressions. This observation has also been made [Thywissen 2006], that even goes a step further in arguing "Risk is seen as a function of hazard, vulnerability, exposure and resilience, while the mathematical relationship between the variables is unknown". In this sense also the above collected risk Def. (2-1) to Def. (2-5) are not to be understood too mathematically, but rather illustrative to emphasise the composition of disaster risk. The only clear mathematical formula to quantify risk, which is known by the authors, is the PEER equation for earthquake risk that is provided in [Baker, Cornell 2003].

In the next section a fully developed disaster management methodology is presented that clearly outlines the important sub-steps of risk management and supplies unambiguous definitions of the risk defining terms. After this has been introduced, the theoretical background is sufficient to demonstrate how the above listed definitions interrelate and can be included in the framework.

### 2.2.2 Risk management concept

Similar to the state of definition of risk as explained above, also for the term risk management a huge variety exists in literature. The first definition of risk management, which was offered into health sciences [NRC 1983] is subsequently given:

"A decision-making process involving the consideration of information of political, social, economic and technological nature, in addition to data concerning risks, in order to develop, analyze and compare regulatory options; the goal of this process is to select the most appropriate response with respect to the potential risks that may pose a chronic threat to health."

The proposed risk management framework presented in this section has been developed in close cooperation to [Pliefke, Sperbeck, Urban 2006] and is extended in compliance with [AS/NZS 4360 1999] that defines a risk management process as the:

"Systematic application of policies, procedures and practices to the task of identifying, analysing, evaluating, treating and monitoring risk."

As illustrated in Fig. 2-6 the three main components of the framework are given through risk identification, risk assessment and risk treatment and are performed sequentially throughout the risk management process, accompanied by a risk review step and continuous risk monitoring. The risk review process is assigned to the task to constantly include all new information, knowledge and experience about the risk and to indicate its evolution within the process over time. Thus, the risk is updated on a regular basis. It should be emphasised that the risk review process is only performed for risks that have already run through the whole process at least once. Consequently, in each risk review iteration the effectiveness of possibly implemented risk reduction interventions is indicated. The risk monitoring procedure in contrast, captures the exchange of information of all persons actively or passively involved or participating in the risk management process. This exchange of information is necessary to guarantee a smooth collaboration between interdisciplinary researchers and to discover new hazards due to the ever changing environment.

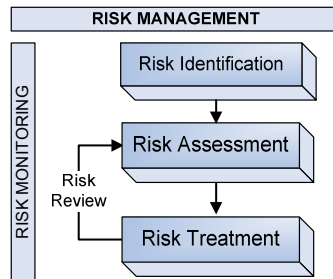


Fig. 2-6: The general risk management framework [Pliefke et al. 2007]

### 2.2.2.1 Risk identification phase

The prerequisite for performing the risk identification phase and therefore to initiate the operation of the risk management chain is the condition of being aware of a dangerous situation. If this is done, first of all the boundaries of the model domain have to be circumscribed by defining the system under analysis. The system can be composed of a single building or infrastructure element, a city, a region or even a whole country. Next, all sources of events that are able to endanger the functionality of the system have to be identified and are characterized by the term hazard. Thus, the risk identification step leads to an answer to the question “what can happen and where?” As soon as this analysis is completed for a particular location, it is proceeded with the risk assessment phase.

### 2.2.2.2 Risk assessment phase

After having outlined the model domain and identified all possible hazards to the system, the risk assessment phase starts to operate, representing the first crucial step of the risk management framework. The risk assessment itself consists of two sub-procedures, the risk analysis and the risk evaluation module, whose tasks are to be seen in quantifying the risk and comparing it to other competing risks, respectively.

#### a) Risk analysis

The risk analysis procedure (depicted in Fig. 2-7) represents the most sophisticated part of the risk assessment phase, whose major objective lies in the quantification of the risk defining pa-

rameters and finally the risk itself, most desirably in monetary units per time unit (i.e. \$/year). In order to reach this ambition, first of all a hazard analysis is being performed where the intensity and frequency parameters of each identified hazard type with respect to the predefined system are estimated. Once the hazard data are quantified, it has to be analysed, which components of the system are exposed, i.e. potentially endangered by the impact of the hazard. In this way, a subdivision of the system into elements at risk (EaR) and elements at non risk (EaNR) is performed, depending on the hazard under consideration. As the EaNR are by definition not exposed, they are not threatened by the hazard and can therefore be excluded from the further analysis. An EaR on the contrary, represents a building or another arbitrary infrastructure element that is characterised by several parameters that have to be determined. Among these are precise location parameters within the system, information about the functional use (residential, commercial, industrial), occupancy (inventory of contents, number of people living or working inside) and construction type (building material, number of storeys, construction year). A detailed discussion about the EaR parameters is provided in [Grossi, Kunreuther 2005]. Furthermore, to facilitate the analysis, EaR with similar characteristics can be grouped together into EaR classes, depending on the hazard under consideration. Then, the further analysis can concentrate on one typical representative out of each EaR class, assuming that all other EaR of the same category will show similar behaviour.

After all the EaR (classes) have been identified and clearly delineated, the structural behaviour of each EaR (class) has to be predicted depending on the hazard load. The damage module of an EaR is strongly dependent on the structural response of the EaR and captures the physical harm only. It can be expressed by a large variety of measures, e.g. water height, crack width and storey drift, which are used to derive damage states. It has to be clearly emphasised that damage is not measured in monetary values. The relation between the hazard intensity and the resulting damage is called structural vulnerability. Thus, the structural vulnerability is an EaR (class) specific characteristic that indicates the degree of physical susceptibility towards the impact of the hazard.

Subsequent to the prediction of the structural behaviour of all EaR (classes), the consequences for the system that might go in line with a given level of damage of the exposed elements have to be analysed. For this investigation the characteristic parameters of each EaR (class) have to be taken into account. It is distinguished between direct consequences, that occur simultaneously to the time the disaster takes place and indirect consequences that occur with a time shift as a result of the direct consequences. Whereas direct consequences are in a straight line linked to the coping capacity of the system, i.e. the ability to withstand the natural forces and to provide immediate help, indirect consequences are linked to the resilience, i.e. the capacity to remain functional and recover from the disaster. In addition, each consequence class is further subdivided into tangible or economic consequences, that are directly measurable in monetary terms and intangible consequences, that are not directly appraisable, e.g. injuries and fatalities, pollution of the environment, loss of cultural, social and historical values etc. An overview of the consequence division is provided in Fig. 2-7 and Fig. 2-9.

After all possible consequences for each EaR (class) and thus for the system have been determined, loss appraises and eventually accumulates all direct and indirect consequences at the time the disaster takes place. In this respect, the indirect consequences that occur later in time have to be discounted on basis of a properly defined discount rate that is specific for each consequence class. In this context, system vulnerability is an EaR (class) specific characteristic that links the hazard parameters directly to the loss and indicates the total potential the hazard has on the EaR (class). Thus, it indicates the physical susceptibility of the EaR (class) itself, its contents as well as the resulting degree of disruption of its functionality within the system. Consequently, the structural vulnerability is included in the broader concept of system vulnerability.

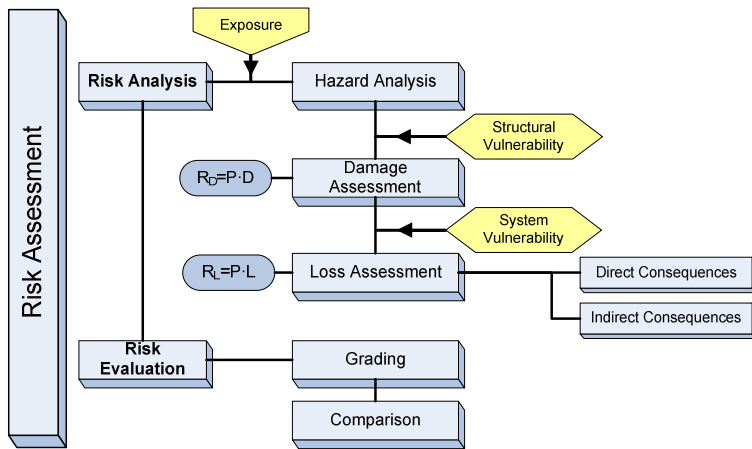


Fig. 2-7: The risk assessment phase [Pliefke et al. 2007]

The risk analysis phase terminates with the quantification of risk where all the previously collected information is comprised. It is distinguished between two different types of risk. Firstly, risk can be calculated by taking the product of the annual probability of occurrence of the hazard multiplied by the expected damage that goes in line with it.

$$\text{Structural Risk} = \text{Probability} \cdot \text{Damage} \text{ [Damage measure / year]} \quad \text{Def. (2-6)}$$

It is being referred to as structural risk. Evidently, the structural risk is of primary importance for engineers in order to predict the behaviour and the response of a structure or structural element under potential hazard load. The second way to express the risk is to take the product of the annual probability of occurrence of the hazard and the expected loss.

$$\text{Total Risk} = \text{Probability} \cdot \text{Loss} \text{ [Loss unit / year]} \quad \text{Def. (2-7)}$$

It is being referred to as total risk. The total risk may comprise all consequences, both tangible and intangible, if a reasonable way has been found to convert the primarily non appraisable harms into monetary units. Alternatively, this transformation of intangible outcomes does not need be done and the total risk can be split according to the respective consequence classes to indicate their relative contribution to risk. In any case the total risk is more exhaustive than the structural risk as the full hazard potential to the system is taken in account.

## b) Risk evaluation

Adjacent to the termination of the risk analysis procedure, the risk evaluation phase is initiated. The purpose of risk evaluation is to make the considered risk comparable to other competing risks to the system by the use of adequate risk measures. In this context, so called exceedance probability curves have found wide acceptance as a common tool to illustrate risk graphically. In an exceedance probability curve the probability that a certain level of loss is surpassed in a specific time period is plotted against different loss levels. Hereby, the loss to the system can be specified in terms of monetary loss, of fatalities or of other suitable impact measures. An insightful overview of common risk measures and tools to compare risks is provided in [Proske 2004].

Finally, after having analysed the risk on basis of adequate risk measures, it may be graded into a certain risk class, depending on individual risk perceptions.

2.2.2.3 Risk treatment phase

After the risk to the predefined system has been analysed and graded into a risk class, the last procedure of the risk management framework, the risk treatment phase, begins to operate. This procedure is assigned to the task to create a rational basis for deciding about how to handle the risk in the presence of other competing risks. Based on several analytical tools from decision mathematics, economics and public choice theory, a decision whether to accept, to transfer, to reject or to reduce a given risk can be derived. In the latter case, risk mitigation initiatives are implemented. Fig. 2-8 visualises the process of risk treatment schematically.

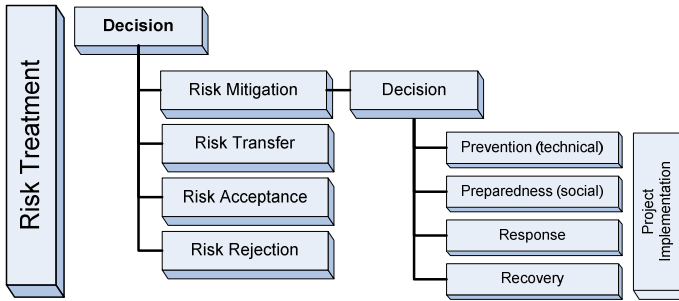


Fig. 2-8: The risk treatment phase [Pliefke et al. 2007]

If the risk is to be mitigated, decision makers are able to choose among several opportunities to implement a risk reduction project. All the possible risk reduction strategies have in common that they reduce the vulnerability of the system. Depending on the specific strategy that is chosen, they can either reduce structural vulnerability by increasing the resistance of structures or system vulnerability by strengthening the system to recover from the disaster as quickly as possible. The strategies are subdivided with respect to the time the risk reduction project is implemented.

Firstly, so called pre-disaster interventions, such as prevention and preparedness, are available. Prevention includes technical measures like structural strengthening that are to be performed with an accurate time horizon before the disaster takes place. Typical examples are dykes against floods or dampers against dynamic actions. Preparedness in contrast contains all social activities, e.g. evacuation plans and emergency training, that are necessary to limit harm shortly before the disaster takes place.

Secondly, postdisaster strategies can be pursued to reduce the risk. Among these, response covers all activities that are performed immediately after the occurrence of the disaster, such as the organisation of help and shelter for the injured and harmed as well as the coordination of emergency forces. Recovery on the contrary, subsumes all activities that need to be taken until the predisaster status of the system is restored again. Obviously, also a combination of the mentioned possibilities can be applied to mitigate the risk. Eventually, for clarity reasons Fig. 2-9 reviews the entire risk management framework schematically.

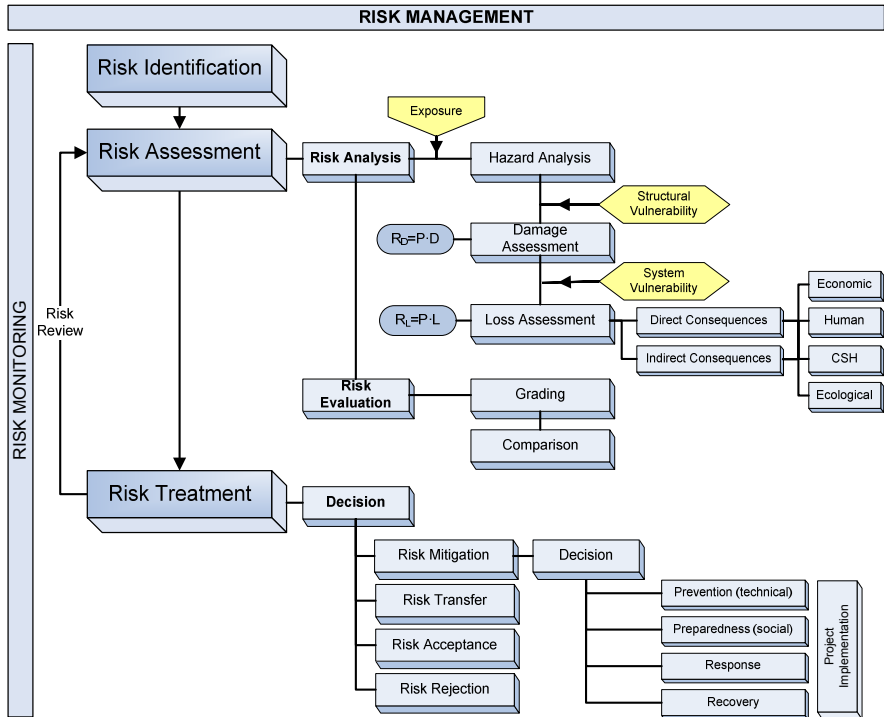


Fig. 2-9: Overview of the whole risk management process [Pliefke et al. 2007]

### 2.2.3 Evaluation and integration of most common definitions

After the general risk management framework has been introduced in the last section, at this point it is discussed, how the risk definitions Def. (2-1) to Def. (2-5) have to be seen in relation to each other. Even if the referenced authors might have had different understandings in their risk characterisations, it is shown now, how the diverse formulae can be retraced in the above described methodology. This ambition is approached, by taking the previously established basal terms and definitions as a baseline for argumentation. In the following, the review of the risk Def. (2-1) to Def. (2-5) is separated in two passages with respect to the affinity of formulation.

The Def. (2-1) and Def. (2-2) have the hazard and the vulnerability module in common, while Def. (2-1) contains an additional exposure multiplier. Therefore, Def. (2-1) is better suited for the analysis of entire systems that are composed both of endangered objects (EaNR) that are distributed unevenly within the system. Consequently, the exposure term has to be included in the definition in order to first identify the exposed elements for which the further analysis is being performed. Def. (2-2) on the contrary is superior in application for risk analysis of one single structural element, where the exposure to the impact of the hazard is a prerequisite for initiating the investigation. In this case, risk is sufficiently described by the product of hazard times vulnerability. In both definitions of risk it is to be specified, whether structural vulnerability or system vulnerability is employed to calculate the risk. If structural vulnerability is taken into consideration, Def. (2-1) and Def. (2-2) are conceptually identical

to Def. (2-5), as structural vulnerability links the hazard to the damage state of each exposed element of system or the single EaR respectively. If system vulnerability is used instead, Def. (2-1) and Def. (2-2) are analogous to risk Def. (2-4) as system vulnerability connects the hazard module directly to the loss of the system or the single EaR. By incorporating all direct and indirect consequences that might go in line with the disaster and transforming them to the time the disaster takes place.

Secondly, risk Def. (2-3) to Def. (2-5) are considered jointly as they differ in their understanding of hazard outcome, while they have the hazard impact implicit in their probability multiplier. There are basically two ways to interpret the probability multiplier. On the one hand it can refer to the probability that a hazard occurs, while on the other hand the probability of an adverse outcome, specified in terms of consequences, loss or damage could be meant. The variation in the outcome term in contrast, is directly related to the depth of investigation as well as the width of demonstration.

In this respect, the use of the term consequence in Def. (2-3) is most general and makes a detailed listing of the diverse harms to the system necessary. The depth of analysis cannot be judged upon based on the formula. It can either finish with the determination of the physical harm to the considered system or include the total spectrum of adverse outcomes over time. Therefore, Def. (2-3) is most suitable to be applied in political decision processes as in this area, it is essentially to know which parts of the system are especially endangered by the hazard and to which extend. With this information specific tailored risk reduction interventions can be implemented to guarantee an adequate safety level throughout the population.

The use of loss (Def. (2-4)) and damage (Def. (2-5)) as an outcome measure however, usually entails an evaluation of the consequences on basis of a suitable impact measure, and differ in the depth of analysis. If loss is taken into account, it is implicit in the definition that all possible consequences, both direct and indirect, need to be considered and evaluated, dependent on their occurrence in time. Hereby, the loss can either be subdivided by consequence classes, so that it is distinguished between economic loss, loss of life etc. or accumulated in one single number, which entails finding a common scale of evaluation for both tangible and intangible consequences. The use of loss as an outcome indicator is predominantly advantageous in economic considerations, where it is important for instance to express disaster risk as a percentage of national income. Furthermore, on a loss basis it can be judged on the effectiveness of risk reduction interventions, as the benefits in terms of reduced loss can directly be incorporated in cost-benefit analysis. Also in insurance industry it is essential to rely on loss in the calculation of premiums for disaster insurance.

Finally, if damage is taken to convey the outcome, the consideration will be restricted to the physical harm of the elements of the system. Only the immediate reactions of the structures are included in the analysis without questioning the aftermaths. Consequently, the expression of risk in terms of damage is of primary importance in civil engineering, to indicate the structural behaviour under hazard load. Based on this consideration, the engineer can decide for instance whether a strengthening measure of a building is necessary to reduce the structural risk. All important definitions included in the presented methodology are briefly summarised in Appendix A.

### **2.3 Measuring risk**

#### **2.3.1 General remarks**

On the one hand the variety of risk definitions is enormous, on the other hand the risk measures are based besides different assumptions. Hence, knowledge about the means of measure is very important to judge results of risk analyses, as the following simple example regarding methods of travelling illustrates. If the number of fatalities is related to the distance of travelling (e.g. per

kilometre or hour), airplanes are the safest methods, as commonly known. In that case, the probability of dying is

- $4.19 \cdot 10^{-9}$  for airplanes,
- $4.67 \cdot 10^{-6}$  for cars and
- $2.13 \cdot 10^{-5}$  for trains [Proske 2004].

Moreover, it is to notice that these data compare the probability of an accident - not necessarily including fatalities - with the probability of dying. Thus, the numbers above cannot really be compared, because they relate accidents to deaths. However, more important is the general critic regarding the means to relate the numbers to the travel distance. Other means are suggested, for instance to relate it to the take-offs and landings. If the number of fatalities is related to the number of travelling, airplanes are the least safe transportation method, as depicted in Fig. 2-10.

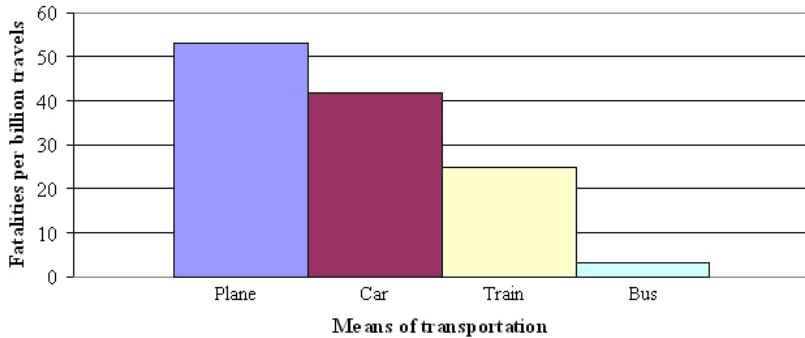


Fig. 2-10: Number of fatalities per travel for different means of transports [Proske 2004]

In the methodology and understanding of risk given above, risk is defined by the product of damage or loss and their probabilities. Subsequently, different means to measure risk are listed and briefly explained. It is distinguished between parameters to describe physical damage and parameters which may be used to express the loss.

### 2.3.2 Damage parameters

First of all, a very famous measure, the probability of collapse – respectively its inverse the target reliabilities - is discussed, which is included in most building codes. This can be seen as a very early risk-based approach. However, it is not a damage parameter. If the collapse is seen as a single state of physical damage, the failure probability is the related likelihood to calculate the risk by the definition used for this study. The risk would be the collapse times the failure probability, which is often not really reasonable. Moreover, the collapse is only the last state in a grading of damage states. For a reasonable risk management it is essential to take into account also partial damage.

Such partial physical damages can be described by a lot of parameters. In general, for structures under seismic loading storey drift, plastic strains and stresses are commonly used for the calculations. On the real structure, damages as crack width and displacements are of interest. Especially for the numerical modelling of masonry, a material model (see Section 4.3.3.2) is used in this study, which provides mortar damage and unit damage. First of all, in the following chapters the basic knowledge is provided to assure a well and easy understanding of all used damage parameters which are finally described in detail in Section 4.3.4.

## 2.3.3 Loss parameters

The estimation of loss is a very difficult subject and a relative new research field still in progress, which is shown due to the suggestions and improvements discussed in literature. To describe the consequences of disasters, the physical damage parameters explained above can usually not be directly used. Concerning tangible loss in the structure itself (without inventory), the following four parameters defined in [ASTM 1999] are quoted subsequently. The original names regarding [ASTM 1999] are used here, despite ‘damage’ should be replaced by ‘loss’ considering the above introduced risk management concept. For instance, the simplest one, the Damage Ratio  $DR$  as given in Eq. (2-1), should be termed as Loss Ratio ( $LR$ ), which is defined by the repairing costs  $C_r$  and the replacement construction cost  $C_c$ , or also called value of a structure before the damage occurred.

$$DR = \frac{C_r}{C_c} \quad \text{Eq. (2-1)}$$

It should be less than one to ensure an economic rehabilitation. The Mean Damage Ratio  $MDR$  (or better the Mean Loss Ratio) is the expected value  $E$  of the  $DR$  conditioned on the earthquake intensity  $I_E$  as shown in Eq. (2-2)

$$MDR(t) = E[DR | I_E] \quad \text{Eq. (2-2)}$$

This parameter is used in the insurance industry to calculate the insurance premium. The monetary consequences of the seismic structural damage, which are related to a certain exceedance probability in a time period, are designated as Probable Loss  $PL$ . The  $PL$ -values are determined by means of a consistent statistical procedure, which includes the probability density functions of the earthquake intensity and structural damage caused by this intensity.  $PL$ -values are stated either for return periods or exceedance probabilities. The last parameter quoted here is the Scenario Loss  $SL$ , which expresses the loss in percentage of the building replacement cost caused by seismic events from specific fault zones or other defined ground motions.

To describe intangible values as the loss of life, some further parameters often used in literature are presented below. A very common and simple one is the mortality rate or the probability of death. Similar to the failure probability, it expresses only the probability of a consequence, not the risk itself. Concerning the presented understanding of risk, the consequence is equal to the loss of life, which has to be multiplied by the probability of death. Since the term ‘mortality rate’ is used in medical science with a different meaning, it is enhanced to speak more generally about the probability of dying, which is usually expressed by the ratio of number of fatalities per year to the size of the population – normally a country. Taking the German population of 82,500,000, the probability of death due to transportation accidents in Germany is 6,087. As a result, the number of accidents divided by the population gives the quote of  $7.4 \cdot 10^{-5}$ . Probabilities of dying can be easily applied and serve acceptable risk values for persons. Unfortunately, the time spent performing an activity is not contained in the probability of dying.

By the use of the Fatal Accident Rate ( $FAR$ ) this problem can be solved. It includes the time period spent in performing an activity. The number of fatalities per unit population is then standardised to an exposure time of  $10^8$  hours (approximately 11,415 years) to avoid very low numbers [Urban 2007]. As the probability of death, the  $FAR$  is used to determine acceptable levels for human risk, neglecting the fact that also the  $FAR$  expresses only the probability.

The age of the people dying is not included in all these measures mentioned above. The death of younger persons appears to be very terrible. From another point of view, dying at an old age seems usual and is accepted by the society. To account for this problem Cohen developed the Lost Life Expectancy ( $LLE$ ), as published in [Cohen 1991], [Cohen 2003]. The  $LLE$  relates risks

in terms of comprehensible commonplace experience. To calculate the *LLE*, the difference in the mean life expectancy is subtracted by the mean age people die while performing an action or being exposed. Therefore, the death occurring by unnatural causes of an elderly person influences the result less than the premature death of a young person.

A further important social indicator that is especially designed to support managing risks to life is the Life Quality Index (*LQI*). Several sub-definitions exist. By means of the *LQI*, fatalities can be related to monetary units. This may appear inhuman, however expressing every type of loss in equal units is essential to allow a comparison. The changes in the quality of life can be calculated by several parameters. They depend on the type of application and may be roughly subdivided into medical, social, economic and engineering life quality factors. Economic life quality considers productivity, life expectancy and income. Hagerty [Hagerty et al. 2001] gives a large and widespread study, including more than twenty different life quality indices. Regarding civil engineering, the most important parameter is the engineering life quality. Originating from Nathwani [Nathwani, Lin, Pandey 1997], it was promoted in Europe especially by Rackwitz [Rackwitz 2004], who applied the *LQI* to the optimisation of acceptable risk levels for technical facilities. This engineering life quality is determined by a function of three parameters. The main formula is given briefly in Eq. (2-3).

$$LQI = g \frac{w}{1-w} \cdot e \quad \text{Eq. (2-3)}$$

It includes the gross national product  $g$ , the time spend in paid work  $w$  (used as a life quality measure), and the mean life expectancy  $e$ . A detailed improved derivation of the *LQI* and his basics can be found in [Pliefke, Peil 2008]. The *LQI* is to be interpreted as an anonymous individual utility function deriving its life quality to unequal parts from longevity and consumption [Pliefke, Peil 2007].

## 2.4 Risk evaluation

As a basis for decisions to take in the risk treatment phase, the risk has to be ranked. The decision maker has to know whether a risk is high or low, if it can be accepted or not. Therefore, a grading is necessary. In the following some basic knowledge is given as well as a practicable suggestion for a classification of masonry buildings, which is used for this study.

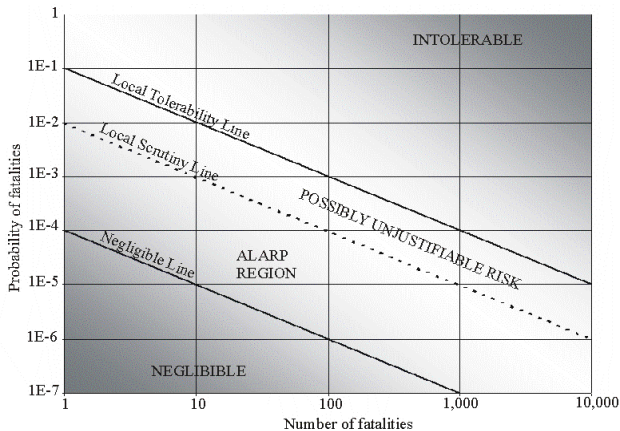


Fig. 2-11: Tolerable risk as a function of severity [Helm 1996]

To determine acceptable risk bases, Frequency-Number diagrams (F-N-diagrams) or Probability-Damage or (P-D diagrams) were developed (see Fig. 2-11). On the one hand the frequency is used in literature, on the other hand the probability. Sometimes the authors confuse frequency and probability. The number of fatalities is commonly used. However, any damage or loss parameter may be used instead. The societal risk of nuclear power stations has been already assessed until 1967 by means of the P-D diagrams, which plot the consequences of extreme events, e.g. the losses versus their probability in a logarithmic scale [Urban 2007]. Usually, the reference time equals one year, nevertheless should also be indicated on the vertical axis. Sample results of studies are shown in Fig. 2-11. These diagrams suit well to compare different risks, as may be seen. In this illustration, two lines are shown, which are labelled marginally accepted and unaccepted. In Fig. 2-11 the regions of risk are presented. The diagram displays loss as a function of probability. Simplified, these ranges can also be used without dependency of probability or frequencies. In [Porter 2002] the regions are described, which Helm has already examined for variety of industrial and other technological hazards that can produce large numbers of fatalities. Such risks go in line with the characteristics of earthquakes: The society is exposed to potentially disastrous, involuntary and occasional events. Helm assessed the tolerability of these hazards as a function of frequency and number of deaths. He found an inverse linear relationship between the severity of damage/loss (number of deaths) and tolerability.

Four general regions of the frequency-versus-severity space result in the graph characterise the tolerability of risk. Helm used the expression 'tolerable risk' rather than 'acceptable risk', because fatalities are not acceptable. Regarding [Porter 2002], the four regions (see Fig. 2-11), are as follows:

- Intolerable: High frequency and severe consequences exceed local acceptability of deaths from industrial and other accidents. In this region, "risk cannot be justified except in extraordinary circumstances."
- Possibly unjustifiable: Risk is "tolerable only if risk reduction is impractical or if its cost is grossly disproportionate to the improvement gained." This is the upper portion of the region Helm denotes ALARP (as low as reasonably practicable), meaning the risk is tolerable as long as all reasonably practical steps are taken to reduce the risk further.
- Lower ALARP: Risk is non-negligible, but is "tolerable if cost reduction would exceed the improvement gained."
- Negligible: Below the negligibility line, frequency and severity are low enough for the risk to be considered broadly acceptable.

The relationship frequency-severity-tolerability of Helm is useful especially for the assessment of need risk mitigation, for several reasons that a quote below after [Porter 2002]:

- It allows one to characterise risk acceptability in both its dimensions of frequency and severity.
- It acknowledges that vast grey areas of acceptability exist.
- It recognises that costs and benefits of a hazard are relevant when the risk is moderate, but become irrelevant as the risk increases.
- It acknowledges that for moderate to high-risk hazards, there is a distinction between reasonable and unreasonable cost for risk reduction.

Regarding Fig. 2-11 the question occurs, if a decision-maker should assess risk in terms of the isolated system (over which he has control, for instance one house), or within more extensive range, such as considering all similar buildings that might be affected by the same seismic action. The number of potential casualties in an earthquake ranges from zero to the maximum occupancy of the building. For one building, this is the loss that might be controlled by the owner. Therefore, the seismic risk should be plotted maybe for one building.

Several further suggestions can be found in literature to grade risk. In the last time, the discussion started in the field of economic and decision theory, whether such diagrams are correct. It is neither the purpose nor the aim of this thesis to discuss such questions. Instead it seems more relevant to suggest a reasonable way for the risk calculation. In the framework of engineering purposes and reasons of practical efficient applicability, the separation into risk classes seems to be meaningful. Naturally, the risk classes used depend highly on the handled problem. Here, only the problem of seismicity related to the structural damage of masonry is focussed. Regarding this damage, a lot of damage parameters exist, as already mentioned. All may be handled in the same way.

It is suggested here, to use damage classes - as given by the macro intensity scales like the European Macroseismic Scale (EMS-98) (see Tab. 3-3) - to calculate the risk. For every damage class the related risk can be calculated, by multiplying the value of the damage parameter with the probability that the damage occurs. It is to take care specially for the calibration of damage parameters to the damage classes of EMS-98, because it describes only the macro state of a building, not the values of such damage parameters itself. Lang proposes to use the push over curve for a grading of damages classes [Lang 2002] as depicted in Fig. 2-12. More details are given in Chap. 8.

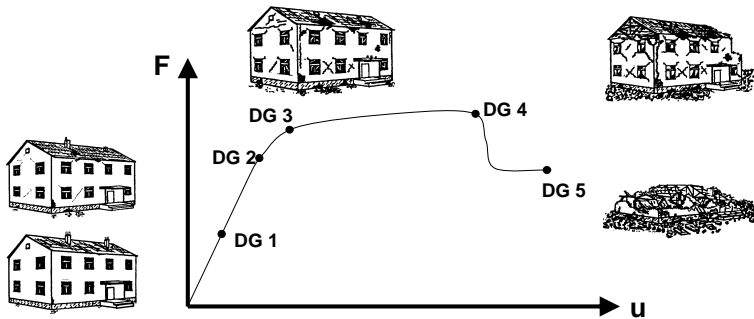


Fig. 2-12: Connection of the EMS-98 damage to a pushover curve [Lang 2002]

## 2.5 Summary

First of all, concerning catastrophes and actual trends, some reasons to apply the risk management as well as the importance of uncertainties in this context are shown. Especially the difference between developing and industrial countries is elaborated, which indicates the necessity of improved seismic design and the application of rehabilitation measures in developing and newly industrial countries. In Section 2.2 it is demonstrated how widely the definitions and understandings of the term risk can range. Applied across various disciplines and often used in multidisciplinary collaborations, so far no consistency in delineating the borders of disaster risk could be reached. By providing some exemplary risk definitions out of literature and extracting classes of risk calculation formulae, it is shown that the heterogeneity of risk definitions is mainly due to different understandings of the basic terms hazard, vulnerability, exposure, consequences, damage and loss. These terms that occur repeatedly throughout the diverse risk definitions, are often used interchangeably and so far no clear concept to distinguish the terms from each other has been developed. This lack of a harmonised concept is addressed by introducing a clear and flexible risk management framework that provides assistance in analysing, comparing and treating

disaster risk. Each step in this chain is precisely defined and graphically illustrated, leaving some range for problem specific modifications. Finally, the initially listed risk definitions are integrated in the concept and their interrelations are shown. It is illustrated how the definitions vary with respect to the object or system under consideration and differ in the depth of analysis as well as the level of detail. To conclude, the question which formula to use depends strongly on the field of application, which makes it necessary to emphasise certain aspects of the risk composition. Therefore, none of the risk formulae can be shown to be superior to another and even less to be universal. However a 'communication in the same language' is indispensable for an efficient multidisciplinary collaboration in implementing all the sub-steps of the risk management chain. Some parameters and tools to measure and grade risk are summarised. Regarding an efficient and practicable calculation of risk, the separation into risk classes on the base of the EMS-98 is recommended.

### 3 Earthquakes and structural response

#### 3.1 General remarks

Hazards associated with earthquakes are referred to as seismic hazards commonly, which can be subdivided into ground shaking, structural hazards, liquefaction, landslide, lifeline hazards, tsunamis etc. In fact, ground shaking can be considered to be the most important of all seismic hazards because all the other hazards are caused by ground shaking [Kramer 1996]. Thus, this work focuses on ground shaking leading to structural hazard.

Seismic hazards can be caused by volcanic activity, collapse of underground cavities, artificial events (explosions) and reservoir induced quakes. But these reasons are usually neglected in earthquake hazard analysis because of the small energy and local limitation. The main part of seismic hazards is caused by plate tectonic. On the boundaries of major plates and microplates deformations leads to such tectonically caused earthquakes (see Fig. 3-1). Ruptures of the earth's crust go in line with a sudden release of energy that creates seismic waves. These waves are distinguished regarding the propagation and transaction type as well as their velocity. The main categories are body and surface waves. Body waves, which can travel through the interior of the earth, are subdivided in p-waves (analogous to sound waves and involves successive compression and rarefaction of the material) and s-waves (cause shearing deformations). The s-waves are further subdivided into SV and SH, regarding vertical and horizontal direction of particle movement. Surface waves result from the interaction between body waves and the surface and travel along the earth's surface. They are subdivided in Rayleigh waves (which are analogous to water waves and are produced by interaction of p- and SV-waves) and Love waves. The last result from the interaction of SH-waves with a soft surficial layer.

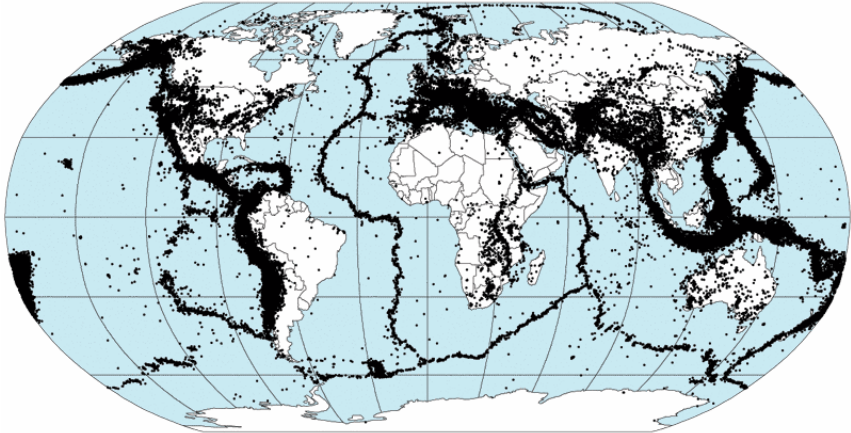


Fig. 3-1: Preliminary determination of epicenters, 358 214 events from 1963 until 1998 with all magnitudes [NOAA, USGS 1996]

The point where the rupture begins is called hypocenter or source (Fig. 3-2). From there the rupture spreads across the fault. Although fault rupture can extend through the surface, the source is located at some hypocentral depth or focal depth below the ground surface. The point directly above the source on the ground surface is called epicentre. The observer or receptor somewhere on the surface, for instance a building, is of main interest in the hazard analysis. The distance between this receptor and the hypocenter is called hypocentral distance. The very common source-pathway-receptor model divides the seismic hazard into three components of source,

pathway and site effects. Source effects contain mechanisms occurring directly at the fault. The distance and medium through which the event propagates (e.g. influence of subsoil and ground conditions) are included in the pathway. Finally, the receptor includes all local site effects as well as parameters describing the exposure and the value of the structure.

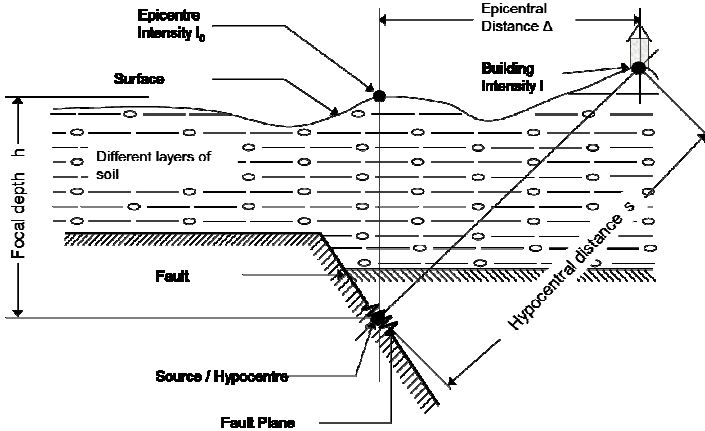


Fig. 3-2: Source pathway receptor model [Urban 2007]

Regarding these three components of the source-pathway-receptor model the uncertainties involved in the seismic hazard analysis may also be distinguished in three main groups, which are summarised in Tab. 3-1.

Type of uncertainties	Examples
Source uncertainties	Fault type, depth, rupture surface, location, magnitude, occurrence time, occurrence interval, seismic history, geology
Path uncertainties	Distance, regional soil type, attenuation function
Site uncertainties	Local soil profile, topography

Tab. 3-1: Different types of uncertainties in earthquake engineering

Usually it is distinguished between low and high seismicity. In zones of low seismicity usually small damages - leading mainly to economic and CHS loss - occur, but the cost can be very high. Thus, a reduction of damage is very interesting. Very high damage, collapse or partial collapse go in line with high seismicity and causes in addition a high human loss. Therefore, the main task is to avoid complete or partial collapse of the structure. Of course the damage and loss not only depend on the low or high seismicity, but also on the structures. In developing countries, an earthquake of similar intensity often causes much higher human loss, as in high developed countries.

In [Eurocode 8] the following suggestion is given for a distinction of the seismicity:

‘It is recommended to consider as low seismicity cases either those in which the design ground acceleration on type A ground,  $a_g$ , is not greater than 0.08 g (0.78 m/s<sup>2</sup>), or those where the product  $a_g \cdot S$  is not greater than 0.1 g (0.98 m/s<sup>2</sup>).’

In the recent German Standard [DIN 4149] the maximal design ground acceleration  $a_g$  of  $0.8 \text{ m/s}^2$  on type A ground is given. So, the German earthquake zones belong nearly to the low seismicity zones. Here, the main interest is to reduce or avoid damage. In zones of high seismicity, like Italy or Turkey, also the avoidance of collapse is an important task.

Earthquakes are characterized by their extreme randomness. Not only the seismic event itself is uncertain, but also the main parameters to describe it. Numerous intensity parameters exist, that intend to describe the severity of an earthquake. Some are already mentioned above. The describing parameters have to be assessed. In the following subchapter, the most important parameters are briefly explained, based mainly on the information given in [Meskouris, Hinzen 2003], [Kramer 1996] and [Pocanschi, Phocas 2003].

### 3.2 Description of earthquakes

The engineering seismology parameters can be roughly distinguished into parameters which are related to the receptor (site) and parameters related to the source. So, the magnitudes and the seismic moment try to quantify the earthquake activity at the source, however the intensity is a macroscopic measure of the vibration on the site.

#### 3.2.1 Magnitudes and seismic moment

The magnitude is commonly referred in the media and scientific publications. Different types of magnitudes exist. Very often used in media is the Richter magnitude  $M_L$ , which is usually referred to as local magnitude in scientific publications. Relying on a database of earthquakes in California, Richter has derived an empirical relation. The Richter local magnitude is not directly related to physical characteristics of the earthquake's source and it was originally developed for epicentral distance below 600 kilometres and only for the Wood-Anderson seismometer used by Richter.

$$M_L = \log_{10} A - \log_{10} A_0 \quad \text{Eq. (3-1)}$$

$A$  is the maximum recorded amplitude of measured ground displacement and  $A_0$  a standard value as a function of distance. Furthermore,  $M_L$  does not distinguish between different types of waves. Due to the drawbacks of the local magnitude, further magnitudes mentioned below have been developed.

The surface wave magnitude  $M_s$  is obtained from

$$M_s = \log_{10} A + 1.66 \cdot \log_{10} \Delta + 2.0 \quad \text{Eq. (3-2)}$$

where  $A$  is the maximum ground displacement in micrometers and  $\Delta$  is the epicentral distance of the seismometer.  $M_s$  is a magnitude scale based on the maximum ground displacement amplitude of Rayleigh waves. Therefore, it can be determined from any type of seismograph. For deep-focus earthquakes, surface waves are often too small to attain a reliable evaluation of  $M_s$ .

The body wave magnitude  $m_b$  is a worldwide magnitude scale based on the amplitude of the first cycles of p-waves which are not strongly influenced by the focal depth.

$$m_b = \log_{10} A - \log_{10} T + +0.01\Delta + 5.9 \quad \text{Eq. (3-3)}$$

where  $A$  is the p-wave amplitude in micrometers and  $T$  is the period of p-waves. Moreover, the Energy Magnitude  $M_E$  (which is related to the wave energy) and the Moment Magnitude  $M_w$  (calculated by means of the seismic moment  $M_0$ ) shall be briefly mentioned only. All these mag-

nitudes are not related to each other. A comparison between the different magnitudes may be found in [Kramer 1996].

The parameter most closely related to the fault itself is the seismic moment  $M_0$  representing the physical strength of an earthquake:

$$M_0 = G \cdot A_f \cdot D_s \tag{Eq. (3-4)}$$

where  $G$  is the shear modulus near the rupture area  $A_f$  and  $D_s$  the average amount of slip over the fault plane.  $M_0$  is strongly correlated to the magnitude.

### 3.2.2 Amplitude parameters

The most common way to describe a ground motion is with the time history. The motion parameters may be acceleration, velocity and displacement (see Fig. 3-3). Only one of these is measured typically with the others computed by differentiation or integration. The maxima of these time histories are called peak ground acceleration (PGA), peak ground velocity (PGV) and peak ground deformation (PGD).

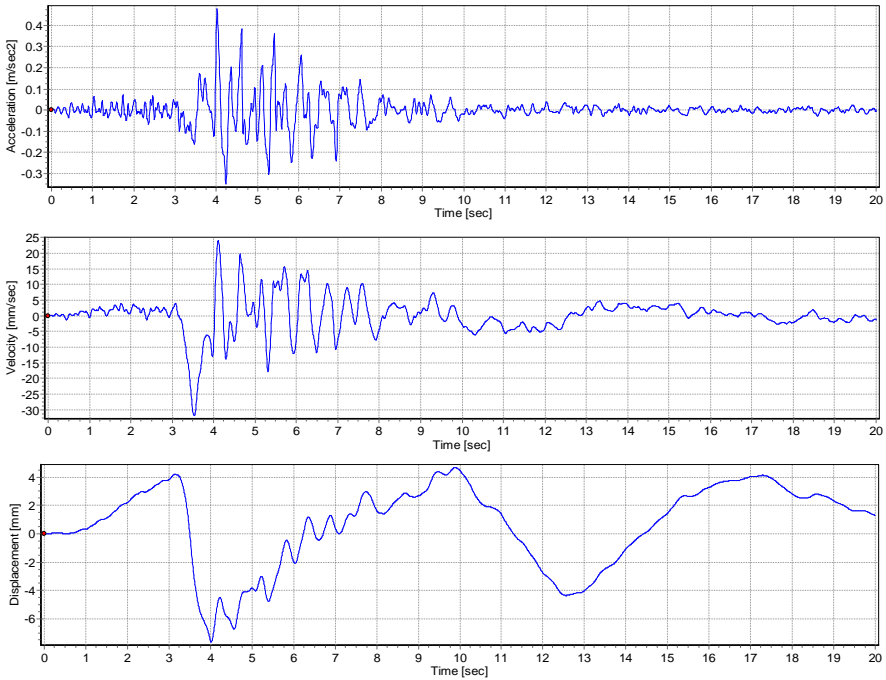


Fig. 3-3: Time histories of acceleration, velocity and displacement of the Friuli earthquake of 1976 (Italy)

### 3.2.3 Duration

Intuitively, the duration should have a considerable effect on the damage. So, it can be argued that many physical processes, such as degradation of stiffness and strength would lead to higher

damages. Nevertheless, the general scientific proof of its importance is to some degrees still missing. The discussion is somewhat confused since several measures for the time duration are used in literature. For engineering purpose, only the strong-motion portion of the load is of interest. So, different approaches have been taken to the problem of evaluating the duration of strong motion. In the following some important definitions are explained.

The significant duration  $D_{s95}$  is defined widely and was already defined as the time between 5% and 95% of the Arias intensity, which is visualized in red in Fig. 3-4. Sometimes the value being referred to is  $D_{s75}$ , including only the time between 5% and 75%. The next type of time, the bracketed duration  $D_{b0.05}$ , is defined as the time interval between the first and last exceedance of a given threshold, usually taken as 0.05g. Related to the latter measure is the uniform distribution  $D_u$ , which is defined as the sum of time intervals in which the threshold is exceeded.

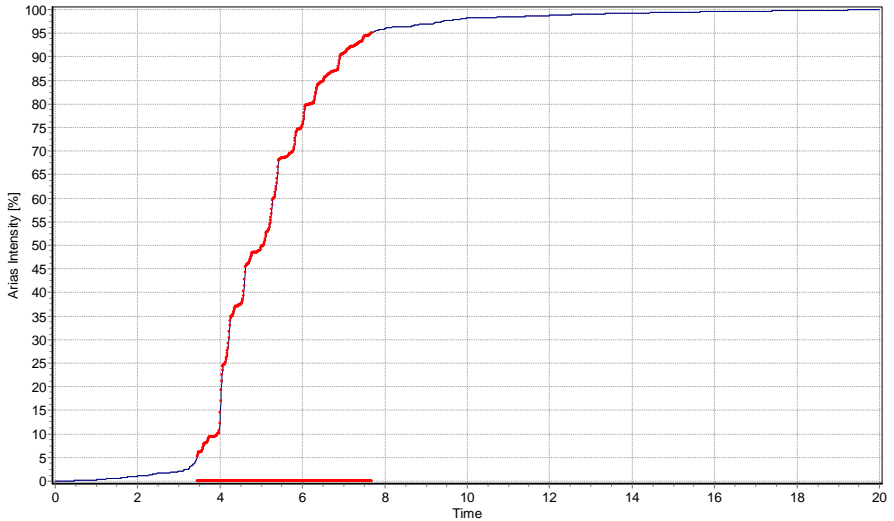


Fig. 3-4: Arias intensity in dependency on the time of the Friuli earthquake of 1976 (Italy)

### 3.2.4 Intensity

First of all, the different intensity definitions try to capture the seismic activity at the site (or receptor). Roughly it can be distinguished between time domain parameters and damage intensity scales, which are explained in the following two subchapters.

#### 3.2.4.1 Time domain

An important value defined by Arias in 1970 and used frequently is the Arias intensity  $AI$ :

$$AI = \frac{\pi}{2 \cdot g} \cdot \int_0^{T_0} a_g^2(t) dt \quad \text{Eq. (3-5)}$$

where  $g$  is the acceleration of gravity,  $a_g$  the ground acceleration and  $T_0$  the total duration of the record. Thus,  $AI$  is independent from the method to define the duration of strong motion. It is shown in [Urban 2007] that this measure is very well correlated with the structural damage be-

cause it takes into account the intensity of PGA over a period of time. The characteristic intensity  $I_c$ , is defined as [Park, Ang 1985]:

$$I_c = (a_{rms})^2 \cdot \sqrt{T_d} \quad \text{Eq. (3-6)}$$

where  $a_{rms}$  is the root mean square of the acceleration and  $T_d$  the duration.  $I_c$  is related linearly to an index of structural damage due to maximum deformations and absorbed hysteretic energy.

### 3.2.4.2 Damage intensity scales

Seismic intensity scales are not determined by the physical parameters, but rather from the damage caused to structures or the behaviour of objects within a building and the way it is perceived by human beings. Different intensity scales exist in Europe. The most common are the Modified Mercalli Intensity (MMI) scale [Wood, Neumann 1931], the Medvedev-Sponheuer-Karnik (MSK) scale and the European Macroseismic Scale (EMS-98) [Grünthal 1998], which is used in this study. Therefore only this scale is mentioned in detail (see Tab. 3-2 and Tab. 3-3). Further intensity scales for earthquakes are the Rossi-Forel scale (RF) and Japanese Meteorological Agency scale (JMA) The four scales are graphically compared in Fig. 3-5.

EMS intensity	Definition	Description of typical observed effects (abstracted)
I	Not felt	Not felt.
II	Scarcely felt	Felt only by very few individual people at rest in houses.
III	Weak	Felt indoors by a few people. People at rest feel a swaying or light trembling.
IV	Largely observed	Felt indoors by many people, outdoors by very few. A few people are awakened. Windows, doors and dishes rattle.
V	Strong	Felt indoors by most, outdoors by few. Many sleeping people awake. A few are frightened. Buildings tremble throughout. Hanging objects swing considerably. Small objects are shifted. Doors and windows swing open or shut.
VI	Slightly damaging	Many people are frightened and run outdoors. Some objects fall. Many houses suffer slight non-structural damage like hair-line cracks and fall of small pieces of plaster.
VII	Damaging	Most people are frightened and run outdoors. Furniture is shifted and objects fall from shelves in large numbers. Many well built ordinary buildings suffer moderate damage: small cracks in walls, fall of plaster, parts of chimneys fall down; older buildings may show large cracks in walls and failure of fill-in walls.
VIII	Heavily damaging	Many people find it difficult to stand. Many houses have large cracks in walls. A few well built ordinary buildings show serious failure of walls, while weak older structures may collapse.
IX	Destructive	General panic. Many weak constructions collapse. Even well built ordinary buildings show very heavy damage: serious failure of walls and partial structural failure.
X	Very destructive	Many ordinary well built buildings collapse.
XI	Devastating	Most ordinary well built buildings collapse, even some with good earthquake resistant design are destroyed.
XII	Completely devastating	Almost all buildings are destroyed.

Tab. 3-2: European Macroseismic Scale (EMS-98), classification of intensity Description of typical observed effects [Grünthal 1998]

	<p><b>Grade 1: Negligible to slight damage</b>  <b>(no structural damage, slight non-structural damage)</b>                  Hair-line cracks in very few walls.                  Fall of small pieces of plaster only.                  Fall of loose stones from upper parts of buildings in very few cases.</p>
	<p><b>Grade 2: Moderate damage</b>  <b>(slight structural damage, moderate non-structural damage)</b>                  Cracks in many walls.                  Fall of fairly large pieces of plaster.                  Partial collapse of chimneys.</p>
	<p><b>Grade 3: Substantial to heavy damage</b>  <b>(moderate structural damage, heavy non-structural damage)</b>                  Large and extensive cracks in most walls.                  Roof tiles detach. Chimneys fracture at the roof line; failure of individual non-structural elements (partitions, gable walls).</p>
	<p><b>Grade 4: Very heavy damage</b>  <b>(heavy structural damage, very heavy non-structural damage)</b>                  Serious failure of walls.                  Partial structural failure of roofs and floors.</p>
	<p><b>Grade 5: Destruction</b>  <b>(very heavy structural damage)</b>                  Total or near total collapse.</p>

Tab. 3-3: Classification of damage to masonry buildings [Grünthal 1998]

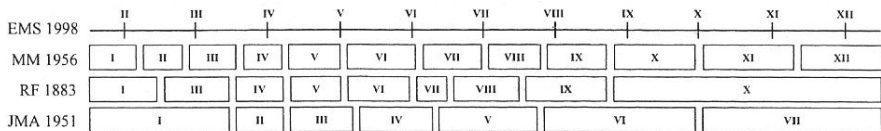


Fig. 3-5: Comparison of European Macroseismic Scale 1998 (EMS), Modified Mercalli Intensity scale (MMI), Rossi-Forel (RF) and Japanese Meteorological Agency (JMA) [Meskouris, Hinzen 2003]

### 3.2.5 Frequency content parameters

The dynamic response of structures is very sensitive to the frequency at which they are loaded. Earthquakes produce complicated loading with components of motion that span a broad range of frequency. The frequency content describes how the amplitude of ground motion is distributed among different frequencies. This can be done by means of tools as the Fourier spectra, power spectra and some more which will not be further explained here. Only the response spectra - used extensively on earthquake engineering practice as well as in this study - is described in the following. Within the frequency domain all measures are related to the frequency content of a given time history. It is important to keep in mind that response spectra are developed by determining the absolute maximum values of a single-degree-of-freedom (SDOF) system with viscous damping as shown in Fig. 3-6. Further basics are given in Section 3.4. The very famous equation of motion - here given in Eq. (3-12) - is solved using the Duhamel integral resulting in the following expression determining the spectral displacement  $S_d$ , which is the absolute maximum of the relative top displacement of the integral in Eq. (3-7) for the SDOF system.

$$\bar{S}_d(t) = u_{rel}(t) = -\frac{1}{\omega} \int_0^t \ddot{u}_{rel}(\tau) e^{-\zeta\omega(t-\tau)} \sin[\omega(t-\tau)] d\tau \quad \text{Eq. (3-7)}$$

Here  $u$ ,  $\omega$  and  $\zeta$  are the displacement, the natural frequency and modal damping of the SDOF system. Now, since the integral term has the unit of m/s, it may be seen as a velocity. This value is also called pseudospectral velocity  $S_v$ , and may be determined as follows:

$$\bar{S}_v = \int_0^t \dot{u}_{rel}(\tau) e^{-\zeta\omega(t-\tau)} \sin[\omega(t-\tau)] d\tau \quad \text{Eq. (3-8)}$$

Using Eq. (3-7) and Eq. (3-8) and including the pseudospectral acceleration  $S_a$ , a relationship between the three components may be derived:

$$S_a = \omega^2 S_d = \omega S_v \quad \text{Eq. (3-9)}$$

Spectral acceleration is not to confuse with peak ground acceleration (PGA). PGA is what is experienced by a particle on the ground. Spectral acceleration is approximately what is experienced by a building, as modelled by a particle on a massless vertical rod having the same natural period of vibration as the building. The pseudospectral velocity is not the same as the absolute velocity spectrum. A full solution for the velocity would cause Eq. (3-10).

$$\dot{u}_{rel}(t) = -\zeta\omega \cdot u_{rel}(t) - \int_0^t \ddot{u}_{rel}(\tau) e^{-\zeta\omega(t-\tau)} \cos[\omega(t-\tau)] d\tau \neq \omega S_D \quad \text{Eq. (3-10)}$$

Nevertheless, pseudo values may easily be applied  $S_d$ ,  $S_v$ ,  $S_a$  Spectra and in combination. The most famous one is the spectral acceleration diagram which used to present the response spectra of the many standards. To show easily a lot important characteristics of an earthquake the spectral velocity is often used. In the capacity spectrum method, spectral acceleration and spectral displacement are coupled in the  $S_a$ - $S_d$ -diagram, also called Acceleration Displacement Response Spectra (ADRS) diagram.

## 3.3 Earthquake records

The prediction of different levels of ground motion and shaking intensities is the major task hazard analysis. Time records to describe earthquakes are already shown in Fig. 3-3. Such can be measurements of natural earthquakes or artificial generated earthquake records.

Recordings of natural earthquakes are available online at several databases. Still, those records are not always of the magnitude, distance or soil conditions which are to be considered in the structural analysis. Additionally, it is sometimes unknown, whether the records are filtered or modulated. Since for this work a large number of different records is going to be needed, the approaches for the applied generations of artificial accelerograms are briefly explained in the following.

For the generation of artificial accelerograms several algorithms exist. In general, they all base on a given response or power spectrum and are created as an inverse Fourier transformation which is then modulated, filtered and iteratively fitted to the given spectrum. An easy and common way in the generation of artificial accelerograms is the summation of different harmonic waves with randomly varying phase angle. Further methods are the modulation white noise and non-stationary approaches. The methods are summarised, compared and described more in depth in [Urban 2007]. For the purpose of this study random phase angle generation is sufficient. The approach is already implemented in programmed codes by [Meskouris, Hinzen 2003] and can be used in combination with the target spectra given in modern codes as [DIN 4149].

### 3.4 Structural dynamic

Some basics of the structural dynamic will be briefly mentioned. A deeper explanation is given in literatures, for instance [Link 2002], [Kramer 1996] and [Meskouris, Hinzen 2003].

#### 3.4.1 Single-degree-of-freedom system

The basics of the structural dynamic can be easily described by means of the single-degree-of-freedom (SDOF) system which is shown in Fig. 3-6. With special regard to earthquakes, it is loaded with a base point excitation, here a ground displacement  $u_g$ . In some methods (e.g. response spectra method) the structure is simplified as a SDOF system to calculate the structural response, which can be the displacement  $u$ .

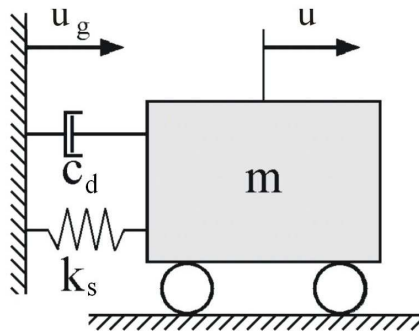


Fig. 3-6: Damped single-degree-of-freedom (SDOF) system with base point excitation

The relative displacement  $u_{rel}$  - simply calculated by Eq. (3-11) - is of greater importance as the absolute displacement of the structure, because it does not include the ground motion.

$$u_{rel} = u - u_g \quad \text{Eq. (3-11)}$$

When a dynamic load is applied to the mass of the system, the tendency for motion is resisted by the inertia of the mass and by forces that develop in the dashpot and spring. The equation of mo-

tion can be derived with a simple force equilibrium and so easily expressed in terms of the dynamic equilibrium of those forces as in Eq. (3-12). It describes the dynamic behaviour of the SDOF system with base point excitation:

$$m\ddot{u}_{rel} + c_d\dot{u}_{rel} + k_s u_{rel} = -m\ddot{u}_g \quad \text{Eq. (3-12)}$$

where  $m$  is the mass,  $c_d$  is the damping coefficient of dashpot and  $k_s$  is the stiffness of the spring. Dividing by  $m$ , the equation of motion is often expressed in the standard formulation as shown in Eq. (3-13).

$$\ddot{u}_{rel} + 2\zeta\omega\dot{u}_{rel} + \omega^2 u_{rel} = -\ddot{u}_g \quad \text{Eq. (3-13)}$$

The natural frequency  $\omega$  and the damping ratio  $\zeta$  are used in this standard expression.

### 3.4.2 Damping

In real systems, energy is lost as a result of friction, heat generation or other physical mechanisms, which dissipate energy. Therefore, the free vibration of response amplitude of a damped SDOF system will diminish with time. A huge amount of damping types exists. Regarding this work the structural damping is significant, which belongs to the inner damping and is caused by material damping and damping in the surfaces of contact. Normally the sum of all damping effects can be described with sufficient accuracy by means of the viscous damping formulation, which is proportional to the velocity and easy to handle. This term of damping is shown in Eq. (3-12).

Damping can be implemented in numerical modelling in different ways. A very common method is the application of the Rayleigh damping. The numerical programs used in this study base also on this method, in which the damping matrix can be broken into a component proportional to mass matrix and a component proportional to the stiffness matrix. So, the Rayleigh damping is described by a mass damping coefficient  $\alpha$  and a stiffness damping coefficient  $\beta$ . The damping matrix is calculated by using these constants to multiply the mass matrix and stiffness matrix. The damping ratio may be determined for each natural frequency  $\omega_i$  for a particular vibration mode  $i$  by means of Eq. (3-14).

$$\xi_i = \frac{\alpha}{2 \cdot \omega_i} + \frac{\beta \cdot \omega_i}{2} \quad \text{Eq. (3-14)}$$

Constant factors over the frequency range of interest may be evaluated by Eq. (3-15). It contains the damping for the lowest (l) and highest (h) frequency and their corresponding damping included in this study.

$$\beta = \frac{2 \cdot \xi_l \cdot \omega_l - 2 \cdot \xi_h \cdot \omega_h}{\omega_l^2 - \omega_h^2} \quad \text{Eq. (3-15)}$$

The damping ratio and the influence of mass damping, which is decreasing with increasing frequency and the importance of increasing stiffness or beta damping is shown in Fig. 3-7. The final values of  $\alpha$  and  $\beta$  were chosen for masonry in general and to represent a larger range of damping ratio for a great frequency range, which bases on previous studies of [Urban 2007].

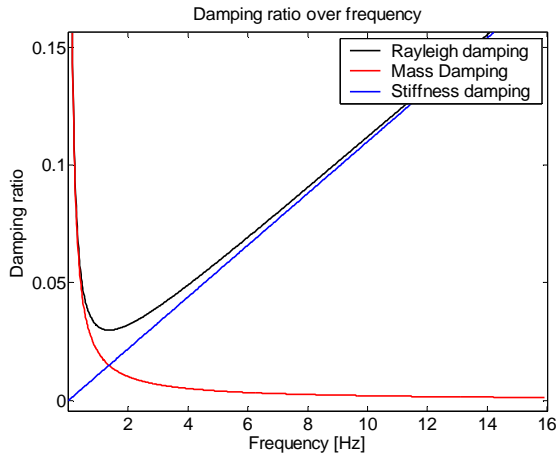


Fig. 3-7: Rayleigh damping versus structural frequency [Urban 2007]

### 3.5 Correlation between strong motion parameters and structural damage

Strong motion parameters describe the strength of an earthquake. Some of them are explained in Section 3.2. In a previous study [Urban 2007] it is already investigated, whether correlation between strong motion parameters and structural damage of the mainly applied masonry material model [Gambarotta, Lagomarsino 1997b] (see Section 4.3.3.2) can be observed, and whether it goes in line with literature regarding other masonry material models. The damage parameters are already introduced in Section 2.3.2. In [Urban 2007] and [Urban et al. 2006] a huge amount of strong motion parameters is taken into account. In order to assess the strong motions effects, a numerical transient sample study was performed. Therefore, an artificial earthquake was generated. This accelerogram will be referred to as basic earthquake. The length of this basic accelerogram was set to eleven seconds with a linearly increasing intensity function during the first second and a decreasing one in the last second. A set of hundred earthquakes was created by multiplying the amplitudes of the root earthquake by factors 0.5 to 5.0 in steps of 0.5 and changing the length of the accelerogram from two seconds to eleven seconds in steps of one second. The set of hundred earthquakes was then applied to the finite element model of a wall with varying height, i.e. different first natural frequencies ranging from 1 Hz to 10 Hz [Urban, Sperbeck, Peil 2006]. To include the natural variation, the study was not only performed for one ‘root’ earthquake, but also hundred time histories were included additionally, of which thirty were natural recordings and seventy were artificial ones developed with different algorithms. Two thousand calculations were evaluated to achieve the correlations. The extension from one basic earthquake to hundred basics earthquakes has not lead to different correlations.

It can be concluded, that reasonable correlations were evidenced. Thus, the material model is able to predict the structural damage in a realistic way. The results go mainly in line with the literature. Only the scatter of damage for lower frequencies resulted higher. This is in contrast to the results presented by [Bommer et al. 2004a] because the material model used there is focused on shear failure, whereas the model applied here includes also the failure due to tension, which governs for low frequencies. If only the damage due to shear was taken into account, similar results would be obtained. The result shows the advantage of the material model used here. As it should be expected, the parameters to describe the strength of the earthquake are well correlated with the structural damage parameters. Quite often, a high correlation is achieved, as it can be

seen especially for high frequencies. This is due to the fact that the rank order correlation coefficient was used. Specifically the Arias Intensity correlates most constantly over the considered frequencies. The duration has also a significant impact on the damage (see Fig. 3-8 left). With the given results it can be also concluded, that for this task it is sufficient to provide estimates of duration and PGA in order to assess the probabilities of damage. The relation of these strong motion parameters and the damage are presented in Fig. 3-8.

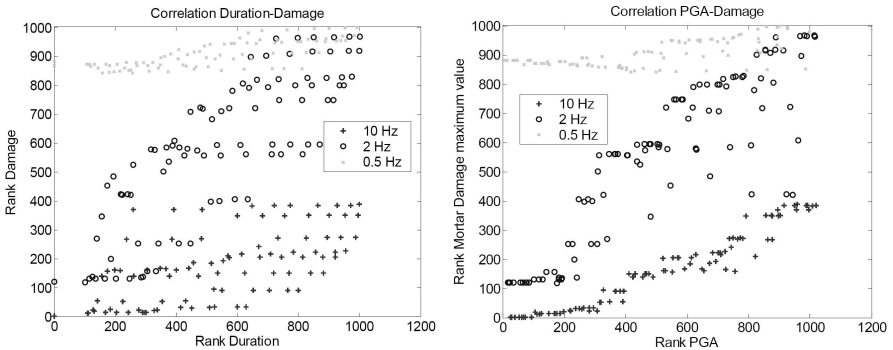


Fig. 3-8: Rank Order Correlations of Maximum Mortar Damage and Uniform Duration with 0.05g threshold for the full range of simulations [Urban, Sperbeck, Peil 2006]

Another important parameter was the natural frequency of the structure itself. Thus, not only the intensity but also the duration and the natural frequency are varied for the probabilistic analyses in this study. Moreover, the presented method to vary a basic accelerogram by means of a factor to implement the different strength of earthquakes leads to realistic results. Anyway, to be on the safe side in this study, different basic earthquakes are used. In detail, another basic earthquake is generated for every duration. It is further explained in Section 3.6.

### 3.6 Probability of earthquake loading

As already mentioned, this thesis does not focus on the hazard analysis. This is already done in previous works on which this study is based. Nevertheless, the hazard analysis is integrated and described in the following. First of all, some basics regarding the assessment of seismic probabilities are mentioned and briefly discussed. Thereafter, the probability of intensity is given for the region of Aachen investigated in this study.

#### 3.6.1 General remarks

The scope of an advanced hazard analysis is to take into account the uncertainties and to describe the probability of exceedance, finally given in terms of probability density functions for further analyses as damage assessment. The current German standard [DIN 4149] or the European code [Eurocode 8] take into account only the return period of 475 years, which corresponds to a probability of exceedance of 10% in 50 years (see Eq. (3-16)). For the different regions (earthquake zones) only one value of design ground acceleration is assigned. Thus, the scattering of earthquake strength is neither included in the return period nor in the acceleration. Regarding these drawbacks, more methods are necessary to generate data for a reasonable hazard analysis in the framework of risk management. The best valid concept is the probabilistic seismic hazard analysis PSHA, which is able to estimate probabilities of occurrence of ground motion characteristics.

In general, to estimate the probability of exceedance  $p_{ex}$  of an event regarding the design working life  $T_L$  of the structure the relation given in Eq. (3-16) is used:

$$p_{ex} = 1 - e^{-\frac{T_L}{T_R}} \quad \text{Eq. (3-16)}$$

where  $T_R$  is the return period of the event. If the design working life is set equal to 100 years and the probability of exceedance has to be below 10% in 100 years, this correspond to a return period of 950 years. The annual probability of exceedance can be calculated by using  $T_L = 1$  year or by means of Eq. (3-17).

$$p_{ex} = \frac{1}{T_R} \quad \text{Eq. (3-17)}$$

As already introduced at the beginning of this chapter, different types of uncertainties in earthquake engineering exist. They are summarized in Tab. 3-1 and they can be taken into account by means of the source-pathway-receptor model (see Fig. 3-2), which is used in many different methods to carry out extending hazard analyses. The methods mainly differ in the laws used to describe the uncertainties. The general common procedure and the fundamentals of PSHA methodologies described in the following are based on the well-established method developed and first published in [Cornell 1968] and explained more in detail in [Kramer 1996]. The similarities may be generalised in four steps, which are summarized in the following and depicted in Fig. 3-9.

In the first step, the earthquake source is identified and characterised by means of probability distributions of potential rupture locations within the source. In most cases, uniform probability distributions are assigned to each zone, implying that earthquakes are equally likely to occur at any point within the source zone. These distributions are then combined with the source geometry to obtain the corresponding probability distributions of source-to-site distance.

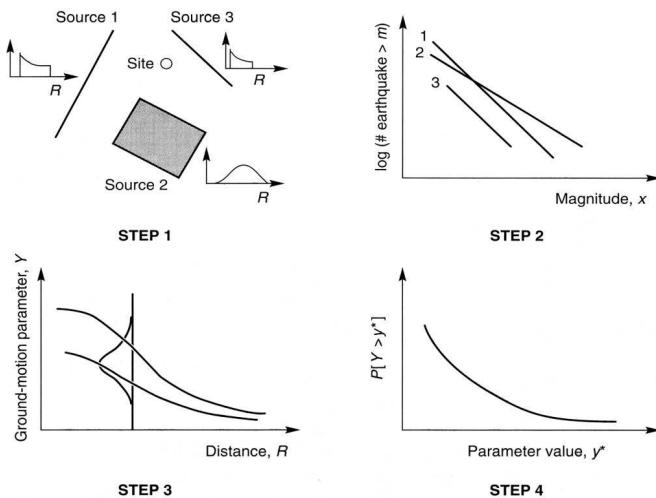


Fig. 3-9: Steps of probabilistic seismic hazard assessment [Kramer 1996]

In the next step, the temporal distribution of earthquake recurrence is characterised. A recurrence relationship, which specifies the average rate at which an earthquake of some size will be exceeded, is used to characterise the seismicity of each source zone. This is done by means of dis-

tributions of the magnitude, which may be described in different ways. The most common is the Gutenberg-Richter relationship - given in Eq. (3-18) – which is extended to the Gutenberg-Richter recurrence law. The use differs in modifications to account for minimum and maximum magnitudes.

$$\log \lambda_m = a - bm \tag{Eq. (3-18)}$$

The mean annual rate of exceedance  $\lambda_m$  of an earthquake of magnitude  $m$  is calculated using the seismic constants  $a$  and  $b$ , which are determined for each region by a combination of historical earthquake data and modern instrumental records. Another way is the description with Extreme Value Distribution Type III, which is sometimes referred to as Inverse Weibull distribution [Sánchez-Silva, Rackwitz 2004]. The probability of occurrence for the magnitude  $F_M(m)$  is calculated as depicted in Eq. (3-19) [Rackwitz 2006]:

$$F_M(m) = \frac{\exp\left[-\left(\frac{M_{max} - m}{M_{max} - w}\right)^k\right] - \exp\left[-\left(\frac{M_{max} - M_{min}}{M_{max} - w}\right)^k\right]}{1 - \exp\left[-\left(\frac{M_{max} - M_{min}}{M_{max} - w}\right)^k\right]} \tag{Eq. (3-19)}$$

where  $M_{max}$  is the upper magnitude and  $M_{min}$  is the lowest magnitude. The constants  $w$  and  $k$  describe the shape of the graph and are thus determined by the maximum likelihood method to best fit the observed data of seismicity in the given region. In Fig. 3-10 the annual exceedance probabilities of the magnitude for different regions are shown, which base on data quoted by [Rackwitz 2006] and [Urban 2007]. A comparison of Gutenberg-Richter relationship and Weibull distribution is given in [Urban, Sperbeck, Peil 2006] and [Urban 2007].

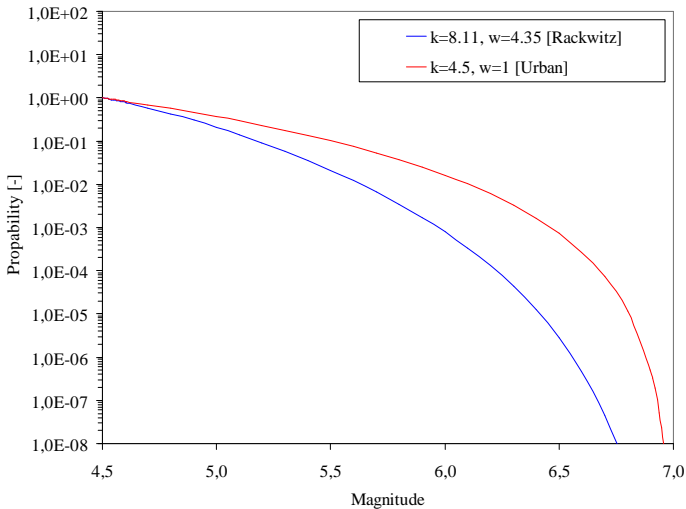


Fig. 3-10: Annual exceedance probabilities of the magnitude for different regions

In step 3, the ground motion produced at the site by earthquakes of any possible size occurring at any possible point in each source zone must be determined with the use of predictive relationships. The uncertainty inherent in the predictive relationship is also considered in a PSHA. The

uncertainty in these ground motions is a function of the scatter in the database from which the predictive relationships were developed.

In the last step, the uncertainties in earthquake location, earthquake size and ground motion parameter prediction are combined to obtain the probability that the ground motion parameter will be exceeded during a particular time period. Therefore, standard methods of probabilistic analysis can be used to combine these quantified uncertainties. Because of the complex and empirical nature of the probability density functions, exceedance probabilities are usually computed by numerical rather than analytical methods. The accuracy of PSHA depends on the accuracy with which uncertainty in earthquake size, location, recurrence, and effects can be characterised.

For many PSHA methods it is highly recommended not to use probabilities of occurrence less than  $10^{-5}$  [Schmitt 2005], [Bommer et al. 2004b], [Abrahamson, Silva 1997]. Also, if dealt with very low annual exceedance rates, the PSHA will always involve a large degree of expert judgement [Bommer et al. 2004b]. Regarding the application examples of PSHA methods, the interested reader is referred to [Schmitt 2004], [Sánchez-Silva, Rackwitz 2004], [Simeonova et al. 2006], [Rackwitz 2006], [Urban, Sperbeck, Peil 2006] and [Urban 2007].

### 3.6.2 Probability assessment for an endangered region and ground motion estimation

In the framework of a hazard analysis, the results of a PSHA carried out by the Institute for Geosciences and Natural Resources Hannover [Schmitt 2004] and [Schmitt 2005] are used. In this PSHA a method is utilized which deduces the causative sources, characteristics, and ground motions for future earthquakes. The analysis methodology is based on the conception that the seismic hazard at a site is a function of three main components: the space geometry of seismic sources, the characteristics and statistics of their seismicity and the attenuation of intensity. The resulting hazard at a specified site is obtained by integrating the effects of ground motion from earthquakes of different size occurring at different locations within different seismic source regions and with different frequencies of occurrence [Simeonova et al. 2006]. For the investigated region of Aachen, the PSHA leads to results shown in Fig. 3-11 by means of the seismic hazard curve for the intensity and summarised in Tab. 3-4.

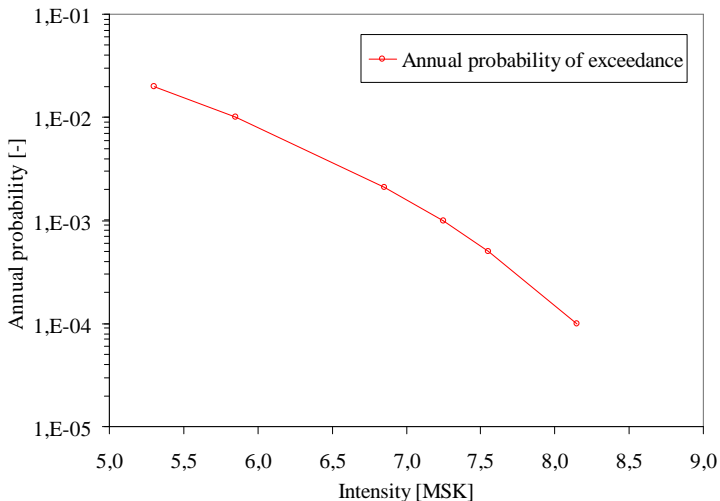


Fig. 3-11: Seismic hazard curve for Aachen, Germany [Schmitt 2005]

The relation between Intensity and *PGA* is determined subjected to Murphy and O'Brien as defined in Eq. (3-20), recommend and applied in [Mistler 2006].

$$PGA = 1.778 \cdot 10^{0.25I} \quad \text{Eq. (3-20)}$$

In Tab. 3-4 all values are summarized. An investigation of the whole range of probabilities – as given by the curve in Fig. 3-11 – in structural analysis by means of probabilistic transient analysis is not reasonable, since many small earthquakes which occur with high probability do not lead to damages. Hence, a huge number of transient calculations is redundant, while not leading to damage. Thus, the following new method is suggested and applied in this study. A minimum threshold is selected which is reasonably fitted to the investigated structure. Therefore, in this work the minimum threshold corresponds to a return period of 475 years, and the maximum to a return period of 10000 years, which belongs to the recommended minimal probability as quoted above. Moreover, a return period of 2000 years is used with the aim to approximate finally fragility curves as result of the risk based analysis in Chap. 8.

Return period	Annual probability of exceedance	Annual probability of exceedance	Intensity	PGA
[a]	[-]	[%]	[MSK]	[m/s <sup>2</sup> ]
50	0.0200	2.00	5.30	0.38
100	0.0100	1.00	5.85	0.52
475	0.0021	0.21	6.85	0.92
1000	0.0010	0.10	7.25	1.15
2000	0.0005	0.05	7.55	1.37
10000	0.0001	0.01	8.15	1.94

Tab. 3-4: Seismic hazard data regarding for the region of Aachen, Germany [Schmitt 2005]

For this study transient analyses are performed (see Chap. 6, 7 and 8). Therefore, time histories are necessary. The PGAs given in Tab. 3-4 are used to generate one scaled aim response spectra in accordance to [DIN 4149] for each return period of interest as recommended by [Mistler 2006]. The geological ground type R in combination with foundation soil type C is used. Corresponding to each aim response spectra, four time histories are artificially generated, which differ in duration and characteristics. For the return period the data are given in the following as the pseudo-velocity diagrams (see Fig. 3-12), the spectral acceleration diagrams is depicted in Fig. 3-13, finally the different durations and corresponding parameters of each time history are given in Tab. 3-5. All diagrams and tables related to the return periods of 2000 and 10000 years are printed in Appendix B.

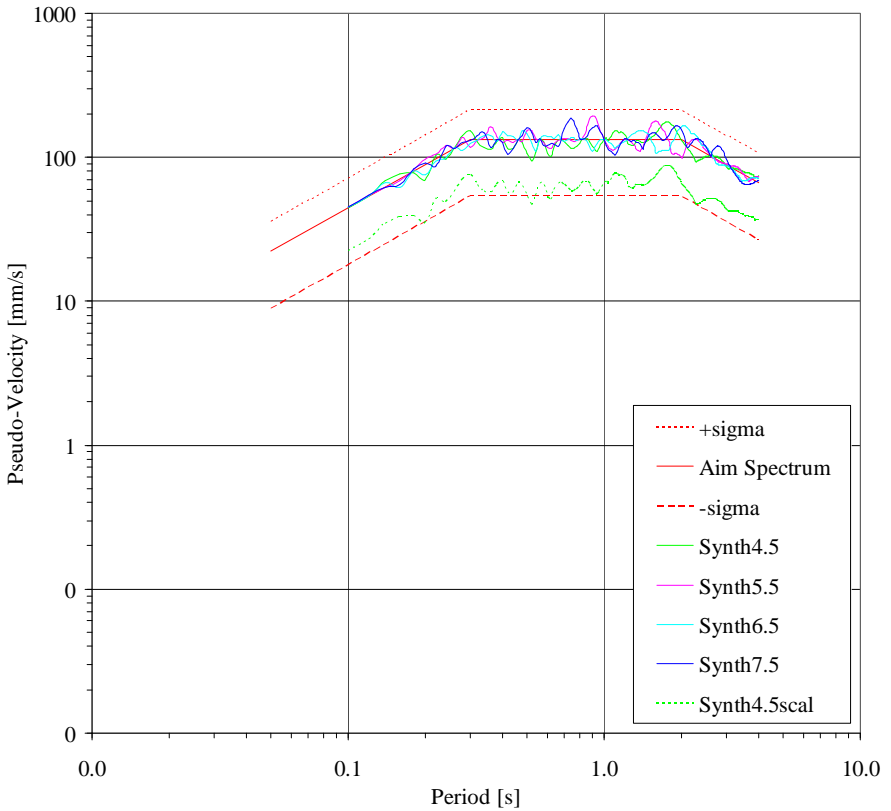


Fig. 3-12: Pseudo-velocity diagram, return period of 475 years

As shown in Fig. 3-12 and Fig. 3-13 the artificial generated earthquakes scatter around the aim spectra. Moreover, in the probabilistic transient structural analyses the time histories scatter by means of a scaling factor, within a range of a lognormal distribution with standard deviation 0.5 and a mean value of 1.0 – normalized value. In accordance with [Rackwitz 2006], [Hosser et al. 1986] and several other authors the response spectra scatter in a range defined by a lognormal distribution with a standard deviation of 0.6. In the transient structural analyses for the time histories scattering a standard deviation of 0.5 is chosen, since small variation of the generated accelerograms already exist. Both together lead to a standard deviation of 0.6 as recommended by the quoted literature. This is also shown in Fig. 3-12 and Fig. 3-13, where the dashed red line depicts the standard deviation of 0.6 and dashed curves represent the earthquake scaled by a factor of 0.5.

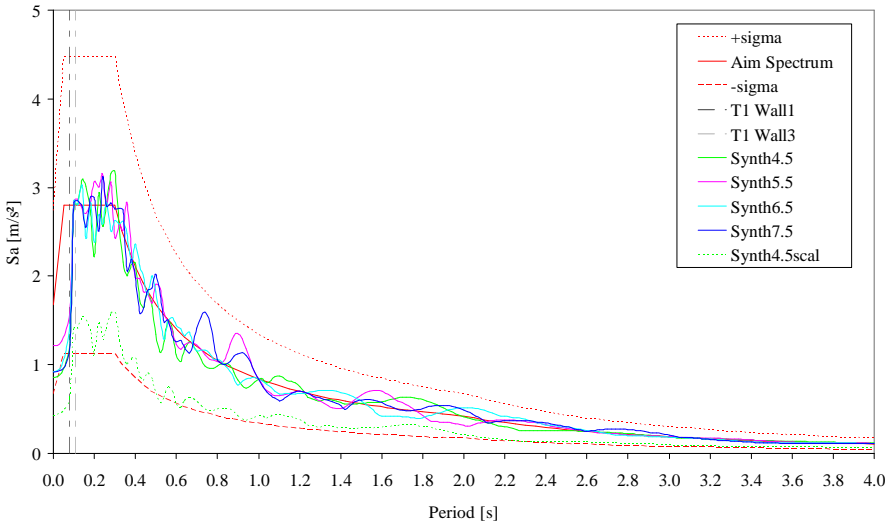


Fig. 3-13: Spectral acceleration diagram, return period of 475 years

No.	Over-all time [s]	Increasing time [s]	Start of decreasing [s]	Steady phase [s]	Simulation stop [s]	Uniform Duration $D_{u0.15}$ [s]	Significant Duration $D_{s95}$ [s]	Arias Intensity AI [m/s²]
1	10	1.5	6	4.5	8	4.8	6.0	0.1252
2	10	1.5	7	5.5	9	5.6	6.5	0.1499
3	10	1.5	8	6.5	9	5.8	7.0	0.1429
4	10	1.5	9	7.5	10	6.0	7.4	0.1643

Tab. 3-5: Durations and Intensities of the generated accelerograms, return period of 475 years

To investigate structures with a high resistance, artificial earthquakes for a PGA of averagely round about  $4 \text{ m/s}^2$  are generated. The diagrams and tables are shown in Appendix C. By means of the method explained above seven different time histories are generated, one for each duration.

### 3.7 Requirements on the seismic performance of structures

#### 3.7.1 General remarks

For seismic action a lot of design philosophies and methods exist, which aim partly at different requirements on the seismic performance of structures. Here, it is roughly distinguished in two main groups of methods. An older method - in the following called conventional design – bases historically on the use of forces. In this technique, a structure is designed to act only in the elastic range during an earthquake. Modern methods take into account also the plasticity – in the following called inelastic design – and deal often with ductility and displacement (see Fig. 3-14).

To offer a better understanding of this subject, some basics regarding the historical development based on [Priestley 2007] are given subsequently. Currently, seismic design is mostly based on

force rather than displacement. The reason is mainly based historical. Before the 1930's, only some structures were specially designed against seismic loading. In the 1930's several major earthquakes occurred. The structures with design for horizontal wind forces performed better in than those without special resistance against horizontal loading. Therefore, horizontal inertia forces (normally 10% of the building weight) for structures in seismic regions had been implemented in first design codes.

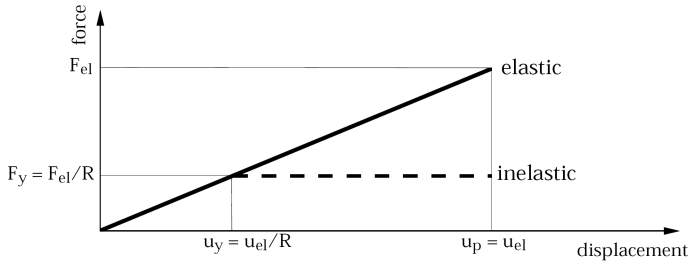


Fig. 3-14: Comparison of elastic and inelastic response

With the development of inelastic time-history analysis and improving knowledge of seismic behaviour and in the 1960's, came understanding that numerous buildings had survived earthquakes capable of inducing inertia forces many times larger than those related to the structural strength. As a result, the concept of ductility has been developed to reconcile the obvious anomaly of survival with apparently insufficient resistance. Coherences between ductility and force-reduction factor, which is also called ductility reduction factor  $R$  (see Fig. 3-14) or behaviour factor  $q$ , such as the 'equal displacement' and the 'equal energy' concepts were advanced as an essential to regularize the proper horizontal resistances. Much investigation effort was directed during the 1970's and 1980's to determine the existing ductility capacity of diverse structures. The considerations of ductility became a fundamental part of design. In order to quantify the available ductility, extensive experimental and analytical studies were performed to determine the safe maximum displacement of different structural systems under cyclically applied displacements [Priestley 2007]. It was an important step in a direction away from a force-based seismic design. In order to determine the necessary resistance, a force-reduction factor was introduced that reflects the observed ductility capacity of structure and material. However, it was still designed in terms of required strength and displacement capacity. The concept of 'capacity design' was introduced [Park, Paulay 1976], in which the identification of preferred locations of flexural plastic hinging becomes important. In contrast, undesirable locations of plastic hinges and adverse modes of inelastic deformation were avoided by choosing their resistance higher than strength that belongs to the desired inelastic mechanism.

It may be seen, that in the beginning design was based on strength, or force considerations using assumed estimates of elastic stiffness. As in the last years, the importance of displacement was more appreciated, the one attempt to modify the existing force-based design to contain consideration of displacement as we find it in [Eurocode 8] and [DIN 4149]. There, the non-linear behaviour is taken into account by means of the behaviour factor  $q$ . For masonry this factor is chosen very conservative. Thus, the real ductile behaviour and the real ability of energy dissipation are much underestimated, which leads to problems in the design of masonry.

Moreover, different design philosophies exist. Structures can be designed for the serviceability level earthquake with the aim to avoid damage. The design level earthquake allows repairable damage. For the extreme earthquake the structures are designed in a way to avoid collapse while allowing irreparable damages. The newest and most complex philosophy is the risk based design, which is already explained in Chap. 2. The definition of risk includes the damage and its prob-

ability. Finally it can be summarised, that the suggested risk management based concept of Chap. 2 offers the possibility to consider the different hazard levels (serviceability level earthquake, design level earthquake and extreme earthquake) and aims on the damage reduction.

Due to their importance the terms ‘shear capacity’ and ‘ductility’ and their relation to design concepts are separately depicted in the subsequent subchapters.

#### 3.7.2 Shear capacity

In this context the term ‘capacity’ is used to express the strength. Since the shear resistance of walls is described with force (not with stresses) the term ‘capacity’ is often used in literature. To avoid misunderstanding regarding the meaning above and since this thesis deals with the in-plane shear behaviour of masonry walls the term ‘shear capacity’ is used.

Regarding the retrofitting against seismic action, the shear capacity is of interest, which is defined by the maximum static or static cyclic shear resistance which the structure can carry. If the shear capacity is increased, usually also the elastic range is increased. Hence, a strengthened structure behaves more elastic than a non-strengthened structure. In areas of low seismicity or to design a structure for the serviceability level the shear capacity is often increased. The aim is an elastic structural response and so a complete avoidance of damage. Nevertheless, high strengths require big cross sections, which lead to high costs.

#### 3.7.3 Ductility

The capability of plastic deformation while carrying the load is called ductility. Roughly it is distinguished in local ductility of a structural element (e.g. plastic hinges) and global ductility of the whole structure. Several suggestions exist to define values for the ductility. In general it can be done by means of ‘equal displacement’ or ‘equal energy’ approximation

A high ductility avoids brittle failure, which is desirable. Moreover, in case of dynamic action energy is well dissipated, when the structure behaves plastically. Thus, the loading is reduced, because plasticity leads to reduction of stiffness and so to a reduction of dynamic loading which depends on the stiffness. As disadvantage damages occur in case of ductility, and the damage increases with ductility. In areas of high seismicity or to design a structure for extreme earthquake the focus often lies on high ductility to avoid failure and to reduce the dynamic loading. It is not economic and sometimes also impossible to construct buildings which react only in the elastic range during a strong earthquake. Damages are accepted. However it is to ensure that the structure does not collapse.

#### 3.7.4 Conclusion

To ensure the avoidance of collapse in case of unexpected strong earthquake, a high ductility of the structure is definitely important. In fact the utilisation of high ductility in combination with low shear capacities (small elastic range) leads on the one hand to low dynamic forces, and on the other hand to high damages. Regarding a risk based design, which aims at the reduction of damages, an increasing of the shear capacity can be useful, if it reduces the damages. For dynamic action it is to investigate, if retrofitting measures effectively reduce the damages for the huge variety of earthquakes and their interactions with the different types of structure.

### 3.8 Summary

The basics and describing parameters of seismic hazards are briefly explained, as well as differences and drawbacks of naturally and artificially generated earthquake records. Both are used in this work. Moreover, basics of structural dynamic are explained to provide the knowledge for a good understanding of some earthquake parameters and the structural response. Last, it is important to understand significant requirements on the seismic performance of structures, which are essential for the investigation of strengthening measures in case of earthquakes. Two complete different design methods have to be distinguished. On the one hand, the conventional design acts in the elastic range and tries to avoid any damage. On the other hand, the inelastic design uses the ductility for a reduction of dynamic forces and accepts damage. Moreover, a summary of correlations between strong motion parameters and structural damage of masonry is given to identify the most important parameters, which are of interest for sensitivity and probabilistic studies described in Chap. 6, 7 and 8. Consequently, it is reasonable for the probabilistic analyses to implement the variety of earthquake intensity (by means of peak ground acceleration), duration as well as the natural frequency of the structure. For a reasonable risk assessment as performed in Chap. 8 the probability of earthquake loading is necessary. Therefore, some basics regarding seismic probabilities are briefly given as well as values of the probability for the region of Aachen investigated in the study.



## 4 Masonry

Masonry is one of the oldest materials and still most commonly used for construction. Advantageous properties as simple applicability, fire resistance, durability, and aesthetical appearance have led to a widespread resorting. Masonry may be distinguished in a large amount of classes regarding several parameters as material used, manner of assemblage, strength, age or sense of application. In this thesis, only some important groups are mentioned. The interested reader is referred to basic literature as [Merritt, Ricketts 2001] and [Gunkler, Budelmann 2007]. First of all, unreinforced masonry is elucidated, in the sense of normal masonry without any retrofitting, strengthening and rehabilitation measures. Essential knowledge is given in the subchapter below, which provides the base for retrofitted masonry as prestressed one, explained subsequently. After all, the numerical modelling of the complex material behaviour of masonry is explained.

### 4.1 Unreinforced masonry

#### 4.1.1 Mechanical properties of masonry

In order to estimate the resistance of masonry walls, a lot of mechanical properties need to be determined, which depend on the model used for the prediction. Furthermore, many different experimental tests can be found in literature to determine the same parameters. It is neither the purpose nor the intention of this thesis to discuss this topic or suggest further test. Instead some parameters are briefly given to provide basic information.

##### 4.1.1.1 Material behaviour of units and mortar

Masonry is a rather complex composite material. Its properties depend strongly upon the properties of its components. A huge variety of incombustible materials, such as natural stones, bricks, structural clay tile, concrete block, calcium-silicate bricks, gypsum block, glass block, or adobe brick are commonly used to produce the units, which are available in an almost unlimited number of sizes. Units without cores or with core areas up to 25% of the gross cross section are called solid units, which are rarely used nowadays. Hollow units have core areas up to a maximum of about 50% of the gross area. Core patterns typically vary dependent on manufacturer. Due to the cores and sometimes also due to the material, the units are anisotropic. Moreover, the masonry as a whole is anisotropic, caused in addition by the joints and bond pattern. In case of dry stone masonry no mortar is utilised. Nowadays, also thin bed mortar is deployed frequently. Especially, historical masonry can be composed of gypsum mortar. In the last decades portland cement based mortars in combination with hydraulic lime are applied in general. The numerous types of mortar show widespread properties.

A number of material properties is determined separately for units and mortar, as the tensile and compression strength as well as related moduli of elasticity, Poisson's ratio, density, ductility and fractured energies. A further property is the softening or post-peak behaviour described by gradient of the sloping curve part, which differs significantly for brittle and ductile materials. As outlined in Fig. 4-1 this can be also related to the fracture energy  $G_f$  and  $G_c$ . This behaviour depends also on the load direction (compression or tension) for materials masonry consists of. In general, compressed mortar or units behave more ductile than tensioned ones.

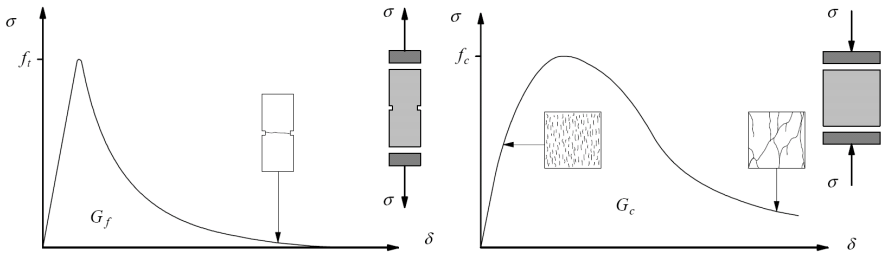


Fig. 4-1: Behaviour of quasi-brittle materials under uniaxial loading and definition of fracture energy, Left: tensile loading ( $f_t$  denotes the tensile strength), Right: compressive loading ( $f_c$  denotes the compressive strength) [Lourenço 1996]

4.1.1.2 Compression behaviour of masonry

For the determination of parameters to characterise the interface of mortar and units as the adhesive tensile strength, composite specimens are used. Also a more accurate determination of the compressive strength of masonry ensues on the composite as explained below. The interaction of units and mortar joints has attracted the interest of numerous researchers. In general, the mortar in the joints tends to have larger transverse strains than the masonry units under load. The units are stiffer than the mortar joints, leading to failure of masonry under compression, which is firstly proved by Hilsdorf [Hilsdorf 1965]. A predominant triaxial compression state of stress occurs in the mortar joint, while due to the lateral expansion of the mortar joints a triaxial compression-tension-tension state of stress predominates. If this lateral tension stress in the units is greater than its tensile strength, the process of vertical cracking in the units starts.

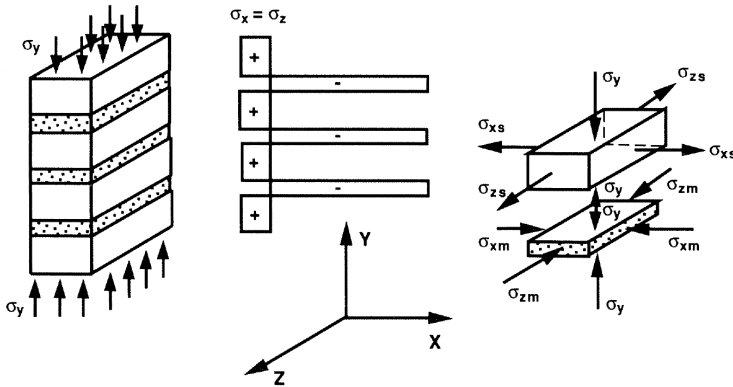


Fig. 4-2: Interaction of units and mortar joints - Prism under uniaxial compression and stresses in unit and mortar [Ganz 1990a]

Thus, under uniaxial compression perpendicular to the bed joints a splitting type of failure is usually observed in the units, as depicted in Fig. 4-3. However, this fact has not yet been universally recognized, thus some national standards still base the masonry compressive strength on unit and mortar strength.

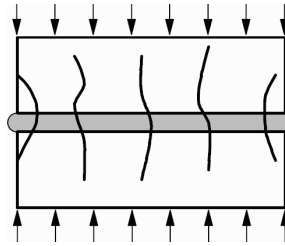


Fig. 4-3: Compression perpendicular to the bed joints and splitting [Lourenço 1996]

#### 4.1.1.3 Tension behaviour of masonry

In case of tensile loading perpendicular to the bed joints three failure types are possible or a mix of them. On the one hand the mortar strength may be the lowest. In that case the crack occurs in the mortar itself. On the other hand the adhesive tensile strength or also called bonding tensile strength, which characterises the bond between unit and mortar, could be the lowest. Often these occur in combination. The third possibility is a tensile failure of the unit, which is rarely observed due to the fact that the unit resistance is usually much greater than the mortar resistance. The tensile failure mode of the unit-mortar interface is often referred to as mode I in literature.

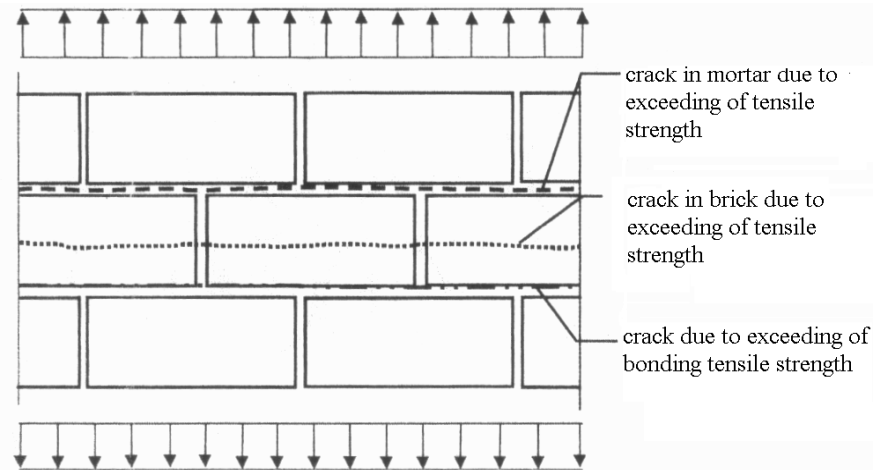


Fig. 4-4: Tensile loading on masonry and failure possibilities [Huster 2000]

#### 4.1.1.4 Shear behaviour of masonry

Regarding seismic loading the shear behaviour is the most important one. Shear strength and friction coefficient are properties of high interest to predict shear failure. In addition, the fracture energy is also used sometimes. In literature, the shear failure mode of the unit-mortar interface is often referred to as mode II. A possible experimental set-up used for tests in Braunschweig, Germany, is depicted in Fig. 4-5. A complete characterization of the masonry shear behaviour is presented in [Van der Pluijm 1993], for solid clay and calcium-silicate units. Compressive

stresses were applied with three different levels: 0.1, 0.5 and 1.0 N/mm<sup>2</sup>. The shear tests results are shown in Fig. 4-6, which clearly depicts the enhanced shear strength with increasing normal load level and revealed its Coulomb-friction nature. The results yield an exponential shear softening curves with a residual dry friction level. The area defined by the stress-displacement diagram and the residual dry friction shear level defines the mode II fracture energy  $G_f^{II}$ . Its value depends also on the level of the compression stress [Lourenço 1996]. For numerous specimens with higher compressive stresses, shearing of the unit-mortar interface was accompanied by diagonal cracks in the unit. This shows, that the shear behaviour cannot be exhaustively described by merely consideration of the unit-mortar interface.

Especially for parts of masonry walls greater than two-unit or three-unit specimens, the behaviour is more complex. As outlined in Fig. 4-7, it is to distinguish between three failure types. The first one, shear failure of the joint is already explained above. It occurs in case of low normal stresses. Increasing of this level leads to diagonal cracks in the units due to diagonal tensile stresses. If the normal load level is very high approximately vertical cracks can be observed in the bricks. This may be seen as a combination of shear and compression behaviour.

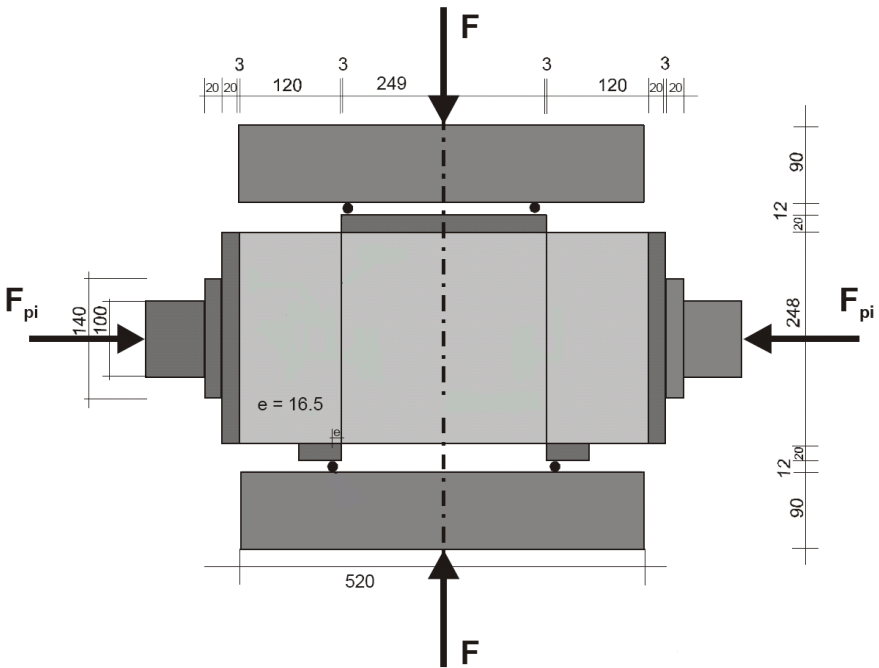


Fig. 4-5: Experimental setup of a shear test [Budelmann et al. 2004]

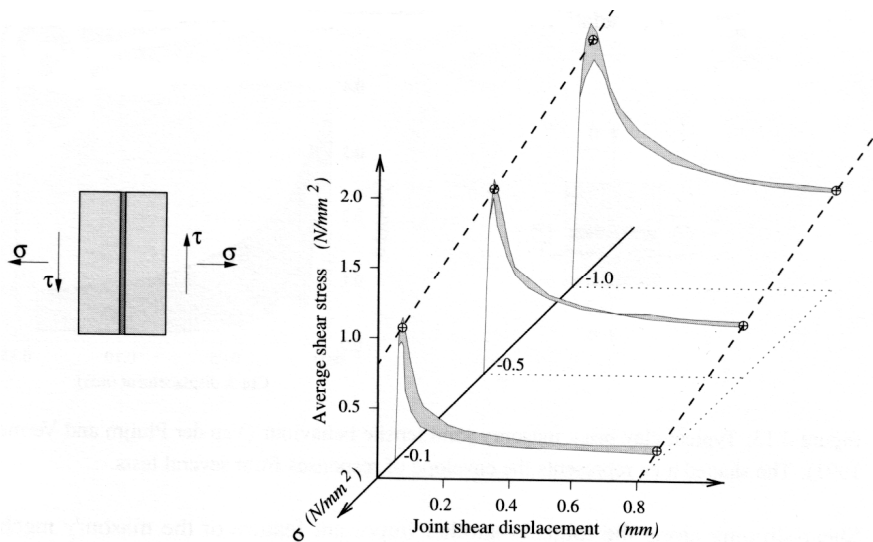


Fig. 4-6: Typical shear bond behaviour of joints for solid clay units, showing average shear stress-displacement at various normal stress levels (the shaded areas represent the envelopes of several tests) [Van Zijl 2000]

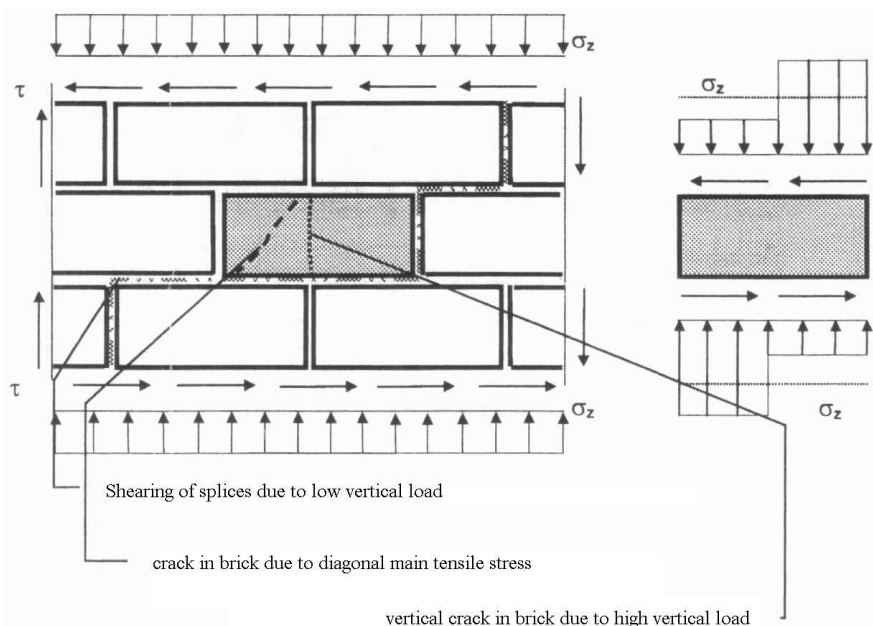


Fig. 4-7: Shear loading on masonry and failure possibilities [Huster 2000]

## 4.1.2 Support conditions of masonry walls

Before discussing the failure modes of in-plane loaded masonry walls, essential basics of the support conditions are given due to their significant impact on the failure mechanism. In this work it is distinguished between two theoretical extreme cases support condition 1 (SC 1), support condition 2 (SC 2) and the reality, which is something between the extreme cases, as outlined in Fig. 4-8.

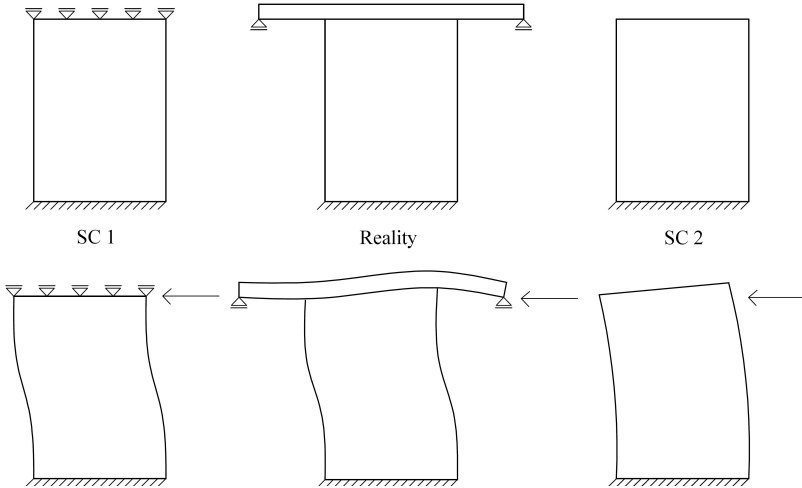


Fig. 4-8: Support conditions of shear walls and resulting deformations, Left: Support condition 1 (SC 1), Middle: Realistic condition, Right: Support condition 2 (SC 2)

In case of SC 1, the top of the wall is constrained, on account of that it stays horizontal. Mainly shear loading occurs. For case SC 2, the top of the wall is free and can rotate. Thus, the wall behaves like a cantilever, and in-plane bending loading occurs primarily. Fig. 4-8 shows walls with these support conditions and the resulting deformed shapes. In reality this condition exists very rare. Merely SC 2 can be found for free standing walls or towers. However in reality, the support condition of the walls is between these extreme cases, since usually the walls are located between floor slabs. The realistic support condition depends on the behaviour of the floor slabs. To predict the behaviour realistically, beams or slabs should be modelled as depicted in the middle of Fig. 4-8. Below, the impacts are explained in more detail. To gain deeper insight, case studies are performed, which are given in Chap. 6.

## 4.1.3 Failure mechanisms of horizontal in-plane loaded masonry walls

The anisotropic behaviour is reflected by the different failure modes of masonry encountered for general loading conditions such as combined shear and axial loads or introduction of concentrated loads. For horizontal in-plane loaded masonry walls the failure modes are usually distinguished in:

- Bed joint sliding (shear failure of the joints),
- Diagonal tension (shear failure of the units) or some times also named diagonal cracking,
- Rocking and
- Toe crushing (failure of the corner)

as it is recommended in [FEMA 306], [FEMA 308] and [FEMA 356]. Below this failure types are described in depth.

Bed joint sliding has to be further subdivided. On the one hand stepped cracks occur, which involve failure of different bed joints and head joints as shown in Fig. 4-9 left. On the other hand only one bed joint can fail, which leads to the movement of an upper rectangular block. Both cases are depicted in Fig. 4-10. The shear strength is a sum of the adhesive shear strength which describes the resistance of the bond between unit and mortar, and the friction. The last corresponds to the residual shear strength after initiation of sliding and is expressed by the Coulomb-friction law, which includes the vertical loading and the friction coefficient. These two failure types of bed joint sliding are very ductile, due to the Coulomb-friction mechanism acting in the bed joints until the end of a stepped course. Moreover, this mechanism dissipates a lot of energy (see Fig. 4-10 right). Both high ductility and high energy dissipation are desirable for a good seismic performance. The horizontal loading capacity is relative low.

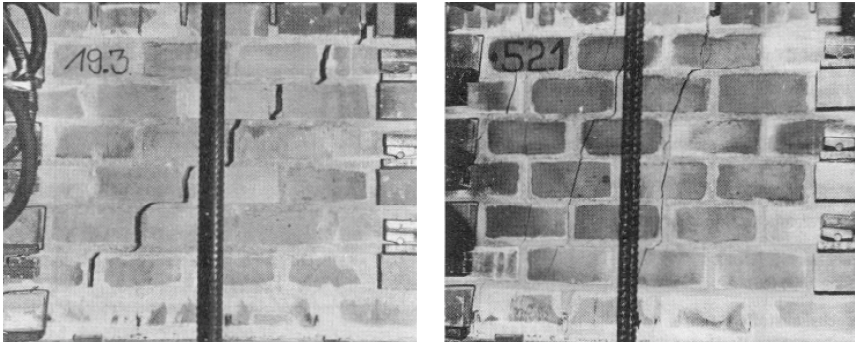


Fig. 4-9: Shear crack patterns, Left: Joint failure, Right: Unit failure [Mann, Müller 1978]

The term diagonal tension expresses the incidence of diagonal tension cracks in the units as presented in Fig. 4-9 right and Fig. 4-11. Quite high horizontal loading can be carried, however the ductility is usually lower as in case of bed joint sliding or rocking, since the upper wall triangle shears off and is no more supported. In case of cyclic loading the hysteresis includes usually a smaller area and therefore less energy is dissipated (see Fig. 4-11 right) as in case of bed joint sliding.

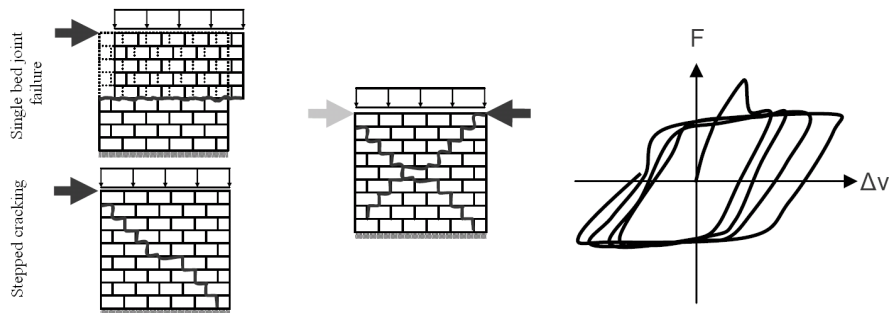


Fig. 4-10: Bed joint failure, Left: Static loading, Middle: Static cyclic loading, Right: Static cyclic load displacement diagram [Mistler 2006]

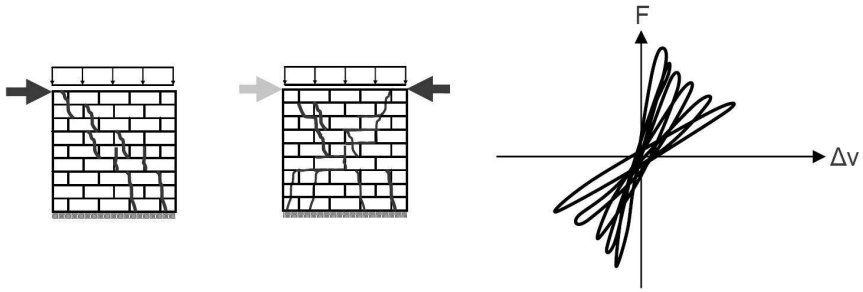


Fig. 4-11: Diagonal tension, Left: Static loading, Middle: Static cyclic loading, Right: Static cyclic load displacement diagram [Mistler 2006]

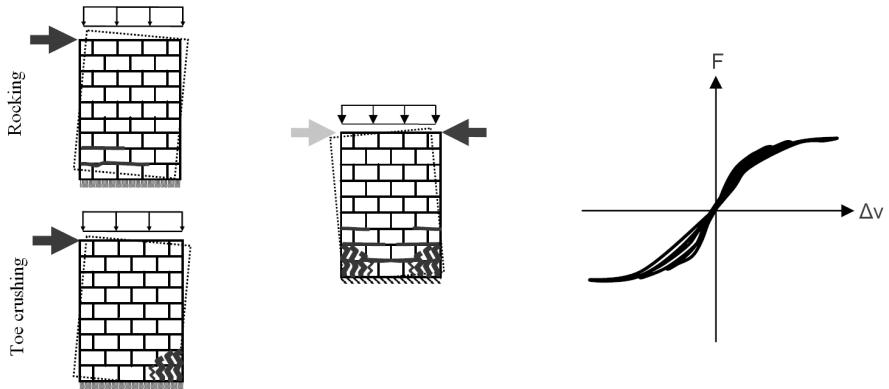


Fig. 4-12: Rocking and toe crushing, Left: Static loading, Middle: Static cyclic loading, Right: Static cyclic load displacement diagram [Mistler 2006]

The phenomena rocking can also lead to stability problems and is especially observed for slender walls. It describes the overturning of a panel (see Fig. 4-12), which goes in line with gaping joints due to tensile failure of the unit-mortar interface on the bottom and on the top, if the top is supported. The rotating wall itself is not significantly damaged. However, the area of non-cracked bed joint becomes smaller, which leads to higher stresses. In case of rocking the dissipated energy is very low. However the ductility can be very high if toe crushing is avoided. This last mechanism (toe crushing) is usually a result of rocking. Due to the decreasing bed joint area and the increasing stresses, the units fail on the high loaded corners. Toe crushing depends highly on the unit properties. The units of the corner of a turned masonry panel fail. Toe crushing is a very brittle failure mode [Ötes, Löring 2006], which is very dangerous and has to be avoided especially in case of seismic action. Given the brittle nature of this failure mode, very low energy is dissipated. A further limit state can be a successive failure (see Fig. 4-14 left) of such slender wall, which rotates.

Finally, it is to be mentioned, that this different failure modes can occur in combination and often cannot completely separated. For instance, failure of units and joints can be often observed in one wall as shown in Fig. 4-16. Only for some special cases one mechanism is observed. This highly depends on many parameters as explained below.

#### 4.1.4 Influencing parameters on failure mechanisms

##### 4.1.4.1 Vertical load level, slenderness and support conditions

The failure modes of horizontal in-plane loaded masonry walls elucidated above depend on a lot of parameters. The most important ones are:

- The vertical load level and
- The slenderness of the wall [Mistler 2006].

Of course:

- the support conditions as depicted in Fig. 4-8 and
- the material parameters of masonry

have also a significant impact. Subsequently, the relations are explained more in detail.

As well known the vertical load level influences the shear capacity significantly. Moreover, it has an essential impact on the failure type. For low vertical loading generally bed joint sliding occurs, whereas diagonal tension arises from low vertical load levels as compared in Fig. 4-9. For very high vertical loading nearly vertical cracking results, which goes in line with compression failure (see Fig. 4-3).

In this work slenderness is defined as the height/width ratio of a wall. The slender the wall, the easier rocking occurs, due to the bending loading. Compact walls tend to bed joint sliding or diagonal tension in dependency of the vertical load level. Thus, gaping joints appear on the top and, if the bottom is supported, as well there. The occurrence of gaping joints depends also on the vertical load level, as it is recognised on shear wall tests of the university Eindhoven (see Section 4.1.5.1) by Vermeltoort and Raijmakers [Vermeltoort, Raijmakers 1993]. For low vertical loading tensile failure of the first and the last bed joint is recognised, however for higher vertical stresses this phenomenon could not be observed as presented in Fig. 4-16.

Whether gaping joints ensue or not depends moreover on the support condition. For SC 1, which impedes vertical movement and thus lower rotation effects, gaping joints are rarer than in case of SC 2 (see in Fig. 4-14). The support conditions influence the behaviour and failure mechanisms strongly, as recognised in experimental test like [Ötes, Löring 2006] as well as further literature and own simulations (see Section 6.2). Fig. 4-13 shows SC 1, where the top of the wall cannot rotate, which leads to a restrained system counteracting panel rotation. Thus, mainly shear loading and so bed joint sliding or diagonal tension results. Only small gaping joints can be observed. Furthermore, the tendency of the wall to rotate and the vertical support, which impedes a vertical movement, leads to additional vertical forces due to this constrain. Walls with SC 2 (the upper beam can rotate) are illustrated in Fig. 4-14. This leads to a non-restrained system. In-plane bending occurs mainly and causes primarily rocking with huge gaping joints.

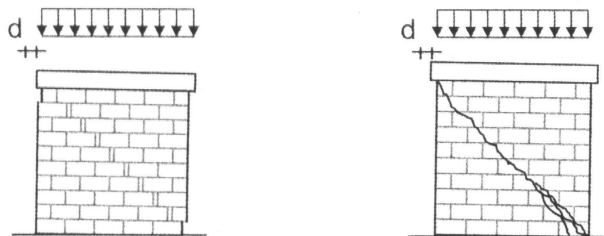


Fig. 4-13: Limit state of shear loading capacity for SC 1 (applied displacement  $d$ ), Left: Joint failure, Right: Unit failure [Ötes, Löring 2006]

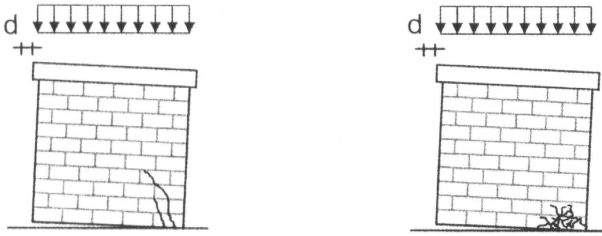


Fig. 4-14: Limit state of shear loading capacity for SC 2 (applied displacement  $d$ ), Left: Successive failure, Right: abrupt failure [Ötes, Löring 2006]

In dependency of the rotation level and the material also toe crushing can result. The author agrees with [Ötes, Löring 2006] regarding this distinction of the support condition. Concerning the resulting failure modes a deeper description is necessary. So, it depends also highly on the slenderness which failure mode occurs. For slender walls very often rocking is observed independently on the support condition. Moreover, rocking and diagonal cracking can take place in combination as pointed out in [Vermeltoort, Raijmakers 1993] and own simulations. The extremes can be summarised as follows. SC 1 and compact walls lead to shear behaviour (small rotation of the wall), which results in bed joint sliding or in case of high vertical loading diagonal tension. In case of SC 2 and slender walls bending behaviour dominates (high rotation level of the wall), which causes rocking and toe crushing.

#### 4.1.4.2 Material parameters of masonry

Regarding shear behaviour the main resulting failure modes bed joint sliding (see Fig. 4-13 left) and diagonal cracking of the units (see Fig. 4-13 right) are distinguished. In reality, numerous parameters influence the occurrence of these failure types. Stepped cracks as a result of bed joint sliding are located in the head and bed joints, which shows the dependency of this phenomenon on the unit sizes, on the width/height ratio of the units as well as on the bond pattern and the related overlapping. The following summarised material parameters have an impact on the cracking of the units.

- Aspect ratio of the units
- Size of the units
- Tensile strength of the units
- Overlapping
- Stiffness and thickness of the mortar joints
- Mortar filled or unfilled head joints
- Shear strength of the unit mortar interface

Concerning bending behaviour successive failure as outlined in Fig. 4-14 left and abrupt toe crushing (see Fig. 4-14 right) may be distinguished, as explained above. Due to the rotation of the wall rocking is observed and the corners are highly loaded. Tension and compression behaviour of masonry are important, and are influenced by the following factors.

- Type of unit (high impact)
- Tensile strength of the mortar joints (small impact)

## 4.1.5 Experimental tests of shear walls

### 4.1.5.1 Eindhoven

The static behaviour of masonry walls was investigated for instance at the university Eindhoven [Vermeltoort, Raijmakers 1993]. The shear walls, here named JD, had a height/width ratio of one with dimensions 990 mm × 1000 mm, built up with 18 courses, from which 16 courses were active. The first and the last course were fixed in steel beams as shown in Fig. 4-15. The masonry walls were made of 10 mm thick mortar joints and solid clay bricks with dimensions 210 mm in length, 52 mm in height and a thickness of 100 mm. For all specimens SC 1 (no rotation of top and bottom) was used. Different vertical compression uniformly distributed forces  $p$  were applied to the walls, before a horizontal load was increased under top displacement control  $d$ . Different initial vertical loads  $p$  were applied. For walls:

- J4D and J5D the load  $p$  equals 0.30 N/mm<sup>2</sup> (30 kN),
- J6D the load  $p$  equals 1.21 N/mm<sup>2</sup> (120 kN) and
- J7D the load  $p$  equals 2.12 N/mm<sup>2</sup> (210 kN).

The material data are obtained from samples collected for each wall and from existing results on compression, tension and shear tests as summarised also in [Lourenço 1996] and [Rots 1997]. The micro-properties for the different materials are obtained from Raijmakers and Vermeltoort [Vermeltoort and Raijmakers 1993].

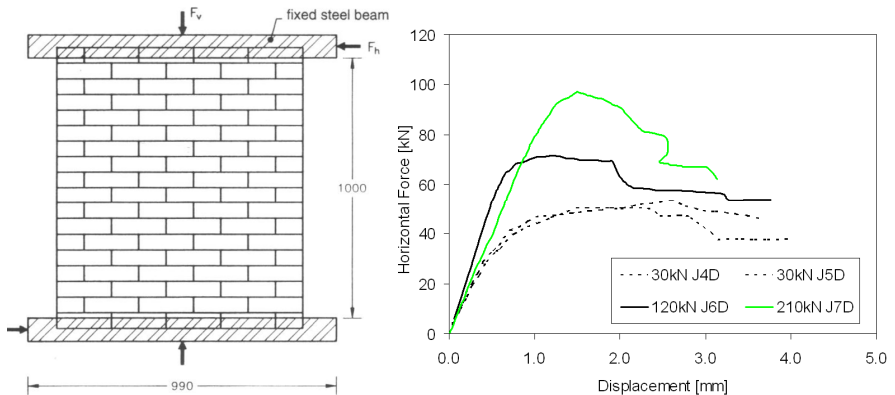


Fig. 4-15: Eindhoven shear walls, Left: Experimental setup [Rots 1997], Right: Load displacement curves [Lourenço 1996]

In Fig. 4-16 the experimental crack patterns for the different wall tests are given. A similar behaviour of the walls can be seen. In case of wall J4D and wall J5D with lower initial vertical load, horizontal tensile cracks develop at the bottom and top of the wall at an early loading stage. For all walls, a diagonal stepped crack leads to collapse, simultaneously with cracks in the bricks and crushing of the compressed toes.

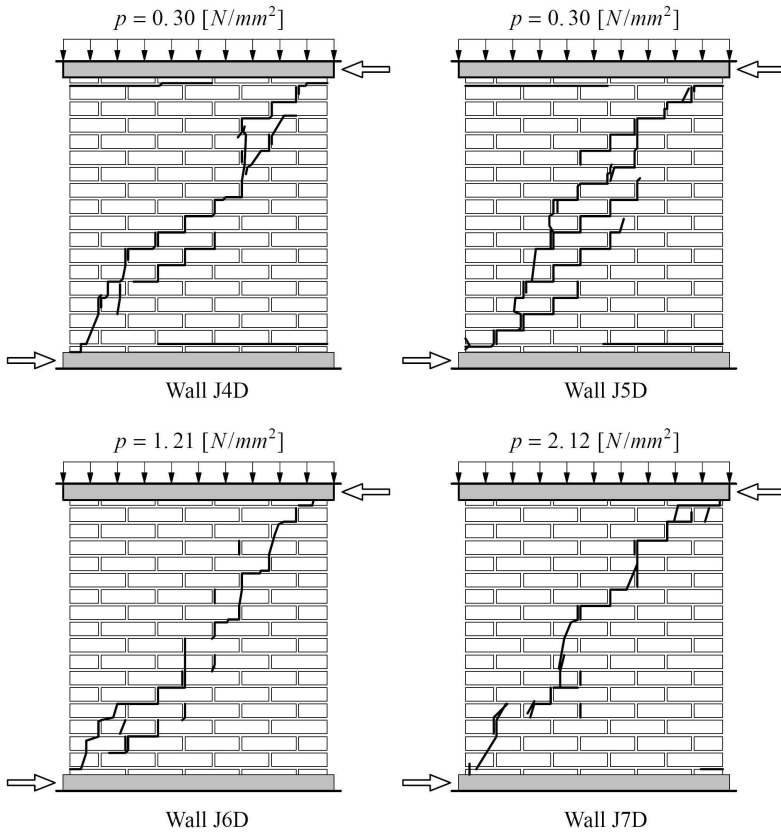


Fig. 4-16: Experimental crack patterns of the Eindhoven shear walls [Lourenço 1996]

## 4.2 Vertical prestressed masonry

### 4.2.1 Means to apply vertical prestressing in practice

Several manners to apply prestressing on existing and new masonry constructions are available. They may differ in their impacts on the mechanic behaviour of the masonry walls. Thus, it is roughly distinguished in external and internal prestressing. Important possibilities and sub-variations are categorised below.

- External prestressing
  - External forces
  - External tendons
- Internal prestressing
  - Internal tendons with full bond
  - Internal tendons with contact
  - Internal tendons without contact and bond

External forces are often applied in experimental tests, which can be done in a very easy and economic way. The vertical load level is simply increased. However, any tendons/strands are not used, as depicted in Fig. 4-16. For the practical application this variation is not meaningful. Instead external tendons may be quite easily applied in practice, especially for existing structures, as shown in Fig. 4-45. The tendons are placed exterior the wall, which may be outside, inside or both. If it is done only on one side, additional bending moments usually originate. Furthermore, the length of the strands is strongly influenced by the temperature of the presented climate. In case of a summer day a strand placed outside can be stretched significantly due to temperature and insolation, which may lead to a significant reduction of the prestressing forces. The opposite would happen in cold zones during the winter time. In addition the ductility of steel tendons can be significantly reduced in zones of extreme low temperature like Alaska. This phenomenon is well known for steel structures in such zones, where unexpectedly brittle failure may occur. Since high strength steel has to be used for tendons, which is characterised by brittle failure, this problem has to be in mind regarding an external prestressing in such areas.

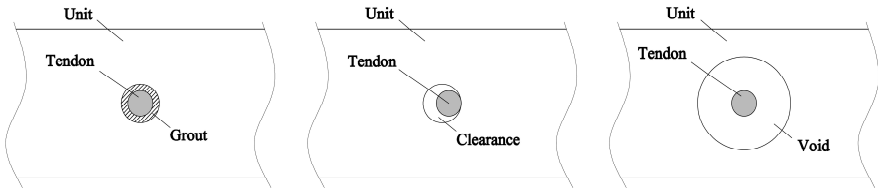


Fig. 4-17: Types of internal prestressing, Left: Internal tendon with full bond, Middle: Internal tendon with contact during the loading, Right: Internal tendon without contact and bond

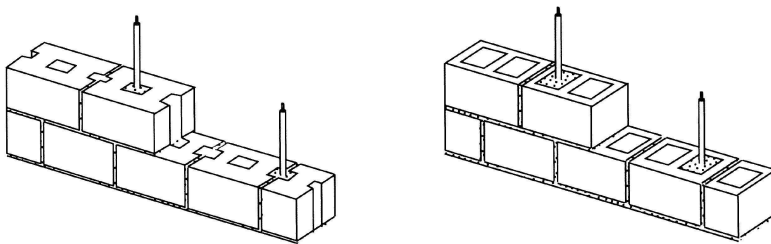


Fig. 4-18: Layout of vertical tendons in masonry walls, Left: In cores and head joints, Right: In cores only [Ganz 1990a]

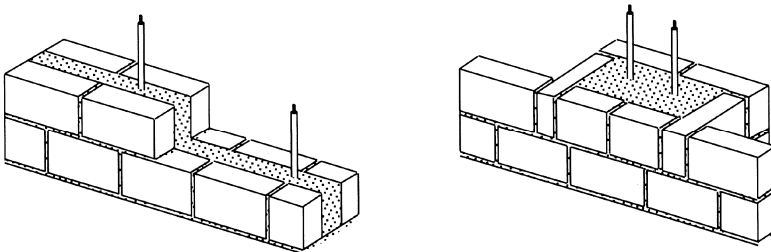


Fig. 4-19: Layout of vertical tendons in masonry walls, Left: In cavities, Right: In pockets [Ganz 1990a]

The term ‘internal prestressing’ means the availability of tendons inside the wall. The different possibilities can be roughly distinguished as presented in Fig. 4-17. Bond between tendons and masonry can be reached by means of pressure grouting. The gap is filled with cement grout, consequently force can be transferred. The most common method for prestressed masonry with internal tendons ensures only contact during the horizontal loading. This includes a small clearance between masonry and tendon, which is not filled with grout. After reaching an initial horizontal displacement, the tendon contacts the masonry and force can be transferred. If the distance between masonry and tendon is very high, also in case of huge horizontal displacement contact is excluded, here named ‘internal tendons without contact and bond’. Some possibilities for a practical execution of prestressing are outlined in Fig. 4-18 and Fig. 4-19. Instead of prestressing with tendons, either bars, wires, or strands may be used.

4.2.2 Function of prestressing

In masonry walls prestressing forces may be used to reduce or eliminate tensile stresses, to improve the shear capacity and the bending capacity. In the following the function of vertical prestressing on essential structural behaviour is described.

4.2.2.1 Shear behaviour

The dependency of shear capacity on the vertical load level is already mentioned in Section 4.1.1.4 and is illustrated in Fig. 4-6. An increased shear capacity of masonry walls results from enhanced normal forces, due to its Coulomb-friction nature. This phenomenon is utilised in case of vertical prestressing. Investigations of the shear behaviour of prestressed masonry walls led to an interaction law [Ganz 1990b] as presented in Fig. 4-20 by means of a diagram with normalised shear capacity  $s_u$  and normalised normal forces  $n_u$  as functions of lateral forces  $S$ , normal forces  $N$ , length  $l_0$ , height  $h_0$ , thickness  $d$  and masonry compressive strength  $\beta_{D,mw}$ . The yellow marked area in Fig. 4-20 presents the benefit of shear capacity  $\Delta s$ , which follows from vertical prestressing forces  $P$ . Moreover, the threshold of prestressing forces becomes easily visible. A further increase of prestress does not lead anymore to an enhancement of shear capacity. Instead, failure caused by high axial loading occurs, which is elucidated in Section 4.1.1.2. A reasonable threshold of the overall normal forces depends on the problem, like damages to minimise, creeping and shrinkage of the material.

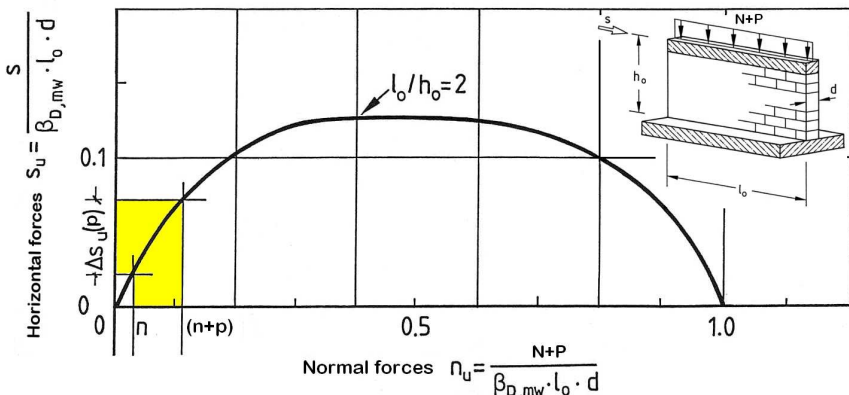


Fig. 4-20: Interaction of shear capacity and normal forces for masonry walls [Ganz 1990b]



due to the interaction of normal forces and ultimate moment  $M_u$ , as depicted in Fig. 4-22 by means of an interaction diagram with normalised bending capacity  $m_u$  and normalised vertical forces  $n_u$  as functions of normal forces  $N$ , prestressing force  $P$ , length  $l_0$ , height  $h_0$ , thickness  $d$  and masonry compressive strength  $\beta_{d,mw}$ .

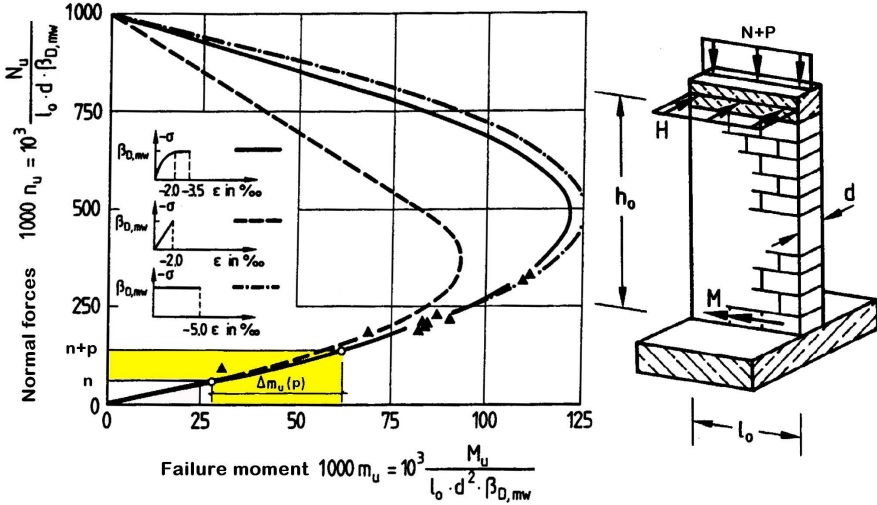


Fig. 4-22: Interaction of out-of-plane bending and normal loading for masonry walls [Gunkler 1993]

The curves are theoretically calculated. However, the experimental results of [Gunkler 1993] are labelled with small triangles and show a good agreement with the theoretical results. The increased normalised out-of-plane bending capacity  $\Delta m_u$  of masonry walls due to enhanced normal forces is marked in yellow. Similar to the interaction of normalised shear capacity and normalised axial forces, also here the ultimate moment is limited. For the bending-normal loading interaction a balance point is very clearly visible.

4.2.2.3 Stability

Stability problems refer in this context to horizontal deformation leading to out-of-plane buckling of the wall. The stability highly depends on the vertical load level and the means of practical execution of prestressing regarding the three types ‘internal tendons with full bond’, ‘internal tendons with contact during the loading’ and ‘internal tendons without contact and bond’, which are outlined in Fig. 4-17, as well as external prestressing. In case of ‘internal tendons with full bond’, ‘internal tendons with contact during the loading’, small horizontal deformations cause vertical restoring forces, which counteract a horizontal deformation. Thus, the stability is not endangered despite the higher vertical loading. However, for ‘internal tendons without contact and bond’ and external prestressing such restoring force cannot occur, due to the missed contact. On the other hand the vertical forces are higher due to the prestressing, which leads to a negative impact on the stability. Therefore buckling is more probable. To avoid out-of-plane buckling ‘internal tendons with full bond’ or at least ‘internal tendons with contact during the loading’ are recommended by the author.

#### 4.2.2.4 Cracking

To guarantee the serviceability of structure a limitation of crack width or a completely avoidance of cracks is necessary, which depends on the purpose of the construction. Reasons can be prevention of water entering or a utilisation as fair-faced masonry. Vertical or diagonal cracks can be repaired by using horizontal prestressing tendons. Gaping bed joints caused by eccentric loading can be closed again by installing vertical prestressing tendons.

The mitigation of horizontal cracks due to imposed wall end rotations can be reached by means of prestressing as given in Fig. 4-23. A combination of wall thickness reduction (over the full height or only by using a soft strip below the slab) with an increase of axial load by introducing prestressing will yield optimum benefits both for crack width and for strength of the wall [Ganz 1990a], as presented in Fig. 4-23, where the non-dimensional crack width (ratio of crack width  $w$  to wall thickness  $d$ ) and the wall end rotation angle are used. For a constant wall end rotation angle the increase of normal forces leads to a lower non-dimensional crack width. Also, Gunkler confirms in [Gunkler 1999] the enhanced safety against such cracking due to prestressing.

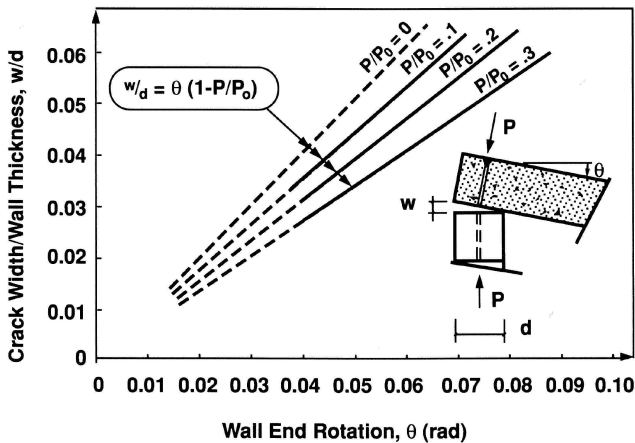


Fig. 4-23: Mitigation of bending cracks by means of post-tensioning [Ganz 1990a]

Regarding out-of-plane bending load of masonry walls and resulting cracks in masonry walls, Zimmerli declares in [Zimmerli 1999] that increased normal forces cause an optimal distribution of curvature across the whole wall and therefore reduce the incidence of cracks. This phenomenon is besides observed in experimental tests [Falkner, Gunkler 1994]. Moreover, it is pointed out in [Budelmann, Gunkler, Wigger 2003], that prestressing leads to a bigger compression zone and thus, the depth of bending cracks is reduced, which also decreases the probability of reinforcement corrosion.

#### 4.2.3 Comparison of historical and modern masonry regarding a reasonable application of vertical prestressing

Concerning a reasonable use of strong influential strengthening measures like vertical prestressing the distinction in historical and modern masonry is fundamental, as elucidated below. The terms 'historical' and 'existing' should not be confused. In this work historical masonry refers to be older than at least hundred years, which is in addition characterised by a historical value such as old churches, cathedrals, palaces, town centres and bridges. Natural stones and ancient bricks

are usually used in numerous types of shape, assemblages and various combinations. The strengths as well other material properties of mortar and stones show a huge scattering, are not standardised and often unknown. In Europe such types of masonry structures usually consist of walls with several layers as depicted in Fig. 4-24.

Regarding preservation of historical structures, experts discourage an application of measures, which strongly influence the load carrying behaviour [Pieper 1983]. Regarding earthquake and impacts of strengthening on the dynamic behaviour special attention is necessary as damages and collapses of retrofitted constructions have shown in the last decades. Numerous strengthened historical masonry buildings in Italy showed significant damages after earthquakes.

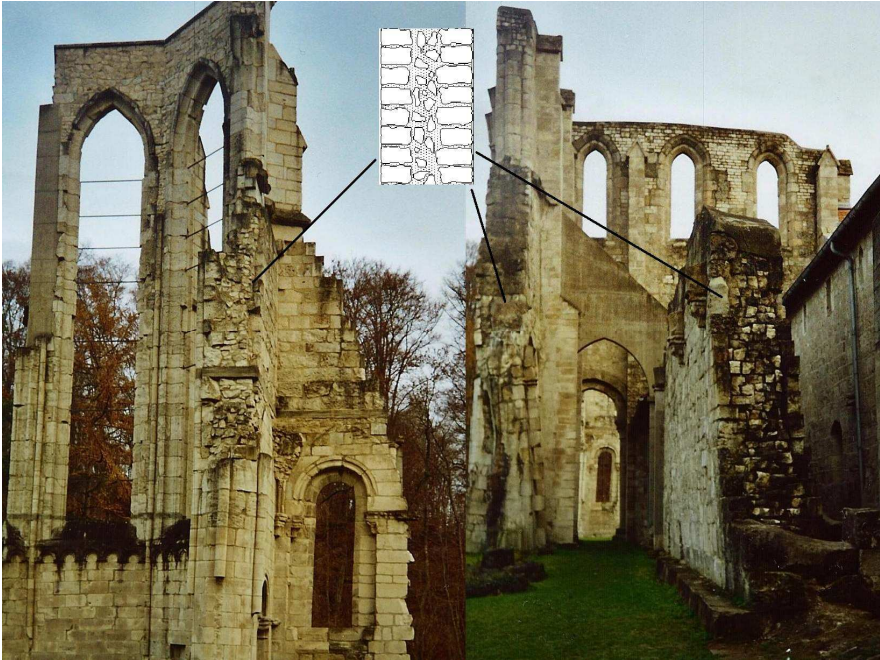


Fig. 4-24: Historical masonry with typical three layer cross section of historical masonry walls

In consequence of these mentioned reasons, the application of vertical prestressing is not recommended for historical constructions showing the drawbacks explained above. Especially for walls consisting of several vertical layers, enormous stability problems can occur. Depending on the structure and structural details, special investigation regarding a reasonable application of vertical prestressing is necessary. This cannot be done extensively in this study for the wide-spread range of possibilities. Moreover, there is still a significant lack of knowledge of the dynamic behaviour of prestressed masonry at all, which requires firstly investigations on simple masonry such as modern masonry, which are more reliable to describe. The term 'modern masonry' is used here for structures made of industrial and standardised masonry units. The material properties of mortar and units are known, the assemblages are regular and vertical layers with insufficient bond do not exist.

## 4.2.4 Experimental tests of prestressed shear walls

### 4.2.4.1 Dortmund

Static cyclic tests of slender shear walls were carried out at the university of Dortmund [Ötes, Löring, Elsch 2002]. Four equal walls strengthened with different methods were tested. Of interest is here the prestressed wall, named T 3. Every wall had a height/width ratio of approximately two with dimensions 2.50 m x 1.24 m, built up with 20 courses. The experimental set-up (see Fig. 4-25) was equal for all walls, which were built on a bottom plate anchored to the testing hall. On the top of the wall a head beam was located, as shown in Fig. 4-25, with support conditions allowing a rotation of the top (SC2). In the prestressed wall, two cavities were available also at the bottom plate for stick-trough of the tendons, located in a conduit (no adhesion with the mortar) and the brick laying starts whereas the void space of the channel section (U-section) was filled with mortar. At the head beam, the rods are put through holes and elongated by means of a tensioning jack. To hold the prestressing force, anchor nuts are fasten to the top of the tendons. For all walls the axial forces were applied with prestressed external steel threaded rods and kept approximately constant with an arrangement of soft disc springs. The horizontal loading was displacement-controlled applied on the head beam in 37 steps from 1 to 40 mm respective -1 to -44 mm, moving from positive to negative in each step.

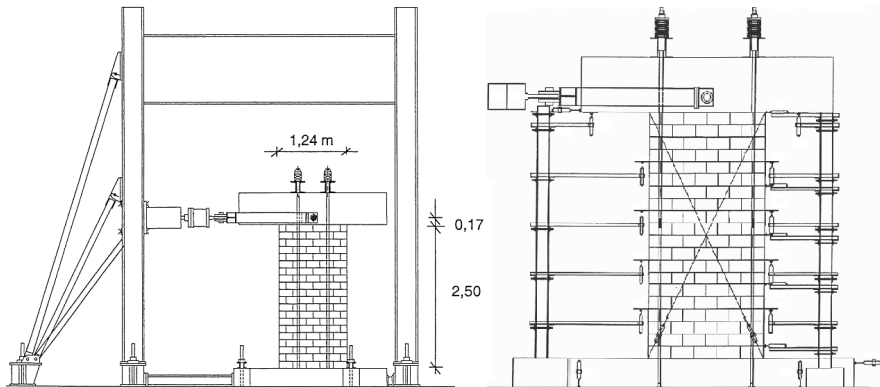


Fig. 4-25: Experimental set-up, Left: Complete set up, Right: Detail set-up [Ötes, Löring, Elsch 2002]

For the first 28 steps no damage was visible. Then, at step 29, first diagonal cracks can be seen in the lowest layer in both corners. In the next steps, 30 and 31, more cracks appeared in both corners, at the left side a small part of the corner split off. At step 32, rocking and stepped cracks occurred. In the next steps more and more damage was visible at the corner areas up to failure of the compression zone. In Fig. 4-26 the measured lateral force and the related horizontal displacement is presented. Up to a lateral force of approximately 50 kN the wall is under full compression. In conjunction with the occurrence of gaping joints, the wall stiffness is essentially determined by the spring properties of the tendons. The lateral force is growing up to 90 kN and then, with increasing crack width and damage of the corners, the resistance of the wall decreases.

An absolute maximum horizontal displacement of 43 mm and an absolute maximum horizontal force 91 kN could be reached. By increasing the normal force due to prestressing, shear failure was avoided. After reaching the proportionate bending design resistance as a result of prestressing, the resistance was increased due to additional elongation of the prestressing bars (caused by the rotation) up to the time in which the compression zone failed. In this condition, the elastic limit of the prestressing steel was not reached.

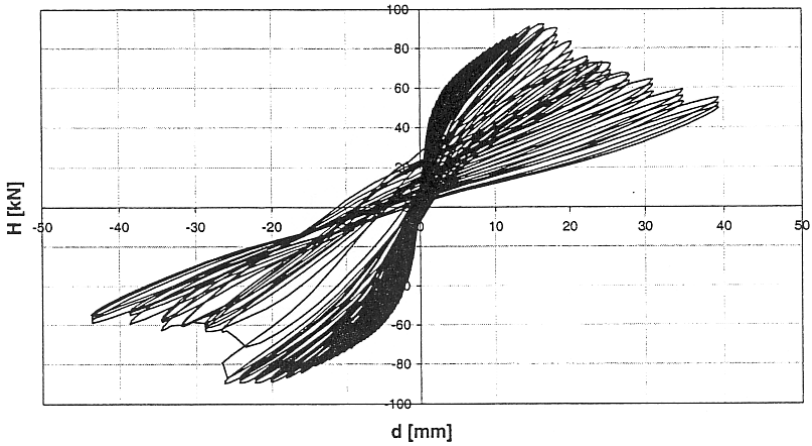


Fig. 4-26: Horizontal load displacement diagram of wall T 3 [Ötes, Löring, Elsch 2002]

4.2.4.2 iBMB tests of Braunschweig

The static cyclic experimental tests of prestressed shear walls were carried out at the iBMB in Braunschweig [Budelmann et al. 2004]. Four walls were tested, with dimensions and extra loads like walls used for stiffening of buildings with three floors. Only the ground floors were considered as they are most critical under seismic action. For all walls, two strands (tendons) have been used for vertical prestressing. The complete experimental set-up is depicted in Fig. 4-27 on the left for wall 1 (W 1). Furthermore, another position of the strands closer to the middle was investigated in wall 2 (W 2). The influence of slenderness was taken into account by means of two different length, therefore wall 3 (W 3) and wall 4 (W 4) were constructed with a slenderness of two (see Fig. 4-30). To ensure correct support conditions also a floor slab and their supporting walls on the ends were erected (see Fig. 4-27 and Fig. 4-30). These conditions were equal for all walls, except wall 4. There the floor slab was supported only on one end as outlined in Fig. 4-30 on the right. The geometrical properties of the walls, the strands positions as well as support conditions are listed in Tab. 4-1. The material properties were equal for all walls and are given in [Budelmann et al. 2004].

Wall	Properties of wall					Support
	Length	Height	Thick-ness	Distance of tendon to edge	Distance of tendons	
	[m]	[m]	[m]	[m]	[m]	
W1	2.5	2.50	0.175	0.25	2.00	On two sides
W2	2.5			0.625	1.25	
W3	1.25			0.25	0.75	
W4	1.25			0.25	0.75	On one side

Tab. 4-1: Geometrical properties of the walls [Budelmann et al. 2004]

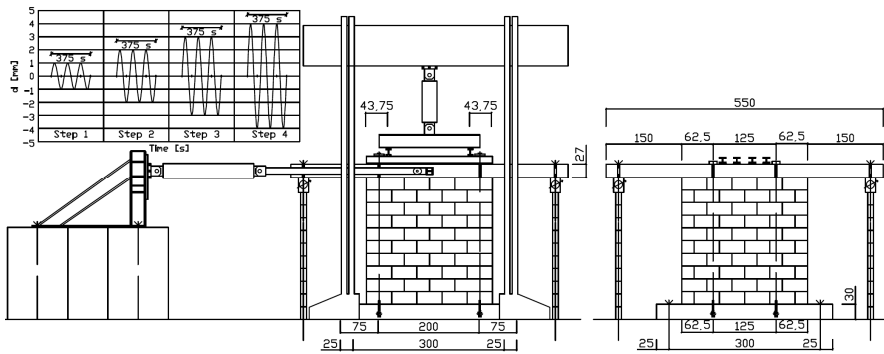


Fig. 4-27: Experimental set-up, Left: Complete set-up for wall 1 and cyclic load curves, Right: Wall 2 [Budelmann et al. 2004]



Fig. 4-28: Crack pattern, Left: Wall 1, Right: Wall 2 [Budelmann et al. 2004]

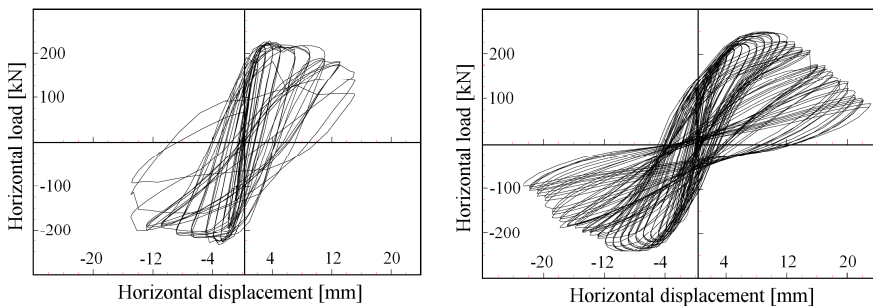


Fig. 4-29: Horizontal load displacement curves, Left: Wall 1, Right: Wall 2 [Budelmann et al. 2004]

The horizontal loading – in reality caused by upper storeys and traffic load - was applied by means of a jack (see Fig. 4-27 on the left) and kept constant. The prestressing forces were pro-

duced by strands. A horizontal displacement was applied on the centre of the concrete slab in a static cyclic way in different increasing step with three cycles per step and equal amplitude, as depicted in Fig. 4-27 on the left. The crack patterns are shown in Fig. 4-28 and Fig. 4-31. The diagonal crosses are very typical of earthquake damage. None of the four walls failed completely before the displacement limit of the test equipment was reached, despite the high unit damage which was observed in the final state. However, wall 2 and wall 3 collapsed partially as presented in Fig. 4-28 and Fig. 4-31 each on the left. A mixture of different failure types as bed joint sliding and diagonal tension occurred. In Fig. 4-29 and Fig. 4-32 the load displacement curves are displayed, which show the most desirable behaviour regarding seismic performance for wall 2. The shear capacity and the ductility are very high. The area enclosed by the hysteresis represents the energy dissipation, which is very good for wall 2 and also good for wall 3 taking into account that slender walls in general do not dissipate much energy.

Measured values like the displacement  $u$  and the horizontal load  $H$  are summarised in Tab. 4-2 for all walls. The index  $u$  means the ultimate point of loading, whereas  $cr$  indicates the occurrence of cracks. The sum of prestressing forces of two strands is denoted  $2xP_0$ . The dead load of the wall and upper storeys as well as traffic loads are expressed by  $G+F$ . In the last column, the forces in the prestressing elements after reaching the ultimate loading point  $(2xP_0)_u$  are given. A significant decrease was observed. Moreover, the different types of failure are listed. Unfortunately, no foundation was available to investigate equivalent non-prestressed walls within this research project.

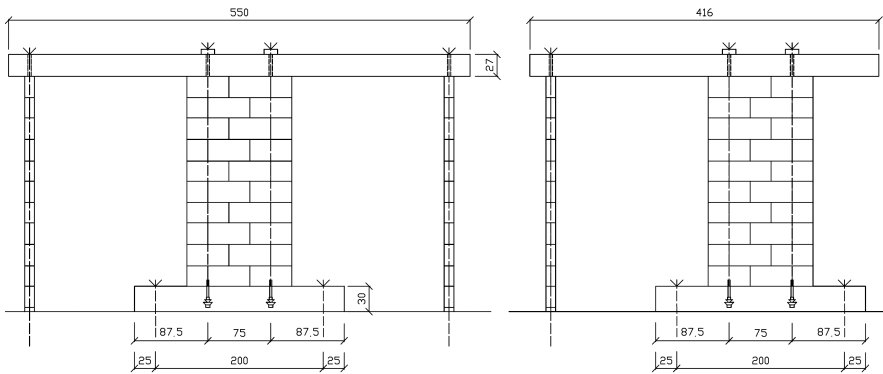


Fig. 4-30: Experimental set-up, Left: Wall 3, Right: Wall 4 [Budelmann et al. 2004]



Fig. 4-31: Crack pattern, Left: Wall 3, Right: Wall 4 [Budelmann et al. 2004]

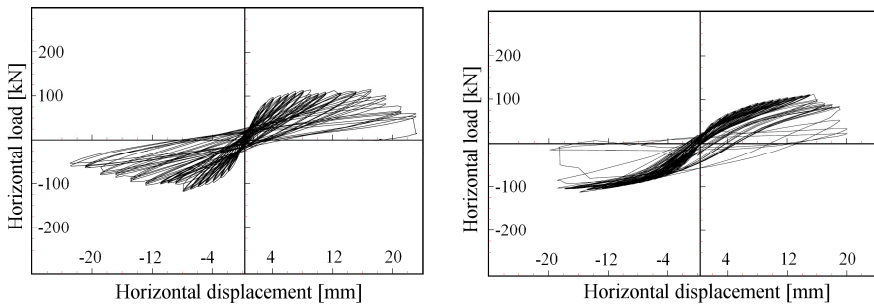


Fig. 4-32: Horizontal load displacement curves, Left: Wall 3, Right: Wall 4 [Budelmann et al. 2004]

Wall	Measurement categories								
	$2xP_0$	G+F	$H_{cr}$	$u_{cr}$	$H_u$	$u_u$	Type of failure	$(G+F)_u$	$(2xP_0)_u$
	[kN]	[kN]	[kN]	[mm]	[kN]	[mm]		[kN]	[kN]
W1	360	245	+217 -227	3	+109 -105	17	Max. displacement of the testing equipment	245	260
W2	356	245	+223 -220	6	+89 -94	23	Partial collapse of the wall	245	128
W3	352	110	+110 -114	7	+60 -60	23	Max. displacement of the testing equipment	110	260
W4	274	110	+101 100	11	+34 -16	20	Partial collapse of the wall	110	140

Tab. 4-2: Loading and results [Budelmann et al. 2004]

## 4.2.5 Wall-tendon interaction

Up to now, the high resistance and ductility of the prestressed walls of Braunschweig [Budelmann et al. 2004] were explained just due to the high vertical loads. In literature about experimental shear wall tests, several authors report about low ductility in case of high vertical loads as for instance [Page, Samarasinghe, Hendry 1980], [Mann, Müller 1982], [Oliveira 2003], [Jäger, Schöps 2006], [Schlegel 2004]. In consequence, the high vertical loading would usually lead to low ductility of in-plane loaded masonry shear walls. In contrast, this is not observed in case of the prestressed walls of Braunschweig as well as the prestressed wall of Dortmund [Ötes, Löring, Elsch 2002]. The author of this thesis developed a theory of wall-tendon interaction of internal prestressed shear walls, which explains this contradiction. Correspondingly, the tendons inside the wall are the correct reason for the good ductility values, not the high vertical load itself. For all these prestressed walls in [Budelmann et al. 2004] and [Ötes, Löring, Elsch 2002] the tendons were located inside the wall and the tendons could contact the masonry during the horizontal loading process as outlined in Fig. 4-17 middle. A skew slide down of the wall part outside the tendons indicates an effect of hooping (or a tie up effect). This means, the tendons also act as a kind of helical reinforcement. Thus, a loadbearing behaviour similar to cables occurs in addition to the prestressing.

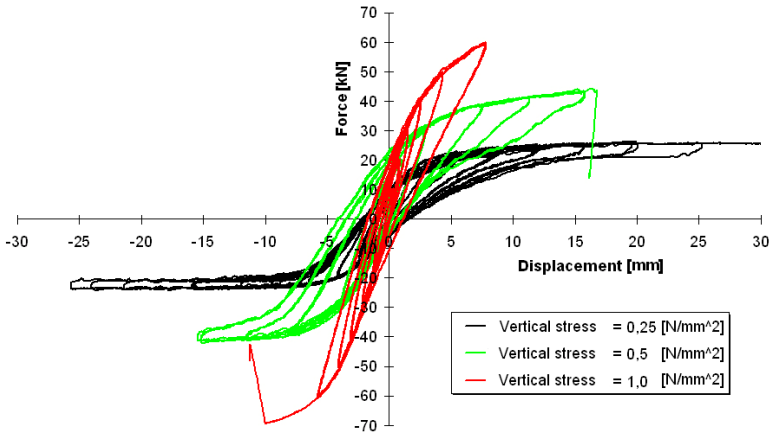


Fig. 4-33: Comparison of static cyclic tested shear wall for three different vertical load levels [Mistler et al. 2007]

This is confirmed by the experimental tests of the iBMB [Budelmann et al. 2004]. Especially in case of wall 3 and wall 4, a slide down of the wall parts outside the strands (see Fig. 4-28 and Fig. 4-31 each on the left) indicates the wall-tendon interaction. The partial collapse due to diagonal cracking takes place only beyond the tendons. Whereas, the inner part (also diagonal cracked) still remains in the wall and carries the loads. In particular for wall 4, it is very clearly visible in Fig. 4-31, how the sliding wall parts contact the prestressing bars and bend it in the final stage. As well experimental tests of Fehling and Stürz [Mistler et al. 2007] with different vertical load levels confirm the authors' theory of a wall-tendon interaction. Their results of shear walls without tendons are depicted in Fig. 4-33, which clearly show the lower ductility with increased vertical loading. The red curve belongs to a vertical load level of  $1.0 \text{ N/mm}^2$ , which is even lower for the prestressed walls of Braunschweig. There, vertical stresses of  $1.38 \text{ N/mm}^2$ , up to  $2.11 \text{ N/mm}^2$  result from the vertical loading. Despite this high vertical loading, a higher ductility was observed for the prestressed walls by means of tendons in the walls.

Probably, no ductile behaviour can be observed in experimental tests for external tendons, internal prestressing elements without contact and internal tendons close to the middle of the wall. For these cases a sliding down of wall parts non lateral supported by the tendons after diagonal cracking. To prove the wall-tendon-interaction theory, complementary experimental tests of reference walls with equal material properties and vertical loads would be necessary, however applied with external tendons. A comparison would probably show the lower ductility of external prestressed walls.

The described effect of wall-tendon interaction should be important for compact walls, which usually collapse due to diagonal tension, however less important for slender walls – in particular for SC 2 - which fail due to rocking and finally toe crushing. Toe crushing cannot be avoided by means of vertical prestressing with internal bonded tendons or strands.

#### 4.2.6 Examples of application

Vertical prestressing was employed in the 80's to strength masonry bracing walls against wind loading. In the last time this idea is followed up to improve the resistance against seismic action. Below some important examples are presented.

##### 4.2.6.1 Salvation Army Citadel

In the early 80's the main building of the citadel of the US military in Warrington, United Kingdom as presented in Fig. 4-34 was partly built of prestressed masonry walls. The main hall is 25 m long, up to 8.5 m high, and 15 m in width. Due to economic reasons hollow masonry walls have been prestressed by means of the Macalloy Bar System (see Fig. 4-36). Due to a surrounding strip-line light, the hall could not be braced spatially.



Fig. 4-34: Salvation Army Citadel, Left: Elevation, Right: Wall section [Ganz 2003]

The wall consists of an exterior and inner leaf, and is separated into several segments. Every segment is prestressed by two tendons with a diameter of 32 mm each and a prestressing force of 1035 MPa.

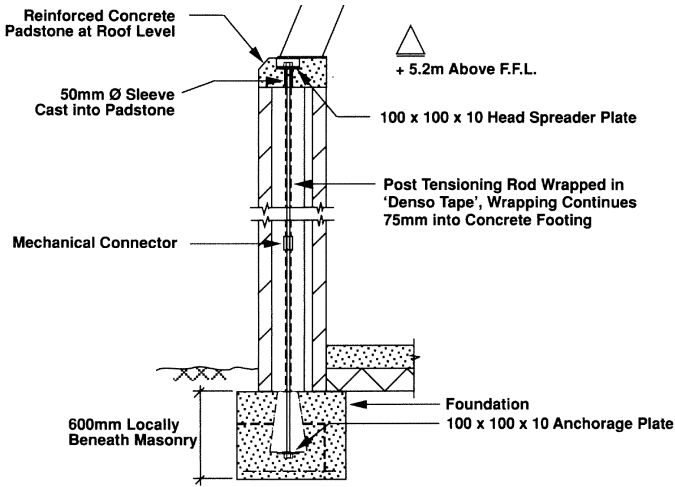


Fig. 4-35: Wall section Orsborn Memorial Hall [Ganz 1990a]

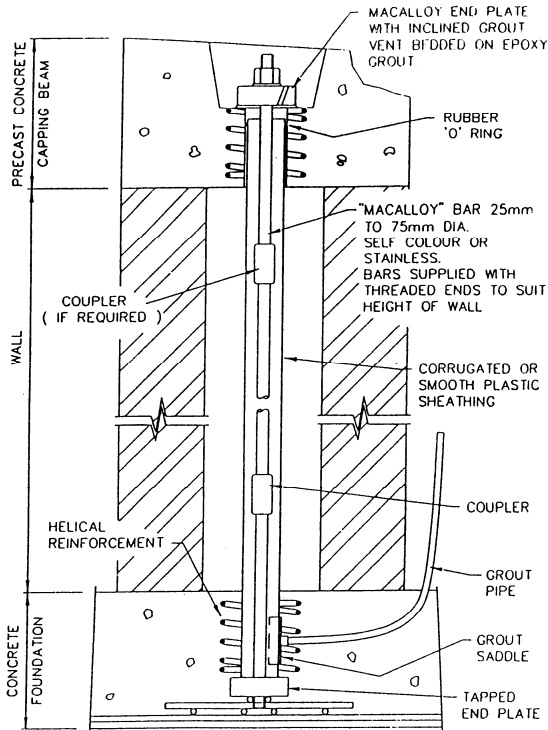


Fig. 4-36: Mechanical drawing of the Macalloy Bar System [Prestressing method Macalloy Bar System 1993]

## 4.2.6.2 Kindergarten Zurich

In the Kindergarten in Zurich, Switzerland, the VSL Post-Tensioned Masonry System was applied in for two brick cavity walls, where the inner leaves were post-tensioned (see Fig. 4-37) in order to provide the necessary resistance against out-of-plane lateral wind action. The internal leaves with large window openings are made of clay bricks and have a thickness of 140 mm. They achieve a height up to 4 m. The walls are supported horizontally on top by means of a steel frame in the roof. For each wall, Five monostrand tendons were used. The dead-end anchorages were located in a floor slab with thickness of 250 mm. The stressing anchorages were placed in precast concrete elements whose height had to be kept to an absolute minimum of 130 mm to avoid visibility in the interior of the room [Ganz 1990a]. To resist bursting forces, ordinary bed joint reinforcement was put under the elements. Every tendon was tensioned with 180 kN.

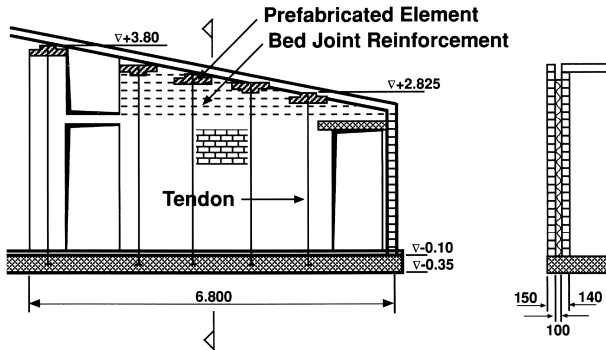


Fig. 4-37: Kindergarten Zurich, Left: Wall dimensions and tendon layout, Right: Wall section [Ganz 1990a]

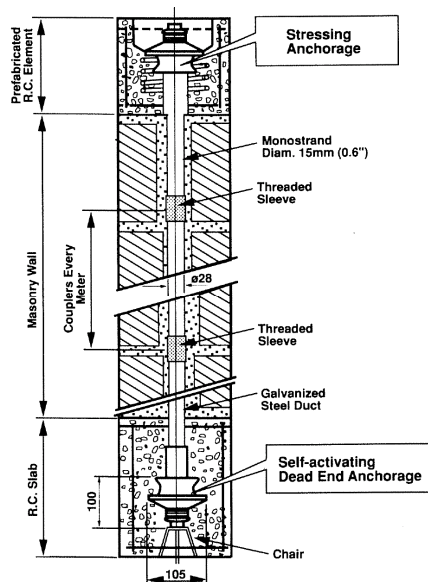


Fig. 4-38: VSL System for prestressed masonry [Ganz 1990a]

Due to the very small dimensions of the prefabricated concrete elements, preliminary tests were carried out to verify the safety for the application of the prestressing force into the masonry. Unbonded monostrands are used in case of the VSL System for masonry. This can be high tensile steel strands. To achieve maximum corrosion protection, they are greased and coated with extruded plastic. A third protection layer is provided by durable tube around the monostrand. In Fig. 4-38, a typical VSL masonry tendon is illustrated. It consists of a monostrand (15 mm diameter), a galvanized steel or plastic tube, a stressing anchorage placed in a concrete element, and a dead-end anchorage. The last is cast inside an in-situ concrete at the lower end of the tendon. The wall construction starts after casting and tube segments are threaded to the anchorage or duct segments that are previously placed. When the final wall height is reached, the final duct segment is cut to the required length and a prefabricated concrete element containing the stressing anchorage and a sleeve for the duct is placed on top of the wall [Ganz 1990a]. After the masonry reaches the demandable strength, the prestressing forces may be applied.

#### 4.2.6.3 Factory Regensdorf

In 1988, the Post-Tensioned Masonry System was employed in a second project in Switzerland. A 250 mm thick fire proof wall in a factory in Regensdorf (see Fig. 4-39 and Fig. 4-40) near Zurich, 36 m long and up to 8.8 m high, was prestressed with seventeen tendons. The wall consists of calcium silicate units and was designed to withstand a wind velocity of 21 m/s as a cantilever.

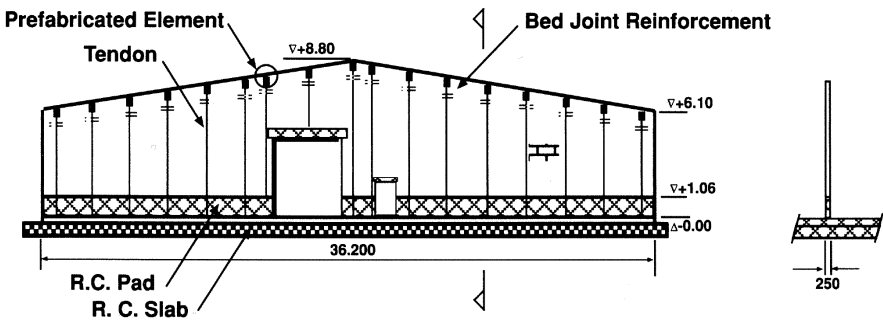


Fig. 4-39: Factory Regensdorf, Left: Wall dimensions and tendon layout, Right: Wall section [Ganz 1990a]



Fig. 4-40: Factory Regensdorf [Ganz 1990b]

Below the masonry, the dead-end anchorages were placed in a 1 m high in-situ cast concrete pad. It was connected to an existing floor slab by means of anchors. Prestressing anchorages are located in prefabricated concrete cubes that have a side length of 250 mm. Two layers of bed joint reinforcement were placed below each anchor. In contrast to the Kindergarten-project, here the dimensions of the precast elements were chosen such as to limit the bearing stresses under a maximum jacking force of 200 kN that means 75% of ultimate, to 40% of the uniaxial masonry strength. The last value was presumed to provide a sufficient factor of safety against local failure, also in case of early stressing after seven days.

#### 4.2.6.4 Hall 8 iBMB

The Institute of Building Materials, Concrete Construction and Fire Protection (iBMB) and the material testing institute (MPA) erected in 2004 the Hall 8 in Braunschweig, Germany (see Fig. 4-41). It consists of a basement, a hall and a three storeys office complex. The whole building has dimensions of 25.8 m in length, 24.5 m in width and 14.0 m in high.



Fig. 4-41: Hall 8 of iBMB, Braunschweig, Left: Finished hall [Budelmann et al. 2006], Right: Construction process

The bracing system against lateral wind and crane runway action consists of seven prestressed masonry walls, which are marked in red in Fig. 4-42. The prestressing system of SUSPA-DSI is applied which uses monostrands. Two different means of sand-lime brick masonry are used. For the walls of Pos. 1 to Pos. 6, they are built up by means of variation A with thin bed joints, whereas for Pos. 8 variation B with normal joints is used. All wall panels are prefabricated, thus an efficient, economic production and high quality is ensured. Thus, the construction process took place rapidly by means of a crane to install the wall panels, as shown in Fig. 4-41 on the right. For Pos. 1 to Pos. 3 two strands are located in each wall, whereas three are used for the Pos. 4 to Pos. 6, and four prestressing elements for Pos. 8. All have a diameter of 15.7 mm (0.62'') and are surrounded by plastic conduits. The small space between the masonry and the conduits is filled with grout. It is to differentiate between execution type A and type B regarding the strands, which are outlined in Fig. 4-43 on the right. In case of Pos. 8 type A is used to install the strands. A dead-end anchor is casted into concrete on the lower end, while the prestressing anchor is located on the top. For the Pos. 1 to Pos. 6 type B is applied. That means the prestressing anchor is in a wall recess on lower part of the wall (see Fig. 4-42). With an innovative measuring method the prestressing forces are permanent controlled. The strands are non-bonded, which allows a regulation of the tension, for instance in case of an observed decrease of prestressing forces. The wall (Pos. 8) is of interest for calculation in the following chapters.

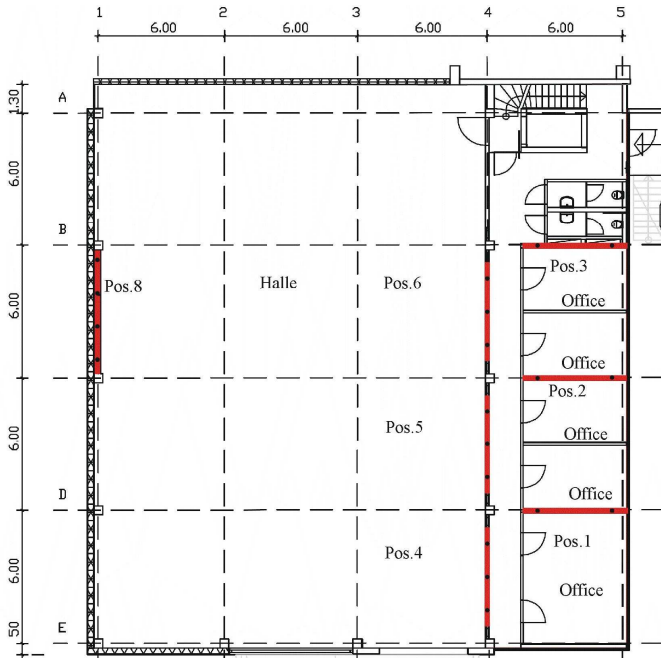


Fig. 4-42: Hall 8 of iBMB, Braunschweig - Top view [Budelmann et al. 2006]

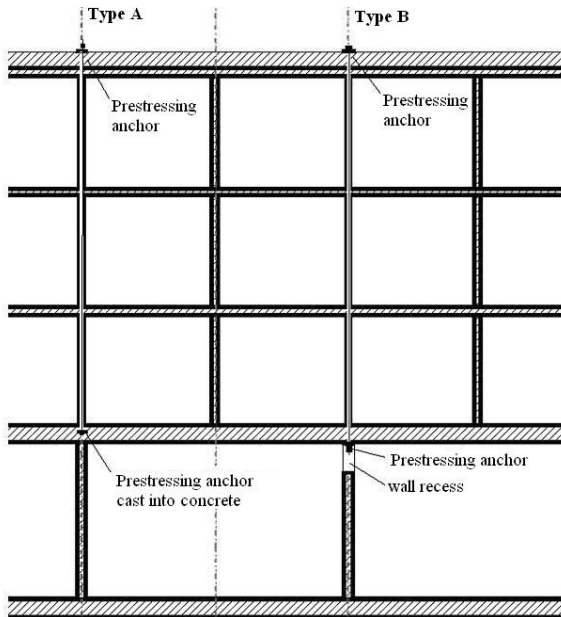


Fig. 4-43: Hall 8 of iBMB, Braunschweig - Wall section [Budelmann et al. 2006]

#### 4.2.6.5 EMPA-building in Dübendorf

In the framework of a check, regarding the earthquake resistance in the region of Zurich, essential buildings as schools and meeting-places had been investigated. The following data are quoted of [Bachmann 2007]. As a result rehabilitation measures are necessary to ensure the safety of some buildings of the Swiss Federal Laboratories for Materials Testing and Research (EMPA) in Dübendorf close to Zurich, Switzerland. They were erected in the 1950's. In detail, the administration and laboratory buildings, which are presented in Fig. 4-44, are strengthened in 2006 and 2007 by means of vertical prestressing. The administration building is three storeys high, 50 m long and 18 m in width. With dimensions of 120 m in length and 20 m in width, the four storey high laboratory building is much bigger.



Fig. 4-44: Administration building and laboratory building of the EMPA, Dübendorf, Switzerland [Bachmann 2007]



Fig. 4-45: External prestressing of the administration building of the EMPA [Bachmann 2007]

Both structures consist mainly of reinforced concrete frameworks and reinforced concrete bracing walls. However, the head facades are made of 38 cm thick masonry walls. In case of ground acceleration in transverse direction these masonry walls have to carry an essential part of the seismic loading. The seismic investigation identifies three of these four walls as weak points, which are mainly caused by numerous openings for doors and windows as well as the relative low vertical loading. It is expected, that the applied vertical prestressing improves the behaviour of the walls. Steel strands with a diameter of 32 mm are located outside the two walls of the laboratory building. A vertical load of 500 kN is produced. The weak wall on the north facade of the administration building is prestressed by means of external prestressing elements made of carbon-fibre-reinforced plastic (CFRP). The wall and the tendons are shown in Fig. 4-45. The eccentric position requires additional steel beams on the roof and a counterbalance of concrete.

#### 4.2.6.6 The bell tower in Trignano

For historical masonry merely the example of a prestressed bell tower is found, which is quoted in [Desroches, Smith 2002] and [Fugazza 2003]. The S. Giorgio Church, located in Trignano (S. Martino in Rio, Reggio Emilia, Italy) was struck by a 4.8 Richter magnitude earthquake on October 15, 1996, resulting in significant damage to the bell tower within the church. Following the earthquake, the tower was rehabilitated using shape memory alloys (SMAs). Four vertical prestressing steel tie bars with SMA devices were placed in the internal corners of the bell tower to increase the flexural resistance of the structure, as shown in Fig. 4-46. The SMA devices were made up of 60 wires, 1 mm in diameter and 300 mm in length. An important effect of SMA is the dissipation of energy. The bars were anchored at the top and bottom of the tower. Consequently, two rehabilitation measures are applied on this historical structure. On the one hand the SMAs to improve the dynamic behaviour, on the other hand the prestressing to increase the resistance of masonry.

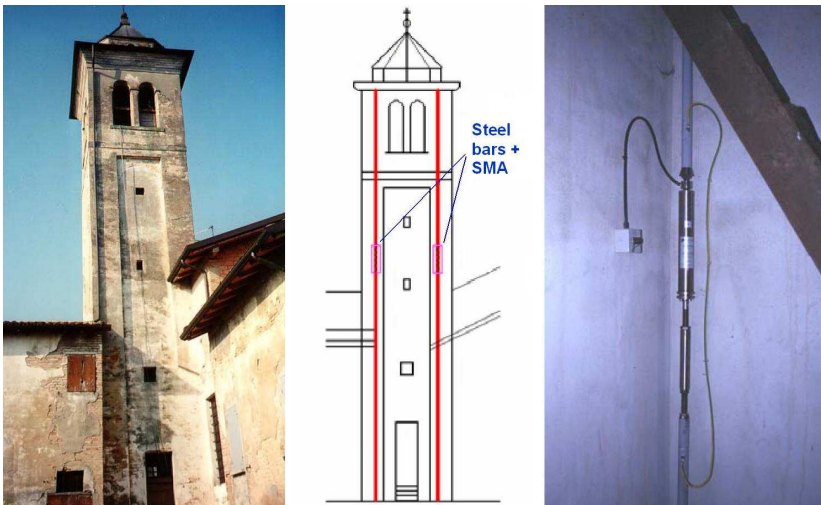


Fig. 4-46: Bell tower of the S. Giorgio church, Left: East wall [Indirli et al. 2001], Middle: Intervention scheme [Indirli et al. 2001], Right: SMADs after assembling [Castellano 2001]

The goal was a limitation of force applied to the masonry by post-tensioning the SMA devices, thus guaranteeing constant compression acting on the masonry walls and keeping the applied

force below 20 kN. The retrofit was tested by a minor  $M_L = 4.5$  Richter magnitude earthquake on June 18, 2000, with the same epicenter as the event in 1996. After the main shock, the tower was investigated and no evidence of damage was present.

### 4.3 Numerical modelling

To predict the structural behaviour and to assess the damage, numerical methods based on the finite element method (FEM) are used in this thesis. In following some basics, regarding the simulation of masonry, are briefly given. Essential basics of the FEM itself are given in fundamental literature as [Ahrens, Dinkler 1994], [Müller, Groth 2001] or [Link 2002]. First of all, an overview of modelling strategies for masonry is given. Thereafter, the used material models are described as well as the used damage parameters and their definitions. Finally, possibilities to model prestressing are discussed.

#### 4.3.1 Modelling strategies for masonry

The anisotropic and discontinuous nature of this material is caused by its composites (units and mortar), their assemblage, and the anisotropy of numerous unit types. Several methods to simulate masonry were developed. A famous categorisation of computational modelling frameworks for structural masonry is given below. In the literature several terms are used for the same method. Perhaps the most appropriate strategies come from the university of Delft [Rots 1997] and [Lourenço 1996] where three principal modelling strategies are identified as depicted in Fig. 4-47.

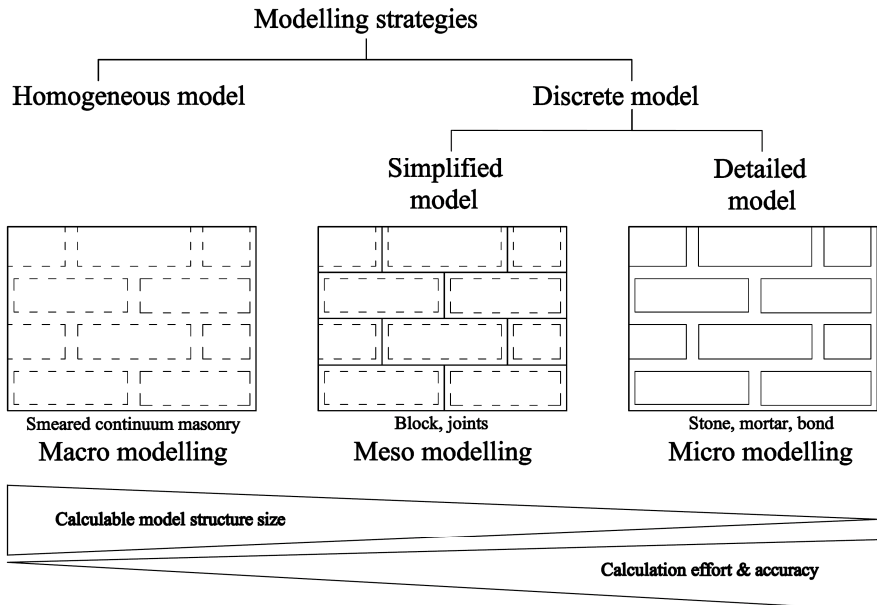


Fig. 4-47: Overview of modelling strategies for masonry structures

The modelling strategies are briefly listed subsequently:

- Macro-modelling – where all three principal features of structural masonry are represented by an equivalent continuum
- Meso-modelling – ‘geometrically expanded’ continuum units, with discontinuum elements covering the behaviour of mortar joints and interfaces
- Micro-modelling – units and mortar in the joints represented as continuum, whereas the unit/mortar interfaces are modelled by discontinuous elements

The first method, macro-modelling - also referred to as smeared, continuum or homogenised model - does not make a distinction between individual units and joints. Masonry is treated as a homogeneous anisotropic continuum. The second approach is an agreement between macro- and micro-modelling, which is named meso-modelling or simplified discrete model. Here, each joint, consisting of mortar and the two unit-mortar interfaces, is simulated as one ‘average’ interface that is located in the middle of the joint and describes the joint as well as the bond properties, while the units are expanded in order to keep the geometry of the structure unchanged. Masonry is thus considered as a set of elastic blocks bonded by potential fracture lines at the joints. Accuracy is lost since Poisson’s effect of the mortar is not included. The last strategy, micro-modelling, is not used in the framework of this thesis, since it goes in line with a high calculation effort. The Young’s modulus and Poisson’s ratio of mortar and stones are taken into account separately as well as, optionally, inelastic properties of both unit and mortar.

The interface represents a potential crack/slip plane with initial dummy stiffness to avoid interpenetration of the continuum. This enables the combined action of unit, mortar and interface to be studied under a magnifying glass. Fields of application are for instance the detailed investigation of mortar joints as done in [Twelmeier, Sperbeck, Budelmann 2008], special impacts of mortar on unit damage, or to give a better understanding about the local behaviour of masonry structures. This type of modelling applies notably to structural details, but also to modern building systems like those of concrete or calcium-silicate blocks, where window and door openings often result in piers that are only a few block units in length. These piers are likely to determine the behaviour of the entire wall and individual modelling of the blocks and joints is then to be preferred [Lourenço 1996]. One modelling strategy cannot be preferred over the others, since different application fields exist for macro, meso and micro models. Macro models are applicable when the structure is composed of solid walls with sufficiently large dimensions so that the stresses across or along a macro-length will be essentially uniform [Lourenço 1996]. Due to the reduced time and memory needs as well as a simple mesh generation, homogenous models are more practice oriented. It allows the calculation of big structures and the application of time consuming analysis as transient and probabilistic simulations. Meso-modelling is most valuable when a compromise between accuracy and efficiency is needed.

#### 4.3.2 Basics of plastic theory

An assessment of seismic loaded masonry structures in the ultimate limit state requires a description of its non-linear material behaviour. Therefore, elastoplastic material models are used in this study, which base on the theory of plasticity. Those are well established and sound numerical algorithms have been implemented. The basics of this theory and the numerical implementation are elaborately illuminated in [Owen, Hinton 1980], [Chen 1982], [Chen, Han 1988] or [Hofstetter, Mang 1995]. Subsequently, some important information are briefly summarised. To describe metals the plastic theory was developed, however it can also be used for quasi-brittle materials as concrete or masonry, if they are loaded in triaxial compression and shear-compression problems where inelastic irreversible strains are observed, [Pijaudier-Cabot, Borderie, Fichant 1994].

As formulated in Eq. (4-2), the assumption of an elastoplastic constitutive model demands essentially, that the overall strain  $\varepsilon$  can be separated in an elastic part  $\varepsilon^{el}$  and an inelastic or also referred to as plastic part  $\varepsilon^{pl}$ .

$$\varepsilon = \varepsilon^{el} + \varepsilon^{pl} \quad \text{Eq. (4-2)}$$

Based on Hook's law, the elastic strain rate  $d\varepsilon^{el}$  is related to the stress rate  $d\sigma$  by the elastic stiffness matrix  $K$  in the elastic range, as given Eq. (4-3).

$$d\sigma = K \cdot d\varepsilon^{el} \quad \text{Eq. (4-3)}$$

Yield functions that limit the elastic domain are an essential notion in the plastic theory. If the stresses  $\sigma$  satisfy the general yield criterion, yielding can only occur. It depends on the stress  $\sigma$  and scalar  $\kappa$  (see Eq. 4-4), which is introduced as a measure for the amount of hardening or softening.

$$F(\sigma, \kappa) = 0 \quad \text{Eq. (4-4)}$$

In general, however, it is extremely complex to describe the material behaviour with a single yield surface and one must resort to the theory of multi-surface plasticity by a number of functions  $F_i$  which define a composite yield surface [Lourenço 1996]. That multi-surface yield criterion can be continuous or discontinuous. In case of a continuous transition as depicted in Fig. 4-48 on the left, the plastic strain rates are equal in the intersection and it is true

$$d\varepsilon^{pl} = d\varepsilon_1^{pl} = d\varepsilon_2^{pl} \quad \text{Eq. (4-5)}$$

In case of a discontinuous transition (see Fig. 4-48 on the right), the plastic strain rates are unequal in the intersection and it is true

$$d\varepsilon^{pl} \neq d\varepsilon_1^{pl} \neq d\varepsilon_2^{pl} \quad \text{Eq. (4-6)}$$

For the numerical treatment of such intersections a number of literatures exist.

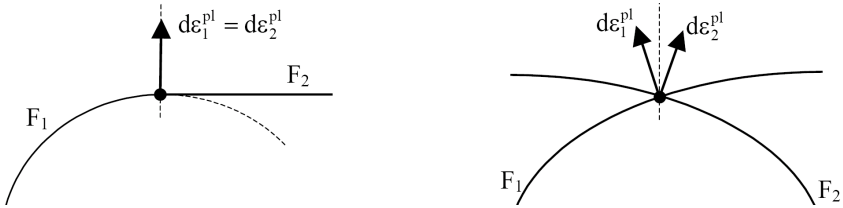


Fig. 4-48: Transition of two yield criteria, Left: Continuous, Right: Cutting edge [Schlegel 2004]

The plastic strain rates  $d\varepsilon^{pl}$  are calculated by means of the yield criteria. In case of an associated flow rule, which is reasonable for steel - the plastic potential  $G$  is equal to the yield surface  $F_i$  and the plastic strain rate is perpendicular to the yield surface.

$$G(\sigma, \kappa) = F(\sigma, \kappa) \quad \text{Eq. (4-7)}$$

However, it describes a dilatation, which can be incorrect for materials like concrete and masonry, since a dilatation is not confirmed by experimental test [Schlegel 2004]. Regarding this phenomenological reason, the use of a non-associated flow rule can be reasonable for a better adjustment. In this case, the plastic potential  $G$  is unequal the yield surface  $F$ , and the plastic strain rate is not perpendicular to the yield surface.

$$G(\sigma, \kappa) \neq F(\sigma, \kappa) \quad \text{Eq. (4-8)}$$

For single surface plasticity, the assumption of a non-associated flow rule leads to

$$d\epsilon^{pl} = d\lambda \frac{\partial G}{\partial \sigma} \quad \text{Eq. (4-9)}$$

Here,  $d\lambda$  is the plastic multiplier rate. If the yield criterion changes due to the load history, hardening or softening occur and the yield surface respectively the plastic potential is modified. This can be taken into account on the one hand by means of work hardening. The parameter  $d\kappa$  should be a work measure and simply reads

$$d\kappa = W^{pl} = \sigma^T \dot{\epsilon}^{pl} \quad \text{Eq. (4-10)}$$

On the other hand, strain hardening (or softening) can be used. The scalar  $d\kappa$  is adequate to the equivalent plastic strain rate  $d\epsilon_{eps}$ , which must always be positive and increasing.

### 4.3.3 Material models

In this section all material model, which are used in this thesis to simulated masonry, are described. The most important one to solve the given problems of this work is the model of Lagomarsino and Gambarotta [Gambarotta, Lagomarsino 1997b] (see Section 4.3.3.2). Nevertheless, more rare used material models are explained as well. A reasonable application of these different models regarding distinctive tasks is discussed in Section 4.3.3.4.

#### 4.3.3.1 Interface material model of Delft

A material model of the Delft University of Technology to describe the behaviour of the interface which can be used for micro- and meso-modelling (see Section 4.3.1) is precisely explained in [Lourenço 1996] and [Rots 1997] as well as briefly in [Lourenço, Rots 1997]. Lourenço developed a constitutive model for the monotonic behaviour of interface elements within the incremental theory of plasticity [Lourenço 1994]. This model was checked by means of experimental data. In reproducing experimental results, well accuracy was observed. Nevertheless, the model is not able to predict stiffness degradation and energy dissipation, as observed in experimental results that are loaded cyclically. Note, that pure elastic behaviour during unloading from the yield surface is assumed in case of classical plasticity. A convex composite yield criterion is used in this rate independent model. The criterion consists of three individual yield functions, where softening behaviour is included for all modes. The yield functions account for tension criterion, Coulomb friction criterion and compressive cap criterion as depicted in Fig. 4-49.

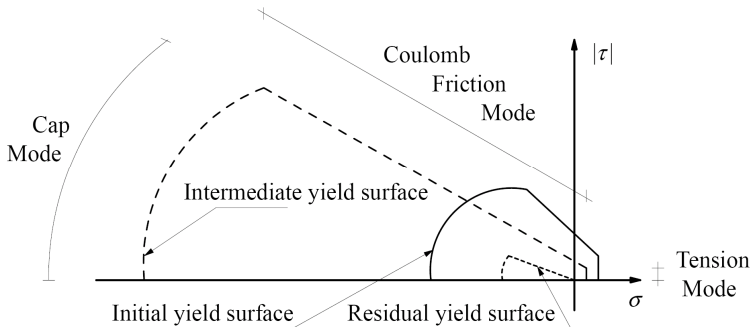


Fig. 4-49: Interface cap model for hardening and softening [Lourenço 1996]

Exponential softening laws are chosen according to available experimental data in order to model tensile and shear failure. While for the compression mode, a hardening/softening law is adopted. The uniaxial behaviour under tensile, compressive and shear loading is reproduced based on these isotropic hardening laws. For tensile and cap modes associated flow rules were adopted. Whereas, a non-associated plastic potential  $G_s$  was assumed for the shear mode with a cohesion  $c$  and dilatancy angle  $\Psi$  as expressed in Eq. (4-11).

$$G_s = |\tau| - \sigma \cdot \tan \Psi - c \quad \text{Eq. (4-11)}$$

Van der Pluijm [Van der Pluijm 1993] has recognised that dilatancy and friction angles are different, therefore a non-associated flow rule for shear is necessary. This material model is available in the finite element code DIANA<sup>®</sup> for interface elements.

#### 4.3.3.2 Material model of Lagomarsino and Gambarotta

In this work, in-plane loaded brick masonry shear walls are mainly simulated by means of a continuum damage model developed by [Gambarotta, Lagomarsino 1997b], which bases on a micromechanical approach and finite element method. It is able to describe tensile versus compressive response of mortar joint. The constitutive equations are obtained on the hypothesis of plane stress condition and considering a homogenisation procedure of two layered mediums: the mortar bed joint layer and the layer representative of the brick. In order to take into account decohesion and slippage in the mortar joint the former is modelled, while the latter considers the damage and failure of bricks. The contribution of mortar head joints is not considered in this model. Fig. 4-50 depicts the simplification described above schematically as well as the definition of coordinate system ( $x$  in direction of the bed joint and  $y$  perpendicular), which is necessary to know the orientation of the mortar bed joints throughout the structure. Input parameters of this material model and their notations are listed in Tab. 4-3.

Parameter	Sym.
Density	$\rho$
Young's modulus of masonry	$E$
Poisson's ratio	$\eta$
Friction coefficient	$\mu = \tan \phi$
Tensile strength mortar	$\sigma_{bm}$
Shear strength of the mortar joints	$\tau_{mr}$
Inelastic deformation parameter for mortar	$c_{mt}$
Softening coefficient mortar	$\beta_m$
Compressive strength of masonry	$\sigma_{br}$
Shear strength of bricks	$\tau_{br}$
Inelastic deformation parameter for brick	$c_{bn}$
Softening coefficient of the masonry	$\beta_b$
Young's modulus of concrete	$E_c$
Rayleigh mass damping	$\alpha$
Rayleigh stiffness damping	$\beta$

Tab. 4-3: Material parameters and related abbreviations of the constitutive model of Lagomarsino and Gambarotta

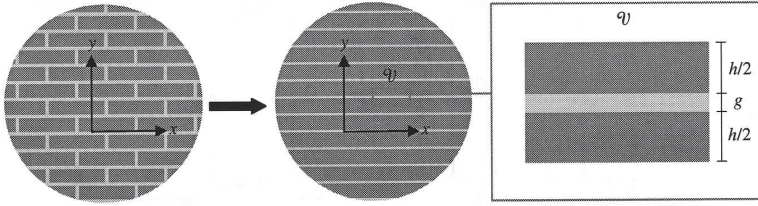


Fig. 4-50: Schematisation and volume of the masonry wall [Calderini 2004]

This model considers inelastic strains in the mortar bed joints  $\varepsilon_m^{pl}$  and in the units  $\varepsilon_b^{pl}$ , while mechanisms of inelastic deformation involving the head joints together with bed joints are neglected. The overall minor strain or also referred to as average strain, is calculated as given in Eq. (4-12) by the elastic compliance matrix  $K_M$ .

$$\varepsilon = K_M \sigma + \varepsilon_m^{pl} + \varepsilon_b^{pl} \quad \text{Eq. (4-12)}$$

The minor strain, as well as the related minor stress, are composed of normal components in the direction normal to the mortar bed joints, tangential components and shear components as noted in Eq. (4-13) and Eq. (4-14). The inelastic strain of mortar and bricks used in Eq. (4-12) may be further divided into extension  $\varepsilon$  and sliding  $\gamma$ , which is shown in Eq. (4-15) and Eq. (4-16).

$$\varepsilon = \{\varepsilon_x, \varepsilon_y, \gamma\}^t \quad \text{Eq. (4-13)}$$

$$\sigma = \{\sigma_x, \sigma_y, \gamma\}^t \quad \text{Eq. (4-14)}$$

$$\varepsilon_m^{pl} = \{0, \varepsilon_m, \gamma_m\}^t \quad \text{Eq. (4-15)}$$

$$\varepsilon_b^{pl} = \{0, \varepsilon_b, \gamma_b\}^t \quad \text{Eq. (4-16)}$$

The last are determined by Eq. (4-17) and Eq. (4-18). The extensional and tangential inelastic compliance parameters  $c_{mn}$  and  $c_{mt}$  characterise the bed mortar joint.

$$\varepsilon_m = c_{mn} \alpha_m H(\sigma_y) \sigma_y \quad \text{Eq. (4-17)}$$

$$\gamma_m = c_{mt} \alpha_m (\tau - f_i) \quad \text{Eq. (4-18)}$$

The Heaviside function  $H$  takes into account the unilateral response of the joint. The friction at the interface  $f_i$  vanishes, if tensile stresses occur, and limits the sliding in case of compressive stresses. Later on, the mortar damage variable  $\alpha_m$  is discussed. Similar it is done for the inelasticity of the brick damage (see Eq. (4-19) and Eq. (4-20)).

$$\varepsilon_b = c_{bn} \alpha_b H(-\sigma_y) \sigma_y \quad \text{Eq. (4-19)}$$

$$\gamma_b = c_{bt} \alpha_b \tau \quad \text{Eq. (4-20)}$$

Where  $\alpha_b$  is the brick damage variable,  $c_{bn}$  and  $c_{bt}$  represent the compressive and tangential compliance parameters of the bricks. The Heaviside function  $H$  in Eq. (4-19) accounts only for the vertical compressive strain in bricks. In fact, the inelastic vertical extension in the masonry is localised in the bed-mortar joint due to their low strength in comparison with the tensile strength of the bricks. The effect of sliding of the brick is negligible compared to the mortar bed contribution, thus if  $\varepsilon_m$ ,  $\varepsilon_b$  and  $\gamma_m$  are known, the strains in the element may be determined. The failure limit states and the related formulae are outlined in Fig. 4-51. The failure type taken into account and the yield surfaces are similar to the already explained material model of Lourenço and Rots

[Lourenço, Rots 1997]. Here, the homogenised material is characterised by three yield surfaces that consider the tensile failure, slippage in the joints including the friction law (where  $\mu$  is the friction coefficient), and the brick failure.

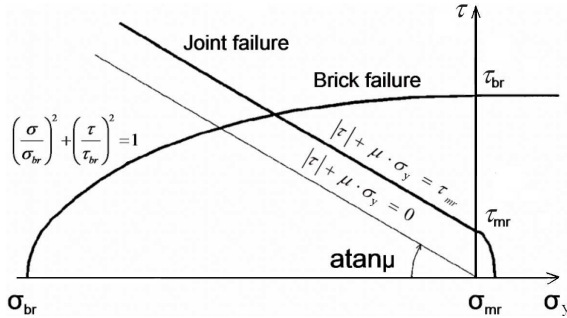


Fig. 4-51: Mortar joint and brick failure domains [Gamborotta, Lagomarsino 1997b]

The tangential compliance parameter for masonry  $c_{bt}$  cannot be entered by a selected value. Instead it is calculated automatically - to reduce the number of input parameters - by the relationship of shear strength  $\tau_{br}$  and the compressive strength  $\sigma_{br}$  of masonry to the inelastic compliance as given in Eq. (4-21).

$$\frac{c_{bn}}{c_{bt}} = \frac{\tau_{br}^2}{\sigma_{br}^2} \quad \text{Eq. (4-21)}$$

If tensile stress acts on the mortar bed joints ( $\sigma_y \geq 0$ ), both damage mechanisms of brick and mortar become active. If bed mortar joints are subjected to compressive vertical and horizontal loads ( $\sigma_y < 0$ ), three different damage mechanisms may become active: the damage of the bricks, the sliding of the bed joint and the damage to the bed joints. The model is able to describe strength and stiffness degrading (see Fig. 4-52) and so hysteretic response to cyclic shearing strains due to activated frictional mechanisms and damage parameters. Especially, in Fig. 4-52 on the left, the difference of unloading curve and elastic stiffness is clearly shown. Subsequently, the determination of damage is elucidated.

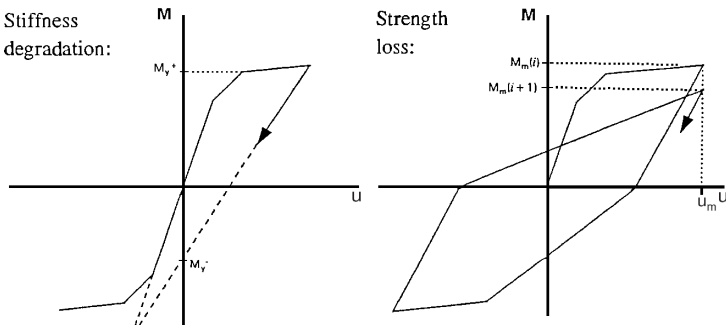


Fig. 4-52: Left: Stiffness degradation, Right: Strength loss [Urban 2007]

As already mentioned, the inelastic contributions are described by these internal variables which evolve through the damage process and are also iteratively fitted in each load step. Moreover, the internal damage parameters determine strength and stiffness degradation of the mortar bed joints

and the bricks. The evolution of damage is described in terms of two damage variables denoting the brick damage  $\alpha_b$  and the damage in the mortar joints  $\alpha_m$ . In this constitutive model only the contribution of the bed joints is included. The damage evolution is defined, in accordance to the toughness function or also named R-curve approach, which is used in the theory of fracture mechanics by imposing the damage energy release rate  $Y_m$  to be less than or equal to the toughness  $R$ . It is assumed that the toughness function  $R(\alpha)$  depends on  $\alpha$ , which is outlined in Fig. 4-53 for the mortar. These damage variables express the loss of toughness at each node of the element. Loss of toughness might be described as the decrease in energy needed to cause further cracking, expressed as the percentage of the energy needed in the undamaged state. The dissipated energy and the damage energy release rate  $Y_m$  have to be determined within the load step and the damage variables have to be calculated iteratively.

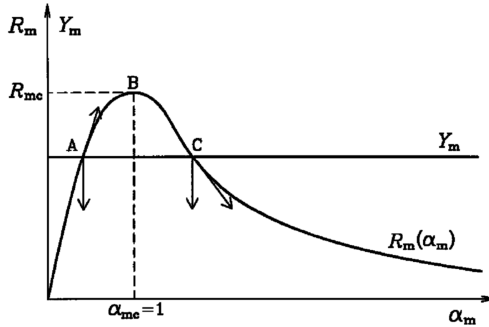


Fig. 4-53: Damage function for the mortar joint; stable and unstable evolution [Gambarotta, Lagomarsino 1997a]

The structure may react very brittle or almost plastic, if cracking takes place. The softening parameter  $\beta$  characterises whether the material reacts brittle. The parameter  $\beta$  would be equal to one in that case. In the contrast, a  $\beta$  of 0 goes in line with ideal plasticity. To account for the post-peak behaviour the resistance towards cracking may be described by Eq. (4-22), which would result in Fig. 4-54 for different values of  $\beta$  [Urban 2007].

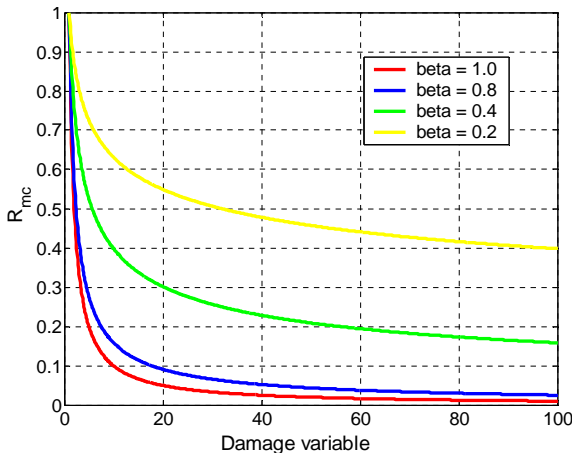


Fig. 4-54: Loss of toughness with increasing damage [Urban 2007]

In the Eq. (4-22)  $R_c$  is the maximum of the toughness function  $R(\alpha)$  and  $\alpha$  is the damage parameter of this material model.

$$R(\alpha) = \begin{cases} R_c \cdot \alpha & 0 < \alpha < 1 \\ R_c \cdot \alpha^{-\beta} & \alpha > 1 \end{cases} \quad \text{Eq. (4-22)}$$

Static and transient analyses either by static, static cyclic or seismic actions are feasible by this constitutive model. The interested reader is referred to [Gambarotta, Lagomarsino 1997b] to gain more detailed information.

#### 4.3.3.3 Material model of Schlegel

At the University of Weimar an advanced and accurate material model for masonry is developed by [Schlegel 2004]. This homogenised approach bases on the plastic theory. Schlegel [Schlegel 2004] implemented it into a finite element code and extended the constitutive model of Ganz [Ganz 1985], to 18 types of failure  $F_i$ . Thus, the model of Schlegel [Schlegel 2004] takes into account also the tensile failure parallel to the bed joint. All failure modes considered in this model are outlined in Fig. 4-55 by means of the crack patterns as well as the related yield criterion notations. To account for anisotropic hardening and softening, each yield criterion is formulated in dependency of the related hardening or softening parameter. The originally failure condition for the plan stress is extend to spatial stress. For in-plane loaded masonry structures, the criterions  $F_1$  to  $F_{10}$  are sufficient, while for three dimensional masonry structures the criterions are extended to  $F_{18}$  in analogy to the criterions  $F_1$  to  $F_{10}$ . Schlegel assumes a masonry, in which the failure mechanisms in both directions perpendicular to the head joint and perpendicular to the longitudinal joint are similar. It can be the model with the same failure criterions, to predict the three dimensional behaviour. An elaborate depiction of the yield surfaces can be found in Fig. 4-56.

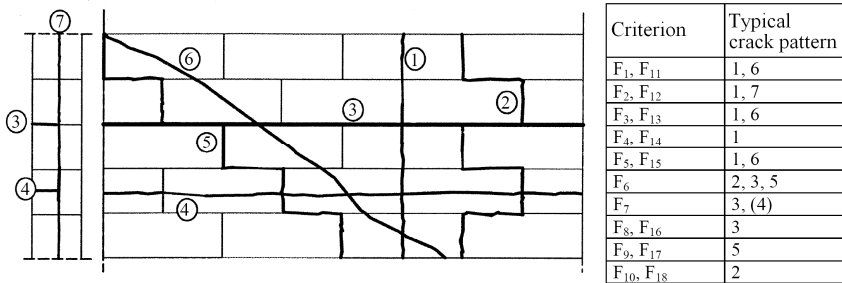


Fig. 4-55: Types of cracks and related flow rules [Schlegel 2004]

Schlegel's material model takes also into account the different types of bond by input parameters  $a_S$  and  $a_L$  for the stone size as well as  $o_y$  ( $o_z$ ) for the overlapping. It is very important to note, that the coordinate system used in [Schlegel 2004] (see Fig. 4-56) is differently defined than in the model of Lagomarsino [Gambarotta, Lagomarsino 1997b] which is explained above and defined in Fig. 4-50. This difference occurs forcedly throughout the thesis in pictures and notations of description as well as in the results between the two material models. The failure domains are briefly described in the following. A detailed explanation is given in [Schlegel 2004]. The yield conditions  $F_1$  to  $F_{10}$  for two dimensional behaviour in the ( $x$ - $y$ -plane) can be simply expressed for the three dimensional behaviour due to an exchange of indexes  $z$  instead of  $y$  and  $zx$  instead

of  $xy$ . Thus, it is not necessary to write the equations here again with two different index notation.

The tensile failure of stones is considered by means of criterion  $F_1$  ( $F_{11}$ ), which Ganz has introduced to limited the principal stresses.

$$F_1 = (1 - \omega_{my})^2 \tau_{xy}^2 + [\omega_{my}(\sigma_x + f_{mx}\Omega_{fm}) - \sigma_y][\sigma_x + \Omega_{fm}(f_{mx} - f_{my}) - \omega_{my}(\sigma_y + f_{my}\Omega_{fm})] \quad \text{Eq. (4-23)}$$

The relation between resisting lateral tensile stresses  $\sigma_y$  and simultaneous occurring of high vertical compression stresses  $\sigma_x$  is expressed (see Eq. (4-23)). The notations are defined in Fig. 4-56. The hardening/softening function  $\Omega$  describes the evolution of hardening/softening of the related strength. The abbreviation  $\omega_{my}$  is given below.

$$\omega_{my} = \frac{f_{fy}\Omega_{fy}}{f_{my}\Omega_{fm}} \quad \text{Eq. (4-24)}$$

Geometrically this criterion  $F_1$  ( $F_{11}$ ) can be modelled as a cone sector. Whereas,  $F_2$  ( $F_{12}$ ) is an elliptical cone, which expresses the compression failure of masonry. To avoid numerical problems Schlegel chamfers the peak of this cone by a second function, which leads to two definition domains  $A$  and  $B$ . For domain  $A$  the yield surfaces is expressed by Eq. (4-25).

$$F_{2A} = \tau_{xy}^2 - (\sigma_x + f_{mx}\Omega_{fm})(\sigma_y + f_{my}\Omega_{fm}) \quad \text{Eq. (4-25)}$$

The shear failure of the units is taken into account by criterion  $F_3$  ( $F_{13}$ ), which is geometrical a cylinder with circular ground with a diameter of the compressive strength in  $y$ -direction  $f_{my}$ , and formulated in Eq. (4-26).

$$F_3 = \tau_{xy}^2 + \sigma_y(\sigma_y + f_{my}\Omega_{fm}) \quad \text{Eq. (4-26)}$$

Analogical to  $F_3$ , the lateral tensile stresses are limited by cylindrical criterion  $F_4$  ( $F_{14}$ ) to model the tensile failure parallel to the bed joint (see Eq. (4-27)).

$$F_4 = \tau_{xy}^2 + \sigma_y(\sigma_y + f_{fy}\Omega_{fy}) \quad \text{Eq. (4-27)}$$

The transition area between  $F_1$ ,  $F_3$  and  $F_4$  is expressed by a tangent plane  $F_5$ , to limit the shear stress in the range of low horizontal stresses  $\sigma_y$ .  $F_5$  is defined in Eq. (4-28).

$$F_5 = |\tau_{xy}| + \sigma_y \frac{1 - \omega_{my}}{2\sqrt{\omega_{my}}} - \frac{1}{2}\sqrt{\omega_{my}} f_{my}\Omega_{fm} \quad \text{Eq. (4-28)}$$

Shear failure of the bed joints is described by  $F_6$ , as usually done with the Mohr-Coulomb law like shown in Eq. (4-29).

$$F_6 = \sqrt{\tau_{xy}^2 + \tau_{xz}^2} + \sigma_x \tan \mu(\kappa_s) - c\Omega_c \quad \text{Eq. (4-29)}$$

Where  $\mu$  is the friction coefficient,  $\kappa_s$  is a scalar hardening variable, and  $\Omega_c$  is the hardening/softening function of the shear strength  $c$ . The tensile stress of the bed joint is limited by failure domain  $F_7$  as follows.

$$F_7 = \sigma_x - f_{ix}\Omega_{fix}, \quad f_{ix}\Omega_{fix} \leq \frac{c\Omega_c}{\tan \mu(\kappa_s)} \quad \text{Eq. (4-30)}$$

The tensile failure of the bed joints in case of high horizontal compression is considered in  $F_8$  ( $F_{16}$ ). The uniaxial horizontal compressive strength, parallel to the bed joint is reduced to the value  $-\zeta f_{my}$ , which accounts for the effect of significant lower horizontal compressive strength than  $f_{my}$  due to early buckling of the bed joint observed in experimental test.

$$F_8 = \sigma_x - f_{tct} \left( \frac{\sigma_y}{\zeta f_{my}} + 1 \right) \quad \text{Eq. (4-31)}$$

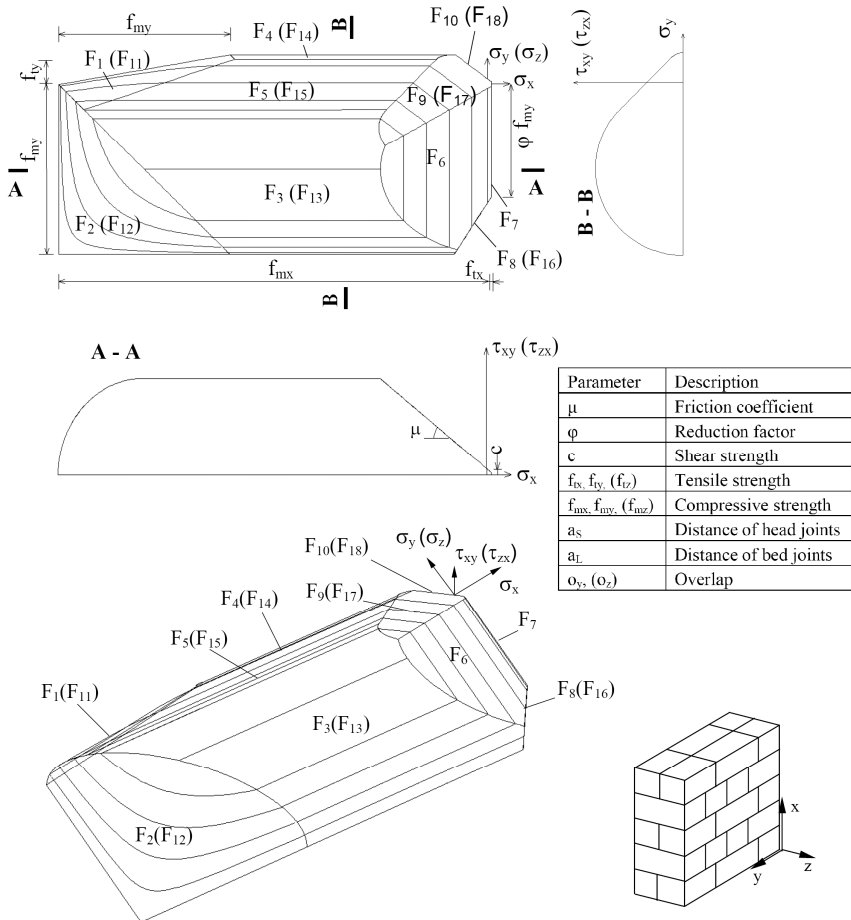


Fig. 4-56: Extended yield surface of Ganz for masonry and parameter description [Schlegel 2004]

Stepped cracking of head and bed joints is described by the yield surface  $F_9$  ( $F_{17}$ ), which is caused due to sliding in the bed joints and goes in line with cracking of the head joints. As explained in 4.1.4.2, this failure mechanism depends on the unit size, the height/width ratio of the unit and on the bond. The yield criterion corresponds to the shear stress criterion determined by

Mann and Müller [Mann, Müller 1978]. The plastic strains are calculated by use of a non-associated flow rule.

$$F_9 = \left| \tau_{xy} \left( 1 + \frac{2a_L}{a_S} \tan \mu(\kappa_S) \right) + \sigma_y \frac{2a_L}{a_S} - (c\Omega_c - \sigma_x \tan \mu(\kappa_S)) \right| \quad \text{Eq. (4-32)}$$

The constitutive law of Ganz is extended with the yield criterion  $F_{10}$  ( $F_{18}$ ) (see Eq. (4-33)) to model tensile failure of masonry parallel to the bed joint.

$$F_{10} = \sigma_y - (c\Omega_c - \sigma_x \tan \mu(\kappa_S)) \frac{a_y}{a_L} \quad \text{Eq. (4-33)}$$

This joint failure results from horizontal tensile stresses. Due to this extension it becomes possible, to consider the significant impact of unit size and the height/width ratio on the crack pattern and failure mechanism. Unfortunately, this accurate and established material model does not include degradation of stiffness and strength and is therefore not really suitable to simulate cyclic behaviour of masonry.

#### 4.3.3.4 Discussion of the models for a reasonable application

The firstly explained micro or meso model of Lourenço and Rots [Lourenço, Rots 1997] is very time consuming and requires much calculation capacity. Moreover, it is not able to consider cyclic loaded masonry, since it does not account for degradation effects, which is also true for Schlegel's model [Schlegel 2004]. In contrast, the model of Lagomarsino and Gambarotta [Gambarotta, Lagomarsino 1997b] takes such effects into account and calculates damages, even separately for mortar and units. It is relative stable, very well established and timesaving. While this thesis deals with earthquakes and risk - to be determinable, the last needs information about damages (see Chap. 2 and Appendix A) - the model of Lagomarsino and Gambarotta [Gambarotta, Lagomarsino 1997b] is most reasonable and thus mainly applied here. The transient analyses are very time consuming. In consequence, a fast material model is necessary. Furthermore, the probabilistic simulations - which are necessary to estimate damage probabilities - increase the calculation effort enormously.

However, the meso or micro model of Lourenço and Rots [Lourenço, Rots 1997] firstly explained and the macro model of Schlegel [Schlegel 2004] are very accurate, due to their considerations of stone sizes, bond and overlapping etc. Thus, they are reasonable and hence used in this work for a few detailed investigations.

#### 4.3.4 Damage parameters

In this section several parameters based on numerical investigations are explained and discussed to describe the physical damage reasonably regarding the topic of this thesis. The final goal is to judge on the usefulness of vertical prestressing in case of seismic action and to calculate risks. As elucidated in Chap. 2, the damage is a very important factor to determine it.

##### 4.3.4.1 Storey drift

In earthquake engineering the storey drift (SD) is commonly used, which is defined as the absolute maximum difference in displacement  $|u|_{max}$  between the basement and the roof for a single storey structure. In case of several storeys it is the difference between the upper and the lower floor slab of a storey. An extension is the interstorey drift (ID), where the difference in displace-

ment  $/u/_{max}$  is divided by the height  $h$  of the storey. A high dependency of storey drift and physical damage is presupposed, like in a manner of increasing storey drift, also an increased damage is expected. However, this assumption cannot be very reasonable, if different structures or strengthening measures are compared. For a good seismic performance, often ductile soft structures with a high ductility are more reasonable than stiff, brittle structures. In this work, some masonry properties in terms of different bonds with different stone size, width/height ratio and overlapping are taken into account, which can lead to a soft structure (high values for the storey drift) with small damage (see Section 7.2.2).

#### 4.3.4.2 Mortar damage

This parameter  $\alpha_m$  is available in the material model of Lagomarsino and Gambarotta [Gambarotta, Lagomarsino 1997b] and characterises the cracks in the mortar or between the stone and the mortar. An advantage of the damage parameters of this material model is that their value always increases, whereas stresses and plastic strains can be removed in case of opposite loading over time. Their maxima can occur somewhere in load history, which have to be in mind and the consideration of this point requires more effort in the evaluation. Regarding the bearing behaviour, the mortar damage is not very interesting, since it has no significant impact on the collapse of the structure. From the practical point of view, mortar damage can be repaired without huge effort. When the mortar is highly damaged the structure is often still safe. For a detailed explanation of this parameter the reader is referred to [Gambarotta, Lagomarsino 1997a] and [Gambarotta, Lagomarsino 1997b] as well as Section 4.3.3.2. In this work, the maximum value is named local damage, whereas the damage, accumulated over the structure per element and divided by the total number of masonry elements, is termed relative global damage.

#### 4.3.4.3 Unit damage

The material model of Lagomarsino and Gambarotta [Gambarotta, Lagomarsino 1997b] performs as well a parameter to express the brick damage  $\alpha_b$  (see Section 4.3.3.2), which describes the cracking of stones. From the practical point of view the unit damage is very important, because it has a significant impact on the failure of the structure and is unrepairable or only with huge effort and costs. The brick damage is a very important damage factor for masonry. When the stones are damaged, the structure is highly endangered (see Section 4.1.3). If the masonry properties are cleverly chosen, the drift can be high, but the unit damage is low (see Section 7.2.2). In analogy to the mortar damage, the maximum value is referred to as local damage throughout the thesis, whereas the sum of all unit damage values of each element divided by the number of nodes is named average global damage.

#### 4.3.4.4 Plastic strains

In general, the occurrence of plasticity goes strongly in line with damages (see Section 4.3.2). Homogenous material models for masonry use the plasticity to describe cracking. The plastic strains express the plastic activity quantitatively. In the evaluation of plastic strains, only the maxima are used in this study. A distinction in local and global strains is not done.

##### a) Vertical plastic strain

The vertical plastic tensile strain goes in line with the tensile failure of mortar joints. For shear walls, the vertical plastic strains in vertical direction are used to deduce on cracks in the mortar

joints, for instance gaping joints due to rocking. The vertical plastic compressive strains indicate unit damage, since units fail in general due to high compression loading for shear walls as illustrated in Section 4.1.1 and 4.1.3.

#### b) Plastic shear strain

By means of the plastic shear strain, shear failure can be expressed, e.g. sliding in the bed joints or other mechanisms in case of shear loading, which are explained in 4.1.1.4 and 4.1.1.3.

#### c) Equivalent plastic strain

As shown in Eq. (4-34), strain components of all directions are considered in the equivalent plastic strain  $\varepsilon_{eq}^{pl}$ . So, it indicates a mechanism independent damage, in contrast to vertical or shear strain. The equivalent plastic strain maybe used as softening parameter [Wang, Shrive 1993] as performed in Schlegel's material model [Schlegel 2004] for masonry (see Section 4.3.3.3). Hence, the equivalent plastic strain is suitable to describe the damage. For a better understanding it is reminded that the equivalent plastic strain is related to equivalent stress for instance regarding the Von Mises plastic distortion hypothesis. The equivalent plastic strain  $\varepsilon_{eq}^{pl}$  is defined as:

$$\varepsilon_{eq}^{pl} = \sqrt{\frac{2}{3} \left\{ (\varepsilon_x^{pl})^2 + (\varepsilon_y^{pl})^2 + (\varepsilon_z^{pl})^2 + \frac{1}{2} [(\varepsilon_{xy}^{pl})^2 + (\varepsilon_{yz}^{pl})^2 + (\varepsilon_{xz}^{pl})^2] \right\}} \quad \text{Eq. (4-34)}$$

where  $\varepsilon^{pl}$  is the plastic strain of the different directions.

#### 4.3.4.5 Plastic activity

The material model of Schlegel – described in Section 4.3.3.3 and [Schlegel 2004] – includes the possibility to print the plastic activity. It shows the plasticity in a qualitative manner. Therefore, the activated failure criterions in the current load step are displayed.

#### 4.3.4.6 Stresses

Stresses do not give information about the plasticity. They cannot be greater than the strength. Also in the elastic range, the strength can be reached without having plastic strains. Moreover, especially in probabilistic analysis, the strengths scatter which makes a comparison of stress and strength quite confusing and complicate. An utilisation of plastic strains to estimate the damage is much more reasonable than stress. Hence, stresses are here not used as damage parameters. Only in elastic material models the stresses are not limited by strength and so the stress indicated damages. However, in the evaluation of simulation results of such elastic models, the strength has to be used in comparisons. For masonry elastic constitutive laws are not reasonable and so far here not used.

### 4.3.5 Numerical modelling of prestressed masonry

#### 4.3.5.1 Means to model vertical prestressing

The vertical prestressing, as used e.g. in [Budelmann et al. 2008], can be modelled in different ways. A very simple one is to consider prestressing only by means of external forces applied on the points where the tendons are anchored. This avoids several problems and is very efficient. An alternative is to model the tendons by specific elements, which is more realistic and accurate. Several reasons approving this kind of modelling are listed in the section below.

A special variation of this second way is to model also the bond or/and contact of the tendons and the masonry. This is not only very time consuming in the construction of the model, but also in the numerical calculation. This is a possibility to account for the wall-tendon interaction as well (see Section 4.2.5). However, several unknown parameters would also be necessary. By virtue of these drawbacks, such a detailed modelling of bond and/or contact is not performed within this study. Nevertheless it can be an interesting research field for further investigations.

#### 4.3.5.2 Reasons to model tendons

For further simulations it is important to know, whether tendons should be modelled, or if it is sufficient to model the prestressing only by external forces. In the following, the reasons to model prestressing by means of tendons are briefly summarised.

- Restoring forces occur (in average round about 10% of the prestressing force per tendon, as shown in Section 6.2.1).
- The restoring forces lead to smaller horizontal displacement as well as smaller rotations (see Section 6.2.1).
- The stiffness is increased due to the restoring force (Fig. 6-7 and Fig. 6-10).
- The change of stiffness has an impact on the dynamic behaviour.
- In a comparison of dynamic simulations with different means to model prestressing, the impact on the dynamic behaviour is shown (see Section 6.2.2).
- The forces in the tendons change even during a static horizontal load (this influence is significant for SC 2 and/or compact walls).
- The forces in the tendon decrease during static cyclic and seismic load. This is observed in experimental tests, and probably caused by the reduction in height of bed joints due to slipping in the joints.
- In the range of high loading (especially for SC 2 and slender walls – going in line with gaping joints) the stiffness of the wall is mainly affected due to the spring properties of the prestressing bars after the occurrence of gaping joints [Ötes, Löring, Elsch 2002].
- The post-peak behaviour differs in dependency on the means to model prestressing (external forces or tendons). Tendons lead to higher resistances.

## 4.4 Summary

After explaining the basics of unreinforced masonry material behaviour and failure mechanism with special regard to in-plane horizontal loading, influencing parameters and their impact on the bearing behaviour are described, which is important for measures to improve the seismic performance of masonry. Moreover, this is elucidated with experimental shear wall test, which are besides used in the following chapters to verify used material models. In analogy, this is done to test prestressed masonry shear walls. The difference of these experiments and theoretical expect-

tations are here explained with an assumed wall-tendon interaction theory. The ductility should decrease significantly by increasing vertical loading. However, the observed ductility of the tested walls was comparatively high. As a further result of the wall-tendon interaction, practical details in application of vertical prestressing are important for the degree of ductility. Consequently, external prestressing and internal tendons without any contact lead to very low ductility, whereas a high one results for internal tendons with full bond and internal tendons with contact during the loading. Finally, some masonry buildings are presented, where vertical prestressing is already applied.

Concerning numerical modelling, fundamental parts of modelling strategies and plastic theory are given, first all. Three material models for masonry, based on FEM, are described and discussed. Regarding transient analysis, especially in combination with probabilistic investigation the constitutive model of Lagomarsino and Gambarotta [Gambarotta, Lagomarsino 1997b] is most suitable and chosen for such analyses. Reasonable damage parameters are explained and discussed, which are used to calculate risks in Chap. 8. Possible impacts of the means to model prestressing on results are theoretically pointed out as well as summarised with regard to simulation results of case studies in the chapters below, where this problem is investigated in depth.

## 5 Impact of prestressing on the dynamic behaviour

To judge if vertical prestressing is suitable to reduce the vulnerability in case of seismic loading, it is important to investigate firstly, whether prestressing has an impact on the dynamic behaviour. If it is the case, prestressing can be disadvantageous regarding the dynamic action. Furthermore, it is of interest in which cases prestressing can be disadvantageous or advantageous. Since prestressing neither changes the mass nor the stiffness significantly, many researchers firstly expect no significant impact on the dynamic behaviour. In the following, many reasons leading to an impact are explained. Moreover, in a lot of transient simulation of this study this impact is shown (see Section 5.2 and 6.2).

In the following some theoretical reasons are given why vertical prestressing should influence the dynamic behaviour. The simplest ones are the increased shear capacity and elastic range, as depicted in Fig. 5-1 regarding, which compares the load displacement curves of a prestressed and a similar non-prestressed wall of experimental test described in [Ötes, Löring, Elsch 2002]. As a consequence also the dynamic behaviour definitely has to be different. On a point where the non-prestressed walls behave already inelastic, the prestressed wall behaves still elastic. Hence, for instance the displacement is smaller (see Fig. 5-1). The blue dashed arrow shows the unloading behaviour of this wall. In contrast to the prestressed wall there is already a plastic part. After unloading, a deformation of wall remains, which causes a hysteresis and energy dissipation.

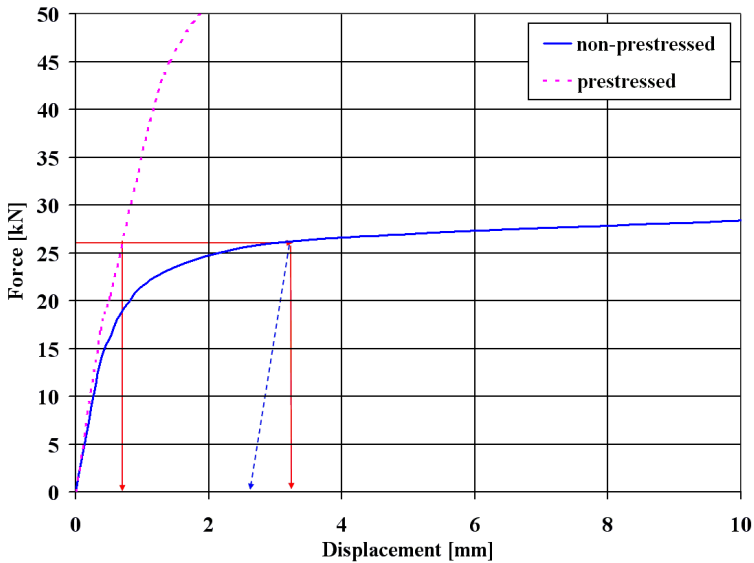


Fig. 5-1: Horizontal load displacement diagram of experimental tested shear walls - different shear capacities and displacements for equal horizontal loading

Another reason for changing in stiffness of the wall due to prestressing is presented below. In the elastic range no significant stiffness changing is to expect. But in the plastic range it can be easily explained. Also for walls it is to distinguish between bending and shear bearing behaviour. The flexural stiffness  $EI$  is a product of the Young's modulus  $E$  and the area moment of inertia  $I$ , which depends on the geometry of the cross section. On the other side the shear stiffness  $GA_s$  is defined by the shear modulus  $G$  and the shear surface  $A_s$ . In case of plasticity, a prestressed wall has another loadbearing cross section as a normal wall. This difference leads to a changing of the

stiffness. In Fig. 5-2 this effect is sketched on the example of different shear surface sizes. It is distinguished between the case of already existing gaping joints (see Fig. 5-2 on the left) and a cross section which is still complete under pressure (see Fig. 5-2 on the right). Due to the higher vertical forces the loadbearing cross section is increased for equal horizontal loading. A gaping joint occurs later when horizontal loading increases for a prestressed wall. The same principle leads to different area moment of inertia. These differences for loadbearing cross sections can be taken into account with the used material models in the numerical simulations. As aforementioned, gaping joints and so this effect occurs primarily for cantilever walls, for which mainly flexural bearing behaviour occurs, because of the high slab rotation.

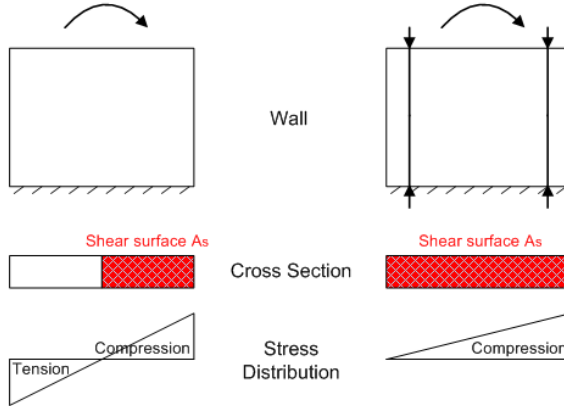


Fig. 5-2: Principle of shear surface  $A_s$  reduction in the plastic range, Left: Non-prestressed wall, Right: Prestressed wall

Such differences of the dynamic behaviour calculated by non-linear dynamic analyses are briefly summarised in Section 5.2. This should also be possible by means of non-linear modal analyses. However, non-linear modal analyses cannot be carried out with ANSYS<sup>®</sup>.

## 5.1 Experimental results

First of all, some literatures mention an influence of the vertical load level on the stiffness of the walls regarding experimental tests. Whereas, other sources do not point out a significant difference of the linear elastic stiffness, as shown in Fig. 5-1 and investigate in Dortmund [Ötes, Löring, Elsch 2002]. The different results could be explained with different masonry materials and different types of walls used for the tests. Regarding this study, it is sufficient to know that vertical prestressing can also change the stiffness of the walls, independent whether or not the linear elastic stiffness is nearly equal. In the following such literature is quoted in detail, as well as literature mentioning an impact of the stiffness of the tendons on the stiffness of the system.

### 5.1.1 Static shear wall tests

The results of static tests mentioned in [Oliveira 2003] are briefly summarised. Tab. 5-1 presents the wall label and the related vertical load level. In Tab. 5-2 and Fig. 5-3 the impact of the vertical load on the stiffness is clearly shown. Not only the shear capacity and the range of elastic behaviour differ, but also the modulus of elasticity and so the stiffness. For these experimental tests the impact is very huge. It cannot be always observed.

Wall designation	Vertical load [kN]	Normal stress [kPa]
SW.30.1	30	150
SW.30.2		
SW.100.1	100	500
SW.100.2		
SW.200.1	200	1000
SW.200.2		
SW.250.1	250	1250

Tab. 5-1: Wall designation and vertical load [Oliveira 2003]

Wall	Young's modulus [N/mm <sup>2</sup> ]		
	$E_{\text{test1}}$	$E_{\text{test2}}$	$E_{\text{calc}}$
SW.30	—	—	566
SW.100	824	688	768
SW.200	969	1302	1057
SW.250	1024	1353	1202

Tab. 5-2: Vertical load level and corresponding test results [Oliveira 2003]

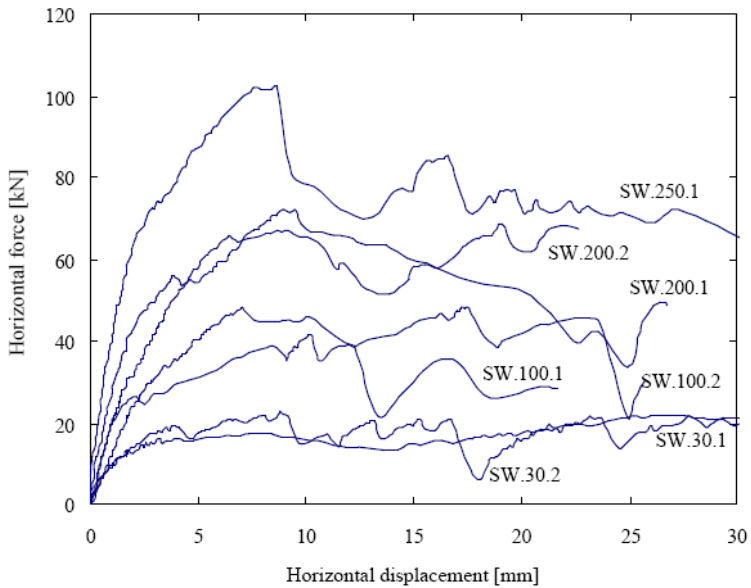


Fig. 5-3: Horizontal load displacement diagrams for different load levels [Oliveira 2003]

### 5.1.2 Static cyclic shear wall tests

At experimental tests in Dortmund (described more in detail in Section 4.2.4.1) also a prestressed wall was investigated and gapping joints were observed [Ötes, Löring, Elsch 2002]. The authors declare that after the occurrence of gapping joints the stiffness of the wall was mainly affected due to the spring properties of the tendons. Hence, not only the prestressing itself but also the means to apply prestressing influences the stiffness and so the dynamic behaviour. Because of that it would be better and more realistic to model the prestressing with tendons (if used in experimental tests) and not only as external forces. This explained effect became only important when the walls are highly loaded and reach the range of shear capacity which goes in line with significant gapping joints. Moreover, gapping joints occur especially for slender walls.

### 5.1.3 Dynamic shear wall tests

In [Magenes, Calvi 1995] is directly depicted that the dynamic behaviour observed in experimental tests with shaking tables differs for different vertical load levels. Two similar walls are compared. The only difference is their vertical load level. On wall 1 a vertical load of 103 kN is applied, on wall 2 a vertical load of 263 kN. The resulting hysteresis are depicted in a load displacement diagram (see Fig. 5-4). For wall 1, which has a lower vertical load a lower stiffness is observed than for wall 2 with a higher vertical load. It can be summarised: The lower the vertical load level, the lower the shear stiffness.

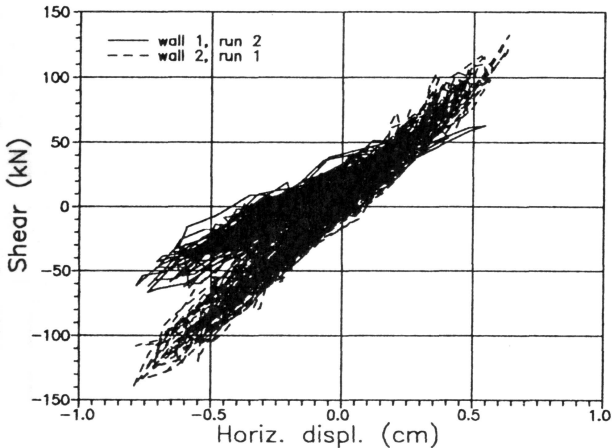


Fig. 5-4: Horizontal load displacement diagrams - Influence of vertical load level on the stiffness of the wall (wall 1 vertical load of 103 kN, wall 2 vertical load of 263 kN) [Magenes, Calvi 1995]

### 5.1.4 Dynamic tests of prestressed beams

In [Gisin, Bachmann 1985] the results of extensive experimental investigation of prestressed beams are given. Materials as lightweight concrete and technologies like prestressing were investigated, because they allow the construction of slender buildings, which can be easily moved into oscillations with big amplitudes. It was a research project at the Institute of Structural Engineering of the Swiss Federal Institute of Technology (ETH) Zurich, Switzerland. The tests aimed at

the investigation of the influence of parameters (e.g. degree of prestressing, cracking, level of excitation) on the dynamic properties (flexural rigidity, natural frequencies, damping characteristics) of lightweight and normal weight concrete beams when they were fully, or partially prestressed, and respond quasi-elastically.

First of all the research program is described. As a part of this project, tests were conducted on two types of prestressed beams, one of lightweight concrete and the other of normal weight concrete. The cross-section was equal (0.4 m width and 0.24 m height). These tests complement the first series of experiments concluded in 1979 on reinforced concrete beams without prestressing. The amount of carried out tests is explained in [Gisin, Bachmann 1985]. The research program comprised the following four phases for each of the two beam types regarding the length  $l$ :

1.  $l = 5.04$  m, full prestress, centric prestressing force.
2.  $l = 7.92$  m, at first full prestressing then without prestressing (permit cracking) finally full prestress, thereafter some of straight rods were replaced by parabolic tendon to investigate effect of cable profile.
3.  $l = 7.92$  m, partially prestress, additional weights on the top, no injected.
4.  $l = 7.92$  m, partially prestress, additional weights on the top, injected.

The following impact on the flexural rigidity was observed. The lower the level of prestressing, the lower the flexural rigidity. Reduction of flexural rigidity from full to partial prestressing for lightweight concrete was less than for normal weight concrete. The static flexural rigidity was less for both kinds of concrete beams than dynamic one. The loading history had a large effect on the rigidity (both static and dynamic).

Regarding the natural frequencies the following relation was determined. The lower the level of prestressing, the less the frequency, caused by the lower stiffness. Reduction of frequency from full to partial prestressing was for lightweight concrete less than for normal weight concrete. The loading history had a large effect on the frequency.

For these beams the damping was independent of the stress level and frequency. Only a dependency of the material was recognised.

## 5.2 Results of non-linear simulations

The non-linear dynamic simulations of the author and their results are elaborately described in Chap. 6. The impact of prestressing on the dynamic behaviour is especially investigated in Chap. 5. For the last an impulse by means of a single horizontal ground displacement is applied on equal walls with three different vertical load levels. The differences in the dynamic behaviour, as pointed out above, are also observed in the transient simulations of this thesis.

## 5.3 Summary

The dynamic behaviour of masonry walls is influenced by vertical prestressing. This is explained by theoretical consideration and confirmed by some experimental results of the literature. Moreover, the own transient simulations go in line with these results. Reasons are for instance the different sizes of the elastic ranges of prestressed and non-prestressed walls, which caused different displacements on equal loading and their different energy dissipation.



## 6 Numerical investigation of non-prestressed and prestressed masonry structures

In this chapter, the prestressing measure is numerically investigated. Therefore, comparisons of prestressed and non-prestressed structures are given. First of all, experimental tests are used in order to verify the models and to calibrate the material input parameters. Furthermore, case studies are carried out, since experimental tests are expensive and results are often not available sufficiently in literature. In the framework of the shear wall tests regarding this strengthening measure, in Braunschweig [Budelmann et al. 2004], exclusively prestressed shear walls were investigated, since the limited project funding. Reference walls to compare the behaviour and damage were not included in the budget. This gap is closed at least by means of additional numerical simulations referring to such non-prestressed reference walls. Moreover, the dynamic behaviour of prestressed shear walls as well as comparisons to non-prestressed shear walls are of high interest to assess the utility of this measure in case of seismic action. However, experimental test with shaking table could not be carried out. Therefore, dynamic simulations are performed. Last are extended to probabilistic simulations including scattering of the loading, support conditions and material parameters to find sensitivities and correlations, but also to receive damage probabilities. In addition, an existing building – Hall 8 of the iBMB/MPA in Braunschweig – is considered to demonstrate the improvement due to prestressing regarding needed shear capacity of bracing walls.

### 6.1 Experimental tests of static loaded shear walls

The experimental tests of the static loaded shear walls carried out in Eindhoven [Vermeltfoort, Raijmakers 1993] are used for a first brief verification of the numerical constitutive models. On the one hand the material model of Lourenço and Rots [Lourenço, Rots 1997] (see Section 4.3.3.1) is applied in a manner of meso-modelling. On the other hand the material model of Lagomarsino and Gambarotta [Gambarotta, Lagomarsino 1997b] (see Section 4.3.3.2) as well as the material model of Schlegel [Schlegel 2004] (see Section 4.3.3.3) are used. The last two base on macro-modelling. The experimental tests are already described in Section 4.1.5.1. For the purpose of this section, the walls J4D and J5D with a vertical load level of 0.3 N/mm<sup>2</sup> are taken into account. By means of the finite element program DIANA<sup>®</sup> the simulation for meso-modelling with the material model of Lourenço and Rots [Lourenço, Rots 1997] are carried out, whereas for macro-modelling ANSYS<sup>®</sup> have to be used to apply the material model of Gambarotta and Lagomarsino [Gambarotta, Lagomarsino 1997b] as well as regarding the material model of Schlegel [Schlegel 2004] via subroutines. The first and the last layer of the walls which are fixed in beams are not modelled, since they were necessary in experiments only for practical reasons. A static horizontal displacement is applied and the resulting crack pattern is computed. The numerical results are compared with observations in the experimental tests. Necessary values of material parameters for the modelling are given in [Vermeltfoort, Raijmakers 1993], [Lourenço 1996] and [Rots 1997]. The used numerical parameters for the three constitutive laws are given in Appendix H. Below, a comparison of the crack patterns and deformations of the tested walls J4D and J5D (vertical loading of 30 kN) with the FEM models of the shear walls is displayed. The crack pattern of wall J4D and J5D can be found in Fig. 4-16.

In Fig. 6-1 on the left, the results of the meso model are presented which simulates separately the bricks and the joints. The unit cracks – coloured depicted and calculated by plastic strains of the units – pass diagonally along the wall. Moreover, the gaping joints are well calculated, which occur on the lower right corner as well as on the upper left corner due to rocking. First of all, a good agreement can be observed between the two modelling strategies regarding the deformed shapes that are displayed in Fig. 6-1, Fig. 6-2 and Fig. 6-3. The crack width itself can be calculated only with meso-modelling. Since, the macro-models cannot directly perform crack patterns,

their plastic activity, plastic strains and damages are presented in Fig. 6-1 on the right, Fig. 6-2 and Fig. 6-3. The types of failure mode and their locations are well expressed by the plastic activity of the Schlegel model [Schlegel 2004] (see Fig. 6-1 on the right) as well as the mortar and unit damage of the Lagomarsino model [Gambarotta, Lagomarsino 1997b]. For the light blue coloured areas (see Fig. 6-1 on the right), unit failure is calculated by means of the Schlegel model, whereas green, yellow and red colours mean the failure criteria for mortar become active. The vertical plastic strain is given on the left of Fig. 6-3, which clearly shows the tensile failure of bed joint, which corresponds well with the gaping joints on the bottom and on the top. This also agrees with the calculated mortar damage in Fig. 6-2 on the left. In addition, this output parameter express also mortar damage due to sliding, which is depicted in the diagonal, where mainly sliding occurs as confirmed by the experimental results and the calculated crack pattern with the meso model. In Fig. 6-1 on the left the crack width of the head joints has the highest values in the middle part of the diagonal and means, three is the highest sliding, which agrees very well with the computed mortar damage of Fig. 6-2 on the left. Furthermore, the calculated plastic shear strain – which is depicted in Fig. 6-3 on the right – expresses this failure mechanism. The parts of maximal plastic shear strain and mortar damage, caused by sliding in the bed joint, fits also very well.

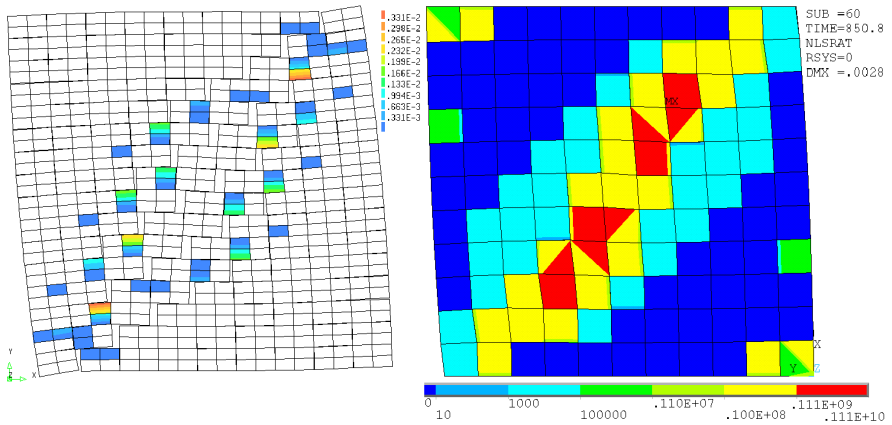


Fig. 6-1: Left: Plastic unit deformation and mortar cracks (meso-modelling), Right: Plastic activity (Schlegel model)

Additionally, in Fig. 6-2 on the right the brick damage is presented. The highest vertical compression loading, which usually leads to cracks in the units, is in the upper right and the lower left corner. Therefore, a very good conformity is in evidence. The same is true for brick cracks along the diagonal. Finally, the load displacement curves of the Eindhoven shear walls J4D and J5D (dashed black) are compared in the horizontal load displacement diagram of Fig. 6-4 with the numerical results of meso-modelling, Lagomarsino [Gambarotta, Lagomarsino 1997b] model and Schlegel model [Schlegel 2004]. All numerical models are able to predict the curve very good. In the plastic range differences may occur. Generally, the numerical results agree well with the experimental data, which shows a relative big scattering. The meso model underestimates the shear resistance somewhat. Further FEM simulations show the increased shear resistance in case of prestressing. The higher the vertical force, the higher the shear resistance.

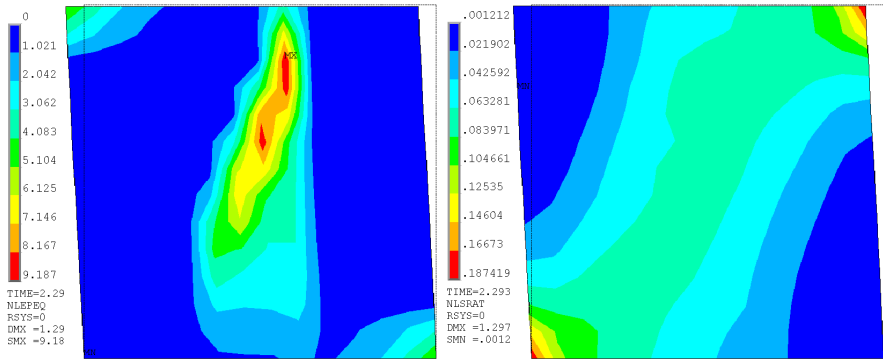


Fig. 6-2: Lagomarsino model results on a horizontal displacement of 1.3 mm, Left: Mortar damage, Right: Brick damage

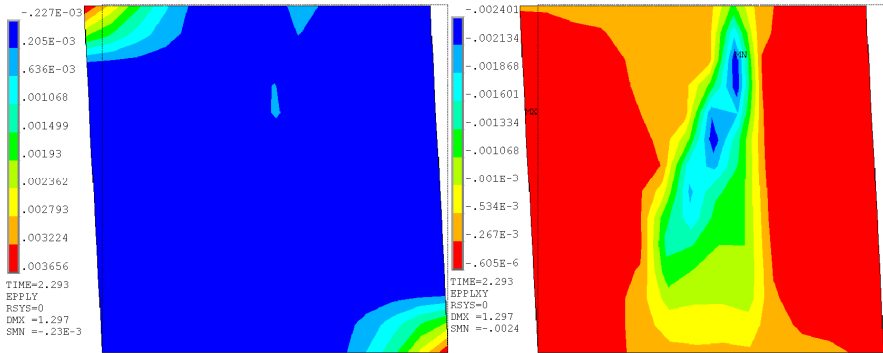


Fig. 6-3: Lagomarsino model results on a horizontal displacement of 1.3 mm, Left: Plastic vertical strain, Right: Plastic shear strain

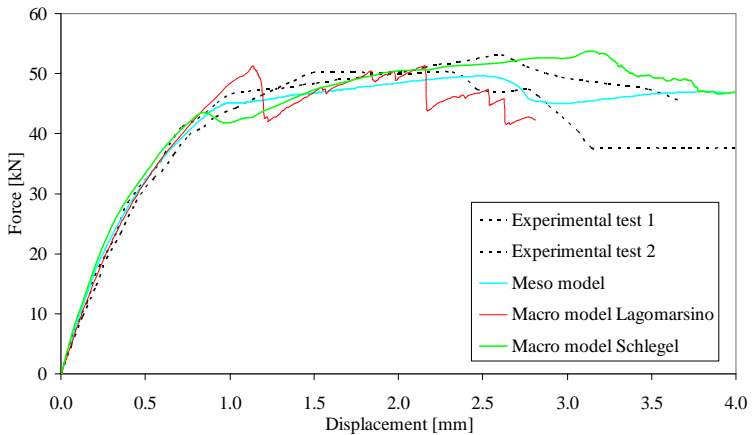


Fig. 6-4: Horizontal load displacement diagram of the Eindhoven shear walls J4D and J5D as well as numerical results of the used material models

## 6.2 Case studies

In this subchapter, the results of a static and a dynamic case study are presented. The static one is carried out in order to investigate several influencing factors, as an important base for deeper investigations and to avoid essential mistakes in the main simulations. Here, manners to model prestressing, restoring force, ductility and others are of interest. The static case study is mainly performed to get a first insight in the impact of prestressing on the dynamic behaviour. In this thesis, an elaborate description of these studies is given, whereas in [Sperbeck, Budelmann 2007] and [Sperbeck, Budelmann 2008] briefer versions can be found.

### 6.2.1 Results of a non-linear static case study

#### 6.2.1.1 Basics of the case study

To get a deeper insight, a huge case study is performed within the following conditions and parameters are varied to investigate their impacts. Four variations of the slenderness  $S$  (0.5, 1, 2, 3) are done. For the different slenderness different heights of 1.25 m, 2.5 m, 5 m and 7.5 m result. The support conditions on the top of the wall SC 1 (see Section 4.1.2) - modelled by means of a ridge L-framework - and SC 2 are used. Moreover, walls with tendons close to the middle are investigated for SC 2. To model prestressing, two means are applied as external forces simply and as tendons (see Section 4.3.5). An overview of this case study is outlined in Fig. 6-5.

The outcome of the static case study is the impacts on:

- Change of prestressing forces in the tendons
- Restoring forces
- Rotation of the top
- Shear capacity
- Ductility

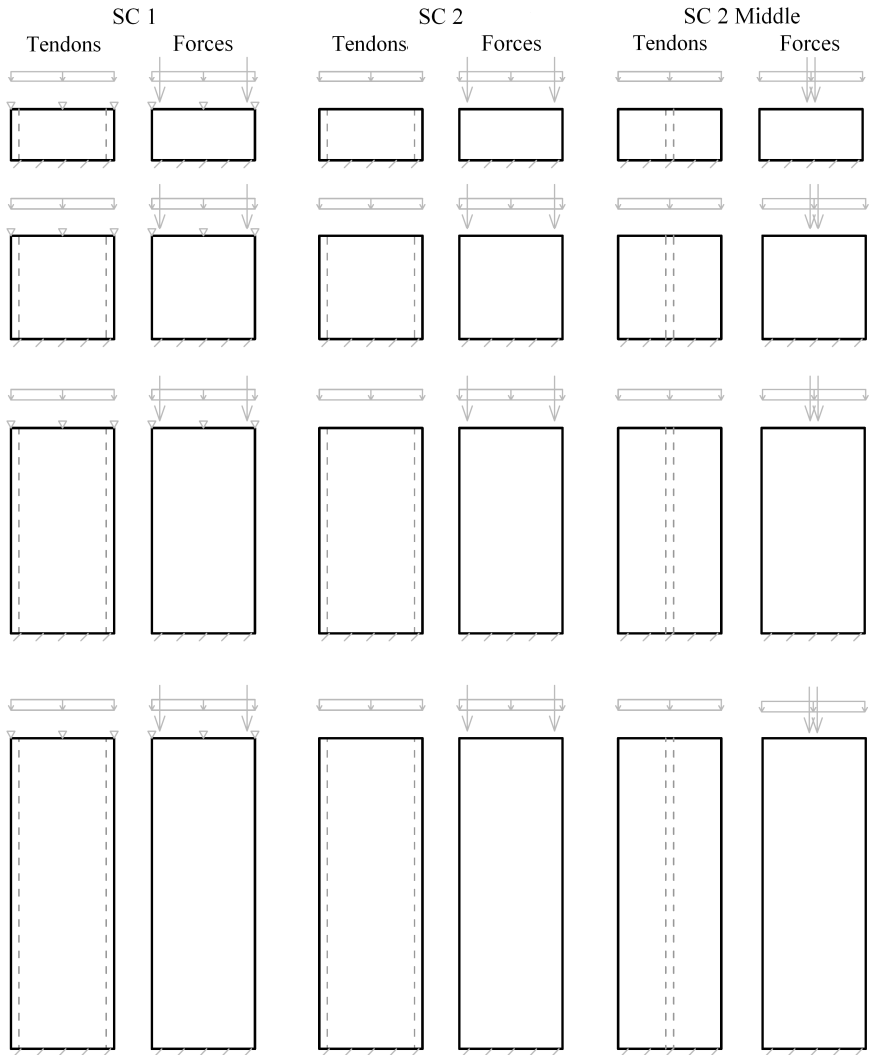


Fig. 6-5: Investigated walls in dependency on the slenderness, means to model the prestressing and tendons position for SC 1 and SC 2

### 6.2.1.2 Model

Following parameters are equal for all variations of the models. The width of the walls is 2.5 m and the thickness 0.175 m. The prestressing force per each tendon is 189 kN. The vertical load of upper storeys is 197.3 kN. This leads to a sum of vertical loads of 575.3 kN. Furthermore, the used material parameters are equal for all models of the case study as listed in Tab. 6-1. In the following the results and findings of this case study are described.

Parameter	Sym.	Value	Unit
Density	$\rho$	2000	kg/m <sup>3</sup>
Young's modulus of masonry	E	2000	N/mm <sup>2</sup>
Poisson's ratio	$\eta$	0.1	-
Friction coefficient	$\mu = \tan \varphi$	0.8	-
Tensile strength mortar	$\sigma_{bm}$	0.15	N/mm <sup>2</sup>
Shear strength of the mortar joints	$\tau_{mr}$	0.2	N/mm <sup>2</sup>
Inelastic deformation parameter for mortar	$c_{mt}$	1	-
Softening coefficient mortar	$\beta_m$	0.6	-
Compressive strength of masonry	$\sigma_{br}$	3.5	N/mm <sup>2</sup>
Shear strength of bricks	$\tau_{br}$	1.5	N/mm <sup>2</sup>
Inelastic deformation parameter for brick	$c_{bn}$	1	-
Softening coefficient of the masonry	$\beta_b$	0.4	-

Tab. 6-1: Material parameters of the model for this case study

6.2.1.3 Impact on change of prestressing forces in the tendon

a) Impact of support conditions

In case of SC 1, only very small changes for the forces in the tendons can be observed (in average round about 4 kN of 189 kN which corresponds to 2%, as given in Tab. 6-2). In contrast, for SC 2 the changes are much higher, which is caused by rotation of the top of the wall (Fig. 4-8).

SC 1			SC 2			SC 2 tendons in the middle		
<b>S 0.5</b>			<b>S 0.5</b>			<b>S 0.5</b>		
	Tendon left	Tendon right		Tendon left	Tendon right		Tendon left	Tendon right
P [N]	173960	183586	P [N]	146267	204124	P [N]	170086	176650
$\Delta P$ [N]	-15063	-5437	$\Delta P$ [N]	-42756	15101	$\Delta P$ [N]	-18937	-12373
$\Delta P$ [%]	-8.0	-2.9	$\Delta P$ [%]	-22.6	8.0	$\Delta P$ [%]	-10.0	-6.5
<b>S 1</b>			<b>S 1</b>			<b>S 1</b>		
	Tendon left	Tendon right		Tendon left	Tendon right		Tendon left	Tendon right
P [N]	184547	184631	P [N]	167292	204814	P [N]	184162	187990
$\Delta P$ [N]	-4476	-4392	$\Delta P$ [N]	-21731	15791	$\Delta P$ [N]	-4861	-1033
$\Delta P$ [%]	-2.4	-2.3	$\Delta P$ [%]	-11.5	8.4	$\Delta P$ [%]	-2.6	-0.5
<b>S 2</b>			<b>S 2</b>			<b>S 2</b>		
	Tendon left	Tendon right		Tendon left	Tendon right		Tendon left	Tendon right
P [N]	187473	187667	P [N]	180757	195614	P [N]	187445	188888
$\Delta P$ [N]	-1550	-1356	$\Delta P$ [N]	-8266	6591	$\Delta P$ [N]	-1578	-135
$\Delta P$ [%]	-0.8	-0.7	$\Delta P$ [%]	-4.4	3.5	$\Delta P$ [%]	-0.8	-0.1
<b>S 3</b>			<b>S 3</b>			<b>S 3</b>		
	Tendon left	Tendon right		Tendon left	Tendon right		Tendon left	Tendon right
P [N]	188218	188395	P [N]	184950	192198	P [N]	188217	188913
$\Delta P$ [N]	-805	-628	$\Delta P$ [N]	-4073	3175	$\Delta P$ [N]	-806	-110
$\Delta P$ [%]	-0.4	-0.3	$\Delta P$ [%]	-2.2	1.7	$\Delta P$ [%]	-0.4	-0.1

Tab. 6-2: Changes of forces in the left and right tendons in dependency on the slenderness, SCs and tendon location

The differences in the changes between SC 1 and SC 2 result from the horizontal position of the top which stays quite equal for SC 1 during the horizontal loading (Fig. 4-8). Therefore, no significant changes in the tendons force are observed. However, for SC 2 the left side moves down

(Fig. 4-8) which leads to a reduction in length of the tendon on the left and to a decreasing of the force. Consequently, in the left tendon the force decreases, but in the right tendon the force increases during the horizontal loading.

### b) Impact of slenderness

It can be observed that for compact walls (here low walls) the changes of forces in the tendons are much higher than for slender walls (Tab. 6-2 and Fig. 6-6). A summary of the forces in the tendons for SC 2 is shown in Fig. 6-6. Achieving the horizontal loading of 5 mm, a significant decrease of more than 20% occurs in case of SC 1, in contrast to SC 1. This effect is huge for low walls ( $S = 0.5$ ). For high walls ( $S = 3$ ) only a small change of 2% exists. Regarding the dependencies on slenderness, attention is necessary. In this study, only the height is varied. The observed relations are mainly caused by the height. For short tendons the same change of length leads to higher stresses than for long tendons. To check, whether the correct trend is recognised, an additional study with a variation of the width is recommended. However, in that case the rotation of the top cannot be compared, since it is related to the width, which has to be a constant input parameter to compare rotations.

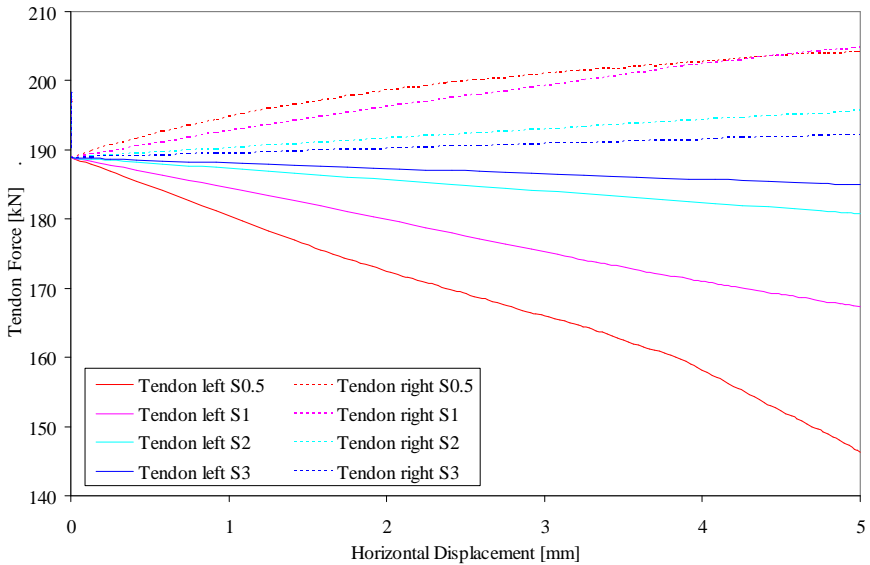


Fig. 6-6: Forces in the left and right tendons in dependency on the horizontal top displacement of the wall for SC 2 and tendons close to the edges

### c) Impact of location of tendons

For SC 2 also the variation 'tendons in the middle' is investigated (see Fig. 6-5). In Tab. 6-2 only small changes for the forces in the tendons can be observed. Close to the middle, the rotation of the top of the wall has merely a small impact on the change of the length of the tendons. Thus, the change of forces is small. This indicates the correctness of the explanation regarding the effects.

6.2.1.4 Restoring forces due to tendons

The main question whether restoring forces can be simulated is investigated firstly. Therefore a comparison is made between a model with tendons and one with external forces only. In addition to this case study the model with a slenderness of 1 and SC 2 is used for load controlled simulations. It could be shown in force controlled simulations that the displacement is smaller for the wall model with tendons, as in an equivalent model (prestressing simulated with external forces). A horizontal force of 130 kN is applied on the top of the wall.

Results for the horizontal displacement  $u_x$ :

Model with tendons	Model with external forces
$u_x = 3.45 \text{ mm}$	$u_x = 3.88 \text{ mm}$

The model with external forces (without the possibility to consider the restoring force) shows a greater displacement in horizontal direction. The difference amount to:

$$\Delta u_x = 0.43 \text{ mm}$$

That is equivalent to round about 10% of the displacement of the model without tendons. It indicates that in the model with tendons restoring forces occur, which leads to smaller horizontal displacement. Moreover, the whole system of the model with tendons has a higher stiffness. A comparison is given in Fig. 6-7 which shows the horizontal load displacement curves.

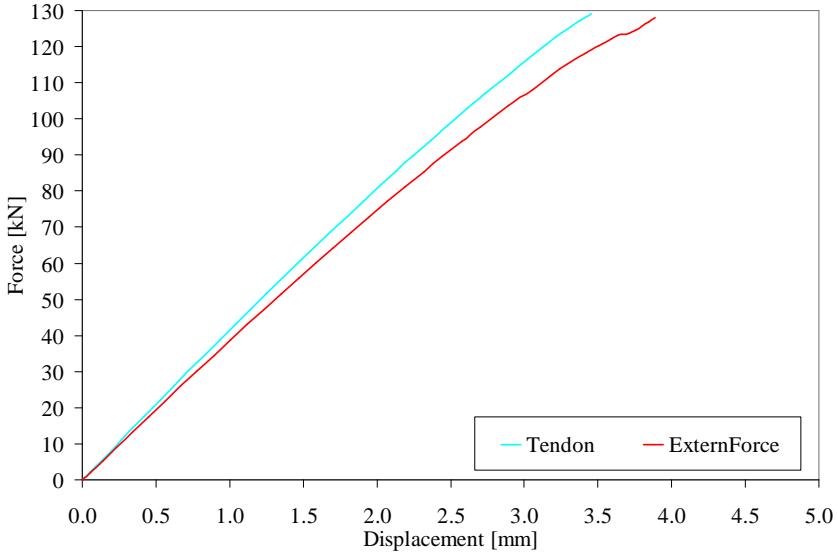


Fig. 6-7: Horizontal load displacement diagram, different stiffness in dependency of the means to model vertical prestressing

Horizontal restoring forces $R_h$ [N]			
Slenderness	SC 1	SC 2	SC 2 tendons in the middle
S 0.5	-770.0*	-40761.0	-6015.0
S 1	-471.0	-14029.0	-996.0
S 2	-185.4	-3976.5	-88.0
S 3	-50.4	-1412.8	-27.2

Tab. 6-3: Restoring forces in dependency on the slenderness, SCs and tendon position on  $u_x = 5 \text{ mm}$  ( $\hat{u}_x = 3.3 \text{ mm}$ )

A comparison of the usual displacement controlled simulations is given in the following. A horizontal displacement of 5 mm is applied on the top of the wall. The difference in the horizontal force of the support shows a value of round about 14 kN for the restoring force (of both tendons). This is also equivalent to around 10% of the horizontal forces in the supports. The restoring forces have to be divided into horizontal and vertical restoring forces. Probably, the first ones mainly cause these differences in the sum of the horizontal load (see also Tab. 6-3) or the differences in the resulting horizontal displacement. However, the vertical component seems to be more important. If a corner of the wall tries to move up (SC 2), the resistance of the tendon hampers this movement, since an increase of vertical strain of the tendon causes greater prestressing forces. Furthermore, the different forces in the right and left tendon during the horizontal loading (Fig. 6-6) cause a restoring moment outlined in Fig. 6-8. The change of the prestressing  $\Delta P$  and the resulting restoring moment  $M(\Delta P)$  are shown for a wall with tendons close to the edges and SC 2.

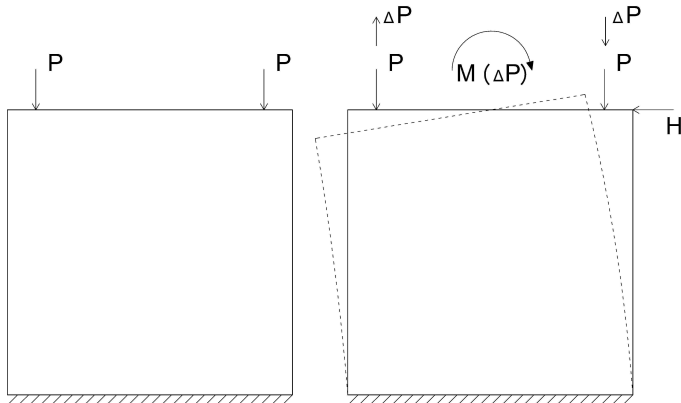


Fig. 6-8: Change of the prestressing for a model with tendons close to the edges and SC 2 – resulting restoring moment

#### a) Impact of slenderness

In dependency on the slenderness, an unexpected result is observed in this study. It seems, the slender the walls, the smaller the restoring forces. Usually the opposite would be expected. But here, the horizontal displacement  $u_x = 5 \text{ mm}$  is the same for all walls. Therefore the angle of rotation of the tendons is much smaller for slender walls as for compact walls. Thus, the horizontal component of the force inside the tendons (which is the restoring force) is smaller for slender

walls (small angles lead to small horizontal components). To investigate the impact of slenderness on the restoring forces, the angle has to be equal for all models and not the horizontal displacement  $u_x$ . Moreover, the forces in the tendons depend on the slenderness and on  $u_x$ . It is depicted in Fig. 6-6 and Tab. 6-2, that for slender walls the prestressing forces stay relative constant during the horizontal displacement, but change significantly for compact walls. If all this is considered and the restoring force amount only to 10% of the prestressing forces, it is not reasonable to investigate the impact of slenderness on the restoring forces more in detail.

#### b) Impact of support conditions

For SC 2 the impact on the restoring forces is much more significant than for SC 1, as shown in Tab. 6-3. For SC 1 the effect of restoring forces due to the means of modelling the prestressing can be neglected.

#### 6.2.1.5 Rotation of the top

In this work, the rotation *rot* of the top is defined as the ratio between the difference in height  $\Delta h$  of the left and the right upper corners and the width  $w$ . The value is here expressed in [%]. This evaluation is made for  $u_x = 5$  mm and only for SC 2. For SC 1 no rotation of the top occurs. As already mentioned the restoring forces have to be divided in a horizontal and a vertical part. The vertical restoring forces depend mainly on the change in length of the tendon during the loading and the basic length. This mechanism influences the rotation. The following trends are observed in the results of this case study (see Appendix D). The rotation of walls with tendons is less than for modelling with external forces. Therefore, the means to model prestressing as tendons is important. In case of prestressing close to middle, this difference is much smaller, which also shows the usefulness of prestressing close to the edges. For a slenderness of one, the highest rotation is observed always. If the wall is more slender or more compact than one the rotation is lower. For a slenderness from one to three it is observed: The slender the wall, the smaller the rotation. More investigations are necessary to find the correct reason for these trends. It has to be in mind that the rotation is always estimated for horizontal displacement of 5 mm. Due to the different geometry, different rotations are caused. It should be investigated for an equal angle of the wall rotation instead of an equal horizontal displacement.

#### a) Impact of means to model the prestressing

If the prestressing is modelled as tendons, lower rotation of the top occurs. It is a mixture of SC 1 and SC 2. The higher the stiffness of the tendon, the lower should be the rotation, due to vertical reaction forces inside the tendon, which occur when an upper corner of the wall tries to move up. In case of modelling prestressing by means of external forces, there are no additional reaction forces, which reduce the movement of the corner.

#### b) Impact of location of tendons

Above it is mentioned that only for SC 2 the modelling of tendons is important. For this support condition a location of the tendons close to the middle is investigated as well. Especially, tendons in the near of the edges of the wall lead to smaller rotation of the top. The elongation of the tendon is the reason. If the corner moves up, tendons close to the edges become longer than tendons close to middle. Hence, for the last one only a small increasing of tendon forces can occur. As a result, this movement is hampered only small. An efficient location of tendons is close to the

edges. It could be assumed, that the lever arm of the prestressing forces would be a significant reason. Although, the rotations of models with external forces close to the edges and close to middle are approximately equal. There is a huge difference of the lever arms, but the difference in rotation can be neglected. However, for the models with tendons more significant differences in rotation occur. Consequently, the lever arm is not the main reason. It is the change in length of the tendons.

### c) Impact of slenderness

In this case study the width is constant and the height differs. It is important to realize that the slenderness does not have a huge impact on the phenomena, as already described above. Hence the results should not be generalised regarding the slenderness.

#### 6.2.1.6 Shear capacity

To achieve information about the shear capacities and ductilities, it is necessary to apply a horizontal loading greater than 5 mm, which the following in results account for, while the previous are mainly related to a maximum horizontal displacement of 5 mm.

### a) Impact of support conditions

As already explained and shown in previous reports, the shear capacity depends strongly on the support condition. For SC 1 the capacity is higher than of SC 2. Fig. 6-9 depicts moreover that the walls with SC 1 have a higher stiffness. For slender walls the shear capacity for SC 1 is reached earlier than for SC 2. In case of compact walls there is no significant difference in displacement.

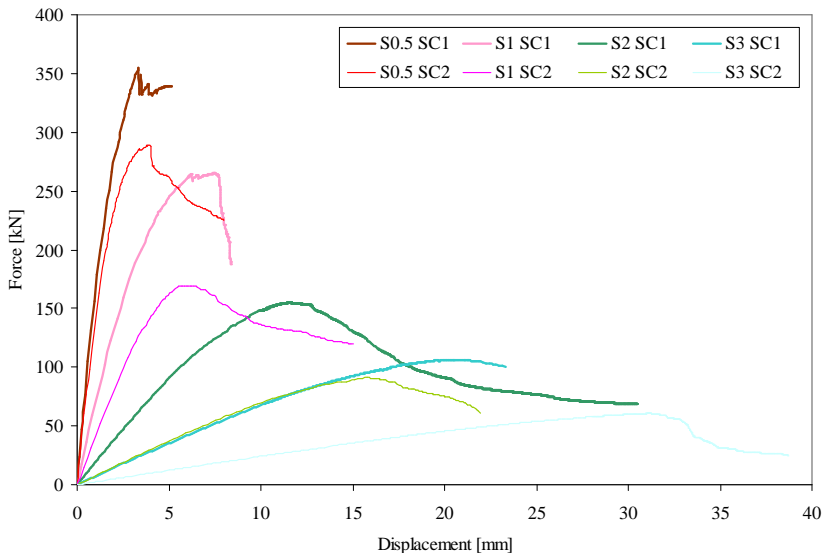


Fig. 6-9: Horizontal load displacement diagram for models with tendons close to the edges in dependency on SCs and slenderness

b) Impact of slenderness

The results of previous experimental tests and simulations of other authors are confirmed by this case study. The higher the slenderness, the lower the shear capacity. For slender walls, high deformations are necessary to reach the peak of load displacement curves. Very compact walls have a very high shear capacity as shown in Fig. 6-9, Fig. 6-10 and Fig. 6-11.

c) Impact of means to model prestressing

In Fig. 6-10 and Fig. 6-11, the load displacement curves are given for the four different slender-ness in combination with support condition SC 2.

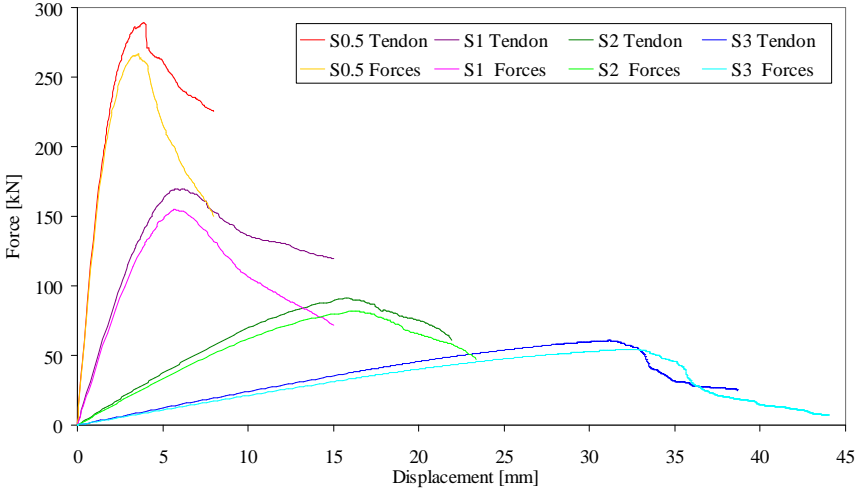


Fig. 6-10: Load displacement diagram for SC 2 and tendons close to the edges, dependent on the means to model prestressing

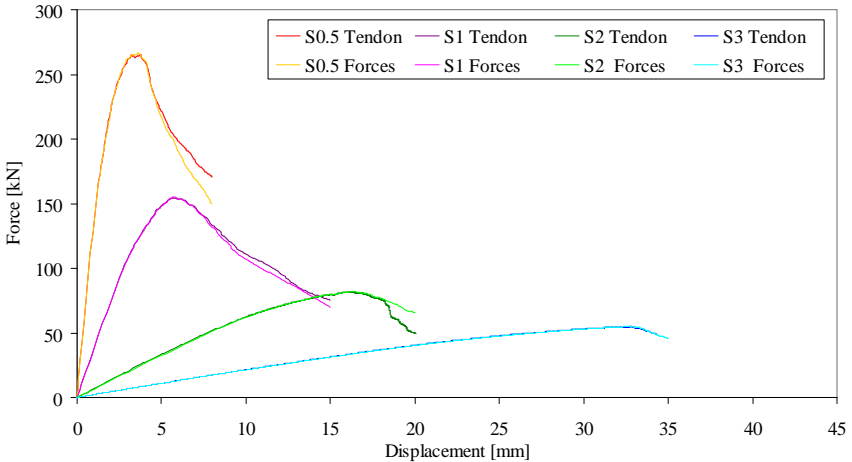


Fig. 6-11: Load displacement diagram for SC 2 and tendons close to middle, dependant on the means to model prestressing

The difference between the modelling of prestressing by means of tendons or external forces is investigated. Fig. 6-10 depicts the results for tendons and forces close to the edges. The shear capacity of models with tendons is significantly higher, whereas the behaviour of walls with prestressing close to middle is shown in Fig. 6-11. The differences regarding the means to model prestressing can be neglected here.

#### d) Impact of location of tendons

A comparison between different positions of tendons as given in Fig. 6-12 proves that tendons close to the edges lead to higher shear capacities. A significant difference between models with tendons and external forces can be observed in Fig. 6-10 (tendons close to the edges). While, the behaviour for walls with tendons close to the middle behaves rather equal (Fig. 6-11). This proves that a position near the sides of the walls is useful, as expected.

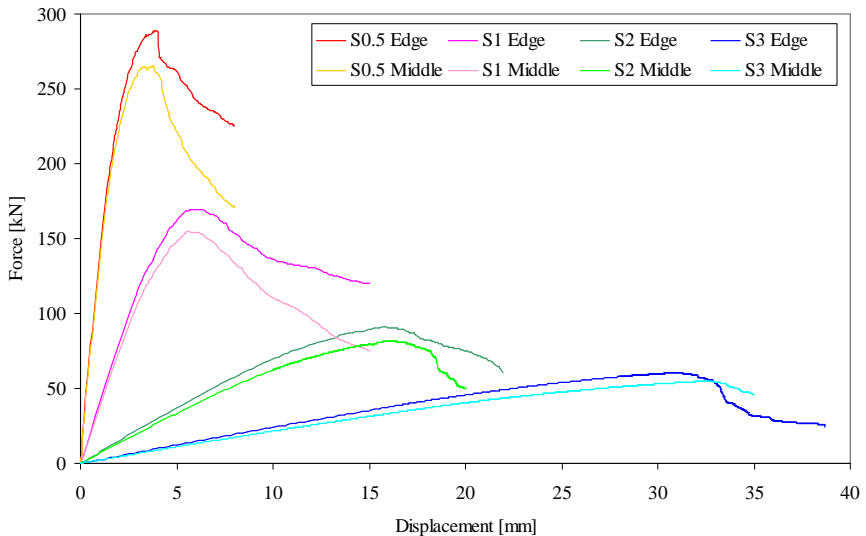


Fig. 6-12: Horizontal load displacement diagram for the model with SC 2 in dependency on tendon position and slenderness

#### 6.2.1.7 Ductility

##### a) Impact of slenderness

The higher the slenderness, the more ductile the wall behaves. For very compact walls, a very brittle behaviour can be noted (Fig. 6-9, Fig. 6-10 and Fig. 6-11), as already observed by other researchers. Although, the post-peak behaviour of models with tendons is more useful. Higher horizontal forces can be applied. Obviously the tendons carry tensile loads when tensile failure is already occurred in the wall.

b) Impact of support conditions

Fig. 6-9 compares the load displacement curves for SC 1 and SC 2. Slender walls behave more ductile in case of SC 2. For compact walls, no significant difference exists between the two support conditions. The peak nearly occurs on the same displacement.

c) Impact of means to model prestressing

Fig. 6-10 depicts, that slender walls modelled with external forces behave more ductile than walls with tendons, in case of prestressing close to the edges. If it is close to the middle no important differences can be observed, like shown in Fig. 6-11.

d) Impact of location of tendons

The comparison in Fig. 6-12 shows, that slender walls with tendons in the middle behave a little bit more ductile than walls with tendons on the edges. But the difference is not significant in framework of this case study.

#### 6.2.1.8 Summary of unexpected and important results

In general, the means to simulate prestressing is important for SC 2 especially when the tendons are close to the edges. For SC 1 this phenomenon can often be neglected. The findings of this case study regarding the impact of slenderness cannot be generalised, since the width is constant as well as the horizontal top displacement. For many comparisons, an equal angle would be necessary instead of an equal horizontal displacement. Moreover, the height of the wall has an important influence, because it corresponds to the basic length of the tendons. Small differences in length lead to huge differences of the forces inside of short tendons. For long tendons much higher differences in length are necessary to reach huge changes of such inner forces. Restoring force occurs and can be simulated when the prestressing is modelled by means of tendons. The restoring forces have to be divided in a horizontal and a vertical part. The last one is important only for SC 2. In this study, the vertical movement of the corners (during the top rotation) leads to changes in length of tendons. A change of the prestressing forces in the tendons results, which decrease in tendons on the lower corner and increase in tendons on the upper corner. In case of low walls, the top rotation leads to significant changes of the prestressing forces in the tendons. It is smaller the higher the walls (see Fig. 6-6). For models with tendons close to the edges the rotation is lower, but the tendons have to be modelled. If simply external forces are used to model the prestressing, no significant difference can be asserted.

## 6.2.2 Results of a non-linear dynamic case study

### 6.2.2.1 Basics of the case study

The increasing of stiffness, as mentioned above, affects the dynamic behaviour as shown in Fig. 6-13. A small case study was performed to investigate further. The vibration behaviour of prestressed walls with a slenderness of three modelled with ‘external forces’, ‘tendons’, and for walls without prestressing, is calculated in non-linear dynamic simulations. A ground displacement is applied as an impulse for all mentioned simulations below. The time for the impulse amounts to 0.12 s to move ground and return back to the original position. The three different load functions are time dependent as identified in Fig. 6-13 with dashed lines. Tab. 6-4 gives a short overview of the carried out dynamic analyses, the level of the applied displacement and whether it was possible to attain convergence.

Impulse displacement	Means to model prestressing		
	External forces	Tendons	Without prestr.
5 mm	Yes	Yes	Yes
10 mm	Yes	Yes	Yes
17 mm	Yes	Yes	Yes

Tab. 6-4: Overview of the carried out analyses with impulse loading

For these models the same values for width, thickness and material parameters (Tab. 6-1 and Fig. 6-5) are used as for the static case study above. All have a static vertical load of 197.3 kN. The variations ‘external forces’ and ‘tendons’ have an additional prestressing force of 189 kN per each tendon.

### 6.2.2.2 Results

The results for the vibration behaviour regarding the horizontal top displacement (absolute displacement, not relative displacement) are depicted in Fig. 6-13. For all of the wall models and load levels, the highest value of the roof displacement is reached after 0.12 s. The highest displacement of 34 mm is observed for the non-prestressed wall. As expected, prestressing leads to a reduction of the vibration amplitude. For the models with ‘external forces’ the displacement amounts to 32 mm and for the ‘tendons’ 32.4 mm. The observed difference between the maximum horizontal roof displacement of ‘tendons’ and ‘external forces’ is smaller for lower load levels. The horizontal displacement of the prestressed walls is insignificantly smaller than the prestressed walls for lower vertical load levels (5 mm and 10 mm). Nevertheless, the mortar damage is much less for prestressed walls, than for the non-prestressed wall (Fig. 6-15). This concludes that vertical prestressing is a useful strengthening measure also for dynamic loading. More detailed investigations are still in progress.

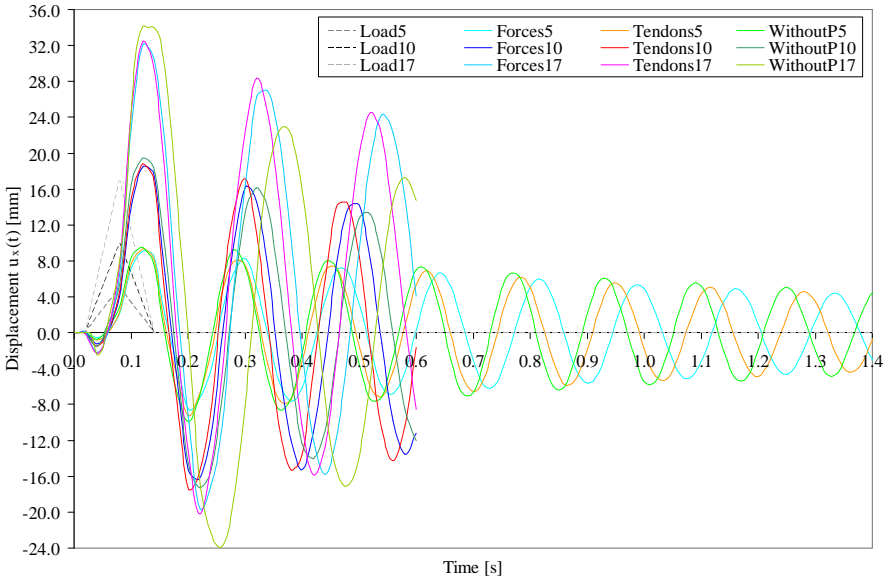


Fig. 6-13: Horizontal displacement of the top time-dependent for modelling of prestressing by means of external forces, tendons, and without prestressing in case of SC 2

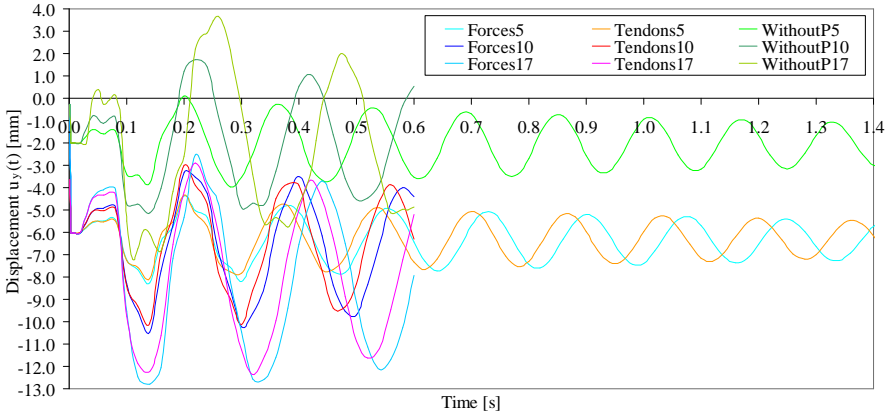


Fig. 6-14: Vertical displacement of the top time-dependent for modelling of prestressing by means of external forces, tendons and without prestressing in case of SC 2

In Fig. 6-14 the vertical displacement of the right upper corner of the wall is displayed. This indicates the rotation of the top, as mentioned above. When high values occur, the rotation of the top is high. For walls where prestressing is modelled by external forces, the rotation is a bit higher, than for modelling by means of tendons. The different vertical top displacements are due to the different vertical load levels of prestressed and non-prestressed walls as seen in Fig. 6-14. The dynamic behaviour is different for all considered walls, as periods vary significantly. The walls with tendons vibrate faster. This means they are stiffer.

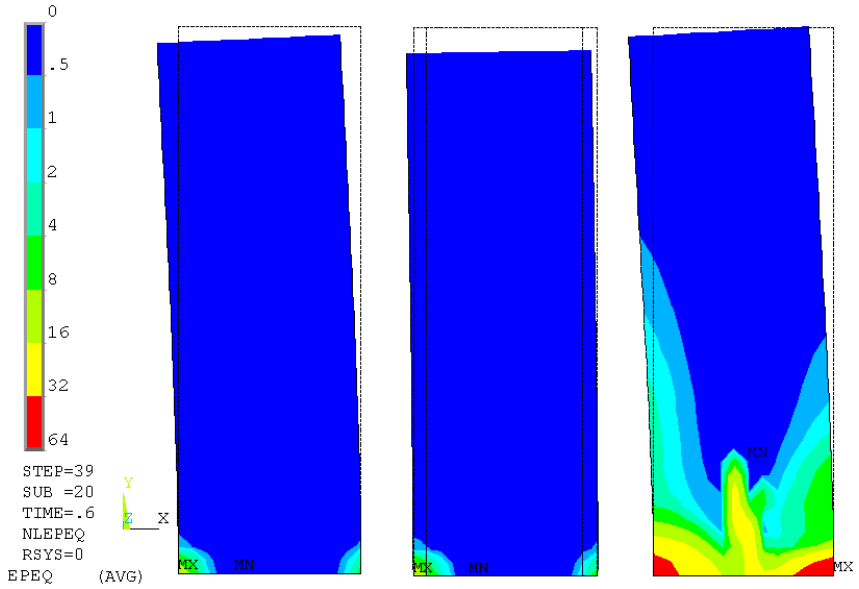


Fig. 6-15: Mortar damage for impulse loading of 10 mm, Left: External forces, Middle: Tendons, Right: Without prestressing

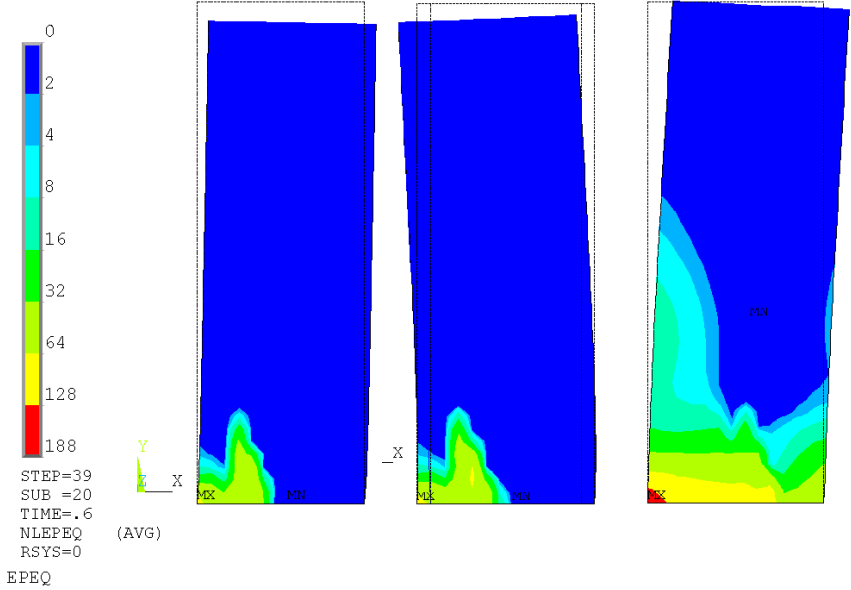


Fig. 6-16: Mortar damage for impulse loading of 17 mm, left: External forces, Middle: Tendons, Right: Without prestressing

Observations of experimental tests lead to a probable reason. Ötes and Löring observed that in the range of high horizontal loading, the stiffness of the wall is mainly affected due to the spring properties of the tendons after the occurrence of gaping joints [Ötes, Löring, Elsch 2002]. This would explain also the bigger difference between ‘tendons’ and ‘external forces’ in case of higher shaking levels. Also, presented static simulations show that the post-peak behaviour differs if the prestressing is modelled as ‘external forces’ or ‘tendons’ (Fig. 6-10). Modelling of tendons leads to higher resistances. In general, the walls vibrate slower, when the ground acceleration is higher. A reason is the higher damage of the walls leading to smaller stiffness, and lower frequencies.

For a higher load level (horizontal ground displacement of 17 mm) also the prestressed walls are significantly damaged. Here, the difference between the two means to model prestressing become larger, but not important. In all these simulations the mortar damage, as well as the brick damage, is a bit higher for tendons, than for external forces.

Impulse displacement	Means to model prestressing		
	External forces	Tendons	Without prestr.
5 mm	no output	no output	16.269
10 mm	13.514	16.136	63.431
17 mm	78.186	85.412	187.33

Tab. 6-5: Maximal mortar damage of the transient analyses

Impulse displacement	Means to model prestressing		
	External forces	Tendons	Without prestr.
5 mm	0.536	0.549	0.301
10 mm	0.914	0.934	0.751
17 mm	15.292	16.091	4.038

Tab. 6-6: Maximal brick damage of the transient analyses

Impulse displacement	Means to model prestressing		
	External forces	Tendons	Without prestr.
5 mm	-0.000627	-0.000658	-0.000276
10 mm	-0.001261	-0.001329	-0.000957
17 mm	-0.015461	-0.016091	-0.005267

Tab. 6-7: Maximal vertical plastic compressive strain of the transient analyses

Below, the maximal values determined in the static analysis are given as well for the prestressed wall (simulated by means of external forces) on a absolute resulting displacement of 47.73 mm on the most moved node of the structure (on the last load step of the softening range as presented in Fig. 6-10), to allow a better comparison:

Max mortar damage: 116.92  
 Max brick damage: 153.00  
 Max vertical plastic strain: -0.0979 (compression)

### 6.3 Simulation of the experimental tests of prestressed walls

In order to verify the material model of Lagomarsino and Gambarotta [Gambarotta and Lagomarsino 1997b] for prestressed shear walls, the experimental tests with internal tendons are used, which are carried out in Braunschweig by the iBMB [Budelmann et al. 2004] and are briefly described in Section 4.2.4.2. For some parameters of the material model experimental data are not available, which requires a model calibration. After extensive parameter studies, to get an idea about sensitivities, several parameter combinations are found to reach a good agreement with the experimental results. Finally, the values for the material parameters given in Tab. 6-8 are used throughout this thesis to simulate the vertical prestressed shear walls of Braunschweig [Budelmann et al. 2004], since this values are a good compromise of numerical stability and agreement with experimental observations.

Parameter	Sym.	Value	Unit
Density	$\rho$	1650	kg/m <sup>3</sup>
Young's modulus of masonry	E	5800	N/mm <sup>2</sup>
Poisson's ratio	$\eta$	0.15	-
Friction coefficient	$\mu = \tan \varphi$	0.436	-
Tensile strength mortar	$\sigma_{bm}$	0.87	N/mm <sup>2</sup>
Shear strength of the mortar joints	$\tau_{mr}$	0.44	N/mm <sup>2</sup>
Inelastic deformation parameter for mortar	$c_{mt}$	0.95	-
Softening coefficient mortar	$\beta_m$	0.3	-
Compressive strength of masonry	$\sigma_{br}$	17.2	N/mm <sup>2</sup>
Shear strength of bricks	$\tau_{br}$	2.5	N/mm <sup>2</sup>
Inelastic deformation parameter for brick	$c_{bn}$	1.1	-
Softening coefficient of the masonry	$\beta_b$	0.4	-
Young's modulus of concrete	$E_c$	14000	N/mm <sup>2</sup>
Rayleigh mass damping	$\alpha$	0.62	-
Rayleigh stiffness damping	$\beta$	0.0003	-

Tab. 6-8: Calibrated material parameter for the prestressed iBMB shear walls of 2004 (Basic F)

#### 6.3.1 Static and static cyclic loading

First of all, the results of the static cyclic experimental test of the iBMB, which are used for the calibration, are compared with the numerical results, in order to demonstrate the capability of the model to simulate the loadbearing behaviour correctly as well as to show the reasonability of the parameter calibration. In the framework of this thesis, the presentation of the numerical investigation is limited on wall 1, wall 3 and wall 4, due to the similarity of wall 1 and wall 2. The damage parameters – introduced in Section 4.3.4 – are utilised to compare the impact of prestressing. A very important one, the horizontal displacement, is often used to evaluate the results, especially in combination with the shear resistance. In [Budelmann et al. 2004] as well as in the diagrams of this thesis, the horizontal displacement  $u_x$  refers to the middle of the wall on the top. However, the pictures with the damage distributions refer to a point of absolute displacement  $u_{abs}$  of the whole structure, since ANSYS<sup>®</sup> plots this value automatically. The last is slightly higher (usually 0.3 mm) than the value for the upper middle point of the wall. To avoid some confusion, this has to be in mind for comparisons of diagrams and the most pictures of damage distributions.

In the subsequent passage, the static cyclic experimental and numerical results of wall 1 are compared. This is best done in Fig. 6-17, by means of horizontal load displacement diagrams. The measured hysteresis is depicted in black and their envelope with a dashed line in Fig. 6-17 on the left. The calculated hysteresis (Fig. 6-17 on the right) describes well the big enclosed area, which is characteristic for compacted walls. For the last significant differences in means to model prestressing by external forces or more accurate by tendons cannot be observed. This is caused due to the concrete slab, which hampers a wall rotation appreciably. Moreover, the simulated static curves are shown in red and blue. Already, in a displacement range of 4 to 7 mm, a small degradation is visible.

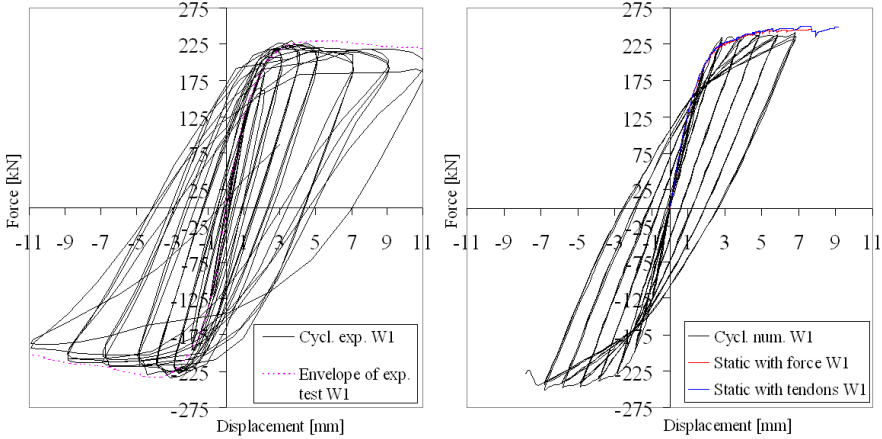


Fig. 6-17: Horizontal load displacement diagram of wall 1, Left: Experimental test (static cyclic curve and envelope), Right: Numerical results (static cyclic curve and static curves)

Due to enormous convergence problems, the cyclic simulations interrupt in a range of 8 mm horizontal displacement. Though this problem, the prediction is sufficient for the target probabilistic earthquake simulations, for which calculations in a very deep plastic range should be avoided. Otherwise the computing time would be very huge as well as the number of numerical fails. The loadbearing behaviour of wall 1 can be qualitatively and quantitatively simulated with good precision. The numerical results are plausible and agree well with experimental ones, which are additionally confirmed by damage distributions of Fig. 6-18 and Fig. 6-19. The crack pattern of the experimental investigations is depicted in Fig. 4-28 for wall 1. The numerical unit damage indicated the occurrence of unit cracking, as given in Fig. 6-18 on the left. The diagonal crack propagation from one corner to the other is well simulated. The lower one is more damaged as also observed in the experiments (toe crushing).

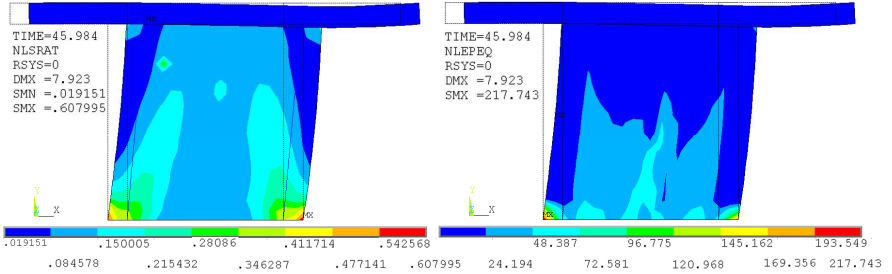


Fig. 6-18: Wall 1 with prestressing for static cyclic loading on  $u_{abs} = 7.9$  mm – Left: Unit damage, Right: Mortar damage

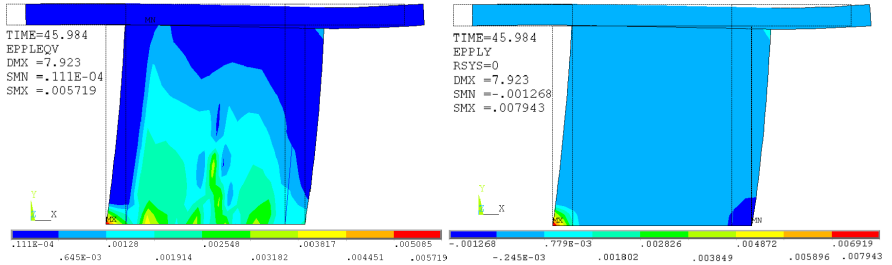


Fig. 6-19: Wall 1 with prestressing for static cyclic loading on  $u_{abs} = 7.9$  mm – Left: Equivalent plastic strain, Right: Vertical plastic strain

In Fig. 6-20 up to Fig. 6-22 the numerical and experimental results are summarised for wall 3. The hysteresis properties of the slender wall 3 differ significantly in comparison to wall 1, which can be simulated very well with the used material model (see Fig. 6-20 and Fig. 6-17).

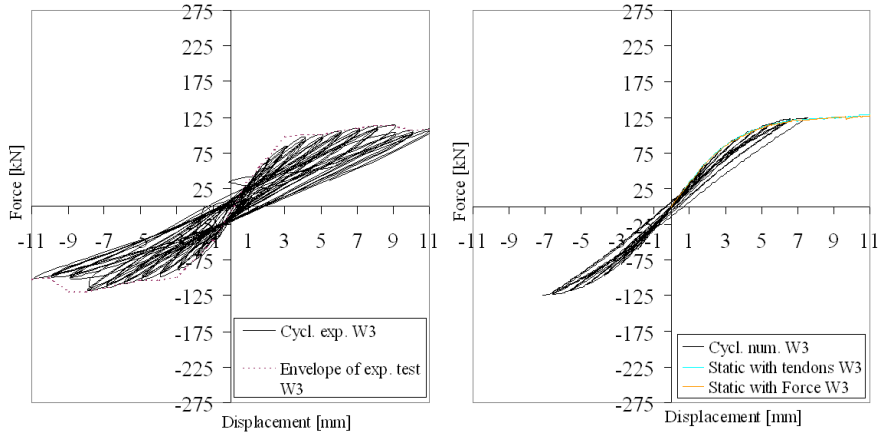


Fig. 6-20: Horizontal load displacement diagram of wall 3, Left: Experimental test (static cyclic curve and envelope), Right: Numerical results (static cyclic curve and static curves)

Regrettably, the mentioned convergence problem occurs likewise for this slender wall. The reason seems to be the stiff support condition on the top leading to increased shear behaviour and failure. Nonetheless, the material parameter calibration is successful and leads to correct and plausible numerical results, which agree well with experiments. With the chosen material parameter combination, the loadbearing behaviour of all walls can be qualitatively and quantitatively simulated with sufficient accuracy as explained in detail henceforth. The experimental crack pattern of wall 3 is depicted in Fig. 4-30, which fits very well with the computed one by means of the unit damage in Fig. 6-21 on the left. Not only the typical diagonal cross is well simulated, but also the higher concentration of cracks in lower part of the wall. There, higher loading acts due to the higher stiffness of the basement in comparison to the more flexural floor slab. This can be seen by means of the vertical plastic compressive strain for wall 1 in the Fig. 6-19 on the right and in Fig. 6-22 on the right for wall 3. Moreover, the high compressive strain due to prestressing becomes visible, except the corners where tensile failure occurs. The equivalent plastic strain – depicted in Fig. 6-19 and Fig. 6-22 on the left – displays the regions of both shear and vertical failure. The last can be subdivided in tensile failure of mortar and unit failure due to high compression stress. These distributions of equivalent plastic strain go very well in line with computed mortar damages, vertical plastic strains and unit damages.

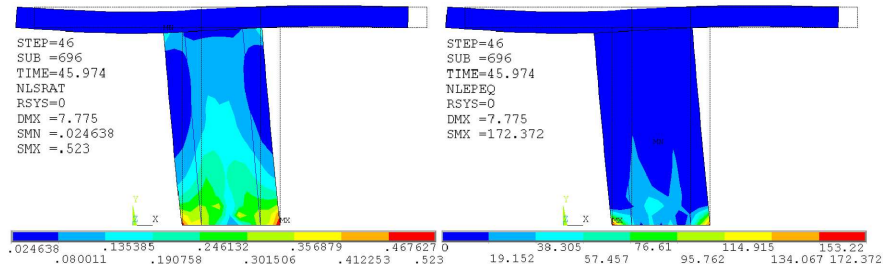


Fig. 6-21: Wall 3 with prestressing for static cyclic loading on  $u_{abs} = 7.7 \text{ mm}$  – Left: Unit damage, Right: Mortar damage

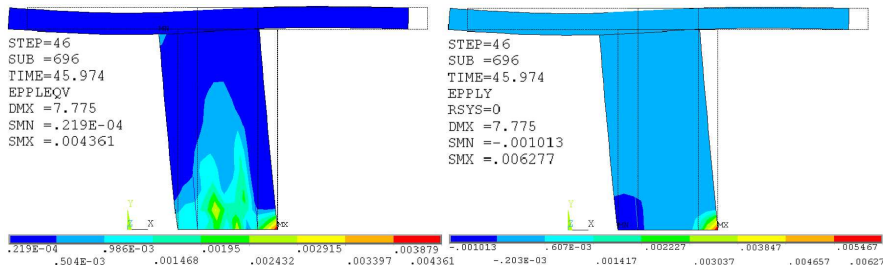


Fig. 6-22: Wall 3 with prestressing for static cyclic loading on  $u_{abs} = 7.7 \text{ mm}$  – Left: Equivalent plastic strain, Right: Vertical plastic strain

As already mentioned, the budget of the experimental project has not included further tests for non-prestressed versions of these four prestressed walls. To close this gap and allow a comparison, the missed non-prestressed walls are numerically investigated here. The results are given subsequently for static loading. Regarding such first comparisons, a consideration of stiffness and strength degradation - which occur in case of static cyclic loading - is not necessary and not reasonable. Moreover, these effects are automatically taken into account in detailed and extensive dynamic investigations, which are presented in Section 6.3.2. The unit damage is compared in Fig. 6-23.

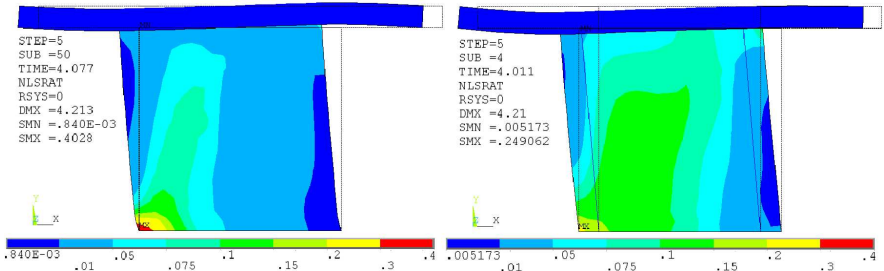


Fig. 6-23: Wall 1 – Unit damage of static loading on  $u_{obs} = 4.2$  mm, Left: Non-prestressed, Right: Prestressed

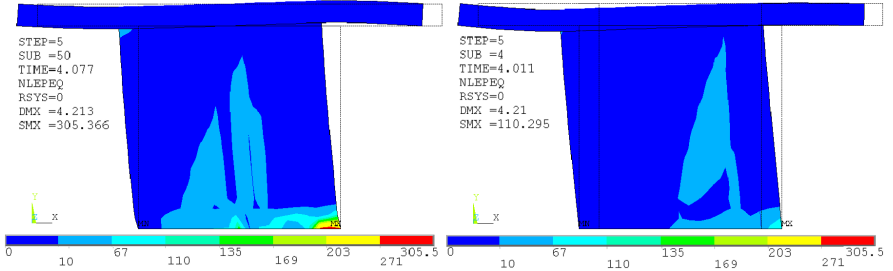


Fig. 6-24: Wall 1 – Mortar damage of static loading on  $u_{obs} = 4.2$  mm, Left: Non-prestressed, Right: Prestressed

For wall 1 the local unit damage is higher for the non-prestressed wall (see Fig. 6-23 on the left) than for the prestressed wall as presented in Fig. 6-23 on the right. However, the distribution shows high damage over greater areas of the prestressed wall. A comparison of Fig. 6-24 on the left and right exhibits a significant reduction of the local and the global mortar damage due to prestressing. Expectedly, the highest mortar damage can be observed on the right lower corner, where vertical tensile stresses lead to mortar tension failure, which is confirmed by the vertical plastic strains of Fig. 6-25.

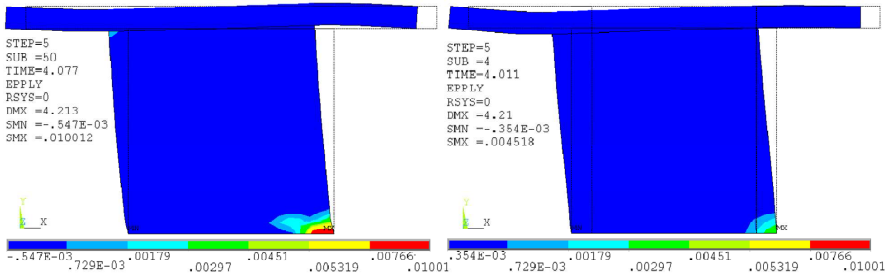


Fig. 6-25: Wall 1 – Vertical plastic strain of static loading on  $u_{obs} = 4.2$  mm, Left: Non-prestressed, Right: Prestressed

In case of prestressing, lower values are observed for the plastic shear strains (see Fig. 6-26) and the equivalent plastic strains (see Fig. 6-27). Besides, their distributions fit very well with the failure mechanisms leading to the mortar and unit damage. Very simplified, it may be imagined:

a superposition of the plastic vertical and shear strain distribution leads to a picture similar as the superposition of unit and mortar damage distribution. The high damaged parts would be shown in one picture produced in two different ways. These numerical results lead to such plausible superposed distributions.

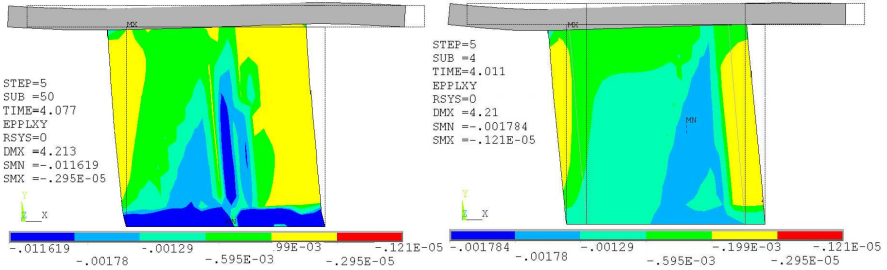


Fig. 6-26: Wall 1 – Plastic shear strain of static loading on  $u_{abs} = 4.2$  mm, Left: Non-prestressed, Right: Prestressed

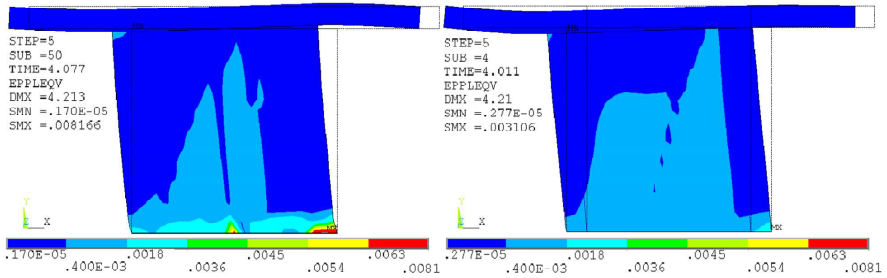


Fig. 6-27: Wall 1 – Equivalent plastic strain of static loading on  $u_{abs} = 4.2$  mm, Left: Non-prestressed, Right: Prestressed

Hereinafter, the results of static loaded non-prestressed and prestressed versions of wall 3 are contrasted. A very different impact of prestressing is obtained regarding the local unit damage. In case of prestressing, this local damage is greater (see Fig. 6-28), even more the global one.

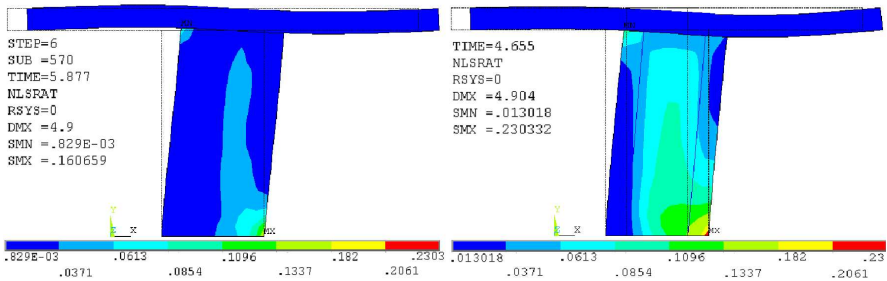


Fig. 6-28: Wall 3 – Unit damage of static loading on  $u_{abs} = 4.9$  mm, Left: Non-prestressed, Right: Prestressed

However, the local maxima are higher for the non-prestressed version in case of all plastic strains (see Fig. 6-30, Fig. 6-31 and Fig. 6-32) and for the mortar damage (see Fig. 6-29), as also ob-

served for wall 1. It is postulated that the higher degree of rotation of wall 3 leads to higher compression loading on the lower corner, which is caused by the greater slenderness and less stiff support condition on the top (the floor slab is longer and more flexible). The results are plausible, since the same agreement of plastic strain distributions of Fig. 6-30, Fig. 6-31 and Fig. 6-32 as well as damage distributions (see Fig. 6-28 and Fig. 6-29) are presented, as detected above for wall 1.

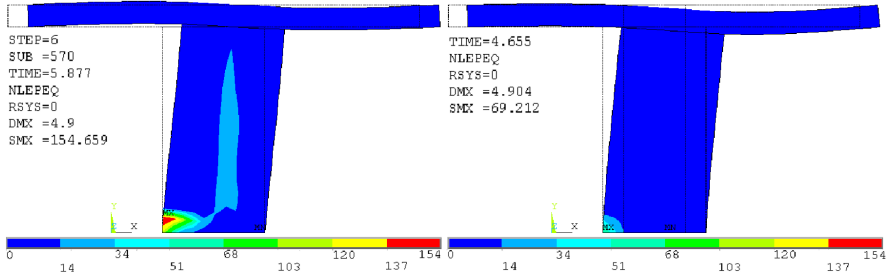


Fig. 6-29: Wall 3 – Mortar damage of static loading on  $u_{obs} = 4.9$  mm, Left: Non-prestressed, Right: Prestressed

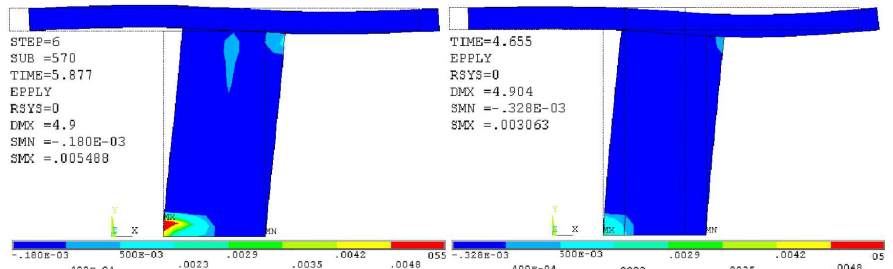


Fig. 6-30: Wall 3 – Vertical plastic strain of static loading on  $u_{obs} = 4.9$  mm, Left: Non-prestressed, Right: Prestressed

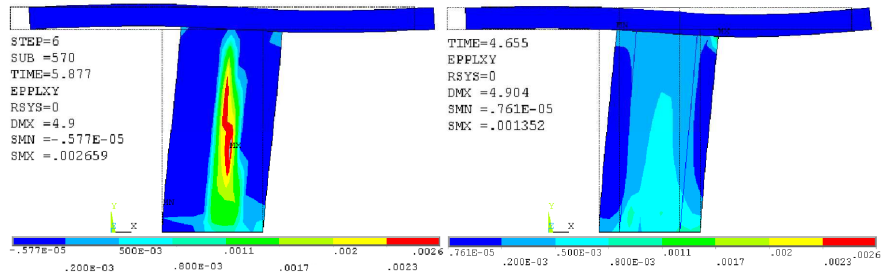


Fig. 6-31: Wall 3 – Plastic shear strain of static loading on  $u_{obs} = 4.9$  mm, Left: Non-prestressed, Right: Prestressed

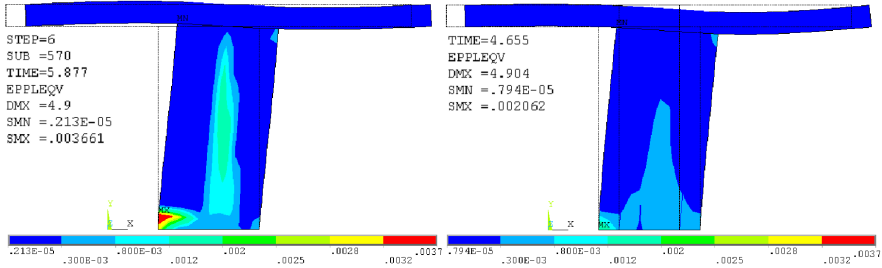


Fig. 6-32: Wall 3 – Equivalent plastic strain of static loading on  $u_{abs} = 4.9$  mm, Left: Non-prestressed, Right: Prestressed

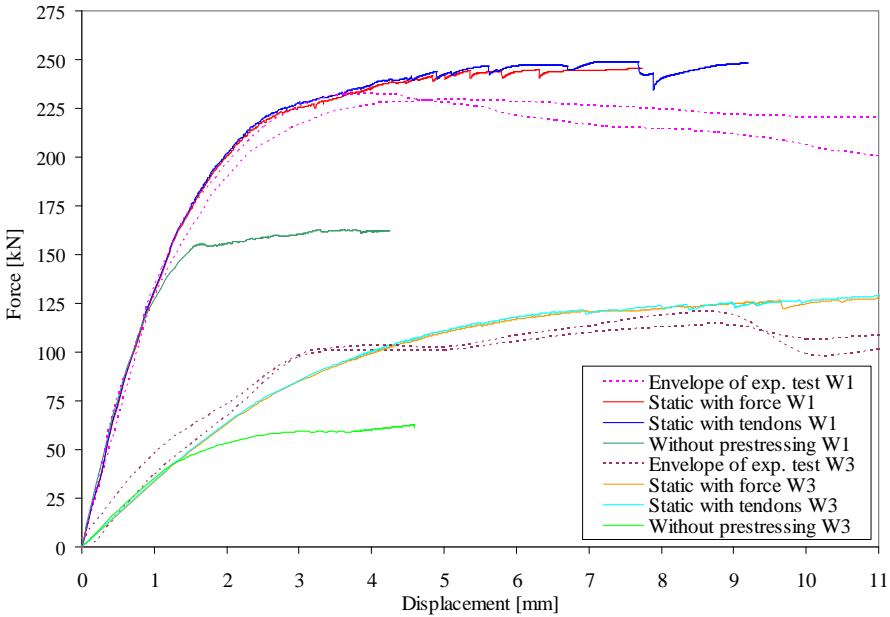


Fig. 6-33: Horizontal load displacement diagram – Numerical results of static loading and experimental envelope of static cyclic loading

The comparison in Fig. 6-33 of simulated load displacement curves without and with prestressing shows clearly the increase in shear resistance, which doubles for wall 3 and is enlarged at approximately 50% in case of wall 1. Due to the similarity of static cyclic simulations mainly static investigations are used for the numerical comparisons of prestressed and non-prestressed walls. The experimental envelope of wall 3 [Budelmann et al. 2004] – which has been produced manually – contains unfortunately a difference between the measured static cyclic curve and fitted envelope in the first plastic range. The difference of the calculated curve and the envelope is mainly caused by this mistake in this range. Moreover, the envelopes scatter for positive and negative displacement, which are shown in the same quadrant of this diagram by means of the same colour and dashing for each wall. In general, the static curves overestimate the measured shear capacity slightly, which is a result of neglected stiffness

and strength degradation, though included in the envelope of static cyclic test, but not considered in the static simulations. Furthermore, the parameter selection for the numerical models could deal with lower strength, which otherwise would lead to convergence problems. The last have to be reduced significantly, to allow probabilistic simulations that base on this parameter calibration. Therefore, this compromise is accepted.

As stated above, the impact of prestressing on the damage of the units differs for the simulations of wall 1 (see Fig. 6-23) and wall 3 (see Fig. 6-28). In addition, this local unit damage is nearly equal for the prestressed and non-prestressed wall 4 (see Fig. 6-37). This damage is slightly greater for prestressing. In case of wall 1 the damage seems to double, if the wall is not prestressed. Consequently, vertical prestressing would be very useful, in contrast to wall 3 and wall 4. The dynamic case study of Section 6.2.2 exhibits likewise greater local damage due to prestressing.

As a first proceeding to find the reason or an interrelation, the progression of local unit damage in dependency of horizontal loading (in terms of top displacement  $u_x$ ) is presented in diagrams. Fig. 6-34 compares not only such damage histories of non-prestressed and prestressed version of wall 1 and 3, but also the two different means to model prestressing by tendons or by external forces. Very interesting is the intersection of the local damage curves of wall 1. Thus, it may depend on the horizontal load level, whether prestressing has an advantageous or disadvantageous influence on the maximal local unit damage. For this compact wall, prestressing reduces the local unit damage up to a drift of approximately 2.3 mm. Thereafter, it increases significantly. In case of wall 3, the prestressing lead to greater local unit damage throughout the whole load history. Closed to 3 mm horizontal displacement, the damage degree is quite similar. If tendons are used to model prestressing, higher damages are computed in the range of high loading, whereas the means of modelling has no impact for low loading.

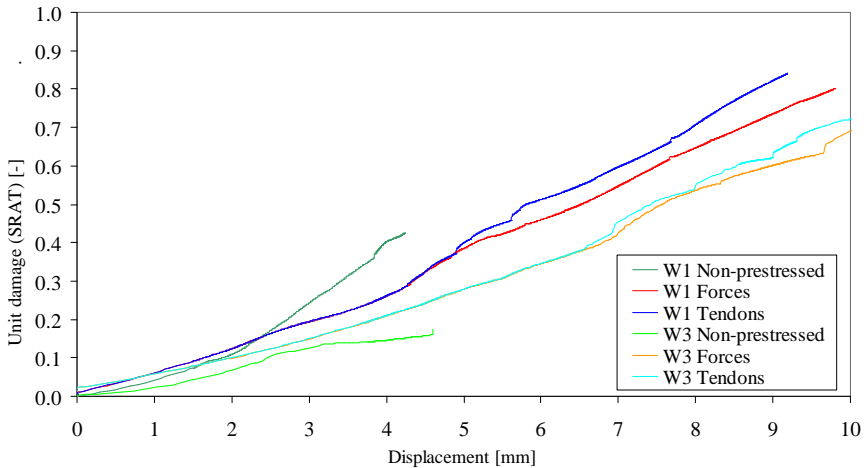


Fig. 6-34: Horizontal displacement versus local unit damage – Numerical results of static loading for wall 1 and wall 3

In addition, the global unit damage is displayed in Fig. 6-35, which exhibits clearly higher global unit damage in the case of prestressing for both walls. Note, that throughout this thesis ‘global damage’ is referred to as average global damage, as already explained in Section 4.3.4. Thus, a comparison of different walls and a use of different numerical meshes is admissible. For both prestressed walls small initial global damage can be observed as a result of vertical prestressing.

The slender wall 3 is more damaged in the initial state than the compact wall. The simple reason is the vertical stress. The cross section of wall 1 doubles, while the prestress level for both walls is nearly equal, as already pointed out in Section 4.2.4.2 (see Tab. 4-2). The high vertical stresses in wall 3 causes greater initial local unit damages. The means to model prestressing has no significant impact on the global damage.

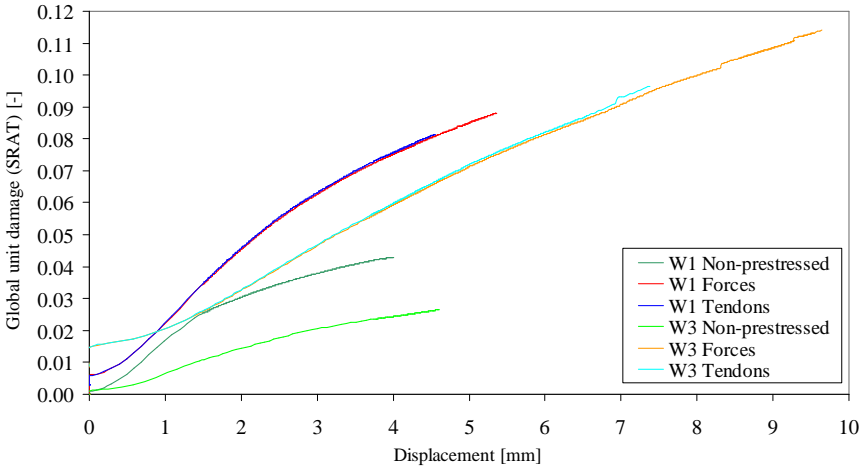


Fig. 6-35: Horizontal displacement versus global unit damage – Numerical results of static loading for wall 1 and wall 3

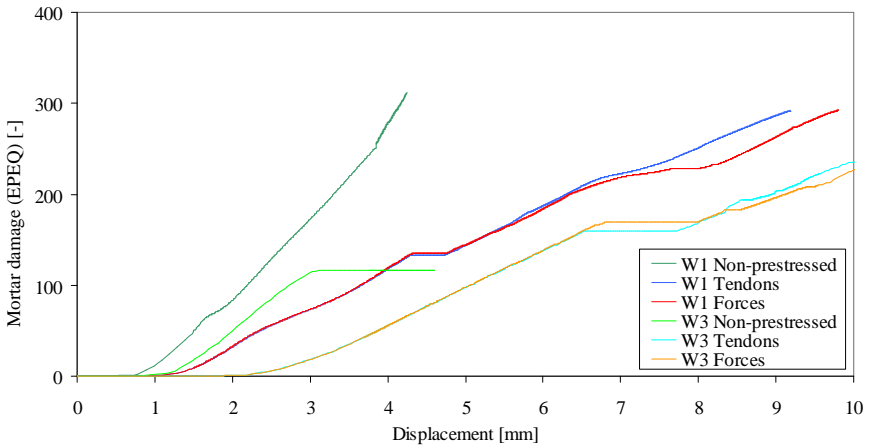


Fig. 6-36: Horizontal displacement versus local mortar damage – Numerical results of static loading for wall 1 and wall 3

To check also the impact on mortar more in depth, the same comparison is given in Fig. 6-36 for the local mortar damage. The positive influence of prestressing on the local mortar damage may be easily seen for both walls. No very important influence of the manner to simulated prestressing becomes visible. Since, the results scatter quite high and especially for the local unit damage contrary impacts occur. The result presentation is briefly extended to wall 4, which is static

loaded as well, for a non-prestressed and a prestressed version. First, the unit and mortar damage distributions are presented in Fig. 6-37 and Fig. 6-38 as well as the meaningful equivalent plastic strain in Fig. 6-39. The last is significantly reduced by vertical prestressing, not only on local contemplation, but also on global one. The prestressing effects slightly greater local unit damage. This is true for the whole load history as shown in the damage displacement diagram of Fig. 6-42. The global unit damage is clearly higher, which is also exactly expressed in Fig. 6-43. The local mortar damage is likewise displayed in a diagram of Fig. 6-41. The same trend than for wall 1 and 3 becomes visible. This damage is strongly reduced by the strengthening measure.

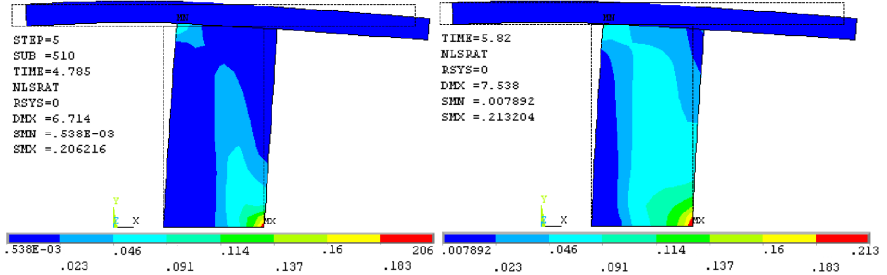


Fig. 6-37: Wall 4 – Unit damage of static loading on  $u_x = 4.35$  mm, Left: Non-prestressed, Right: Prestressed

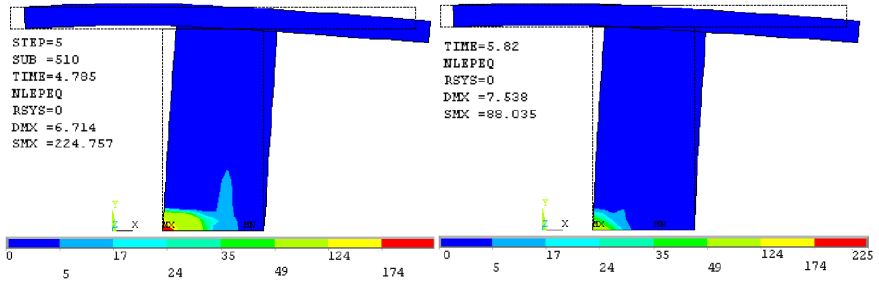


Fig. 6-38: Wall 4 – Mortar damage of static loading on  $u_x = 4.35$  mm, Left: Non-prestressed, Right: Prestressed

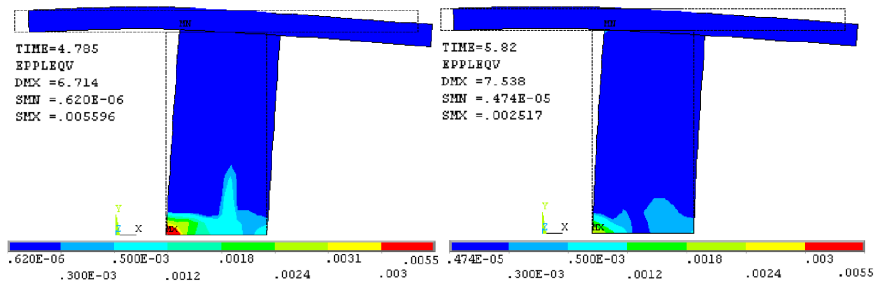


Fig. 6-39: Wall 4 – Equivalent plastic strain of static loading on  $u_x = 4.35$  mm, Left: Non-prestressed, Right: Prestressed

The horizontal displacement  $u_x$  of the upper middle point of wall 4 versus the horizontal reaction forces are presented in Fig. 6-40, in blue for the numerical results of the prestressed wall and in magenta for the non-prestressed one. Also here, the important increase of shear capacity becomes visible. The computed results are related to static loading as well as the distributions of Fig. 6-37, Fig. 6-38 and Fig. 6-39. In addition, the experimental envelopes of the static cyclic tests are depicted in red dashed line. Both curves – of the first and the third quadrant – are shown together in the first one, to express the scatter. As already explained, the static and static cyclic curves are not comparable, strictly speaking. However, it is done to get an idea of the correct trend of the numerical static load displacement curves. In case of prestressing, the numerical static curve is similar to the experimental one. The results are plausible.

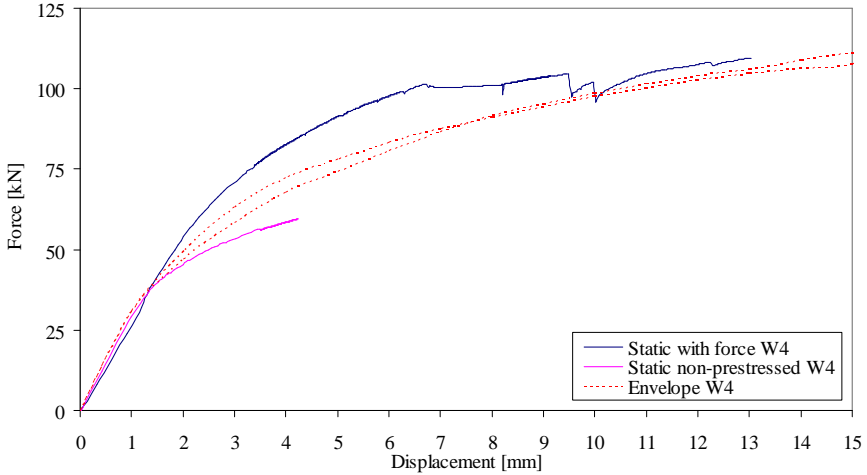


Fig. 6-40: Wall 4 - Horizontal load displacement diagram – Numerical results of static loading and experimental envelope of static cyclic loading

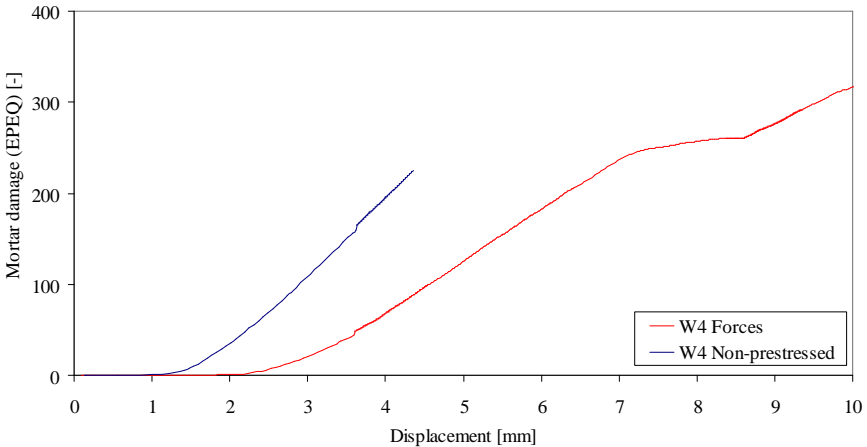


Fig. 6-41: Horizontal displacement versus local mortar damage – Numerical results of static loading for wall 4

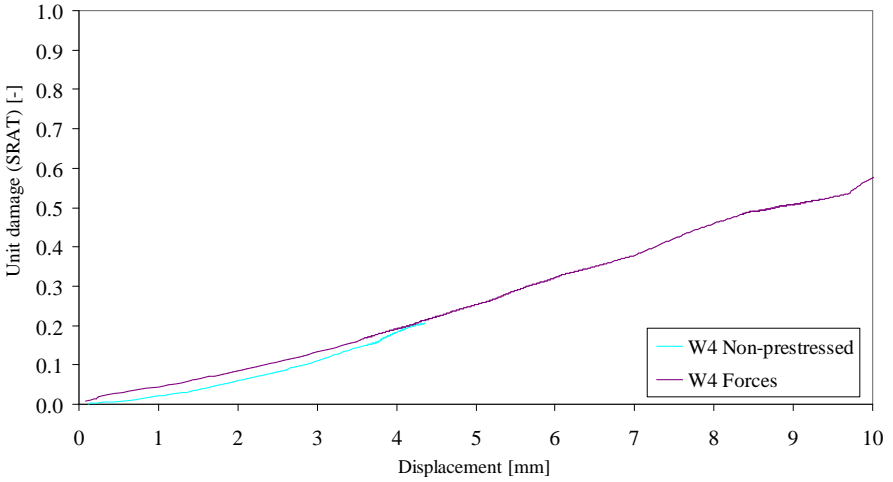


Fig. 6-42: Horizontal displacement versus local unit damage – Numerical results of static loading for wall 4

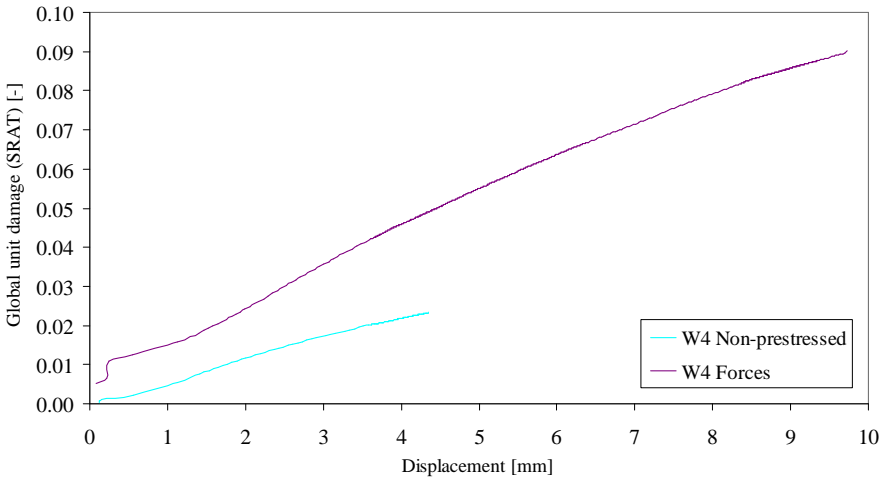


Fig. 6-43: Horizontal displacement versus global unit damage – Numerical results of static loading for wall 4

This section concludes with the recognition, that the used material model of Lagomarsino and Gambarotta [Gambarotta and Lagomarsino 1997b] provides a good description of the loadbearing behaviour and effects of degradation as well as dissipation for all investigated prestressed and non-prestressed walls. Thus, an utilisation for additional dynamic investigations is justified.

### 6.3.2 Earthquake simulation with and without prestressing

In case of static action, the usefulness of vertical prestressing is generally uncontested to achieve an increased shear capacity. Regarding a damage-based design, the results of the previous sections indicate a disadvantage for the unit damage, which usually increases with the vertical loading. Moreover, the impact of vertical prestressing is investigated for dynamic loading. In Chap. 5 the existence of an impact of prestressing on the dynamic behaviour is verified and elaborately explained, additional by numerical simulations for impact loading in 6.2.2. Experimental tests with shaking tables are very costly. Thereupon, a funding to investigate vertical prestressed masonry with tendons inside the walls was not available up to now. To get information about the usefulness of prestressing in case of earthquake, the behaviour of wall 1 as well as wall 3 is simulated. The used earthquakes are the base of the probabilistic investigation given in 6.3.3 and for the risk estimation in Chap. 8. Time histories, related spectra and further describing parameters of these earthquakes are lengthily given in Section 3.6.2 as well as in Appendix B for wall 3 and Appendix C for wall 1.

Also in this Section, the damage is expressed by means of the damage parameters (see Section 4.3.4). In the ANSYS<sup>®</sup>-files and in the optiSLang<sup>®</sup>-files (regarding input as well as output), the abbreviations of Tab. 6-9 are used. The symbols are given as well. First, the results of wall 1 are presented, which is subjected to one earthquake load level only. In contrast three levels are used to investigate wall 3, one for each return period as explained in Section 3.6.2. This is done with regard to an extended risk analysis for wall 3 (see Section 6.3.3.2 and Chap. 8).

Symbol	Abbr. in file	Damage parameter description
$\max  u_{h,rel} $	uhrel	Absolute maximal horizontal top displacement
$\max \alpha_{b,loc}$	SRATloc	Maximal local brick damage
$\max \alpha_{b,glo}$	SRATglob_av	Maximal average global brick damage
$\max \alpha_{m,loc}$	EPEQloc	Maximal local mortar damage
$\max \alpha_{m,glo}$	EPEQglob_av	Maximal average global mortar damage
$\max \varepsilon_{eq}^{pl}$	EQV	Maximal plastic equivalent strain
$\max \varepsilon_{xy}^{pl}$	EPPLXY	Maximal plastic shear strain
$\max \varepsilon_{y,t}^{pl}$	EPPLYtens	Maximal vertical plastic tensile strain
$\max \varepsilon_{y,c}^{pl}$	EPPLYcomp	Maximal vertical plastic compressive strain

Tab. 6-9: Notation of the used damage parameters

For both, wall 1 and wall 3 the same conditions, material parameters (regarding the previous calibration) and vertical loads are used like in the previous section. An exception is the loading of upper storeys. In the static and cyclic simulations forces are used, whereas in the following dynamic simulations the upper storey loads are modelled more realistically with masses to compute the important bracing wall of the first floor. On the one hand, the walls are modelled without prestressing and are subjected to the earthquakes. On the other hand, they are prestressed. This is done by the two different manners with external forces and more accurate with tendons. The results of both walls are summarised in tables, in order to have a good overview about the impact of prestressing in dependency on the different earthquakes and the means to model prestressing. For the selected earthquakes, detailed presentations are given by means of damage distributions and diagrams for the vibration behaviour.

#### 6.3.2.1 Wall 1

In comparison to wall 3, wall 1 has a much higher resistance in terms of shear capacity. Thus, it is subjected to stronger earthquakes. Otherwise, the wall 1 would be loaded only in the elastic

range, which is not reasonable for damage assessment. The earthquakes are elaborately presented in Appendix C. Their characteristics of these seven artificial generated earthquakes are summarised by means of important parameters in the first table of Appendix C. Thereafter, the spectra and time histories are depicted in pictures. The seven earthquakes increase in duration. The steady phase duration is used as label throughout this thesis. The first earthquake has a steady phase duration of 2.5 s, while the last one has such a duration of 8.5 s. Since the steady phase duration is not a common reasonable parameter in seismology, also the related uniform duration is also given in Appendix C.

In Tab. 6-10 the maximal damages of each parameter and each of the three wall models (non-prestressed, prestressing modelled by means of external forces and tendons) are summarised for every earthquake. In order to have a good overview about the impact of prestressing, the maxima of each parameter are underlined per earthquake, while the minima are written in italic numbers. In the event of equality or nearly equality, the numbers are not marked. Hence, it is easily visible, if something has no impact on this damage parameter. The irregularity regarding the impact of prestressing becomes simply clear by the alternation of underlined numbers (representing the maxima) between white fields (which symbols the non-prestressed wall) and coloured field (which symbols the prestressed wall) per each earthquake row. Since the earthquake level is approximately equal (in average approximately  $4 \text{ m/s}^2$ ), it cannot be the reason for the unexpected alternating tendency.

Probably, the different characteristics of each time history cause these results, taking into account the different frequency contents and natural frequencies of the walls, which change during the earthquake. Earthquake 2.5 leads to higher damages in the non-prestressed wall for all parameters, except the global unit damage. This goes in line, with the results of the static analysis of wall 1 in Section 6.3.1 (see Fig. 6-23, Fig. 6-34 and Fig. 6-35). For the remaining earthquakes the mortar damage, the equivalent plastic strain, the plastic shear strain and the vertical plastic tensile strain are reduced by prestressing. However, the storey drift is slightly higher for all earthquakes, except earthquake 2.5. The results for the local unit damage differ strongly. No correlation can be found in this table. As to expect, the vertical plastic compressive strain is always greater for prestressing. This is not true for earthquake 2.5.

Earthquakes			Wall	Damage parameters								
Steady Phase Duration	Arias Intensity AI	PGA	1	max $ u_{h,rel} $	max $\alpha_{h,loc}$	max $\alpha_{h,glo}$	max $\alpha_{m,loc}$	max $\alpha_{m,glo}$	max $\epsilon^{pl}_{eq}$	max $\epsilon^{pl}_{xy}$	max $\epsilon^{pl}_{y,t}$	max $\epsilon^{pl}_{y,c}$
[s]	[m/s]	[m/s <sup>2</sup> ]		[mm]	[-]	[-]	[-]	[-]	[%]	[%]	[%]	[%]
2.5	1.94	4.31	Non-prestr.	<u>2.09</u>	<u>0.145</u>	<i>0.043</i>	<u>145.9</u>	<u>3.55</u>	<u>3.89</u>	<u>1.94</u>	<u>5.68</u>	<u>-0.13</u>
			Forces	1.85	0.126	<u>0.052</u>	33.3	0.47	1.05	0.42	1.54	-0.12
			Tendons	<u>1.70</u>	<i>0.117</i>	0.048	<u>19.3</u>	<u>0.26</u>	<u>0.68</u>	<u>0.33</u>	<u>0.99</u>	<u>-0.11</u>
3.5	2.27	3.76	Non-prestr.	2.79	<u>0.268</u>	<i>0.048</i>	<u>128.1</u>	<u>6.80</u>	<u>3.49</u>	<u>3.53</u>	<u>5.12</u>	<u>-0.31</u>
			Forces	<u>3.49</u>	0.255	0.086	75.1	4.22	2.18	1.96	<u>3.21</u>	-0.36
			Tendons	<u>3.48</u>	<i>0.254</i>	0.086	<u>74.8</u>	<u>4.01</u>	2.19	2.07	<u>3.22</u>	-0.36
4.5	2.45	3.50	Non-prestr.	3.37	0.305	<i>0.061</i>	<u>166.3</u>	<u>7.83</u>	<u>4.36</u>	<u>4.64</u>	<u>6.27</u>	<u>-0.38</u>
			Forces	4.00	<i>0.287</i>	0.094	<u>116.1</u>	<u>5.10</u>	<u>3.21</u>	<u>2.82</u>	<u>4.61</u>	-0.42
			Tendons	<u>4.45</u>	<u>0.321</u>	<u>0.100</u>	132.9	5.67	3.60	<u>2.40</u>	<u>5.14</u>	<u>-0.50</u>
5.5	2.38	3.95	Non-prestr.	2.93	<u>0.261</u>	<i>0.053</i>	<u>278.7</u>	<u>6.29</u>	<u>6.77</u>	<u>4.19</u>	<u>9.61</u>	<u>-0.31</u>
			Forces	<u>3.46</u>	<i>0.253</i>	<u>0.089</u>	85.6	3.25	2.51	<u>1.71</u>	<u>3.65</u>	<u>-0.35</u>
			Tendons	error								
6.5	2.21	4.40	Non-prestr.	2.77	<i>0.213</i>	<i>0.050</i>	<u>270.7</u>	<u>6.46</u>	<u>6.64</u>	<u>3.60</u>	<u>9.59</u>	<u>-0.24</u>
			Forces	<u>3.25</u>	<u>0.242</u>	0.085	61.9	2.49	1.90	1.36	2.76	-0.32
			Tendons	<u>3.19</u>	0.241	<u>0.086</u>	68.8	2.65	1.98	1.48	2.88	-0.32
7.5	2.58	4.17	Non-prestr.	<u>3.28</u>	<u>0.30</u>	<i>0.051</i>	<u>185.1</u>	<u>6.78</u>	<u>4.91</u>	<u>3.71</u>	<u>6.83</u>	<u>-0.38</u>
			Forces	3.45	<i>0.247</i>	0.089	154.2	4.80	4.07	2.12	5.87	-0.34
			Tendons	<u>3.91</u>	0.268	<u>0.090</u>	<u>108.8</u>	<u>4.44</u>	3.03	2.47	<u>4.40</u>	<u>-0.39</u>
8.5	2.44	4.50	Non-prestr.	3.03	0.265	<i>0.052</i>	<u>151.9</u>	<u>6.50</u>	<u>4.09</u>	<u>4.04</u>	<u>5.84</u>	<u>-0.31</u>
			Forces	3.77	0.269	0.093	98.7	4.53	2.80	2.20	4.02	-0.39
			Tendons	<u>3.91</u>	<u>0.285</u>	0.093	113.1	5.06	3.19	3.28	<u>4.57</u>	<u>-0.42</u>

Tab. 6-10: Maximal damage parameters summarised for the related earthquakes, wall 1, maxima (underlined) and minima (italic) are marked per column

In Fig. 6-44 until Fig. 6-48 the behaviour for earthquake 7.5 is presented in detail. First, the unit damage is compared for the non-prestressed wall and prestressing with tendons in Fig. 6-44. The maximal local damage occurs in the non-prestressed wall, as well for the mortar damage (see Fig. 6-45).

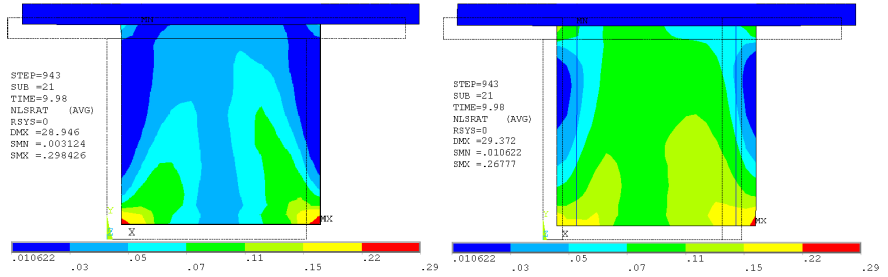


Fig. 6-44: Wall 1, steady phase duration of 7.5 s – Unit damage of static loading on  $t = 9.98$  s, Left: Non-prestressed, Right: Prestressed

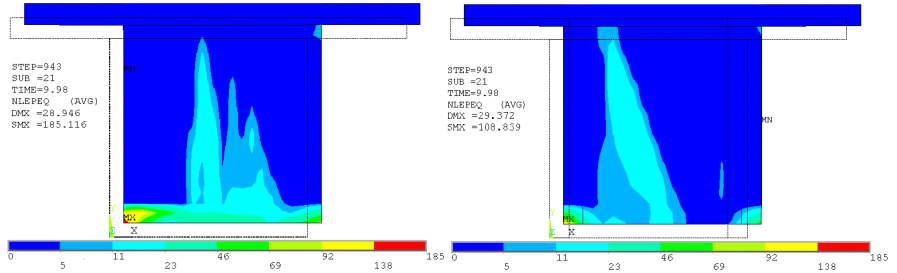


Fig. 6-45: Wall 1, steady phase duration of 7.5 s – Mortar damage of static loading on  $t = 9.98$  s, Left: Non-prestressed, Right: Prestressed

The vibration behaviour of the non-prestressed and prestressed wall is quite similar (see Fig. 6-46). The greater amplitudes can be observed for the prestressed version.

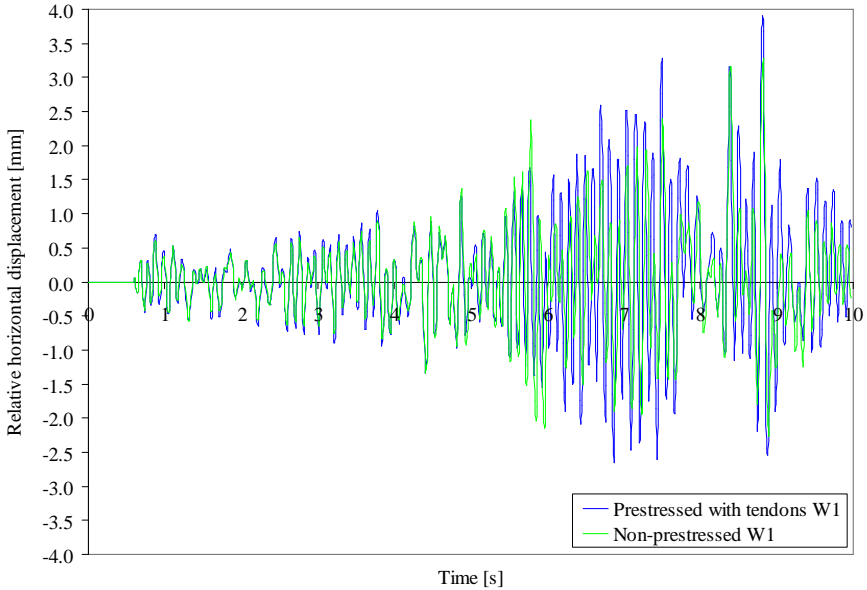


Fig. 6-46: Storey drift in dependency of time for non-prestressed and prestressed wall 1, steady phase duration of 7.5 s

Thereafter, the unit damages are presented, local one in Fig. 6-47 and global damage in Fig. 6-48. Both develop stepwise. Whereas, the sudden increases goes in line with the maximal storey drifts, which are caused by acceleration peaks. Especially, Fig. 6-47 exhibits, that the local damage is irregularly greater for the prestressed or the non-prestressed one, which depends on the time. For the most time the local unit damage is higher in case of prestressing (blue curve). However, in the end of the calculation the absolute value of local unit damage is greater for the non-prestressed wall (green curve). Despite this value is shown in Tab. 6-10 automatically, and represents not the whole truth. Regarding the global damage, prestressing is clearly disadvantageous. Only a slight impact of the means to model prestressing (forces or tendons) on the damage parameters can be observed.

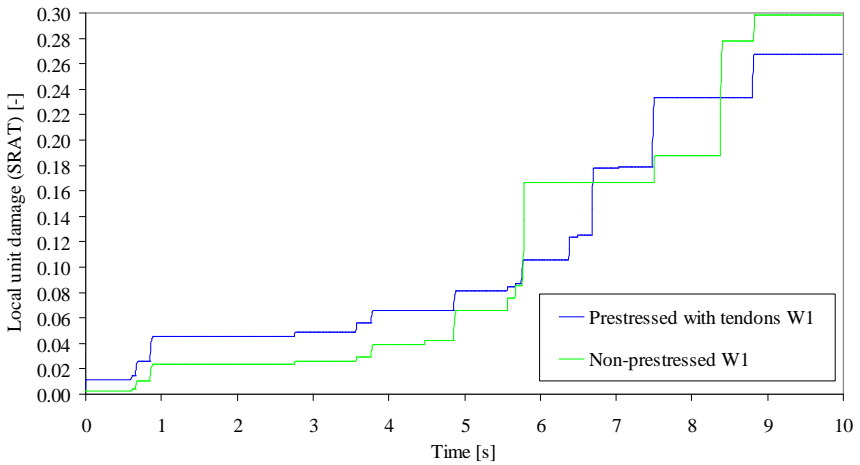


Fig. 6-47: Local unit damage in dependency of time for non-prestressed and prestressed wall 1, steady phase duration of 7.5 s

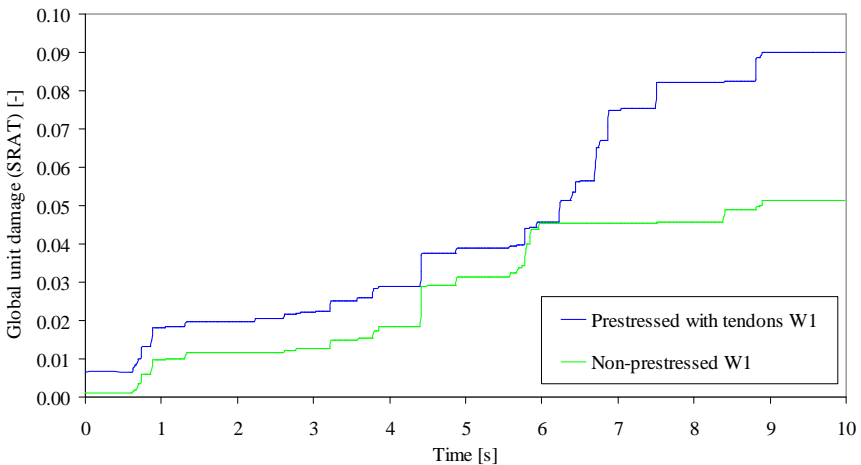


Fig. 6-48: Global unit damage in dependency of time for non-prestressed and prestressed wall 1, steady phase duration of 7.5 s

### 6.3.2.2 Wall 3

Subsequently, the dynamic results of wall 3 are presented for each of the three return periods (earthquake load levels), which are the base for the probabilistic and risk analysis (see Chap. 8). The earthquake is described in Section 3.6.2 and Appendix B. Here, only four different steady state durations are taken into account. This means, only four different accelerograms are applied and the difference in duration is smaller. Related to each return period, the maximal damages of each parameter and each of the three wall models are summarised for every earthquake in Tab. 6-10 until Tab. 6-13. As already pointed out above for wall 1, the maxima of the each pa-

parameter are underlined, while the minima are written in italic numbers for every earthquake row, in order to improve the visibility. For the low level earthquakes related to the return period of 475 years, significant differences between the two manners to model prestressing cannot be observed often.

Numerous damage parameters are zero for the prestressed wall. The irregularity appears to be more complex in case of wall 3 and increases with the level of seismic excitation. Anyway, throughout all earthquakes, the mortar damages and the equivalent plastic strain is reduced by prestressing. The unit damages – both local and global – are increased due to prestressing. Two exceptions exits in for the 10000 years return period (see Tab. 6-13) for the local unit damage. The plastic shear strain is greater in case of prestressing for low seismic action (return period of 475 and 2000 years). The opposite occurs for strong earthquakes (10000 years return period) as given in Tab. 6-13. The vertical plastic tensile strains are reduced due to prestressing for all earthquakes. In contrast, the vertical plastic compressive strain is always greater for prestressed versions of wall 3, which is also observed above for wall 1. However, the remaining plastic compressive strain is much smaller, than the remaining vertical tensile strain. Thus, the benefit due to the strengthening measure is good regarding these parameters. The storey drift is slightly higher for all small earthquakes that belong to the return period of 475 years, for the non-prestressed wall. The opposite occurs for the medium earthquakes (return period of 1000 years), while the results are very irregular for the strong seismic action (see Tab. 6-13). The local mortar damage is always higher for the non-prestressed wall, which is caused by the high slenderness. In general, these dynamic results go in line, with the results of the static analysis of wall 3 in Section 6.3.1.

a) Return period of 475 years

Earthquakes RP=475			Wall	Damage parameters									
Steady Phase Duration	Arias Intensity AI	PGA	3	max $u_{h,rel}$	max $\alpha_{b,loc}$	max $\alpha_{b,glo}$	max $\alpha_{m,loc}$	max $\alpha_{m,glo}$	max $\varepsilon_{eq}^{pl}$	max $\varepsilon_{xy}^{pl}$	max $\varepsilon_{y,t}^{pl}$	max $\varepsilon_{y,c}^{pl}$	
[s]	[m/s]	[m/s <sup>2</sup> ]		[mm]	[-]	[-]	[-]	[-]	[%]	[%]	[%]	[%]	
4.5	0.13	0.86	Non-prestr.	<u>1.18</u>	<i>0.030</i>	<i>0.009</i>	4.61	0.15	0.19	0.08	<u>0.28</u>	<i>-0.01</i>	
			Forces	1.13	<u>0.065</u>	0.026	0.00	0.00	0.09	0.15	0.00	-0.05	
			Tendons	<u>1.10</u>	0.063	0.026	0.00	0.00	0.09	0.15	0.00	-0.05	
5.5	0.15	1.21	Non-prestr.	<u>1.28</u>	<i>0.033</i>	<i>0.010</i>	8.74	0.22	<u>0.35</u>	0.08	<u>0.52</u>	<i>-0.02</i>	
			Forces	<u>1.15</u>	0.066	0.026	0.00	0.00	0.09	0.15	0.00	-0.05	
			Tendons	1.17	0.066	0.026	0.00	0.00	0.10	<u>0.16</u>	0.00	-0.05	
6.5	0.14	0.93	Non-prestr.	<u>1.53</u>	<i>0.045</i>	<i>0.014</i>	24.86	0.59	<u>0.81</u>	0.12	<u>1.22</u>	<i>-0.03</i>	
			Forces	<u>1.67</u>	<u>0.090</u>	<u>0.035</u>	0.14	0.00	0.14	0.23	0.00	-0.08	
			Tendons	1.62	0.087	0.033	0.09	0.00	0.14	0.23	0.00	-0.08	
7.5	0.16	0.92	Non-prestr.	1.41	<i>0.040</i>	<i>0.013</i>	21.12	<u>0.40</u>	<u>0.71</u>	0.10	<u>1.06</u>	<i>-0.02</i>	
			Forces	1.41	<u>0.077</u>	0.030	0.00	0.00	0.12	0.19	0.00	-0.06	
			Tendons	<u>1.39</u>	0.076	0.030	0.00	0.00	0.12	0.19	0.00	-0.06	

Tab. 6-11: Maximal damage parameters summarised for the related earthquakes, wall 3, return period of 475 years, maxima (underlined) and minima (italic) are marked per column

## b) Return period of 2000 years

Earthquakes RP=2000			Wall	Damage parameters								
Steady Phase Duration	Arias Intensity AI	PGA	3	max $u_{h,rel}$	max $\alpha_{b,loc}$	max $\alpha_{b,glo}$	max $\alpha_{m,loc}$	max $\alpha_{m,glo}$	max $\varepsilon_{eq}^{pl}$	max $\varepsilon_{xy}^{pl}$	max $\varepsilon_{yt}^{pl}$	max $\varepsilon_{yc}^{pl}$
[s]	[m/s]	[m/s <sup>2</sup> ]		[mm]	[-]	[-]	[-]	[-]	[%]	[%]	[%]	[%]
4.5	0.20	1.38	Non-prestr.	<i>1.59</i>	<i>0.047</i>	<i>0.015</i>	<u>23.54</u>	<u>0.59</u>	<u>0.77</u>	<i>0.13</i>	<u>1.16</u>	<i>-0.03</i>
			Forces	<u>1.71</u>	<u>0.091</u>	0.034	0.25	0.00	0.15	0.24	0.01	-0.08
			Tendons	1.70	0.090	0.034	<u>0.21</u>	0.02	0.15	0.24	0.01	-0.08
5.5	0.21	1.42	Non-prestr.	<i>1.91</i>	<i>0.065</i>	<i>0.018</i>	<u>64.70</u>	<u>1.33</u>	<u>1.91</u>	<i>0.18</i>	<u>2.87</u>	<i>-0.05</i>
			Forces	2.22	0.115	0.043	0.94	0.02	<u>0.20</u>	0.33	0.07	-0.11
			Tendons	2.22	0.115	0.043	0.94	0.02	0.21	<u>0.33</u>	0.07	<u>-0.12</u>
6.5	0.25	1.20	Non-prestr.	<i>1.96</i>	<i>0.067</i>	<i>0.018</i>	<u>48.32</u>	<u>1.06</u>	<u>1.34</u>	<i>0.20</i>	<u>2.00</u>	<i>-0.05</i>
			Forces	2.13	0.108	0.040	0.87	0.02	<u>0.19</u>	0.31	<u>0.06</u>	-0.11
			Tendons	<u>2.15</u>	<u>0.111</u>	<u>0.042</u>	0.99	0.02	0.20	<u>0.32</u>	0.07	-0.11
7.5	0.25	1.48	Non-prestr.	<i>1.95</i>	<i>0.067</i>	<i>0.019</i>	<u>81.14</u>	<u>1.63</u>	<u>2.34</u>	<i>0.19</i>	<u>3.50</u>	<i>-0.05</i>
			Forces	<i>1.90</i>	0.102	0.038	<i>0.45</i>	0.01	<u>0.17</u>	0.28	<u>0.02</u>	-0.10
			Tendons	<u>1.98</u>	<u>0.104</u>	<u>0.039</u>	0.54	0.01	0.18	<u>0.29</u>	0.03	-0.10

Tab. 6-12: Maximal damage parameters summarised for the related earthquakes, wall 3, return period of 2000 years, maxima (underlined) and minima (italic) are marked per column

## c) Return period of 10000 years

Earthquakes RP=10000			Wall	Damage parameters								
Steady Phase Duration	Arias Intensity AI	PGA	3	max $u_{h,rel}$	max $\alpha_{b,loc}$	max $\alpha_{b,glo}$	max $\alpha_{m,loc}$	max $\alpha_{m,glo}$	max $\varepsilon_{eq}^{pl}$	max $\varepsilon_{xy}^{pl}$	max $\varepsilon_{yt}^{pl}$	max $\varepsilon_{yc}^{pl}$
[s]	[m/s]	[m/s <sup>2</sup> ]		[mm]	[-]	[-]	[-]	[-]	[%]	[%]	[%]	[%]
4.5	6.12	2.05	Non-prestr.	<i>3.12</i>	<i>0.175</i>	<i>0.031</i>	<u>161.97</u>	<u>4.84</u>	<u>4.11</u>	<u>1.59</u>	<u>6.13</u>	<i>-0.18</i>
			Forces	3.33	0.178	0.061	<u>24.56</u>	<u>0.37</u>	<u>0.81</u>	<u>0.86</u>	<u>1.21</u>	-0.22
			Tendons	<u>3.44</u>	<u>0.187</u>	<u>0.064</u>	29.05	0.48	0.96	0.90	1.43	<u>-0.23</u>
5.5	6.46	1.90	Non-prestr.	<u>3.28</u>	<u>0.209</u>	<i>0.035</i>	<u>217.04</u>	<u>6.14</u>	<u>5.37</u>	<u>3.05</u>	<u>7.94</u>	<i>-0.21</i>
			Forces	2.87	0.149	<u>0.055</u>	12.09	0.18	0.47	0.44	0.69	-0.17
			Tendons	<u>2.54</u>	<u>0.132</u>	0.049	5.67	<u>0.09</u>	<u>0.24</u>	<u>0.38</u>	<u>0.20</u>	<i>-0.14</i>
6.5	6.90	1.96	Non-prestr.	<u>3.24</u>	<u>0.192</u>	<i>0.033</i>	<u>268.01</u>	<u>6.34</u>	<u>6.54</u>	<u>3.05</u>	<u>9.64</u>	<i>-0.20</i>
			Forces	2.75	0.144	<u>0.053</u>	9.76	0.15	0.39	0.42	0.57	-0.16
			Tendons	<u>2.45</u>	<u>0.127</u>	0.048	4.21	<u>0.07</u>	<u>0.23</u>	<u>0.37</u>	<u>0.25</u>	<i>-0.13</i>
7.5	8.17	2.15	Non-prestr.	<i>3.20</i>	<i>0.172</i>	<i>0.031</i>	<u>161.86</u>	<u>5.21</u>	<u>4.20</u>	<u>2.14</u>	<u>6.17</u>	<i>-0.17</i>
			Forces	3.31	0.174	0.063	<u>24.21</u>	<u>0.46</u>	<u>0.83</u>	0.88	<u>1.23</u>	-0.22
			Tendons	<u>3.38</u>	<u>0.181</u>	<u>0.064</u>	28.60	0.54	0.96	<u>0.86</u>	1.42	<u>-0.23</u>

Tab. 6-13: Maximal damage parameters summarised for the related earthquakes, wall 3, return period of 10000 years, maxima (underlined) and minima (italic) are marked per column

In Fig. 6-49 until Fig. 6-53 the behaviour for earthquake 7.5 is presented in detail. First, the unit damage is compared for the non-prestressed wall and prestressing with tendons in Fig. 6-49. The maximal local unit damage occurs in the prestressed wall, as well maximal mortar damage (see Fig. 6-50).

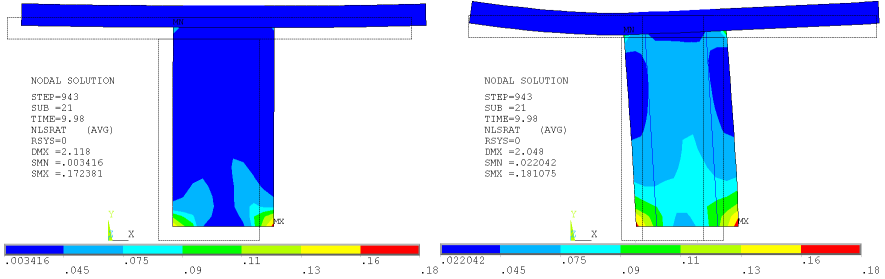


Fig. 6-49: Wall 3, return period of 10000 years, steady phase duration of 7.5 s – Unit damage of static loading at  $t = 9.98$  s, Left: Non-prestressed, Right: Prestressed

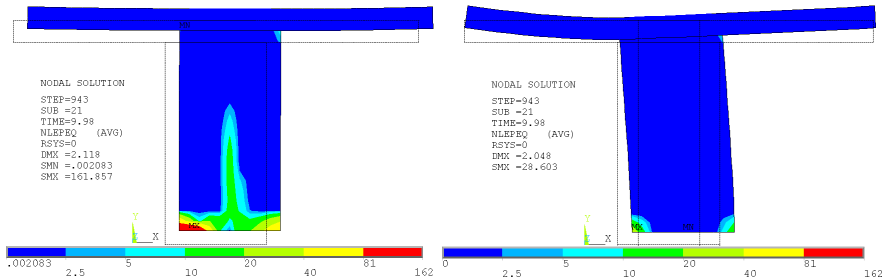


Fig. 6-50: Wall 3, return period of 10000 years, steady phase duration of 7.5 s – Mortar damage of static loading on  $t = 9.98$  s, Left: Non-prestressed, Right: Prestressed

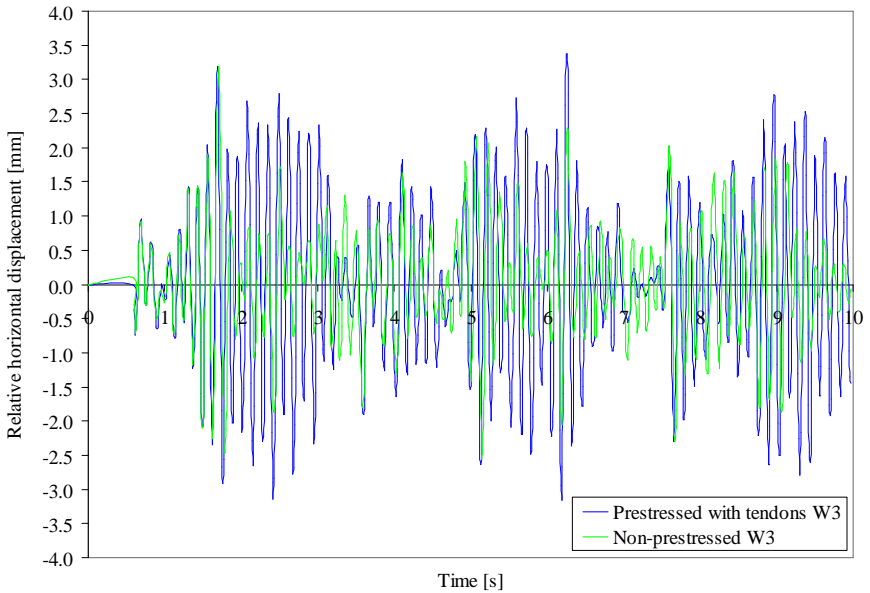


Fig. 6-51: Storey drift in dependency of time for non-prestressed and prestressed wall 3, return period of 10000 years, steady phase duration of 7.5 s

Similar trends between wall 1 (see Section 6.3.2.1) and wall 2 can be observed regarding the damage diagrams in Fig. 6-52 and Fig. 6-53. It depends on the observed time, whether the local unit damage is higher for prestressing. In contrast, the global unit damage is always greater in case of prestressing. In difference to wall 1 (at least for the 2.5 earthquake), the vibration behaviour is more influenced due to prestressing as displayed in Fig. 6-51. This may be not stated for the general vibration behaviour over the whole time, but the differences in the peak amplitudes are significant, not so for wall 1 (see Fig. 6-44). In case of wall 3, the non-prestressed one appears more damped, which is not caused by other damping parameters, since they are equal. Due to the very high mortar damage the wall loses more stiffness and changes so the natural frequency more significantly. In the beginning of the earthquake, the amplitudes and the periods are still equal, while after important seismic excitation the period of the non-prestressed wall become longer. The last confirms stiffness degradation.

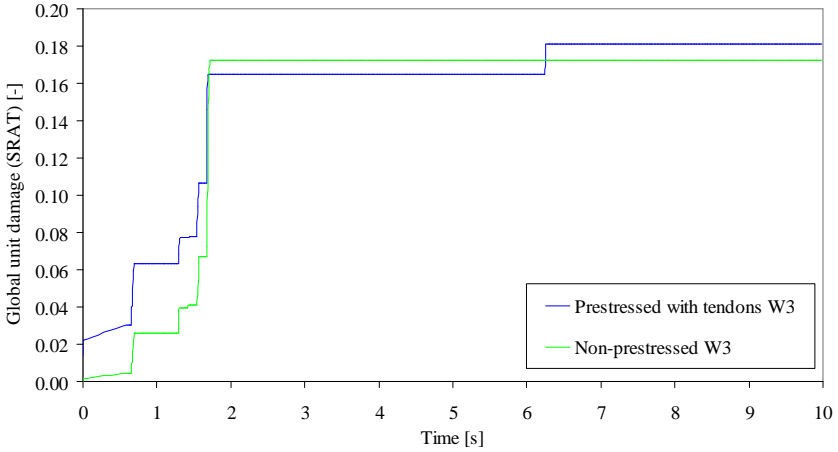


Fig. 6-52: Local unit damage in dependency of time for non-prestressed and prestressed wall 3, return period of 10000 years, steady phase duration of 7.5 s

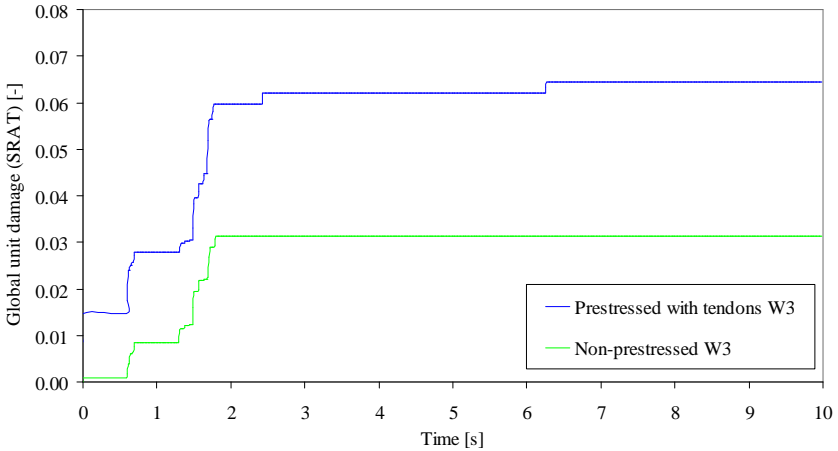


Fig. 6-53: Global unit damage in dependency of time for non-prestressed and prestressed wall 3, return period of 10000 years, steady phase duration of 7.5 s

### 6.3.3 Probabilistic earthquake simulation with and without prestressing

Mainly for the risk assessment in Chap. 8, the probabilistic analyses are carried out. However, further reasons are the observed irregularities in the dynamic results (see Section 6.3.2). The idea is to fix the trends of the impact of prestressing statistically. Of special interest is the unit damage. For this parameter, correlations could not be ensured above. Moreover, this damage parameter is very important, since it can influence the ductility meaningful. For the probabilistic simulations the advanced program optiSLang<sup>®</sup> is used throughout the thesis. It produces the scattering in the samples, executes ANSYS<sup>®</sup> to simulate all samples and evaluates the results statistically.

Latin hypercube sampling is used in the framework of robustness analyses. Sensitivities and probability density functions PDFs for the damage parameters are desired results. By means of the damage parameters – introduced in Section 4.3.4 – the damage is expressed in this section as well as above. Exactly the same numerical wall models and earthquakes of the dynamic analyses are used as mean values. However, these mean values scatter here.

### 6.3.3.1 Wall 1

The allowed range of scattering is defined by PDFs. The sequence of the variables (input parameters), their notation as well as related distribution types are listed in Tab. 6-14 for wall 1. Two probabilistic analyses are performed, one for the non-prestressed and one for the prestressed versions.

No.	Sym.	Abbr.	Variable	Distribution	Expected/mean	Standard deviation	Min.	Max.
Masonry:								
1	$\eta$	nuxy	Poisson's ratio	lognormal	0.15	0.25*0.15=0.0375	-	-
2	$\rho_M$	dens	Density of masonry	normal	1.65E-9 to/mm <sup>3</sup>	0.075*1.65E-9 =0.12375E-9 to/mm <sup>3</sup>	-	-
3	$E_M$	emod	Young's Modulus of masonry	normal	5800 N/mm <sup>2</sup>	0.1*5800=580 N/mm <sup>2</sup>	-	-
4	$\mu$	fric	Friction coefficient	lognormal	0.436	0.185*0.436=0.0807	-	-
5	$\sigma_{mr}$	mtens	Tensile strength of mortar joints	lognormal	0.87 N/mm <sup>2</sup>	0.35*0.87=0.3045 N/mm <sup>2</sup>	-	-
6	$\tau_{mr}$	mshea	Shear strength of mortar joints	lognormal	0.44 N/mm <sup>2</sup>	0.3*0.44=0.132 N/mm <sup>2</sup>	-	-
7	$\sigma_{br}$	comp	Compressive strength of masonry	lognormal	17.2 N/mm <sup>2</sup>	0.17*17.2=2.924 N/mm <sup>2</sup>	-	-
8	$\tau_{br}$	bshea	Shear strength of masonry	lognormal	2.5 N/mm <sup>2</sup>	0.15*2.5=0.375 N/mm <sup>2</sup>	-	-
Support condition - Stiffness of the concrete floor slab:								
9	$E_c$	EmodCon	Young's Modulus of concrete	truncated normal	14000 N/mm <sup>2</sup>	0.4*14000 = 5600 N/mm <sup>2</sup>	0.1	47600
Damping:								
10	$\alpha$	adamp	Rayleigh mass damping	uniform	0.62	-	0.4048	0.8352
11	$\beta$	bdamp	Rayleigh stiffness damping	uniform	0.0003	-	0.0001	0.0005
Loading:								
12	$X_{skal}$	xskal	Scaling factor for horizontal acceleration	lognormal	1	0.5*Mean	-	-
13	$Y_{skal}$	yskal	Scaling factor for vertical acceleration	lognormal	1	0.5*Mean	-	-
14	$\rho_M$	headmass	Density of mass of upper structure parts	truncated normal	2.19164E-7 to/mm <sup>3</sup>	0.4*2.19164E-7 =0.876656E-7 to/mm <sup>3</sup>	1.00E-10	1.15E-06
15	$D$	durat	Earthquakeduration of the steady phase	discrete uniform	-	2.5 3.5 4.5 5.5 6.5 7.5 8.5	2.5	8.5
16	$P$	PreFo	Sum of prestressing forces	lognormal	360000 N	360000*0.35=126000 N	-	-

Tab. 6-14: Parameters varied and applied distribution for wall 1

The results are presented and explained hereinafter. First of all the important correlation matrices are displayed in Fig. 6-54, which shows the linear correlation coefficients for each parameter (input and output). A red diagonal leaps into the eyes immediately, which represents the correlation of the parameters with itself (it has to be one and therefore red). The matrix is divided by

two lines into four parts. The lines separate input and output parameter. The output parameters are highly correlated with each other. In case of the vertical plastic compressive strain, the correlation is negative (blue line), caused by the negative sign. Since in the probabilistic analysis of the prestressed wall also the prestressing force is allowed to scatter, the left matrix contains one parameter more. The high sensitivities of the input parameters  $X_{skat}$  for the horizontal excitation and the head mass are easily visible.

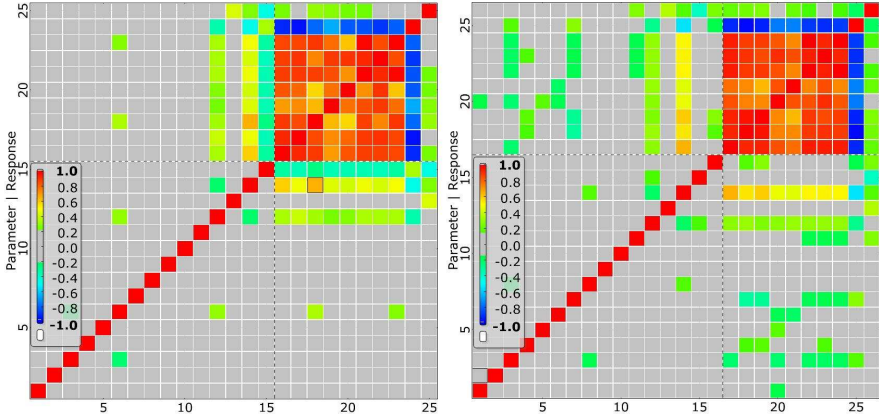


Fig. 6-54: Correlation matrices of wall 1, Left: Non-prestressed (15 input parameters), Right: Prestressed (16 input parameters)

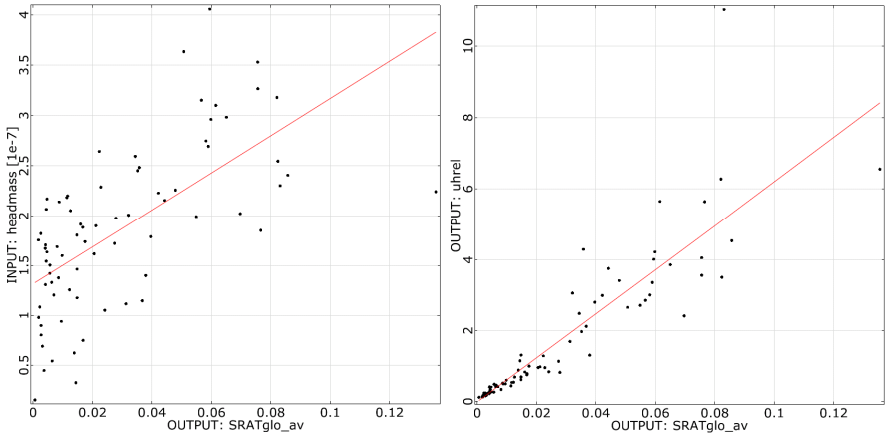


Fig. 6-55: Correlations for the non-prestressed wall, Left: Input parameter head mass with output parameter global unit damage, Right: Output parameters global unit damage and storey drift

For the non-prestressed wall, the correlation of head mass with global unit damage is presented exemplary in Fig. 6-55 on the left. While in the right anthill plot the regression function of the output parameters global unit damage and storey drift are shown. The linear regression coefficients are high. Subsequently, the sensitivities are exemplary presented for the maxima of the important damage parameters  $u_{h,rel}$ ,  $\alpha_{b,loc}$  and  $\epsilon_{y,t}^{pl}$  in Fig. 6-56 for the non-prestressed wall and in Fig. 6-57 for the prestressed wall.

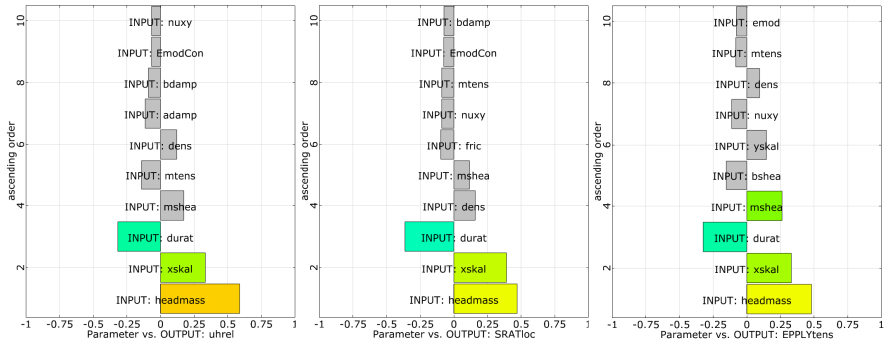


Fig. 6-56: Linear correlation coefficients of the non-prestressed wall, Left: For storey drift, Middle: For local unit damage, Right: For vertical plastic tensile strain

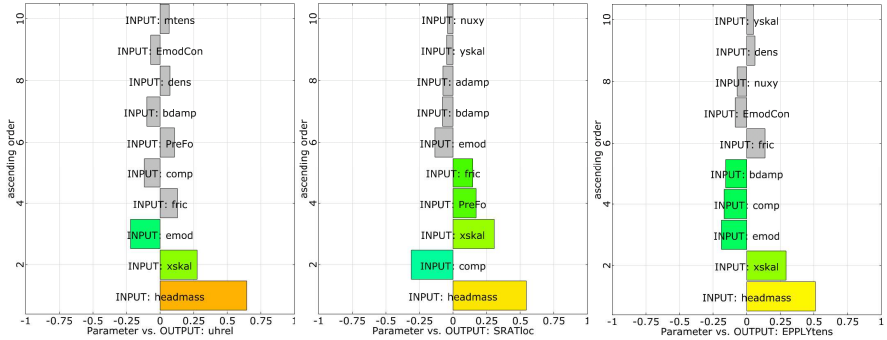


Fig. 6-57: Linear correlation coefficients of the prestressed wall, Left: For storey drift, Middle: For local unit damage, Right: For vertical plastic tensile strain

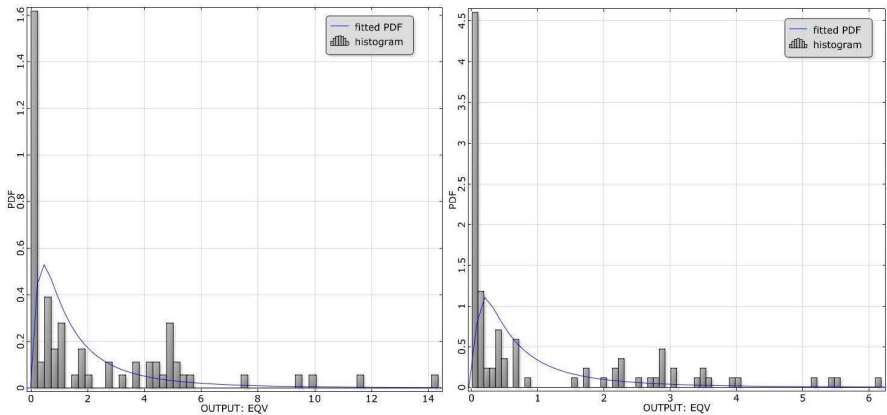


Fig. 6-58: Probability density functions for the equivalent plastic strain [%] - Histogram and fitted lognormal distribution, Left: Non-prestressed wall, Right: Prestressed wall

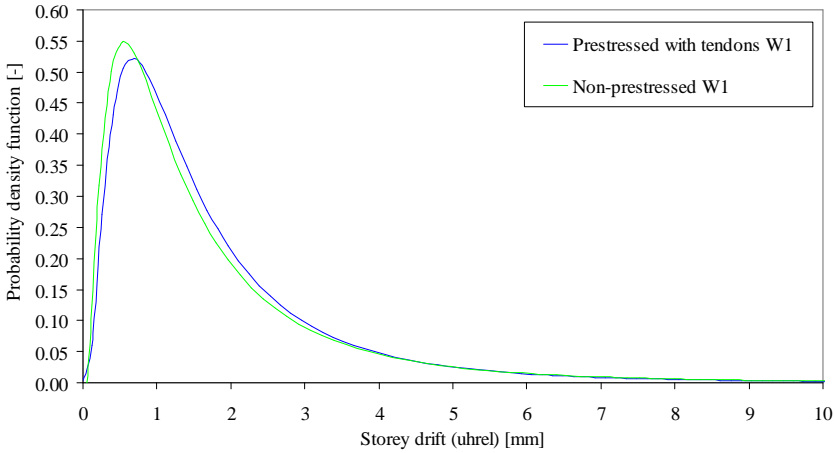


Fig. 6-59: Probability density functions of storey drift for the non-prestressed and prestressed wall

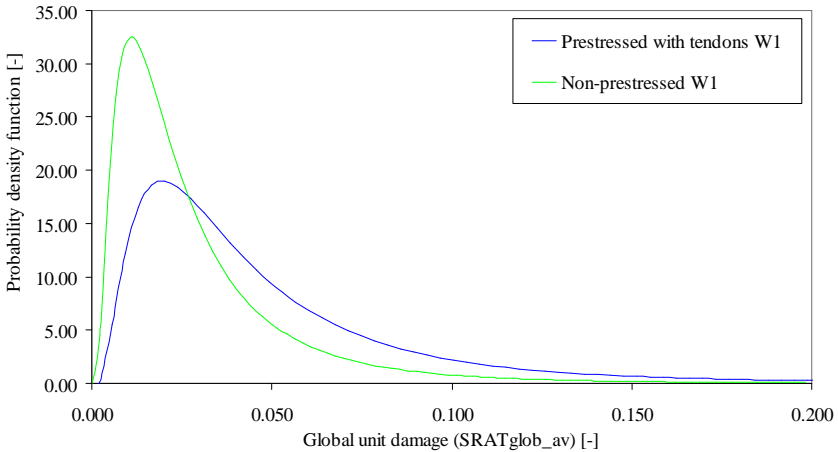


Fig. 6-60: Probability density functions of global unit damage for the non-prestressed and prestressed wall

The leading impact of the input parameters head mass  $\rho_M$  and the scaling factor  $X_{skal}$  (describing the seismic load scattering of the horizontal excitation component) is an important outcome of the probabilistic analyses. Both,  $X_{skal}$  and  $\rho_M$  represent the dynamic loading. They have a high impact on all damage parameters, which is expressed by the coloured lines 12 and 14 in the correlation matrices of Fig. 6-54. The lines number belongs to the number of input parameters given in Tab. 6-14. The sensitivities of the material parameters are quite small and no general impact on all damage parameters can be observed as it is the case for  $X_{skal}$  and  $\rho_M$ . Moreover, the vertical excitation component has also no significant impact on non damage parameter. This is confirmed by previous probabilistic investigations published in [Urban, Sperbeck, Peil 2006] and [Urban 2007]. The observed trends for the sensitivities of non-prestressed walls are also valid for the investigated prestressed wall. For the prestressed one an additional impact of the prestress level

on the local and global unit damage can be seen in Fig. 6-54, as already known from the previous deterministic simulations. In Fig. 6-58 until Fig. 6-60, probability density functions PDFs for the damage parameters equivalent plastic strain, storey drift and global unit damage are depicted, which represent the damage probability. Fig. 6-58 displays not only the fitted continuous log-normal functions, but also the histograms of the produced samples. It can be easily seen for the equivalent plastic strain that prestressing reduces the probability for high damages, but it increases the probability for small damages. In case of global unit damage (see Fig. 6-60), prestressing effects the contrast. Here, high damages occur with higher probability. This confirms the observed trends of the deterministic analyses. Due to the probabilistic investigations, the irregularities become clearer and it can be concluded, that in general not only the local, but also the unit damage is increased due to prestressing for compact walls. The storey drift is not significantly affected by prestressing, since the curves show no great differences (see Fig. 6-59).

### 6.3.3.2 Wall 3

For wall 3 an extended probabilistic investigation is done. In the sum, six different probabilistic simulations are carried out for three different earthquake load levels for return periods of 475 years, 2000 years and 10000 years to account for the different probabilities of exceedance (see Tab. 3-4) regarding the hazard curve for the intensity (see Fig. 3-11). On each seismic level (or return period) two probabilistic simulations are performed, one for the non-prestressed wall 3 and one for the prestressed wall 3.

On each of the three load levels the probabilistic analyses differ slightly concerning the number of investigated scattering input parameters of the resistance. First of all, (regarding some literature and experience) the scattering of the earthquake loading is usually so important that the other scattering could almost be neglected. Furthermore, previous parameter studies and investigations of [Urban, Sperbeck, Peil 2006] and [Urban 2007] have shown very small influences of several material parameters, for which a considering of scatter is not anymore necessary. In addition some parameters influence the convergence enormously, while they have almost no impact on the damage parameters. The influence on the convergence leads to aborted simulation, which reduces the number of samples significantly and insofar the accuracy of the probabilistic analyses. Therefore, some of such material parameters are assumed to be deterministic. However, the significances of almost all material parameters are checked for a return period of 475 years. In this case the impact of the earthquake loading is lower than for the return period of 2000 years and 10000 years. All parameters which scatter - as well as their probabilistic density functions - are listed in Tab. 6-15, Tab. 6-16 and Tab. 6-17 (one table for every seismic level). In the evaluation it was necessary to deactivate some samples due to damage hotspots (wrong calculation of the material model) and nonsensical random parameter selection of optiSLang<sup>®</sup>. An extended presentation is only given for a return period of 475 years. Since, their similarities, a lot of pictures are only shown in the Appendix E for the remaining return periods.

In this paragraph an evaluation of the results regarding the sensitivities is given for all three return periods. The leading impact of the input parameters head mass  $\rho_M$  and the scaling factor  $X_{skal}$  (describing the seismic load scattering of the horizontal excitation component) is already observed in the probabilistic analyses of wall 1. The same can be observed in all analyses of wall 3 for all return periods. Both,  $X_{skal}$  and  $\rho_M$  represents have a high impact on all damage parameters, which is shown by the coloured lines in the correlation matrices in Fig. 6-61, Fig. 6-66 and Fig. 6-67. The lines number of the matrix for the prestressed wall belongs to the number of input parameters given in each related Tab. 6-15, Tab. 6-16 and Tab. 6-17. The matrices are very similar. In the bar charts, the enormous impact is very noticeable. This high impact of  $X_{skal}$  and  $\rho_M$  increases with the earthquake strength (return period). For a direct comparison the Fig. 6-62 and Fig. 6-68 for a non-prestressed as well as Fig. 6-63 and Fig. 6-69 for a prestressed wall can be

simply used. The diagrams of Appendix E confirm this relation. Moreover, it can be seen that this impact of  $X_{skat}$  and  $\rho_M$  is reduced by prestressing. Furthermore, the prestress level influences the damage. It increases the unit damage, but it decreases the mortar damage and the equivalent plastic strain as for instance depicted in Fig. 6-63 and Fig. 6-69 in the middle. These goes in line with the results of previous deterministic simulations. The stiffness of the floor slab – which is simply modelled by a variable Young’s Modulus for the concrete  $E_c$  – has a medium or small impact on some damage parameters (see e.g. Fig. 6-62 and Fig. 6-63 on the right). However, it is the third most important parameter for the storey drift. The greater  $E_c$ , the smaller the storey drift. The damping parameters are sometimes medium important, but never significant. The sensitivities of the material parameters are quite small and no general impact on all damage parameters can be observed as it is the case for  $X_{skat}$  and  $\rho_M$  or the prestress level and  $E_c$ . The most important material parameter seems to be the compressive strength of the units. With an increased earthquake load level (return period) its impact becomes less important. Also here, the vertical excitation component has also no significant impact on non damage parameter. This is confirmed by previous probabilistic investigations published in [Urban, Sperbeck, Peil 2006] and [Urban 2007].

The probability density function PDFs for the damage parameters are partly presented in Chap. 8 and Appendix E, since they are used in Chap. 8 for the risk calculation.

## a) Return period of 475 years

No.	Sym.	Abbr.	Variable	Distribution	Expected/mean	Standard deviation	Min.	Max.
Masonry:								
1	$\eta$	nuxy	Poisson ratio	lognormal	0.15	$0.25*0.15=0.0375$	-	-
2	$\rho_M$	dens	Density of masonry	normal	$1.65e-9$ to/mm <sup>3</sup>	$0.075*1.65e-9$ $=0.12375e-9$ to/mm <sup>3</sup>	-	-
3	$E_M$	emod	Young's Modulus of masonry	normal	5800 N/mm <sup>2</sup>	$0.1*5800=580$ N/mm <sup>2</sup>	-	-
4	$\mu$	fric	Friction coefficient	lognormal	0.436	$0.185*0.436=0.0807$	-	-
5	$\sigma_{mr}$	mtens	Tensile strength of mortar joints	lognormal	0.87 N/mm <sup>2</sup>	$0.35*0.87=0.3045$ N/mm <sup>2</sup>	-	-
6	$\tau_{mr}$	mshea	Shear strength of mortar joints	lognormal	0.44 N/mm <sup>2</sup>	$0.3*0.44=0.132$ N/mm <sup>2</sup>	-	-
7	$c_{m1}$	IDPGm	Inelastic deformation parameter for mortar	uniform	0.95	-	0.5	1.5
8	$\sigma_{br}$	comp	Compressive strength of masonry	lognormal	17.2 N/mm <sup>2</sup>	$0.17*17.2=2.924$ N/mm <sup>2</sup>	-	-
9	$\tau_{br}$	bshea	Shear strength of masonry	lognormal	2.5 N/mm <sup>2</sup>	$0.15*2.5=0.375$ N/mm <sup>2</sup>	-	-
10	$c_{m2}$	IDPEb	Inelastic deformation parameter for masonry	uniform	1.1	-	0.6	1.55
Support condition - Stiffness of the concrete floor slab:								
11	$E_c$	EmodCon	Young's Modulus of concrete	truncated normal	14000 N/mm <sup>2</sup>	$0.4*14000$ $= 5600$ N/mm <sup>2</sup>	0.1	47600.0
Damping:								
12	$\alpha$	adamp	Rayleigh mass damping	uniform	0.62	-	0.4048	0.8352
13	$\beta$	bdamp	Rayleigh stiffness damping	uniform	0.0003	-	0.0001	0.0005
Loading:								
14	$P$	PreFo	Sum of prestressing forces	lognormal	352000 N	$352000*0.35=123200$ N	-	-
15	$X_{skal}$	xskal	Scaling factor for horizontal acceleration	lognormal	1	0.5*Mean	-	-
16	$Y_{skal}$	yskal	Scaling factor for vertical acceleration	lognormal	1	0.5*Mean	-	-
17	$\rho_M$	headmass	Density of mass of upper structure parts	truncated normal	$2.29358e-7$ to/mm <sup>3</sup>	$0.4*2.29358e-7$ $=0.917432e-7$ to/mm <sup>3</sup>	1.00E-10	1.15E-06
18	$D$	durat	Earthquakeduration of the steady phase	diskrete uniform	-	4.5 5.5 6.5 7.5	4.5	7.5

Tab. 6-15: Parameters varied and applied distributions for wall 3 and a return period of 475 years

The matrices in Fig. 6-61 for the non-prestressed wall on the left and for the prestressed one on the right are very similar. The left matrix misses one line and one row for the variable prestress level. All output parameters are highly correlated with each other. Not so the mortar damages with the storey drift and the unit damage. This becomes less in case of prestressing. The bar charts show negative correlation of many material parameters with the damage. This means for instance: The higher the strength, the lower the damage.

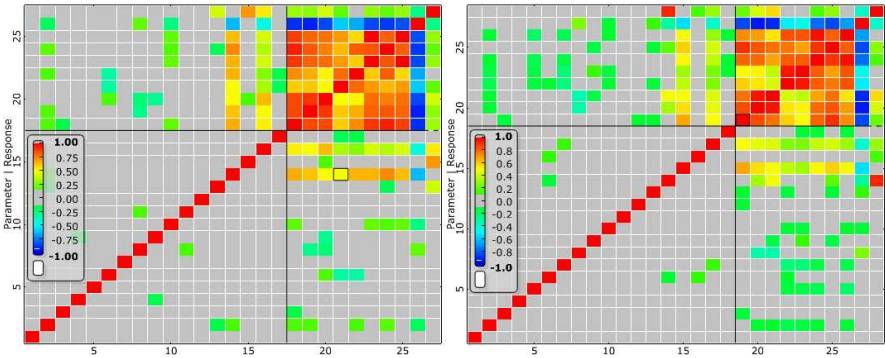


Fig. 6-61: Correlation matrices of wall 3 RP = 475, Left: Non-prestressed (17 input parameters), Right: Prestressed (18 input parameters)

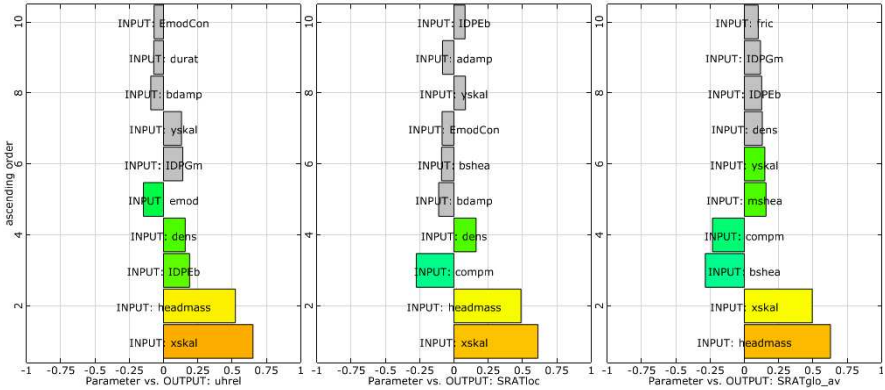


Fig. 6-62: Linear correlation coefficients of the non-prestressed wall, Left: For storey drift, Middle: For local unit damage, Right: For global unit damage

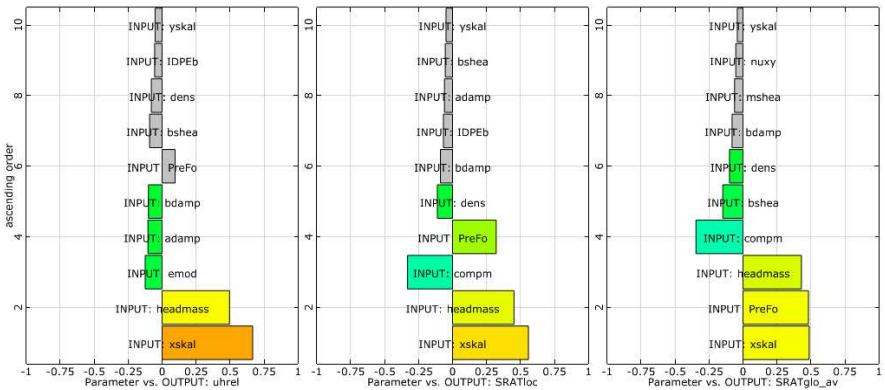


Fig. 6-63: Linear correlation coefficients of the prestressed wall, Left: For storey drift, Middle: For local unit damage, Right: For global unit damage

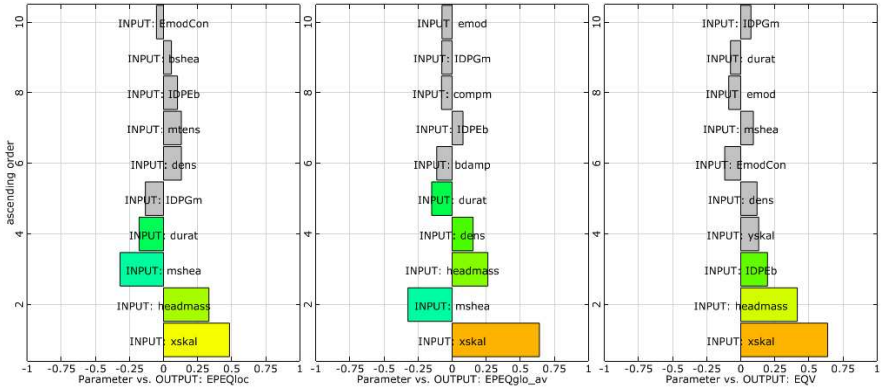


Fig. 6-64: Linear correlation coefficients of the non-prestressed wall, Left: For local mortar damage, Middle: For mortar global damage, Right: For equivalent plastic strain

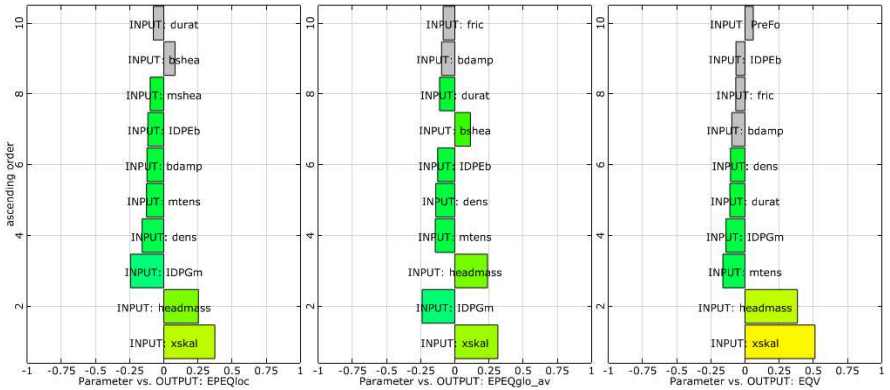


Fig. 6-65: Linear correlation coefficients of the prestressed wall, Left: For local mortar damage, Middle: For mortar global damage, Right: For equivalent plastic strain

b) Return period of 2000 years

Since the most material parameter do not have an important impact on the damage parameters, its number is reduced in the probabilistic analyses of this return period - which is shown by a comparison of Tab. 6-15 and Tab. 6-16 – in order to increase the accuracy of the probabilistic simulations or to allow a smaller amount of samples. The matrices in Fig. 6-66 are less similar than the ones in Fig. 6-61 for the return period of 475 years (lower excitation level). In case of prestressing the correlation of the output parameters decreases relatively strong. The blue lines show the high negative correlation with the vertical plastic compressive strain. This is only due to the negative sign for compression. The bar charts with the linear correlations between the damage parameters and the input parameter are only presented in Appendix E for this return period.

6 Numerical investigation of non-prestressed and prestressed masonry structures

No.	Sym.	Abbr.	Variable	Distribution	Expected/mean	Standard deviation	Min.	Max.
Masonry:								
1	$\eta$	nuxy	Poisson's ratio	lognormal	0.15	0.25*0.15=0.0375	-	-
2	$\rho_M$	dens	Density of masonry	normal	1.65e-9 to/mm <sup>3</sup>	0.075*1.65e-9 =0.12375e-9 to/mm <sup>3</sup>	-	-
3	$E_M$	emod	Young's Modulus of masonry	normal	5800 N/mm <sup>2</sup>	0.1*5800=580 N/mm <sup>2</sup>	-	-
4	$\mu$	fric	Friction coefficient	lognormal	0.436	0.185*0.436=0.0807	-	-
5	$\sigma_{mr}$	mtens	Tensile strength of mortar joints	lognormal	0.87 N/mm <sup>2</sup>	0.35*0.87=0.3045 N/mm <sup>2</sup>	-	-
6	$\tau_{mr}$	mshea	Shear strength of mortar joints	lognormal	0.44 N/mm <sup>2</sup>	0.3*0.44=0.132 N/mm <sup>2</sup>	-	-
7	$\sigma_{br}$	comp	Compressive strength of masonry	lognormal	17.2 N/mm <sup>2</sup>	0.17*17.2=2.924 N/mm <sup>2</sup>	-	-
8	$\tau_{br}$	bshea	Shear strength of masonry	lognormal	2.5 N/mm <sup>2</sup>	0.15*2.5=0.375 N/mm <sup>2</sup>	-	-
Support condition - Stiffness of the concrete floor slab:								
9	$E_c$	EmodCon	Young's Modulus of concrete	truncated normal	14000 N/mm <sup>2</sup>	0.4*14000 = 5600 N/mm <sup>2</sup>	0.1	47600.0
Damping:								
10	$\alpha$	adamp	Rayleigh mass damping	uniform	0.62	-	0.4048	0.8352
11	$\beta$	bdamp	Rayleigh stiffness damping	uniform	0.0003	-	0.0001	0.0005
Loading:								
12	P	PreFo	Sum of prestressing forces	lognormal	352000 N	352000*0.35=123200 N	-	-
13	$X_{skal}$	xskal	Scaling factor for horizontal acceleration	lognormal	1	0.5*Mean	-	-
14	$Y_{skal}$	yskal	Scaling factor for vertical acceleration	lognormal	1	0.5*Mean	-	-
15	$\rho_M$	headmass	Density of mass of upper structure parts	truncated normal	2.29358e-7 to/mm <sup>3</sup>	0.4*2.29358e-7 =0.917432e-7 to/mm <sup>3</sup>	1.00E-10	1.15E-06
16	D	durat	Earthquake duration of the steady phase	diskrete uniform	-	4.5 5.5 6.5 7.5	4.5	7.5

Tab. 6-16: Parameters varied and applied distributions for wall 3 and a return period of 2000 years

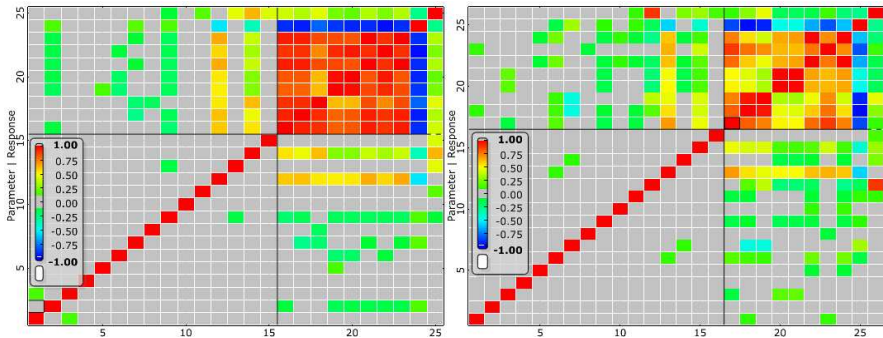


Fig. 6-66: Correlation matrices of wall 3 RP = 2000, Left: Non-prestressed (15 input parameters), Right: Prestressed (16 input parameters)

c) Return period of 10000 years

No.	Sym.	Abbr.	Variable	Distribution	Expected/mean	Standard deviation	Min.	Max.
Masonry:								
1	$\eta$	nuxy	Poisson's ratio	lognormal	0.15	0.25*0.15=0.0375	-	-
2	$\rho_M$	dens	Density of masonry	normal	1.65E-9 to/mm <sup>3</sup>	0.075*1.65E-9 =0.12375E-9 to/mm <sup>3</sup>	-	-
3	$E_M$	emod	Young's Modulus of masonry	normal	5800 N/mm <sup>2</sup>	0.1*5800=580 N/mm <sup>2</sup>	-	-
4	$\mu$	fric	Friction coefficient	lognormal	0.436	0.185*0.436=0.0807	-	-
Support condition - Stiffness of the concrete floor slab:								
5	$E_c$	EmodCon	Young's Modulus of concrete	truncated normal	14000 N/mm <sup>2</sup>	0.4*14000 = 5600 N/mm <sup>2</sup>	0.1	47600.0
Damping:								
6	$\alpha$	adamp	Rayleigh mass damping	uniform	0.62	-	0.4048	0.8352
7	$\beta$	bdamp	Rayleigh stiffness damping	uniform	0.0003	-	0.0001	0.0005
Loading:								
8	P	PreFo	Sum of prestressing forces	lognormal	352000 N	352000*0.35=123200 N	-	-
9	$X_{skal}$	xskal	Scaling factor for horizontal acceleration	lognormal	1	0.5*Mean	-	-
10	$Y_{skal}$	yskal	Scaling factor for vertical acceleration	lognormal	1	0.5*Mean	-	-
11	$\rho_M$	headmass	Density of mass of upper structure parts	truncated normal	2.29358E-7 to/mm <sup>3</sup>	0.4*2.29358E-7 =0.917432E-7 to/mm <sup>3</sup>	1.00E-10	1.15E-06
12	D	durat	Earthquakeduration of the steady phase	discrete uniform	-	4.5 5.5 6.5 7.5	4.5	7.5

Tab. 6-17: Parameters varied and applied distributions for wall 3 and a return period of 10000 years

The matrices in Fig. 6-67 are similar to the ones in Fig. 6-61 for the return period of 475 years. In case of prestressing the correlation of the output parameters do not change much. The mortar damages are lower correlated with unit damage. The local unit damage is less correlated with the plastic strains. Only some bar charts with the linear correlation coefficients of the damage parameters and the input parameter are presented below. Further may be found in Appendix E.

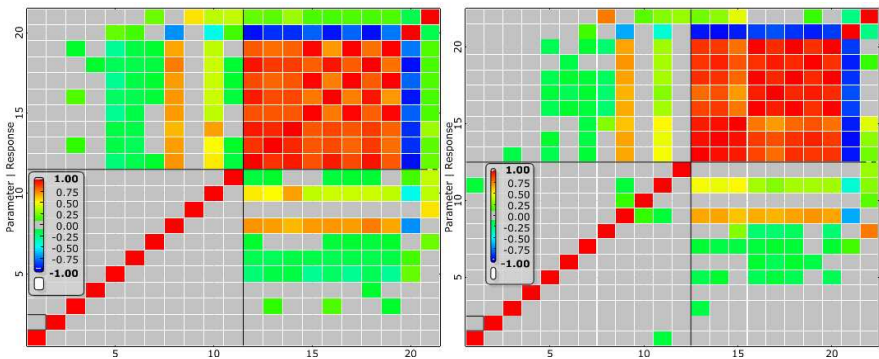


Fig. 6-67: Correlation matrices of wall 3 RP = 10000, Left: Non-prestressed (11 input parameters), Right: Prestressed (12 input parameters)

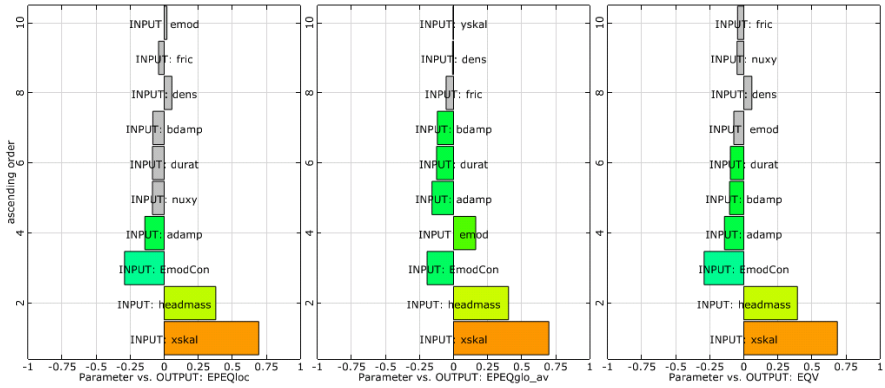


Fig. 6-68: Linear correlation coefficients of the non-prestressed wall, Left: For local mortar damage, Middle: For mortar global damage, Right: For equivalent plastic strain

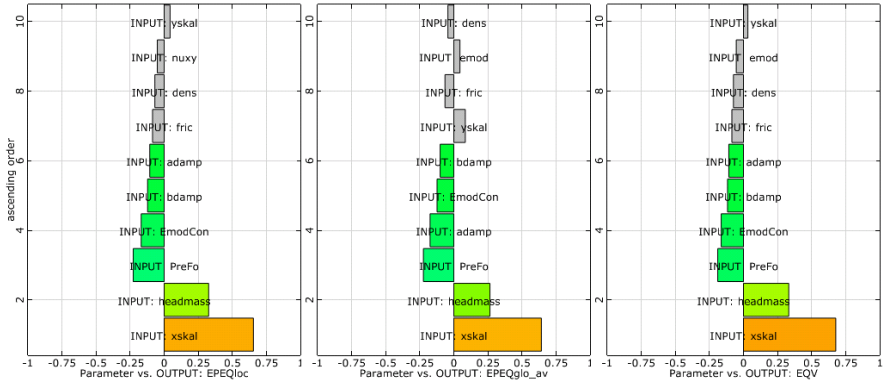


Fig. 6-69: Linear correlation coefficients of the prestressed wall, Left: For local mortar damage, Middle: For mortar global damage, Right: For equivalent plastic strain

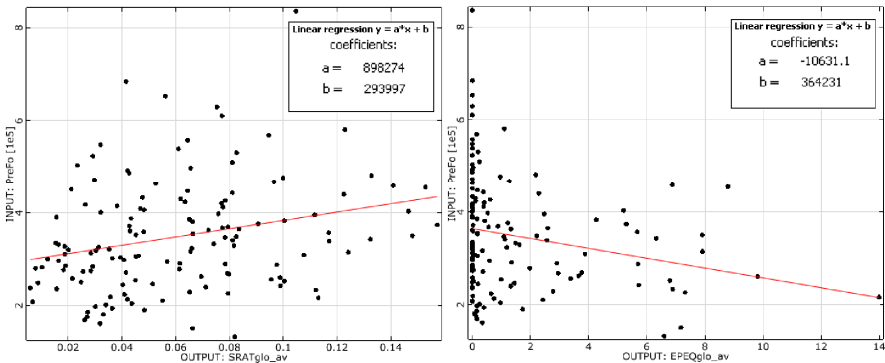


Fig. 6-70: Linear correlation coefficients of the non-prestressed wall, Left: Global unit damage, Right: Global mortar damage

To conclude this subchapter, the linear regressions of the prestressing level with the global unit damage and the global mortar damage are depicted in the anthill plots of Fig. 6-70. It confirms all analyses. The higher the prestressing, the higher the unit damage, the lower the mortar damage.

#### 6.4 Simulation of Hall 8 iBMB

The Hall 8 of the iBMB in Braunschweig, Germany consists of vertical prestressed masonry walls as explained in Section 4.2.6.4. The biggest bracing wall is numerically investigated in this study in cooperation with [Bazrafshan 2008]. Since experimental results of this wall do not exist – it has dimensions of 5.50 m in width and 6.38 m in height – a structural check by special investigations was necessary to get permission for erection, since a standardised structural design calculation is also not available in European codes up to the current time of writing for prestressed masonry. To predict the shear capacity of this important bracing wall the material model of Lagomarsino and Gambarotta [Gambarotta and Lagomarsino 1997b] is used here as well. The input values for the material parameters may be used from the previous model calibration on the basis of the shear wall tests of Braunschweig, which is explained in Section 6.3.1, since the same masonry material and prestressing method is used. Moreover, the usefulness of the numerical model to describe these experimental tests is demonstrated in Section 6.3.1.

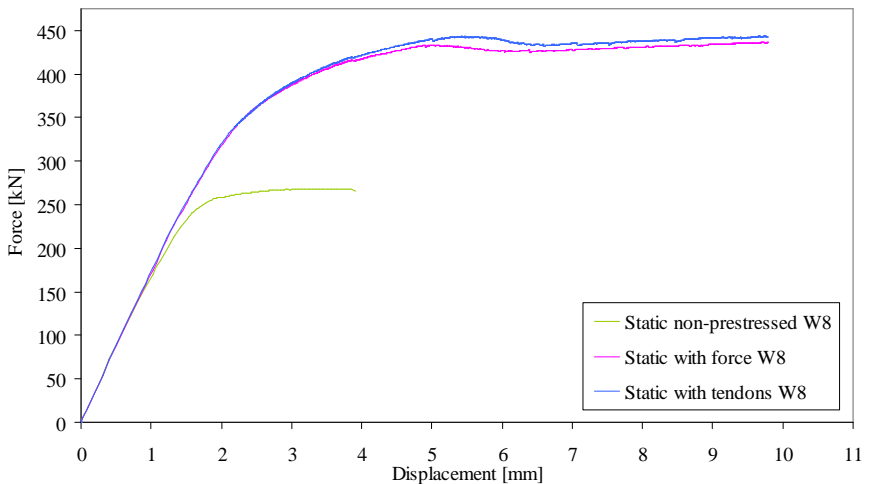


Fig. 6-71: Horizontal load displacement diagram – Numerical results of static loading of wall Pos. 8 in Hall 8 prestressed and non-prestressed

In order to prestress this bracing wall of Hall 8 four tendons have been used, which are modelled on the one hand by four external forces, on the other hand more accurate by additional elements for the tendons. The horizontal load displacement diagram of Fig. 6-71 shows only small difference of the two modelling manners, which are depicted in blue and magenta. Regarding the findings of Section 6.2.1, major differences should be expected, because SC 2 (free rotating top of the wall) is available. However, four tendons instead of two are used, which leads to another loadbearing behaviour. For instance, the tendons close to the middle cause only insignificant restoring forces. For the tendons close to the middle almost no differences occur regarding these types of prestress modelling (see Section 6.2.1). In addition this wall is rather slender. According to the previous case study, the differences are slightly for slender walls. Furthermore, the prestress-

ing forces are smeared by the four strands leading to a uniform distribution of vertical stresses. Here, the comparison of prestressed and non-prestressed version is of interest. Fig. 6-71 clearly presents the high increase of shear capacity that almost doubles. Therefore, the aim of sufficient resistance against horizontal wind and crane runway action is reached. In the next sections, the modelling results of the existing and a non-prestressed state are briefly presented.

6.4.1 Simulation of the existing state

Within this section, the existing prestressed wall is numerically investigated and the two means of prestress modelling are compared. As to expect (respecting the similar load displacement curves), the distributions are very similar for all damage parameters. This is true not only for the quality, but also for the quantity. The unit damage as well as the mortar damage shows the maxima on the corners. On the right lower corner tensile failure occurs (see Fig. 6-73), while on the left one toe crushing can be observed as given in Fig. 6-72.

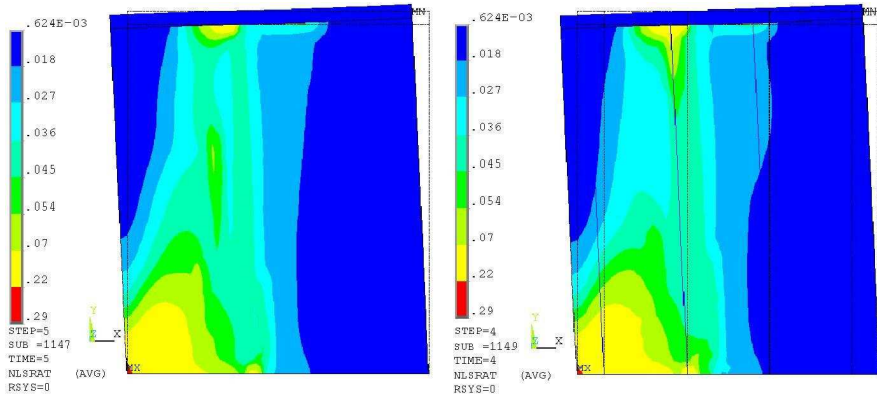


Fig. 6-72: Wall Pos. 8 – Unit damage of static loading on  $u_{abs} = 10.7$  mm, Left: Prestressed by means of forces, Right: Prestressed by means of tendons

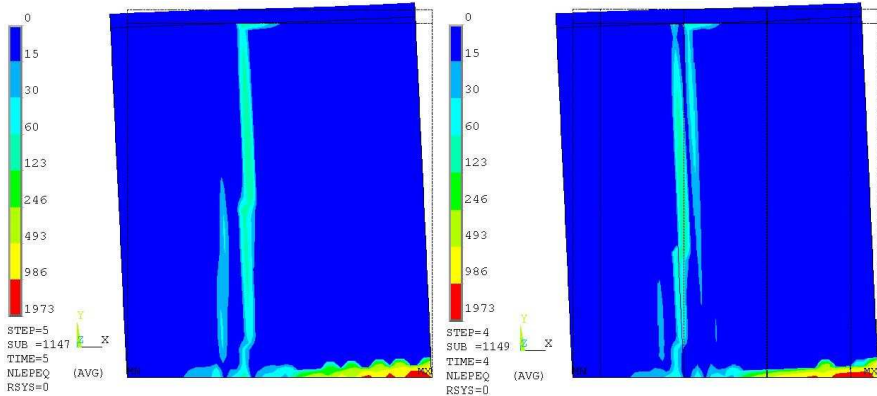


Fig. 6-73: Wall Pos. 8 – Mortar damage of static loading on  $u_{abs} = 10.7$  mm, Left: Prestressed by means of forces, Right: Prestressed by means of tendons

This goes in line with failure mechanisms described in literature and experimental results. A concentration of less damages both mortar and unit damage is visible along a brace between the highly loaded lower left corner and the upper anchor point of the second strand. In this range, compression and shear mechanisms act stronger than in raining wall parts. The reader may anticipate diagonal unit cracking between the diagonal corners. However, in this case of a compression braces appear. The main one (caused by the highest stress) occurs between the lower left compression corner and the upper anchor point of the second tendon. This results are in accordance with truss girder models in [Ganz 1990a] and [Budelmann et al. 2004]. The tensile failure on the corner is detected by the mortar damage in Fig. 6-73 and is confirmed by the vertical plastic strain distribution of Fig. 6-74 with very high values in the lower right part. It plays a major role in comparison to the shear failure on the diagonal as corroborated by equivalent plastic strain of Fig. 6-75. Since it includes components of all directions, and in the distribution no significant plastic equivalent strains are computed, the shear failure impact has to be small.

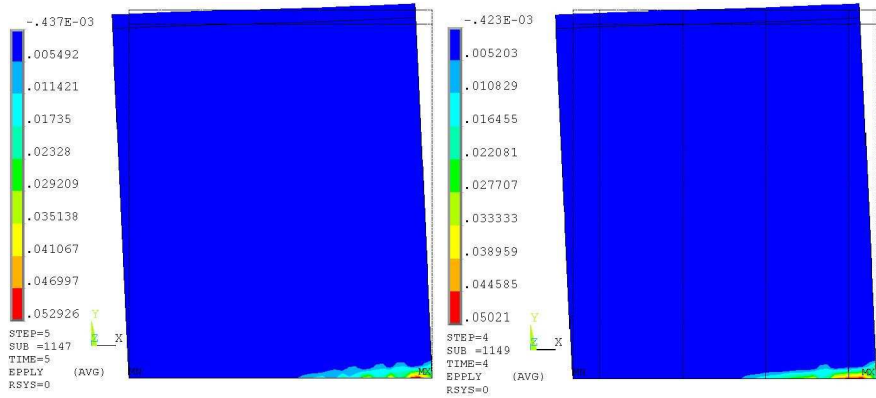


Fig. 6-74: Wall Pos. 8 – Vertical plastic strain of static loading on  $u_{abs} = 10.7$  mm, Left: Prestressed by means of forces, Right: Prestressed by means of tendons

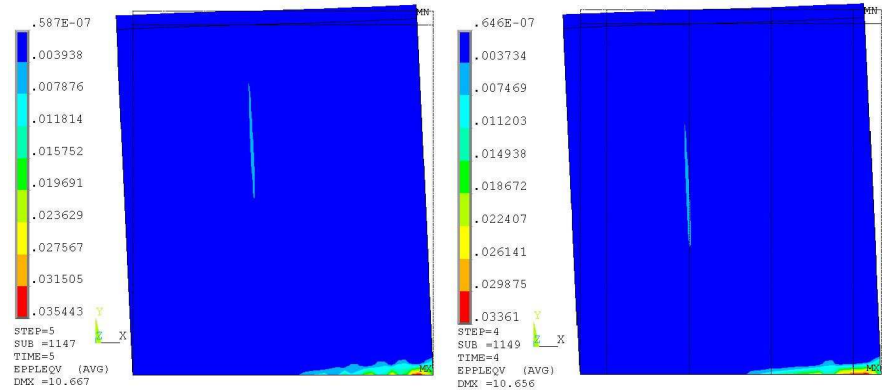


Fig. 6-75: Wall Pos. 8 – Equivalent plastic strain of static loading on  $u_{abs} = 10.7$  mm, Left: Prestressed by means of forces, Right: Prestressed by means of tendons

6.4.2 Simulation without prestressing

Complementary, the consequences of missed prestressing are predicted subsequently. First of all, the shear capacity is essentially lower as shown in Fig. 6-71. The important parameters are depicted in the following as the unit damage in Fig. 6-76 on the left, the mortar damage in Fig. 6-76 on the right and the equivalent plastic strain (see Fig. 6-77 on the left). Moreover the vertical plastic tensile strain is displayed in Fig. 6-77 on the right, which corresponds with the high mortar tensile failure (see Fig. 6-76 on the right) and with the equivalent plastic strain. As already stated for other simulated masonry structures, the mortar damage, the equivalent plastic strain and the vertical plastic tensile strain as well as the global damage are reduced by prestressing. Note, that the values of the figures of the prestressed and the non-prestressed wall cannot be compared, since the different  $u_{abs}$ .

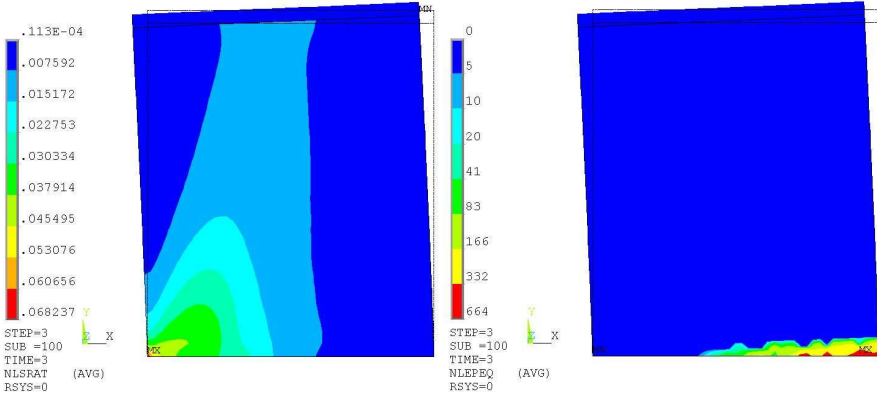


Fig. 6-76: Wall Pos. 8 non-prestressed and static loaded on  $u_{abs} = 4.5$  mm, Left: Unit damage, Right: Mortar damage

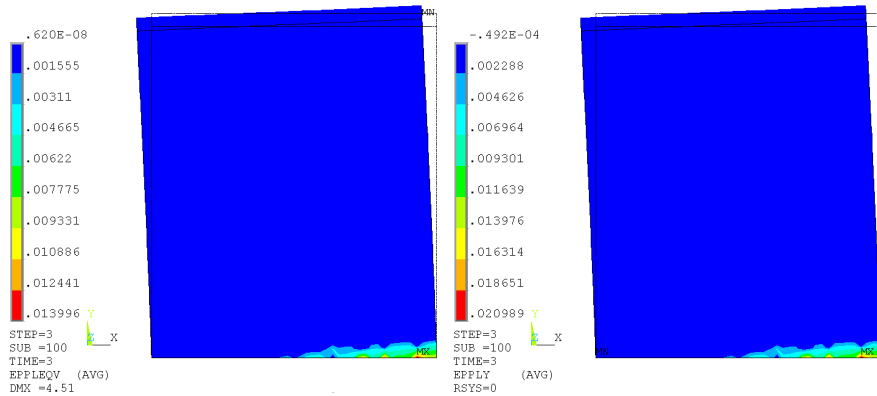


Fig. 6-77: Wall Pos. 8 non-prestressed and static loaded on  $u_{abs} = 4.5$  mm, Left: Equivalent plastic strain, Right: Vertical plastic strain

## 6.5 Summary

In the first subchapter, the capability of the used material models to describe the in-plane behaviour of unreinforced masonry shear walls is verified for static loading, by means of the experimental tests of Eindhoven [Vermeltfoort, Raijmakers 1993].

Thereafter, an extensive static case study is performed to fix important influences. The assumption of a very high importance of the support conditions is confirmed. The existence of restoring forces due to tendons is proved, which can be reasonably taken into account only due to modelling of tendons. The same is valid for the change of prestressing force in the tendons, mainly caused by wall rotation. This effect is much more considerable for short tendons than for long tendons and for constructions allowing a high degree of wall rotation. Locating tendons close to the edges is more reasonable than in the middle of the wall, since restoring forces and moments hamper the storey drift and insofar the damage as well. Afterwards, the impact of prestressing and the impact of the means to model prestressing on the dynamic behaviour are demonstrated in a dynamic case study.

In the third subchapter, the capability of the material model of Lagomarsino and Gambarotta [Gambarotta and Lagomarsino 1997b] is verified regarding prestressed walls and static cyclic behaviour. The numerical results are plausible and agree well with experimental tests of the prestressed shear walls of Braunschweig [Budelmann et al. 2004]. The loadbearing behaviour of all investigated walls is qualitatively and quantitatively well predicted. The used material model of Lagomarsino and Gambarotta is able to describe the material behaviour and effects of degradation and dissipation. Even the different hysteretic behaviour of slender and compact walls is very well simulated. Therefore, it can be utilised for additional dynamic investigations.

Comparisons of static loaded non-prestressed and prestressed versions of wall 1, 3 and 4 show throughout a reduction of the mortar damage, equivalent plastic strain, plastic strain shear stain and vertical plastic tensile strain. The global unit damage is always increased in case of prestressing. The impact of prestressing on the local unit damage is somehow confusing. In case of wall 1 it reduces the local unit damage. However, the local unit damage increases, if prestressing is applied on wall 3. No significant impact can be observed for wall 4. The displaying of the local unit damage over the histories exhibits a dependency of the impact on degree of loading for it.

With the results of the parameter calibration by means of the experimental tests described in [Budelmann et al. 2004], the dynamic behaviour is investigated for wall 1 and wall 3. Of main interest is the impact of prestressing on the damage parameters. The results for the maxima of all these parameters are summarised in Tab. 6-10 until Tab. 6-13 for every earthquake in dependency of non-prestressing or prestressing. The trends for the impact of prestressing from the static analyses are confirmed by the most dynamic simulations. Some additional irregularities can be observed also for other damage parameters. Since the earthquake level is approximately equal (similar PGA) per table, it cannot be the reason for the alternating tendency. Probably, the different characteristics of each time history cause these results, taking into account the different frequency contents and natural frequencies of the walls, which change during the earthquake. The local and global mortar damage is always reduced. For the most earthquakes the equivalent plastic strain, plastic shear strain and vertical plastic tensile strain are reduced by prestressing as well. The storey drift is not significantly affected by prestressing for all earthquakes, and the effect is irregular. For low level earthquakes a general reduction may be seen, whereas for strong seismic action often an increase occurs. The results for the local unit damage differ strongly. No correlation can be found. As to expect, the vertical plastic compressive strain is very often greater than for prestressed walls. For the local unit damage similar irregularities occur as in the static investigations. Moreover, it depends on the observed time, whether the local unit damage is higher for prestressing. In contrast, the global unit damage is always greater in case of prestress-

ing. This can be very dangerous, since it may lead to brittle collapse. Only a slight impact of the means to model prestressing (forces or tendons) on the damage parameters can be observed.

The probabilistic analyses confirm this impact of prestressing of the previous static, cyclic and dynamic simulations. Especially, for the compact wall 1, high irregularity is observed concerning the local unit damage. The probabilistic analyses deliver damage probabilities, which express the general lawfulness. Some exceptions may be possible. The functions depict higher probabilities for high global unit damages in case of prestressing (see for instance Fig. 6-60). Thus, the deterministic irregularities become more clear and it can be concluded, that in general not only the local (see Appendix E), but also the global unit damage is increased due to prestressing for compact walls. The storey drift is not significantly affected by prestressing, since the curves show no great differences (see Fig. 6-59). Concerning the extensive probabilistic analyses of wall 3, the input parameters head mass  $\rho_M$  and the scaling factor  $X_{skal}$  show the highest impacts. The matrices of the different return periods are similar. This high impact of  $X_{skal}$  and  $\rho_M$  increases with the earthquake strength (return period). Moreover, it can be seen that this impact of  $X_{skal}$  and  $\rho_M$  is reduced by prestressing. Besides, the prestress level influences the damage. It increases the unit damage, but decreases the mortar damage and the equivalent plastic strain as for instance depicted in Fig. 6-63 and Fig. 6-69 in the middle. This goes in line with the results of previous deterministic simulations. The stiffness of the floor slab – which is simply modelled by a variable Young's Modulus for the concrete  $E_c$  – has a medium or small impact on some damage parameters. However, it is the third most important parameter for the storey drift. The greater  $E_c$ , the smaller the storey drift.

Finally, an existing building is investigated. The new Hall 8 of iBMB/MPA in Braunschweig is braced by means of prestressed masonry shear walls. The most important one is modelled, also a non-prestressed version. The benefit of the strengthening measure becomes clear.

## 7 Further measures to attain a good seismic performance

This chapter discusses several further measures to achieve a good seismic performance of masonry shear walls. During the investigation of the usefulness of vertical prestressing the author added the following ideas. Some suggestions are related to the microscopic level, other to the macroscopic level. The measures aim mainly on the improvement of ductility as well as on stiffness reduction, in order to make the masonry structure more flexible, ductile and to allow high energy dissipation. This goes in line with a reduction of unit damage, since it causes brittle failure and so ductility reduction. Stiffness reduction and increase of energy dissipation lead to a reduction of horizontal forces in case of seismic action. The ideas are briefly discussed and partly investigated with first simulations. Deeper research is recommended.

### 7.1 Discussion of further measures

#### 7.1.1 Microscopic level - Reasonable material parameter selection for masonry

Regarding the failure mechanisms of masonry walls, which are explained in Section 4.1.3, the material parameters (listed in Section 4.1.4.2) should theoretically be selected as recommended subsequently to reach an improved ductile behaviour.

Concerning to poor shear behaviour, it is important to avoid diagonal cracking of the units, by allowing a high degree of rotation of the units. This can be reached due to:

- Many small units instead of few big units per wall
- Optimised width height ratio of the units (probably a square)
- Optimised overlapping (probably 25%)
- Soft mortar and thick bed joints
- Head joints should be unfilled

For poor in-plane bending – for which rocking and toe crushing are usually the important collapse mechanisms – successive failure and abrupt failure of the corners (especially in case of SC 2 and/or slender walls) occur. The following simple measures should reduce these problems:

- Units with brittle behaviour like vertical coring bricks should be avoid, instead ductile units are suggested.
- A high tensile strength of the mortar joins leads to a higher resistance against rocking. (probably the impact is quite small)

In general:

- The tensile strength of the units should be high and the tensile behaviour should be ductile.

All these theoretical suggestions should still be verified by deeper investigations and experimental tests.

#### 7.1.2 Macroscopic level - Reasonable parameter selection for walls

Masonry walls should theoretically designed as advised in the following, in order to have a ductile behaviour. Wall geometry and vertical load level, elastomer bearing and diverse ideas are suggested and discussed.

### 7.1.2.1 Wall geometry

Regarding the global design of the walls it is probably utile to have several slender walls instead of one long compact shear wall. The reasons are ductile rocking and sliding of slender walls. The findings of previous chapters regarding the aspect ratio of walls indicate the usefulness of a design with several slender walls, instead of one compact wall as outlined in Fig. 7-1. In case of low vertical load level, this leads to a higher ductility [Magenes, Calvi 1995]. As a result of internal vertical prestressing with ensured wall tendon interaction in early loading states, the shear capacity and the ductility would be increased as well (see Section 4.2.5). However, it is also to ensure, that brittle toe crushing can be avoided, for instance to reasonable unit selection as explained in 7.1.1 or by elastomers (see 7.1.2.3).

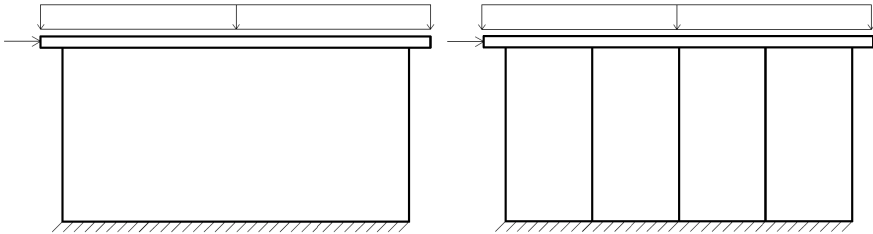


Fig. 7-1: Separation, Left: Basic wall, Right: Wall separated into four slender walls

### 7.1.2.2 Vertical load level

As already explained in Section 4.2.2, the vertical load level can exceed balance points for shear and bending behaviour. This point represents the threshold, on which the improvement achieves the maximal out-of-plane bending or shear resistance. This point is not the optimum, since it goes already in line with diseconomy and increased damages. Instead it is interesting to find an optimum for the prestressing level, which minimises both the unit and the mortar damage. In the previous chapters, it is verified several times that prestressing increases the unit damage, but decreases the mortar damage. The objective function develops oppositely. This requires a Pareto optimisation. The program optiSLang<sup>®</sup> offers such an optimisation. A continuing investigation of this subject is suggested.

### 7.1.2.3 Elastomer bearing

To counteract toe crushing, which occurs especially for slender walls and/or SC 2 – it is recommended to locate elastomer bearings under the lower corners of the wall. This idea is already illustrated in [Schermer 2004].

### 7.1.2.4 Miscellaneous ideas

- A reduction of the rotation due to tendons is also possible, as shown in Chap. 6.
- Ductile behaviour is desirable in combination with high or medium shear capacities. Probably, this can be reached by using a combination of different failure modes. In practice, this could be done by a useful ratio of the before mentioned measures to obtain a ductile behaviour and a reasonable degree of vertical loads.
- Moreover, the tendons inside the wall can avoid a slide down of the triangles which results due to diagonal cracking. So, a ductile behaviour is ensured also in case of diagonal

cracking as observed in experimental tests [Budelmann et al. 2004]. Thus, an internal prestressing is recommended (see Section 4.2.5).

- Especially, bonded prestressing is suggested to achieve an immediate contact (interaction) between wall and tendons in case of slide down. Much space between is disadvantageous as well as external prestressing.

## 7.2 Simulation of further measures

In addition to the theoretical reasoning of the suggested ideas, some measures are simulated in this subchapter, in order to verify the theories or to get an idea about their impact.

### 7.2.1 Division in slender walls as non-prestressed and prestressed version

In this section, macroscopic-level measures are investigated by first numerical simulations. In the sum, four different measures (variations) of a wall are modelled. In Fig. 7-2, an overview of these four measures is outlined. The first is a compact wall, without any macroscopic retrofitting to change its seismic performance. The second is only a prestressed version of the first. Measure three is also equal to the first, except the separation into slender sub-walls (no prestressing). Measure four is a prestressed modification of the third. The prestress level of measure 2 and 4 is equal. The investigated virtual walls have equal dimensions of 4 m in height and 8 m in width. Therefore, they could be bracing walls in industrial halls.

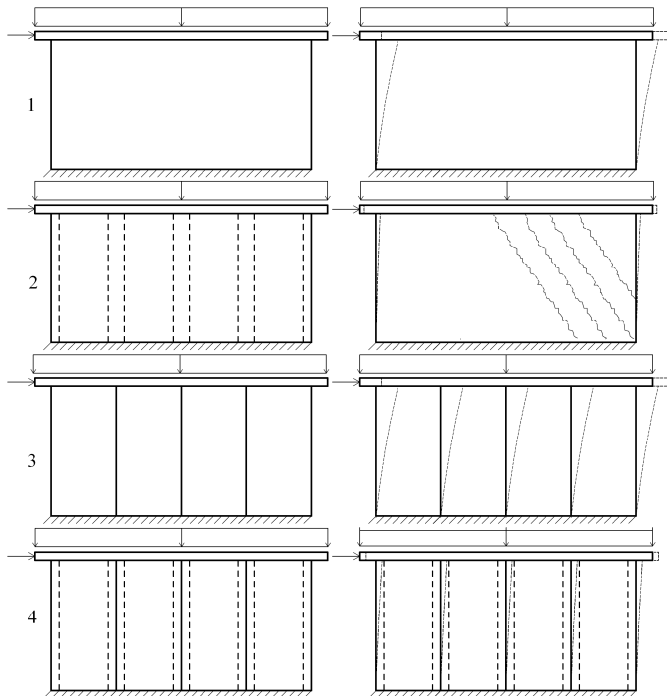


Fig. 7-2: Overview of the investigated measures, Left: Non-deformed, Right: Assumed deformation

For the support conditions on the top SC 2 (free rotation) is modelled, since it leads to less convergence problems. In Fig. 7-2 on the right, the assumed deformations are outlined as well. For the non-prestressed measures 1 and 3, greater storey drift is to expect. In case of prestressing diagonal cracking would occur on the edge under compression. Regarding the prestressed version, a bond of tendons is assumed, which ensures a ductile behaviour of the prestressed walls. The non-prestressed measures 1 and 3 show automatically a ductile behaviour. For these investigations the following material parameters are used which are also a results of parameter calibrations for the prestressed shear wall tests in Braunschweig, however another calibrate combination is used here. This means, the presented virtual wall (measure 1 until 4) consists of the same strong material than the experimental tested prestressed shear wall of Braunschweig [Budelmann et al. 2004]. The material model of Lagomarsino and Gambarotta is used for the simulations.

Parameter	Sym.	Value	Unit
Density	$\rho$	1650	kg/m <sup>3</sup>
Young's modulus of masonry	E	5800	N/mm <sup>2</sup>
Poisson's ratio	$\eta$	0.15	-
Friction coefficient	$\mu = \tan \varphi$	0.436	-
Tensile strength mortar	$\sigma_{bm}$	0.87	N/mm <sup>2</sup>
Shear strength of the mortar joints	$\tau_{mr}$	0.44	N/mm <sup>2</sup>
Inelastic deformation parameter for mortar	cmt	1.0	-
Softening coefficient mortar	$\beta_m$	0.3	-
Compressive strength of masonry	$\sigma_{br}$	17.17	N/mm <sup>2</sup>
Shear strength of bricks	$\tau_{br}$	3.0	N/mm <sup>2</sup>
Inelastic deformation parameter for brick	cbn	1.0	-
Softening coefficient of the masonry	$\beta_b$	0.4	-
Young's modulus of concrete	$E_c$	29000	N/mm <sup>2</sup>
Rayleigh mass damping	$\alpha$	0.62	-
Rayleigh stiffness damping	$\beta$	0.0003	-

Tab. 7-1: Used material parameter investigation of different measures (Study C-KV3)

Previously, static simulations are carried out to get the characteristic load displacement curve of each wall variation. The horizontal load displacement diagram of Fig. 7-3 shows the numerical static results, which characterises the four different loadbearing behaviours of the four measures. Besides, the possibilities to model prestressing via forces or tendons do not influence the behaviour of these walls, since in case of several tendons this impact can be neglected, as already observed for the bracing wall of Hall 8 and explained in Section 6.4.

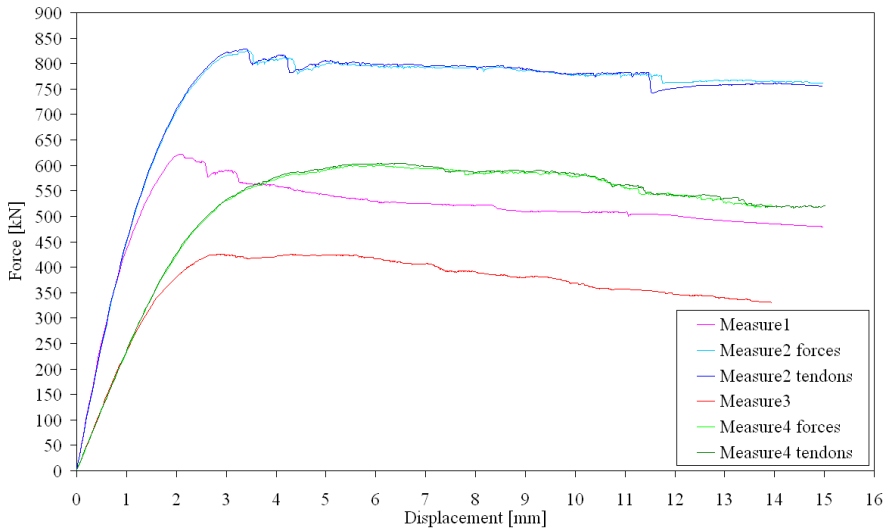


Fig. 7-3: Static load displacement diagram for the four measures and means to model prestressing

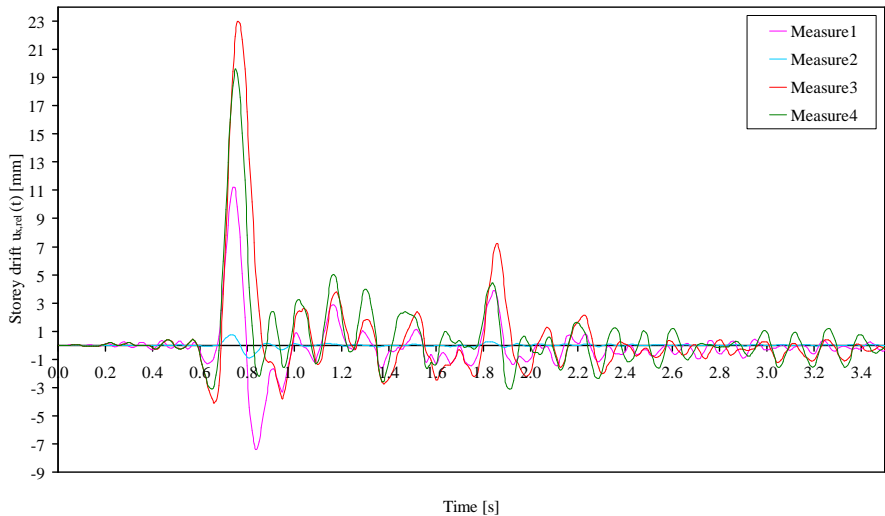


Fig. 7-4: Time depended storey drift for the measure 1, 2, 3 and 4 subjected to the double scaled Northridge earthquake of 1994

The walls are subjected to the Northridge earthquake, which occurred on the 17<sup>th</sup> of January in 1994. The epicenter was located 1 mile SSW of Northridge (20 miles WNW of Los Angeles, CA, USA). It had a moment magnitude  $M_w$  of 6.7. Due to the very high shear resistance of the wall and the low head mass, it was necessary to scale it by the factor two. The related scaled accel-

erograms are given in Appendix F as well as describing parameters. The spectral acceleration diagram is shown in Fig. 7-9.

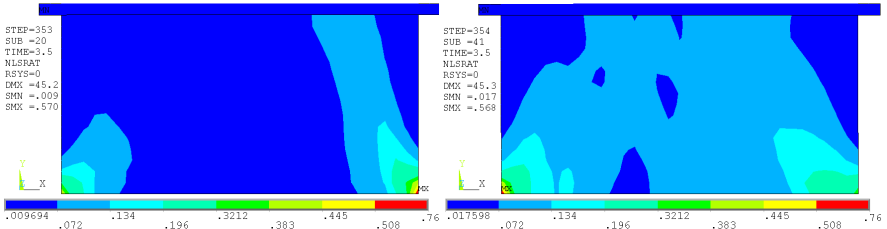


Fig. 7-5: Unit damage for the double scaled Northridge earthquake, Left: Measure 1, Right: Measure 2

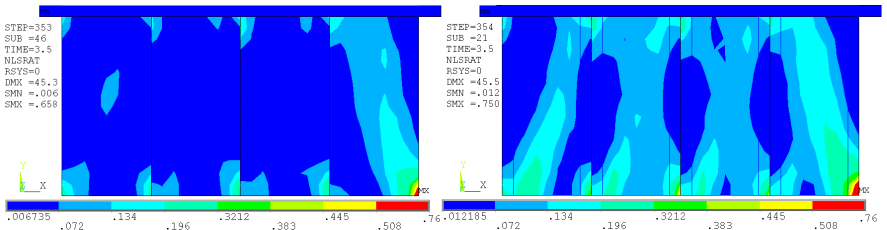


Fig. 7-6: Unit damage for the double scaled Northridge earthquake, Left: Measure 3, Right: Measure 4

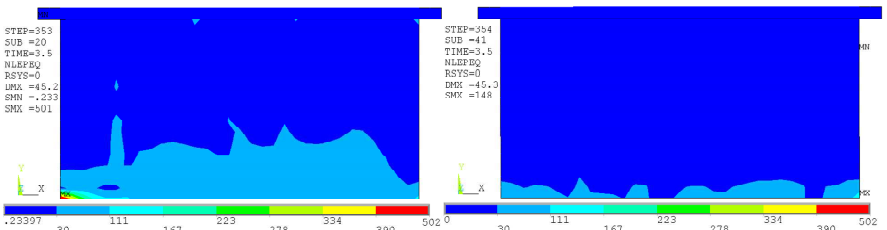


Fig. 7-7: Mortar damage for the double scaled Northridge earthquake, Left: Measure 1, Right: Measure 2

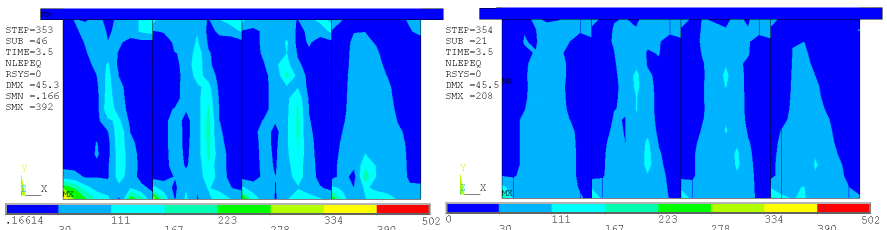


Fig. 7-8: Mortar damage for the double scaled Northridge earthquake, Left: Measure 3, Right: Measure 4

Concerning the unit damage, the separation of the compact wall (measure 1) into four slender walls (measure 3) does not lead to very different crack pattern, which can be observed in a comparison of Fig. 7-5 and Fig. 7-6 each on the left. Merely, on the corners of each slender wall additional damage occurs. However, the main crack band on the right of measure 1 (see Fig. 7-5 on the left) is not significantly reduced due to prestressing. Due to the separation, the mortar damage is distributed over big parts of the wall (Fig. 7-7 on the left), while the compact wall has only a small global mortar damage on the bottom. As summarised in Tab. 7-2, the maximal storey drift is highly increased due to the separation. For the non-prestressed separation (measure 3), the highest value for the storey drift occurs. It doubles in comparison with the non-prestressed compact wall (measure 1). Additionally, measure 3 shows the highest maxima also regarding local mortar damage.

In order to improve the shear resistance and decrease the drift, both wall types are investigated as prestressed versions. Expectedly, the local and the global mortar damage are reduced, especially for the compact wall (see Fig. 7-7 and Tab. 7-2). For measure 4 the mortar damage is higher than for measure 2. Prestressing leads additionally to a reduction of nearly 90% for the drift (see Tab. 7-2) in case of the compact wall, while for the separated version a significant reduction is not achieved.

Measure	$\max  u_{h,rel} $	$\max a_{h,loc}$	$\max a_{m,loc}$	$\max \epsilon_{eq}^{pl}$	1. Natural frequency $f_1$	1. Natural period $T_1$
	[mm]	[-]	[-]	[%]	[Hz]	[sec]
1	11.24	0.571	501.7	0.26	12.81	0.078
2 With forces	-0.89	0.568	148.3	0.38	12.80	0.078
3	22.96	0.658	392.5	0.79	8.96	0.112
4 With tendons	19.62	0.750	208.4	1.10	8.98	0.111

Tab. 7-2: Summarised damages for the different measures and related natural modes

The significant increased unit damage for the prestressed versions (measure 2 and 4) may be easily seen, which is presented in Fig. 7-5 and Fig. 7-6. This goes in line with previous simulation results and the literature. The mortar damage is shown in Fig. 7-7 for measure 1 and 2, while the damage for measure 3 and 4 is given in Fig. 7-8. The impact of prestressing is already known and agrees with other results. The huge reduction of the drift for the compact wall is noteworthy.

Concerning the separation in several slender walls no damage reduction can be observed. This worsening was not expected. The lowest drift, local unit and mortar damage as well as equivalent plastic strain occurs for measure 2 (see Tab. 7-2). However, the global unit damage is increased (see Fig. 7-5). Regarding expectable crack pattern and load bearing behaviour the results are plausible. The unexpected worsening of measure 3 and 4 can be caused by the application of the same earthquake. The natural frequencies of the compact and the separated structure differ significantly, as listed in Tab. 7-2. In Fig. 7-9, this difference is also displayed as well as the consequences. The first natural frequency of the compact wall belongs to a low spectral acceleration, while the separated wall drops nearly a peak of the spectra. Therefore, measure 2 and 4 are higher loaded than the others. Consequently, the results of these earthquake simulations are not really comparable. An earthquake has to be applied with equal spectral acceleration for both natural periods of the structures, or different scaling has to be used. Deeper investigations are necessary to judge on these suggested measures.

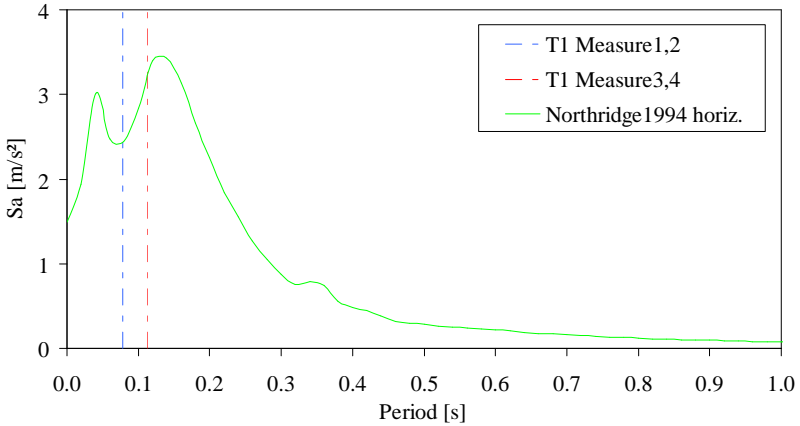


Fig. 7-9: Spectral acceleration diagram of the Northridge earthquake and natural periods of the structures

7.2.2 Unit type, masonry bond and unit size

In the following, some results of measures on the microscopic level are briefly presented. The material model of Schlegel [Schlegel 2004] that bases on macro-modelling (see Section 4.3.3.3) and meso-modelling using the material model of [Lourenço, Rots 1997] (see Section 4.3.3.1) are applied to investigate the impact of different unit types (width/height ratio), and so different bonds. Both models are able to consider such effects. The constitutive models are already checked in Section 6.1 by means of the experimental test results of wall J4D and J5D of the Eindhoven shear wall tests [Vermeltoort, Raijmakers 1993] that are already described in Section 4.1.5.1. To receive more reliable results shear wall J6D is used to control the numerical results. Thereafter, two virtual versions of wall J6D with different unit types are additionally calculated to investigate its impact on the unit and mortar damage. Here, wall J6D is chosen in order to investigate the unit damage better, since higher vertical forces lead to higher unit damage, as shown in the previous chapters. The vertical loading of 120 kN in case of wall J6D was much higher than for the walls J4D and J5D (30 kN). After all, the stone types (width/height ratio) of 200 x 50 as used in the experimental test of wall J6D, 200 x 100 and 200 x 150 are simulated. The resulting bonds are outlined in Fig. 7-10.

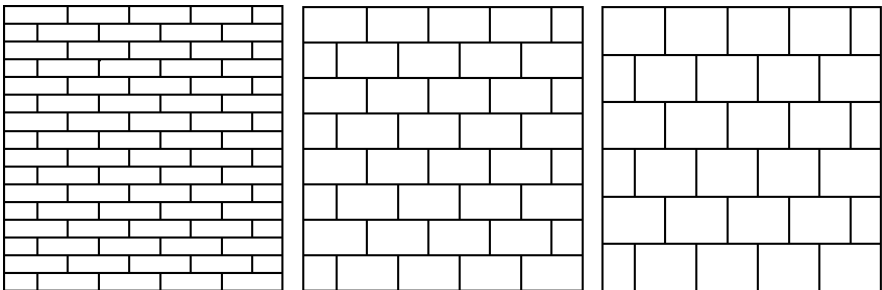


Fig. 7-10: Investigated walls with different unit types, Left 200 x 50 (original experimental test of wall J6D), Middle: 200 x 100, Right: 200 x 150

The used material parameters for both numerical models are given in Appendix H (Tab. H-4 and Tab. H-5). The experimental load displacement curve is depicted in curve Fig. 4-15. A comparison with the two numerical modelling strategies is given in Fig. 7-11. A very well agreement of both models becomes visible.

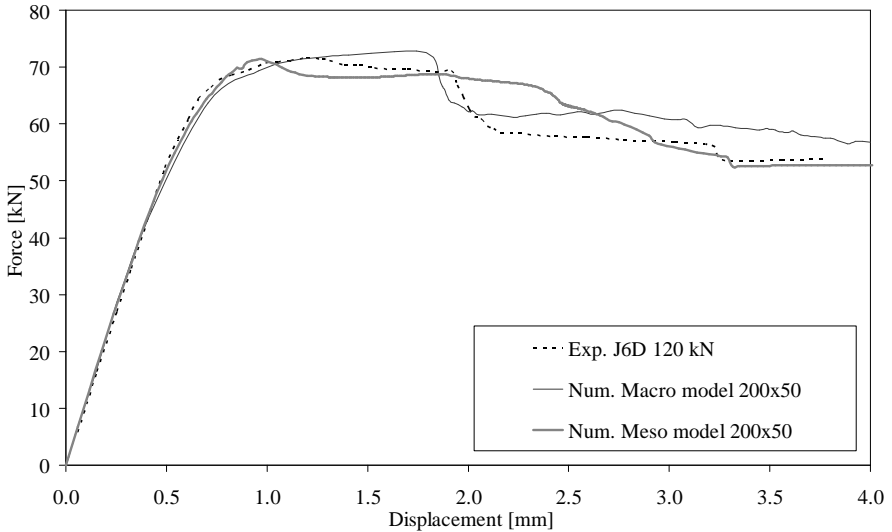


Fig. 7-11: Horizontal load displacement diagram of wall J6D: Experimental versus numerical results

This is also confirmed regarding the experimental crack pattern in Fig. 4-16 on the left in comparison to the equivalent plastic strain (see Fig. 7-12 left) and the plastic activity displayed in Fig. 7-13 on the left. The last presents the activation of yield criteria (see Section 4.3.3.3). Here, light blue colours mean stone failure, while green, yellow and red express mortar failure. Also the crack band width of the wall and the failure types are well computed.

After this well verification of the basic model using calibrated parameters, the impact of unit type on the damage is investigated. In case of higher units (see Fig. 7-10 in the middle and on the right), a higher mortar damage is to expect, while the important units should be less damaged. The simulation results of both constitutive models confirm these predictions. The compact units lead to less brick damage, while many cracks occur in the long units. This is demonstrated in Fig. 7-14 by means of the coloured depicted plastic strain of the units due to meso-modelling and by means of plastic activity (see Fig. 7-13). Here, macro-modelling predicts the activation of unit failure criteria ( $F_1$  to  $F_4$ ) in many regions (light blue elements) as shown in Fig. 7-13 left. For the picture in the middle and on the right, much less activations of unit failure criteria can be observed. Instead more mortar failures occur (depicted by the yellow, red and green regions).

Moreover, the failure region (crack band width of the wall) becomes smaller in case of more compact stones as displayed by the equivalent plastic strain in Fig. 7-12 as well as by the deformed shapes of meso-modelling in Fig. 7-14. In addition, this is indicated by the plastic activity of Fig. 7-13.

It can be summarised that more compact stones should be more useful in case of seismic action, since the unit damage is smaller and the ductility higher. Further, the mortar damage is increased

that usually goes in line with well energy dissipation. However, the shear capacity is decreased in case of compact units.

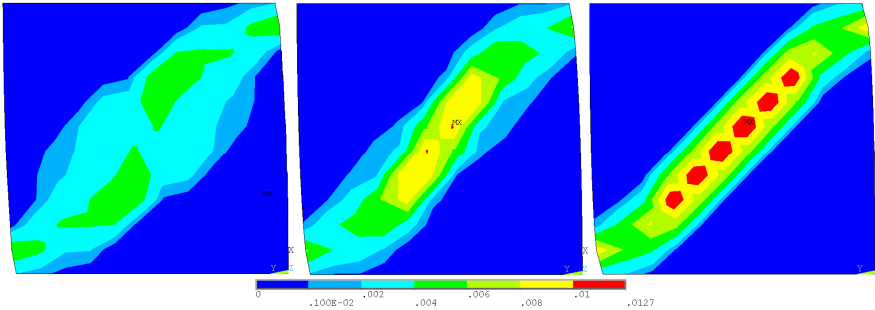


Fig. 7-12: Equivalent plastic strain (drift 3 mm) by Schlegel model, Left 200 x 50, Middle: 200 x 100, Right: 200 x 150

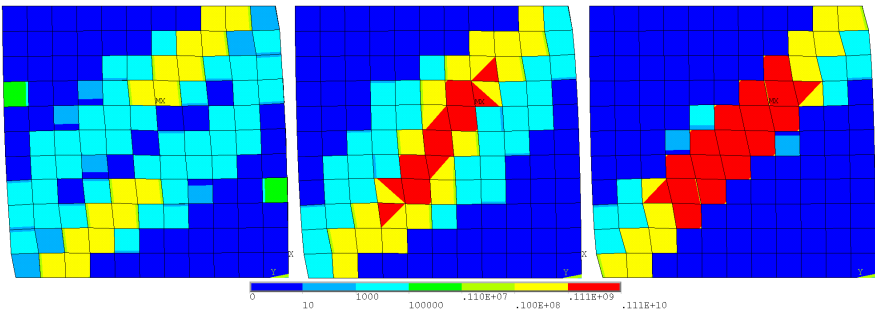


Fig. 7-13: Plastic activity (drift 3 mm) by Schlegel model, Left 200 x 50, Middle: 200 x 100, Right: 200 x 150

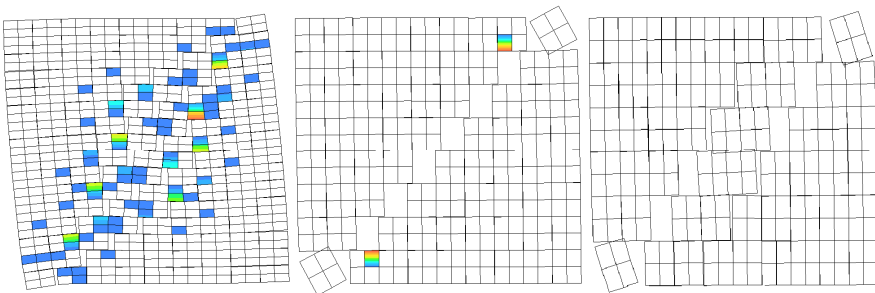


Fig. 7-14: Plastic unit strain (drift 3 mm) by meso-modelling, Left 200 x 50, Middle: 200 x 100, Right: 200 x 150

## 8 Application of the risk management methodology to evaluate different measures

The suggested risk management methodology of Chap. 2 is applied on the problematic of risk reduction by means of vertical prestressing of masonry in case of seismic action. Several informations are already determined and collected in previous chapters. Finally, the different components are compounded here.

### 8.1 Hazard analysis

In Section 3.6 the probability of earthquake loading is given for the example of the region of Aachen. The results of probabilistic seismic hazard analysis PSHA by [Schmitt 2005] is a hazard curve, which is displayed in Fig. 3-11.

If the whole curve is completely integrated in the probabilistic damage assessment, a huge amount of earthquakes would be simulated on a very low excitation level, since small earthquakes have a high probability. Consequently, transient structural simulations related to these low excitation level, would not lead to damages. However, the computational effort increases enormously. Moreover, very small probabilities should not be used in the investigations [Schmitt 2005], since a prediction of this range is very unreliable. A consideration of the whole hazard curve is not reasonable. For this reason, only return periods of 475, 2000 and 10000 years are used in order to assess the damage and to estimate risk on base of such discrete investigation regarding the hazard curve. The related probabilities of exceedance of the hazard  $p_{ex}(H)$  regarding chosen return periods are given in Tab. 3-4.

In each return period further scatter is inherent the occurring strength earthquake action. In accordance with [Rackwitz 2006] and [Hosser et al. 1986], the response spectra scatter in a range defined by a lognormal distribution with a standard deviation of 0.6 is used. For target spectra - on the chosen discrete seismic load levels - artificial earthquakes are generated (see Section 3.6 and Appendix B). The generation includes a small scatter of seismic strength. To reach finally the suggested standard deviation of 0.6, a scaling factor 0.5 is still necessary to regard for the probabilistic variation of earthquake action. The correctness of the finally chosen PDFs for the scaling factor to account for these uncertainties is depicted in earthquake spectra as demonstrated e.g. in Fig. 3-12 Fig. 3-13. The dashed red lines depict the standard deviation of 0.6 and the remaining dashed curves represent the earthquakes scaled by a factor of 0.5. Four different time histories are generated on each chosen seismic load level (return period). The strategy is illuminated more in detail in Section 3.6.

### 8.2 Damage assessment

To express damage, reasonable damage parameters have to be defined firstly. The damage parameters used in this thesis are described in Section 4.3.4. A summary and the parameter notations are given in Tab. 6-9. The damage of seismic loaded masonry walls is predicted by dynamic simulations. This damage assessment, which bases on the generated accelerograms of the hazard analysis, takes into account the uncertainties of seismic loading in a manner described above. An extensive probabilistic damage assessment is carried out for wall 3 in order to estimate risk on base of their results, which are expressed by means of probability density functions for the predicted damages and the related probabilities. In addition, uncertainties of material resistance, support conditions, vertical loading and the degree of prestress level are included as well. The assumed scatter in terms of PDFs, the probabilistic simulations and their results are presented in Section 6.3.3 for wall 3, which is a bracing wall of a three storey terraced house and was investigated in static cyclic experimental tests (see Section 4.2.4.2). The test results are used

for a model calibration (see Section 6.3.1). Thereafter, deterministic transient simulations on base of the generated earthquakes of the hazard analysis are carried out (see Section 6.3.2.2). The wall geometry, vertical loads, support conditions etc. are described in Section 4.2.4.2. In order to analyse the impact of prestressing on damage and its probability, a non-prestressed and a prestressed variation of wall 3 is computed. The results of the probabilistic analyses are presented in 6.3.3.2 and Appendix E. Resulting PDFs for the storey drift and the global unit damage are exemplarily depicted in Fig. 8-1 and Fig. 8-2 for a return period of 10000 years. The deterministic results have shown a small impact of prestressing on the drift (see Tab. 6-11, Tab. 6-12 and Tab. 6-13). This is confirmed by the PDFs, since they show only small differences. Not so the global unit damage. Neither the deterministic simulation, nor the probabilistic ones show a small impact. Instead the probability of great damages increases due to prestressing, while probability for small damages decreases significantly. For the mortar damage, prestressing effects the opposite (see Appendix E).

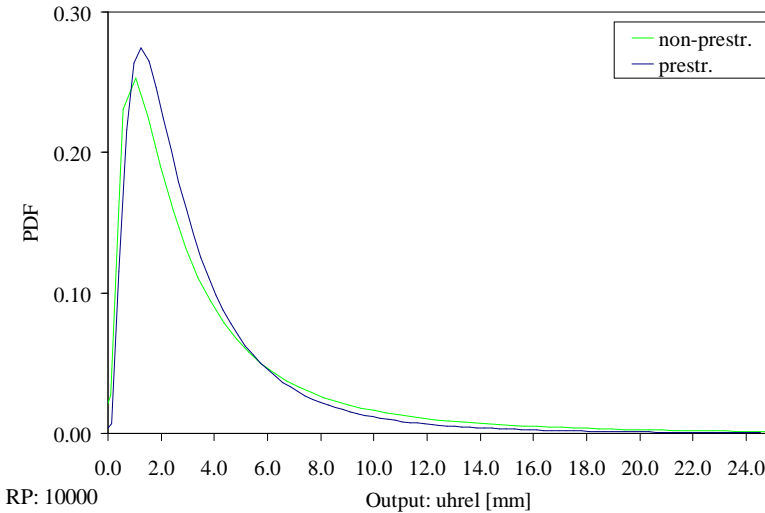


Fig. 8-1: Probability density functions of the storey drift for a return period of 10000 years for wall 3

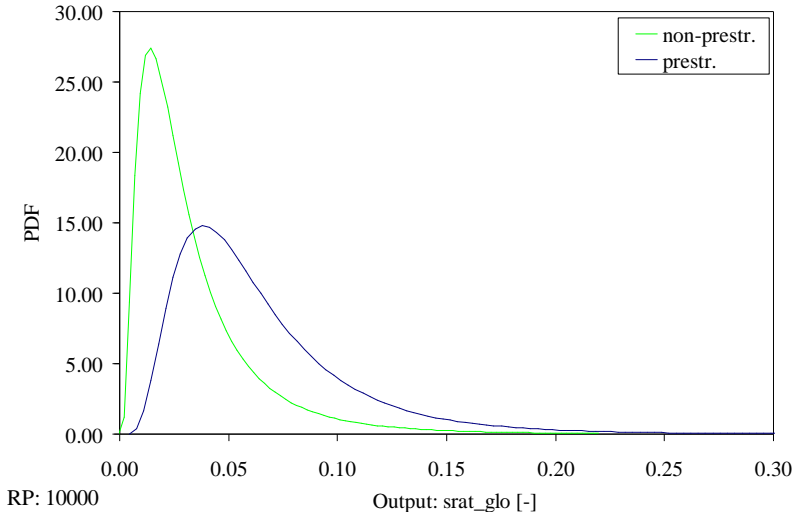


Fig. 8-2: Probability density functions of the global unit damage for a return period of 10000 years for wall 3

### 8.3 Risk calculation

As mentioned before numerous means to express, calculate and compare risks already exist. In this work, the focus lies on the structural risk  $R_D$  (see Section 2.2.2 and Appendix A), which accounts for the physical damage excluding further consequences like repairing costs or victims. It is clarified in Def. (2-6). In practice, the calculation of risk entails several philosophical and practical problems, of which only some can be investigated and solved in this contribution. First of all, the probability of exceedance of the hazard  $p_{ex}(H)$  – which expresses the occurrence of earthquakes in this study – is taken into account. As a result of the hazard analysis, the hazard curve given in Fig. 3-11 and discrete values in Tab. 3-4, provides the needed  $p_{ex}(H)$  for each of the return periods, which are investigated.

The structural risk  $R_D$  which accounts only for the physical damage of the structure is calculated by means of the probability of exceedance of the hazard  $p_{ex}(H)$  and the ‘damage probability’  $p_{ex}(L,R)$  due to resistance and load scatter as a result of the probabilistic damage analysis, as shown in Eq. (8-1). In this study, these analyses account for the scattering of the resistance, e.g. several strengths, Young’s Moduli and damping parameters, as well as the variations in loading. On the one hand, it is the level of prestressing and dead load, here in terms of ‘head mass’. On the other hand, the load intensity of an earthquake, which can scatter as well for each return period. The last is considered by means of the scaling factors  $X_{skal}$  and  $Y_{skal}$  for the horizontal and vertical acceleration histogram and different duration  $D$  (see Tab. 6-15, Tab. 6-16 and Tab. 6-17).

$$R_D = p_{ex}(H) \cdot p_{ex}(L,R) \cdot D \quad \text{Eq. (8-1)}$$

The factor  $D$  represents the damage degree, which can be expressed by several damage parameters in different units.

Afterwards, the risk of the global unit damage is exemplary calculated for a return period of 10000 years. As stated out in Tab. 3-4, a probability of exceedance of the hazard  $p_{ex}(H)$  of 0.0001

is related to this return period. Instead of the fitted PDF, the sampled histogram of the probabilistic damage analysis is directly used to avoid inaccuracy or errors inherent fitting. The resulting distribution for the probability of exceedance is shown in Fig. 8-3 for the global unit damage of the non-prestressed wall. Fig. 8-4 depicts the probability of exceedance of the prestressed one.

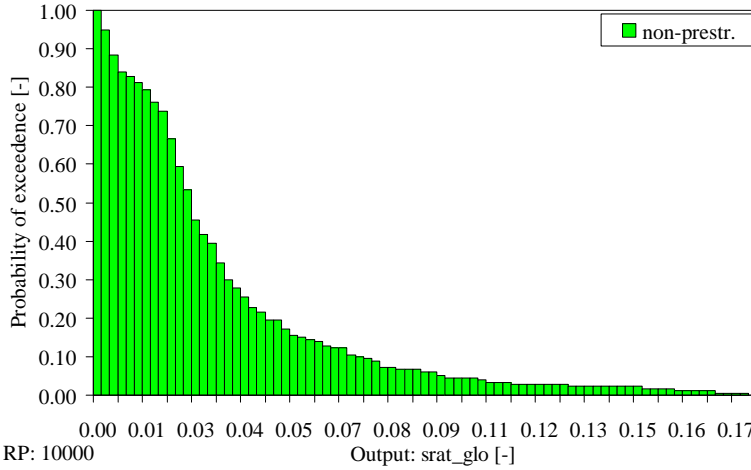


Fig. 8-3: Probability of exceedance of the global unit damage for a return period of 10000 years without prestressing

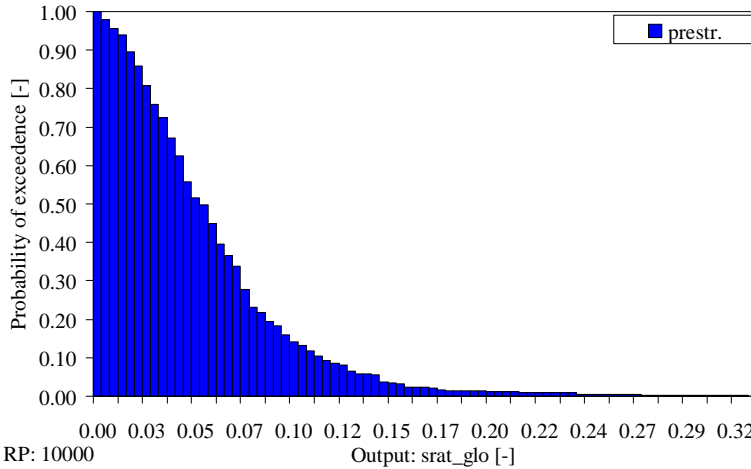


Fig. 8-4: Probability of exceedance of the global unit damage for a return period of 10000 years in case of prestressing

By means of this probability of exceedance and Eq. (8-1), the risk is calculated for every interval of the histograms. The yielding distributions for the risk are presented below. In Fig. 8-5 the risk of global unit damage of the non-prestressed wall is depicted, while Fig. 8-6 shows the unit damage risk of the prestressed wall. The low risk values are caused by the low probability of exceedance of the hazard for the return period of 10000 years, which amounts 0.0001, and the

small values to express this average global unit damage. The number of nodes of the numerical wall model is included there as quotient. Yielding risk distributions of further damage parameters are given in Appendix G.

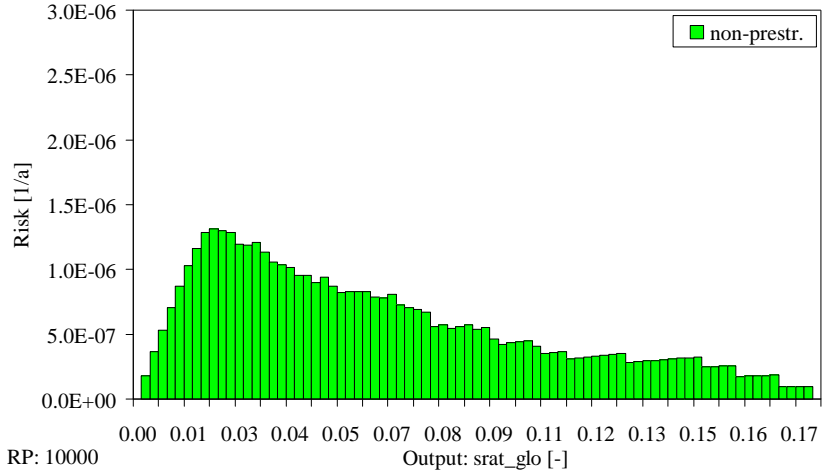


Fig. 8-5: Risk distribution of the global unit damage for a return period of 10000 years without prestressing

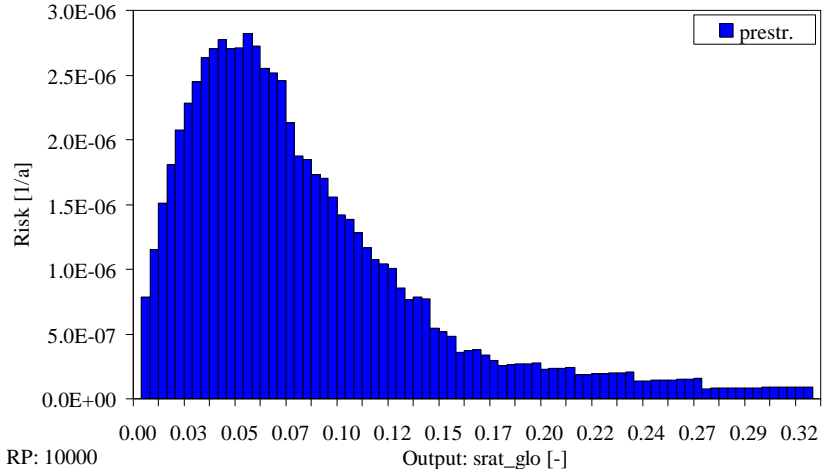


Fig. 8-6: Risk distribution of the global unit damage for a return period of 10000 years in case of prestressing

As an important finding, the calculated values of the cumulative risk can depend on the number of histogram classes (also named number of intervals). The risk can decrease with the number of intervals. This is mainly caused by the value of the damage class in the histogram, since the mean value of the intervals – which is practicably used – changes with the interval width. Consequently, an equal amount of intervals as well as interval width is recommended for a reasonable risk comparison. A standardisation would be desirable. At least the information of used in-

terval numbers and width is important for the decision maker, to avoid wrong adjudications regarding comparisons of different calculations. Moreover, the number of samples of probabilistic analyses and statistical outliers can influence the calculated values for the risk.

#### 8.4 Risk reduction - Comparison of prestressed and non-prestressed walls

In Tab. 8-1 cumulative risk values are given for some damage parameters, exemplarily for the lowest considered return period of 475 years and for the greatest return period of 10000 years. The single risk values of the discrete distributions (see e.g. Fig. 8-5) are simply summed. The impact of prestressing is clearly demonstrated by a percentile risk reduction. For the global unit damage a negative value results. Its meaning is an increase of risk for the unit damage in case of prestressing and seismic action. This goes in line with results of static and dynamic analyses. For local and global mortar damage as well as for the equivalent plastic strain and further damage parameters, the risk is reduced by prestressing. This is valid for all investigated return periods.

Parameter	475 [a]			10000 [a]		
	Risk		Risk reduction [%]	Risk		Risk reduction [%]
	Non-pre.	Prestr.		Non-pre.	Prestr.	
SRAT_glo [-]	6.92E-04	1.36E-03	-96.6	4.60E-05	7.03E-05	-52.92
EPEQ_loc [-]	3.48E+00	9.34E-02	97.31	1.87E-01	4.84E-02	74.15
EPEQ_glo [-]	1.48E-01	2.86E-03	98.06	1.73E-02	2.74E-03	84.15
EQV [%]	9.58E-02	2.44E-02	74.52	6.11E-03	9.40E-04	84.62

Tab. 8-1: Overview of risk values and risk comparison for global unit damage, local and global mortar damage and equivalent plastic strain

#### 8.5 Optimisation

In Section 7.1.2.2, an optimisation of the prestress level is already discussed in order to minimise the different damage parameters. This damage optimisation would entail an optimal risk reduction, since the probability of high damages has to be reduced. For this problem, it is of interest to find an optimum for the prestressing level, which minimises both the unit and the mortar damage. In previous chapters, it is repeatedly verified that prestressing increases the unit damage, but decreases the mortar damage. The objective functions develop oppositely. This requires a Pareto optimisation. The program optiSLang<sup>®</sup> offers such optimisations. In this case, several damage parameters are included in the optimisation procedure.

Above, several risks for different damage parameters are estimated separately (see Tab. 8-1). It is demonstrated, that for the intervention measure ‘vertical prestressing’ e.g. the risk for the unit damage is increased, while for the mortar damage it is significantly reduced. Caused by the units of the damage parameters and relations, only small worsening is observed for the brick damage (-52%), whereas the benefit for the mortar damage appears to be more significant (84%) as shown in Tab. 8-1. The user of such a risk based concept or the decision makers could deduce that within an optimisation, main emphasis should lie on the mortar damage due to its meaningful values. However, from the physical point of view the unit damage is much more important, since it can easily lead to brittle collapse. Therefore, it is better to accept high mortar damages and great numbers for the values of mortar damage risk, also if it would go in line which a small reduction of the brick damage risk.

It is questionable, whether dealing with risk is reasonable for such Pareto-based optimisations. The risk for one damage parameter would increase while the risk for another parameter would decrease. An expression in terms of an overall risk, which includes all damage parameters, would be necessary. However, such a mix can lead to wrong decisions, caused by incomparability of some parameters. Or better expressed: They should not be compared.

## **8.6 Impact of prestressing on the loss**

In Chap. 2 and Appendix A the differences between ‘damage’ and ‘loss’ are already explained in detail. Consequently, ‘damage’ accounts only for the physical damage of the analysed structure. As explained above, it is investigated extensively and precisely by means of advanced complex transient probabilistic analyses with very high computational effort despite the well chosen efficient material model which bases on macro-modelling. In this manner, the structural risk was assessed, which is sufficient to judge on the usefulness of prestressing and to avoid the integration of inaccuracy, which inheres in loss assessment. The last is caused by the lack of knowledge, the missing of well established accurate methods to determine the losses as well as missed profound databases. Another reason is the high degree of subjectivity. For all these reasons, a further effort to estimate losses is neither reasonable, nor necessary in the framework of this thesis.

Despite all that, some statements concerning the impact of prestressing on the loss can ingeniously derived on base of structural results. Due to a wall-tendon interaction (see 4.2.5) prestressing can increase besides the ductility. This reduces not only the probability of collapse enormously, but also the loss. The resulting number of fatalities is therefore reduced as well as costs for business interruption etc. The loss reductions especially in combination with the decreased probability entail a risk reduction, since both factors to calculate risk decrease. In contrast, a wrong application of prestressing (see Appendix I) can lead to brittle collapse, which surely causes higher losses and higher risks. Due to collapse people cannot escape and the loss regarding fatalities and injured person is very high. The estimation of fatalities is very difficult. However, in case of collapse, which avoids an escape, a probability for instantaneous death of 0.3 up to 0.5 is stated out in [Rackwitz 2006]. This does not include the fatalities on posterior data, e.g. after rescue in hospitals.



## 9 Synopsis

### 9.1 Summary

Conventional design concepts base on relative simple strategies, which aim on collapse avoidance and use rough methods to assess the structural behaviour. Partial damage is usually not taken into account. In order to investigate the impact of vertical prestressing on seismic loaded masonry in depth, the complex and innovative concept of risk management is applied in combination with advanced and detailed methods for the structural analysis, which allows an assessment of partial damages. However, the definitions and understandings of terms within risk management spread in a wide range throughout the literature. Even for risk, diverse definitions can be found. This lack of a harmonised concept and definitions is addressed by introducing a clear risk management framework, which provides assistance in analysing, comparing and treating disaster risk. Before the suggested risk management concept is exemplarily applied on an essential bracing wall of a three storey terraced house in the region of Aachen, Germany, several further topics are investigated and components for this example are determined. First of all, significant requirements concerning the seismic performance of structures are introduced, which are essential for the investigation of strengthening measures in case of earthquakes. The hazard analysis is the first component of the risk management chain, which is handled in this thesis. Its result is a description of probability and variety of earthquake loading. It is regarded to the intensity as well as to the variety of earthquake properties, as duration and frequency content. This first component is the basis for a reasonable risk assessment, in which also the damage is assessed in a next step.

The damage assessment is the main part of the thesis and therefore extensively and intensively investigated. Experimental static cyclic tests of prestressed shear walls are an important base, which are *inter alia* used to calibrate numerical models. Moreover, the reason for the well ductile behaviour of the experimentally investigated prestressed walls is stated. Usually, high vertical loading leads to brittle failure of masonry. Since high ductility is very important for seismic action as below explained more in detail, vertical prestressing of masonry would consequently not be useful. However, the tendons inside the tested walls are the reason for the observed well ductile behaviour. The tendons get in contact with the wall during the horizontal loading, which avoid slide down of the upper wall triangle. The wall-tendon interaction averts brittle failure. As a further result of these findings, the practical details in application of vertical prestressing are important for the degree of ductility. Consequently, external prestressing and internal tendons without any contact lead to very low ductility, whereas a high one results for internal tendons with full bond and internal tendons with contact during the horizontal loading. These findings illuminate additional consequences, which are briefly given in the conclusion and are summarised in more detail in Appendix I.

Since, the shear capacity of masonry is significantly increased due to prestressing, its application appears obvious to improve the seismic resistance. The high importance of ductility is already mentioned in the previous paragraph and precisely explained in Section 3.7. Therefore, e.g. external prestressing can be dangerous, since leading to brittle collapse. A damage based design is also helpful for the subsequent distinction. In areas of low seismicity also an external prestressing can be useful. The increase of shear capacity goes in line with an increase of the elastic range, in which nearly no damage occurs. If it can be ensured that during the design life no earthquake loading exceeds the shear capacity, brittle collapse is avoided and the damage is highly reduced. By contrast, in regions of high seismicity these design strategy is not reasonable. On the one hand, sufficient shear capacities cannot be obtained (at least not economically) for very strong earthquakes. On the other hand, great elastic ranges lead to high lateral loads. Ductile structures show a more intelligent behaviour, since the earthquake energy is dissipated and the resulting horizontal forces are limited. However, the damage increases with ductility. External prestressed masonry walls (or prestressed by similar means) fail brittle. Here, internal prestress-

ing can decrease damages and avoid brittle collapse due to wall-tendon interaction. Whenever prestressing avoids collapse, the loss is reduced as well (less fatalities etc.). Damage and loss reductions entail risk reduction, since they are essential factors to calculate risk. Furthermore, a distinction of damage types is important. The numerical simulations show throughout a decrease of mortar damage as well as several plastic strains. However, the global unit damage increases. Incidentally, the unit damage is identified as reason for brittle failure.

Fundamentals of numerical modelling strategies for masonry and plastic theory are given, which are essential to use three explained material models correctly and reasonably. Regarding transient analyses, especially in combination with probabilistic investigations the constitutive model of Lagomarsino and Gambarotta [Gambarotta and Lagomarsino 1997b] is most suitable and chosen for such analyses. The capability of the material model is verified for prestressed static cyclic loaded masonry walls. Its numerical results agree well with the experimental tests. The loadbearing behaviour of all investigated walls is qualitatively and quantitatively well predicted. The model is able to describe effects of strength and stiffness degradation as well as dissipation. Even the different hysteretic behaviour of slender and compact walls is very well simulated. Therefore, it can be utilised for additional dynamic investigations.

Previously, the gap of missing experimental tests of non-prestressed reference shear walls regarding [Budelmann et al. 2004] is closed by corresponding simulations. The results are plausible. Comparisons of static loaded non-prestressed and prestressed versions of several walls show throughout a reduction of the mortar damage, equivalent plastic strain, plastic shear strain and vertical plastic tensile strain. The global unit damage is always increased in case of prestressing. The impact of prestressing on the local unit damage is altering. Moreover, extensive static case studies are performed to discover important influences. The assumption of a very high importance of the support conditions is confirmed. The existence of restoring forces due to tendons is verified. They can be taken reasonably into account due to modelling of tendons, while a simple reflection by means of external forces is not able to account for them. Significant differences in the results are observed merely for compact walls with unsupported tops and two strands on the edges.

With results of the parameter calibration that bases on experimental tests, the dynamic behaviour is investigated numerically, by means of subjection a compact and a slender wall to artificial generated earthquakes. The trends concerning the impact of prestressing from the static analyses are confirmed by the majority of dynamic simulations. Some additional irregularities can be observed. Different characteristics of diverse accelerograms can cause these alternations regarding the impact of prestressing, especially accounting for the different frequency contents of the earthquakes and natural frequencies of the walls, which change during the earthquakes. The local and global mortar damage is always reduced. Also the equivalent plastic strain, plastic shear strain and vertical plastic tensile strain are reduced by prestressing for the most earthquakes. The storey drift is not significantly affected by prestressing for all earthquakes, and the effect is irregular. For low level earthquakes a general reduction may be seen, whereas for strong seismic action the drift of the prestressed wall is often greater. The results for the local unit damage differ strongly.

The probabilistic analyses confirm this impact of prestressing of the previous static, cyclic and dynamic simulations. Especially, for the compact wall 1, high irregularity is observed concerning the local unit damage. The probabilistic analyses deliver damage probabilities, which express the general lawfulness. Thus, the deterministic irregularities become clearer and it can be concluded, that in general not only the local, but also the global unit damage is increased due to prestressing. The storey drift is not significantly affected by prestressing, since the PDFs show no great differences. Concerning the extensive probabilistic analyses of the small wall, the horizontal earthquake scaling factor  $X_{skat}$  and the head mass show the highest impacts. For the investigated walls, the vertical earthquake scaling factor  $Y_{skat}$  is closely not relevant. The support conditions in terms

of stiffness of the floor slab – simply modelled by a variable Young’s Modulus of the concrete  $E_c$  – have a medium or small impact on some damage parameters. However, it is the third most important parameter for the storey drift. The greater  $E_c$ , the smaller the storey drift. The correlation matrices of the different return periods are similar. This high impact of  $X_{skat}$  and head mass increases with the earthquake strength. Moreover, the enormous impacts of  $X_{skat}$  and head mass are reduced by prestressing. Besides, the prestress level influences the damage. It increases the unit damage and decreases the mortar damage as well as the equivalent plastic strain.

This is confirmed by results of previous deterministic simulations as well as with the calculated risks. The observed impacts throughout all simulations go in line not only with the risk distribution, but also with the cumulative risk values. Since, the enormous impact of the earthquake loading - at least in case of high load levels - a damage reduction and so a risk reduction becomes more difficult by means of material improvement or prestressing, which is caused by their small impacts. The results are confirmed by experimental tests and literature.

In addition to the original subject of this thesis, several further measures are suggested in Chap. 7, which could improve the seismic performance of masonry and reduce the unit damage. They are discussed based on existing theories, and first numerical investigations are briefly carried out. The brick damage may be reduced due to more compact units.

## 9.2 Conclusion

The probabilistic damage based design of risk management was very helpful to judge on the usefulness of vertical prestressing. The advanced extensive numerical investigation got a deeper insight and exhibited several problems. The question whether the application of prestressing on earthquake loaded masonry is useful, cannot be answered generally. It is to distinguish in several cases depending on the structure, degree of seismic excitation, level of vertical loading and means of practical execution of prestressing. The relations are summarised in Appendix I.

In case of seismic action, the wall-tendon interaction has a very important impact on collapse, damage and loss. Since, high vertical loading and missing wall-tendon interaction lead to brittle collapse, prestressing can be dangerous. Thus, external prestressing especially in case of high prestressing degrees causes brittle failure, if high earthquake intensities exceed the shear capacity. For regions of high seismicity, a well ductile behaviour has to be ensured by means of further measures, if external prestressing is applied (or internal one without sufficient contact). In regions of low seismicity, the ductility is less important, if a sufficient safety factor guarantees lower horizontal loading than shear resistance. The increased elastic range leads to lower damages up to activation of plasticity.

As an advantage, the mortar damage is always decreased by prestressing in these investigations. However, it is not as important as the unit damage, which is generally increased. The same trends are valid for the related risks.

## 9.3 Outlook

The important impact of the support conditions (e.g. floor slabs) on the loadbearing behaviour and on the damage is verified by static, dynamic as well as probabilistic analyses. Not only for the experimental set-up of shear wall tests, but also for a realistic numerical modelling of bracing walls, deeper investigations are recommended. In this work, the dynamic results of the prestressed masonry base only on one material model. Extend simulations and/or experimental tests are suggested to verify these theoretical results.

The observed high ductility of the shear wall tests using internal prestressing [Budelmann et al. 2004] can be explained with the suggested theory of wall-tendon interaction. Due to the importance of ductility in case of seismic action and concerning the usual brittle behaviour of vertical highly loaded masonry walls, deeper investigations are important, in order to improve and ensure ductile behaviour. Since, prestressing increases the unit damage, but decreases the mortar damage, it is interesting to find an optimum for the prestressing level, which minimises both the unit and the mortar damage. The objective functions develop oppositely, which may be managed by Pareto optimisation.

Different possibilities exist to calculate the risk on base of probabilistic sampled databases. For instance fitted probability density function can be used or directly histograms with a different number of intervals as well as different element widths. Moreover, it can be expressed in several further ways. Only two variations are suggested and used in this thesis, as distribution and as single cumulative number. The impact of different calculation methods and types to express the risk, on the comparison should be investigated more in detail, in order to provide a basis for reasonable risk comparison and standardised methods.

Especially, parameters on the microscopic level – for instance the brick size – could be chosen and optimised to reduce the brick damage, which increases due to vertical prestressing. An additional intensive research and verifications concerning the usefulness in case of seismic action, is neither the aim, nor the purpose of this thesis. However, it is an interesting and promising topic for further research work. Regarding, the presented further measures of Chap. 7 more research work is necessary to get a deeper insight.

## Appendix A: Risk Management Glossary

In this glossary regarding [Pliefke, Sperbeck, Urban 2006] the most important terms of *Risk Management* are briefly defined in a chronological sequence regarding the concept, which is shown in Fig. 2-9.

### System:

The object of investigation for which all sources of *Hazard* are identified and *Risk Analysis* is being performed. The *System* can be composed by a single building or infrastructure element, a suburb of a city, a whole urban region or even an entire country.

### Hazard:

A potentially adverse physical event, phenomenon or human activity that may cause harm to the predefined *System*. Harm can include injury or *Loss* of life, property *Damage*, cultural, social, historical and economic disruption or environmental degradation.

### Hazard Analysis:

Consists of three steps: *Hazard* identification, determination of relevant intensity levels and estimation of the corresponding probabilities of occurrence in a predefined time period. Depending on the size of the *System*, the results may differ for each *Element at Risk*.

### Element-at-Risk (EaR):

A single or a group of persons or objects within the predefined *System* that are susceptible and exposed to the impact of a *Hazard*. In order to guarantee a complete coverage, all *Element at Risk* collectively should compose the entire *System* that is being investigated. This will be referred to as the 'principle of completeness'.

### Exposure:

Inventory of *Element at Risk* that are subjected to a *Hazard*.

### Structural Vulnerability (for each EaR and Hazard intensity):

Is a specific characteristic of an *Element at Risk* that indicates the susceptibility towards the impact of a *Hazard*. Thus, *Structural Vulnerability* links the *Hazard* intensity to the *Damage* of an *Element at Risk*.

### Damage (for each EaR and Hazard intensity):

Describes the physical, biological or chemical effect on an *Element at Risk* caused by the impact of a *Hazard* of a given intensity. Damage captures the material harm and is not expressed in monetary terms.

**System Vulnerability (for each EaR and Hazard intensity):**

Is a specific characteristic of an *Element at Risk*, which indicates the total potential of a *Hazard* of a given intensity. Thus, *System Vulnerability* assigns a *Loss* value to each given *Damage* state of an *Element at Risk*. It is best described by a function that evaluates the *Consequences* of a certain *Damage* state by taking into account the value of the *Element at Risk* itself as well as its designated functionality within the *System*.

**Consequences (for each EaR and Hazard intensity):**

This term captures and quantifies the various adverse effects a natural disaster event of a certain intensity may have on the different *Element at Risk*. *Consequences* can be subdivided into *Direct* and *Indirect Consequences*.

**Direct Consequences** are *Damages* that occur simultaneously to the time the disaster takes place or by immediate follow-on physical destruction such as fires. Therefore they can directly be related to the disaster itself.

**Indirect Consequences** in contrast usually occur with a time shift as a result of the *Direct Consequences*. They can be interpreted as follow up costs that result from the *Element at Risk* being not able to carry out its designated functionality within the *System* after the disaster has occurred.

Moreover, *Direct* as well as *Indirect Consequences* are to be further subdivided and classified into economic, humanitarian, ecological and CSH (cultural, social, historical) *Consequences* due to the measure that is in use for their quantification. As it is possible to assign a monetary value only to economic *Consequences* in a direct way, they will be referred to as **tangible**. All other classes of *Consequences* are termed **intangible**.

In the following several *Direct and indirect Consequences* are outlined divided by consequence classes:

**Direct Consequences:**

**Economic:** Adverse effects on capital stock resulting from physical *Damage* of economic value carrying objects.

**Humanitarian:** Injuries and fatalities due to the *Damage* of objects.

**Ecological:** Ground, air and water pollution, contamination of the environment or other devastating effects on ecosystems caused for instance by releases of toxic substances.

**CSH:** Adverse effects on capital stock resulting from physical *Damage* of CSH value carrying objects.

**Indirect Consequences:**

**Economic:** Business interruption, wage losses, production downtime and other harms on the economy in the long term.

**Humanitarian:** The spread of diseases resulting from the absence of satisfactory hygiene within the affected area, psychological post-disaster effects.

**Ecological:** Penalties due to the violation of environmental regulation rules.

**CSH:** Adverse effects on the wellbeing of society resulting from the abandonment of the CSH value carrying object.

**Loss (for each consequence class and Hazard intensity):**

Subdivided by consequence class this term accumulates all *Direct and Indirect Consequences* a natural disaster of a certain intensity may have at the time the disaster occurs. To quantify the *Loss*, the sum of all *Direct* and discounted *Indirect Consequences* belonging to the considered consequence class for each *Element at Risk* being part of the *System* has to be calculated. In this connection the discounting of the *Indirect Consequences* is dependent on the time the consequences occur and the consequence class specific discount factor that is in use. Then, by definition it can be distinguished between humanitarian, economic, ecological and CHS *Loss*.

**Risk:**

Risk can be expressed in two distinctive ways. One possibility is to express the Risk with respect to the structural *Damage* only (here called '*Structural Risk*'). The second way is to take also the resulting *Loss* (here called '*Total Risk*') into account.

**Structural Risk:**

The *Structural Risk* can finally be calculated by taking the products of the annual probabilities of occurrence and the *Damages*, both given as functions of the *Hazard* intensity, and summing up these products over all *Hazard* intensity levels.

$$\text{Structural Risk} = \text{Probability} \times \text{Damage} \quad [\text{Damage measure} / \text{year}]$$

**Total Risk (for each consequence class):**

For each consequence class the *Risk* can finally be calculated by taking the products of the annual probabilities of occurrence and the losses, both given as functions of the *Hazard* intensity, and summing up these products over all *Hazard* intensity levels.

$$\text{Total Risk} = \text{Probability} \times \text{Loss} \quad [\text{Loss unit} / \text{year}]$$

Consequently, the *Total Risk* is split into the humanitarian, the economic, the ecological and the CSH risk.

**Risk Review:**

Due to the ever changing environment of the *Risk* influencing variables the primary purpose of this step is to constantly include all new information, knowledge and experience about the *Risk* and to perform a *Risk* update, if necessary. It should be emphasised that the *Risk Review* step is only being performed for already identified *Risks* which have run through the *Risk Assessment* and *Risk Treatment* phase at least once. Consequently, in each *Risk Review* iteration the effectiveness of possibly performed *Risk* reduction interventions is indicated.

**Risk Monitoring:**

Accompanying all the steps of the *Risk Management* chain the *Risk Monitoring* procedure captures the exchange of information of all persons actively or passively involved or participating in the *Risk Management* process. It includes the constant awareness of the *System* being endangered by already identified as well as newly discovered *Hazards*. In this regard the *Risk Review* step

can be looked upon as a major sub discipline. As a result of the monitoring procedure the *Risk* evolution within the process over time is registered.

**Risk Management:**

*Risk Management* is defined as the systematic application of management policies, procedures and practices to the tasks of identifying, assessing, treating, communicating, reviewing and monitoring *Risk*.

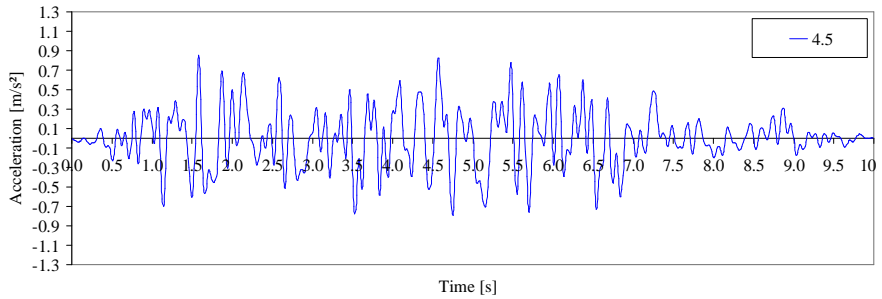
**Appendix B: Data of artificial generated earthquake for probabilistic analyses****a) Return period of 475 years**

Fig. B-1: Accelerogram No. 1 for a steady state phase of 4.5 s

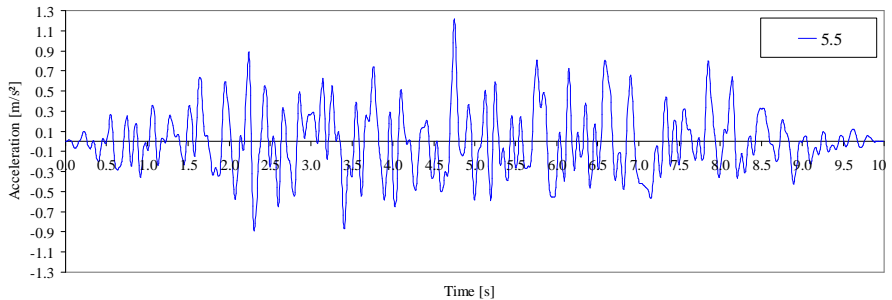


Fig. B-2: Accelerogram No. 2 for a steady state phase of 5.5 s

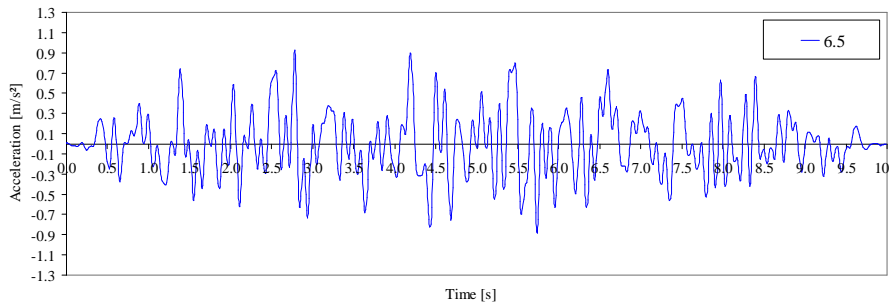


Fig. B-3: Accelerogram No. 3 for a steady state phase of 6.5 s

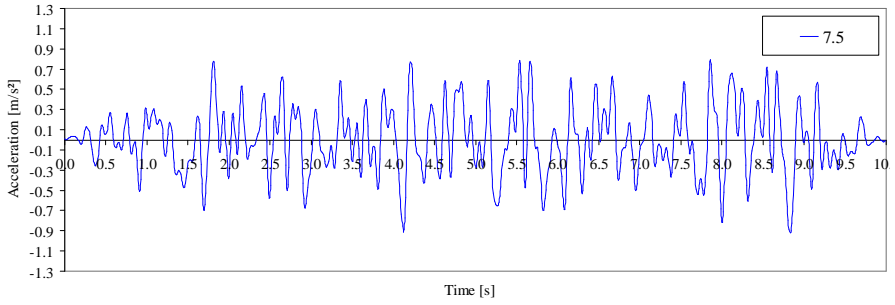


Fig. B-4: Accelerogram No. 4 for a steady state phase of 7.5 s

## b) Return period of 2000 years

No.	Over-all time	Increasing time	Start of decreasing	Steady phase	Simulation stop	Uniform Duration $D_{u0.15}$	Significant Duration $D_{895}$	Arias Intensity AI
	[s]	[s]	[s]	[s]	[s]	[s]	[s]	[m/s]
1	10	1.5	6	4.5	8	5.5	6.4	0.2037
2	10	1.5	7	5.5	9	6.14	6.4	0.2165
3	10	1.5	8	6.5	9	6.4	7.4	0.2467
4	10	1.5	9	7.5	10	6.63	7.7	0.2507

Tab. B-1: Durations and Intensities of the generated accelerograms, return period of 2000 years

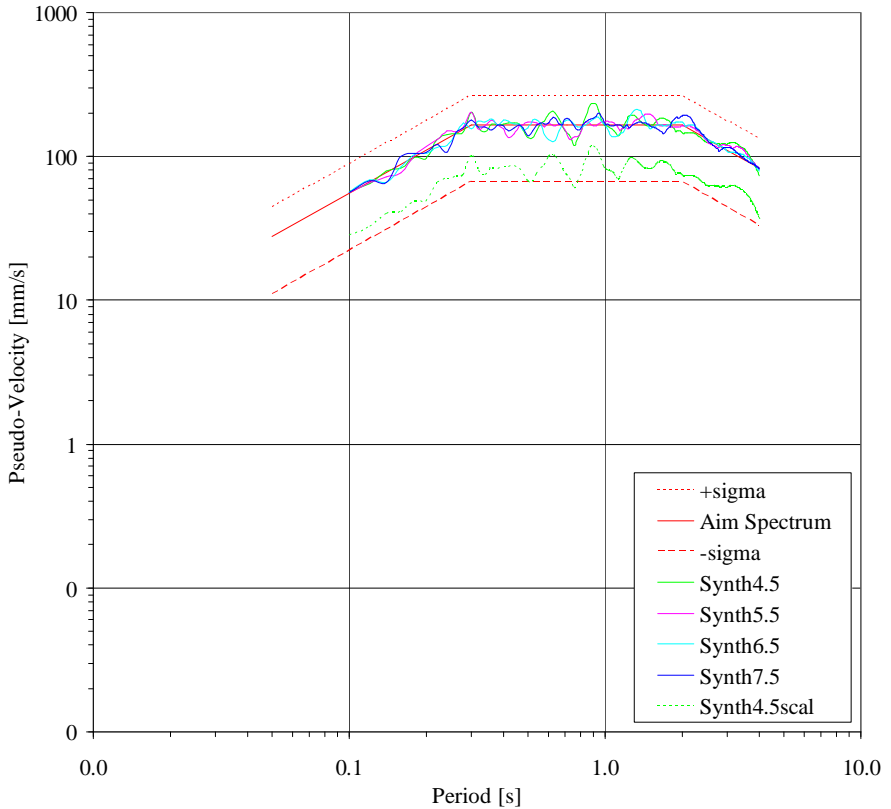


Fig. B-5: Pseudo-velocity diagram, return period of 2000 years

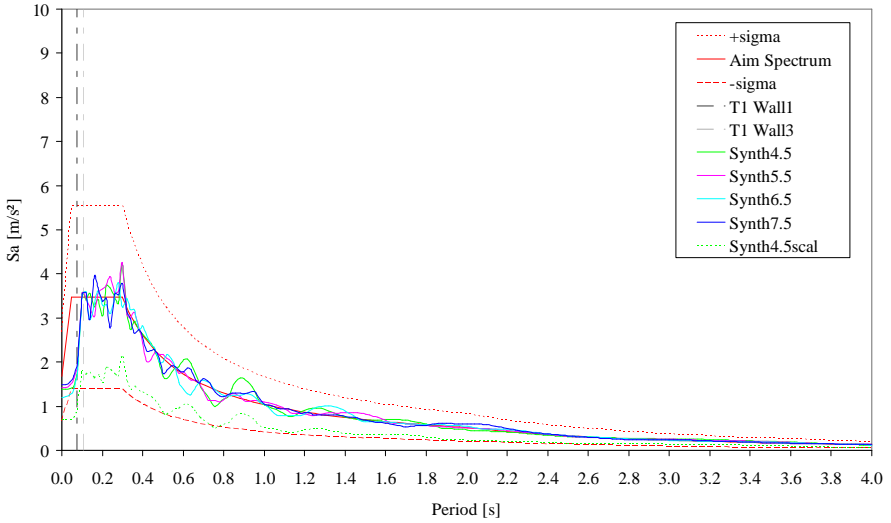


Fig. B-6: Spectral acceleration diagram, return period of 2000 years

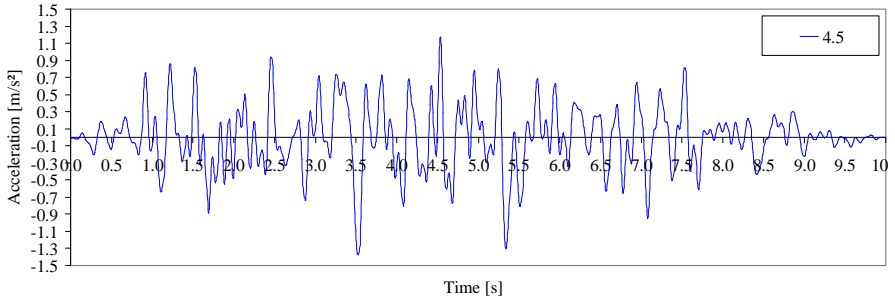


Fig. B-7: Accelerogram No. 1 for a steady state phase of 4.5 s

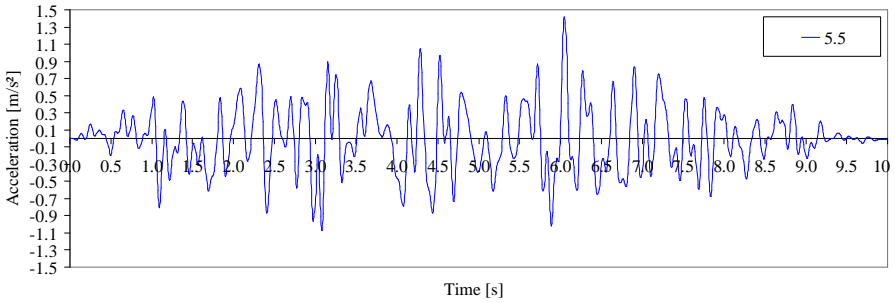


Fig. B-8: Accelerogram No. 2 for a steady state phase of 5.5 s

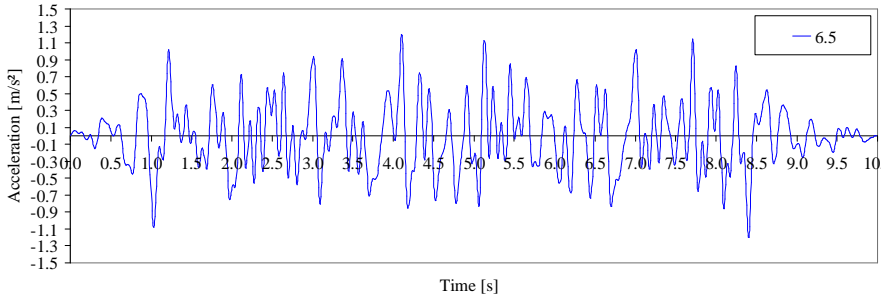


Fig. B-9: Accelerogram No. 3 for a steady state phase of 6.5 s

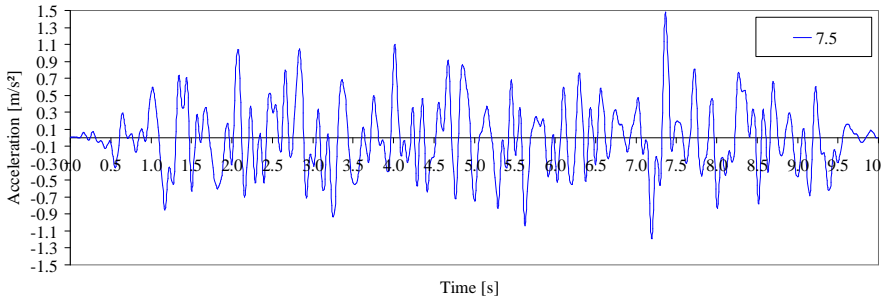


Fig. B-10: Accelerogram No. 4 for a steady state phase of 7.5 s

**c) Return period of 10000 years**

No.	Over-all time	Increasing time	Start of decreasing	Steady phase	Simulation stop	Uniform Duration $D_{u0.15}$	Significant Duration $D_{s95}$	Arias Intensity AI
	[s]	[s]	[s]	[s]	[s]	[s]	[s]	[m/s]
1	10	1.5	6	4.5	7.5	6.71	6.1	0.5801
2	10	1.5	7	5.5	9	7.06	6.5	0.5481
3	10	1.5	8	6.5	9	7.36	6.9	0.5911
4	10	1.5	9	7.5	10	7.86	8.1	0.6511

Tab. B-2: Durations and Intensities of the generated accelerograms, return period of 10000 years

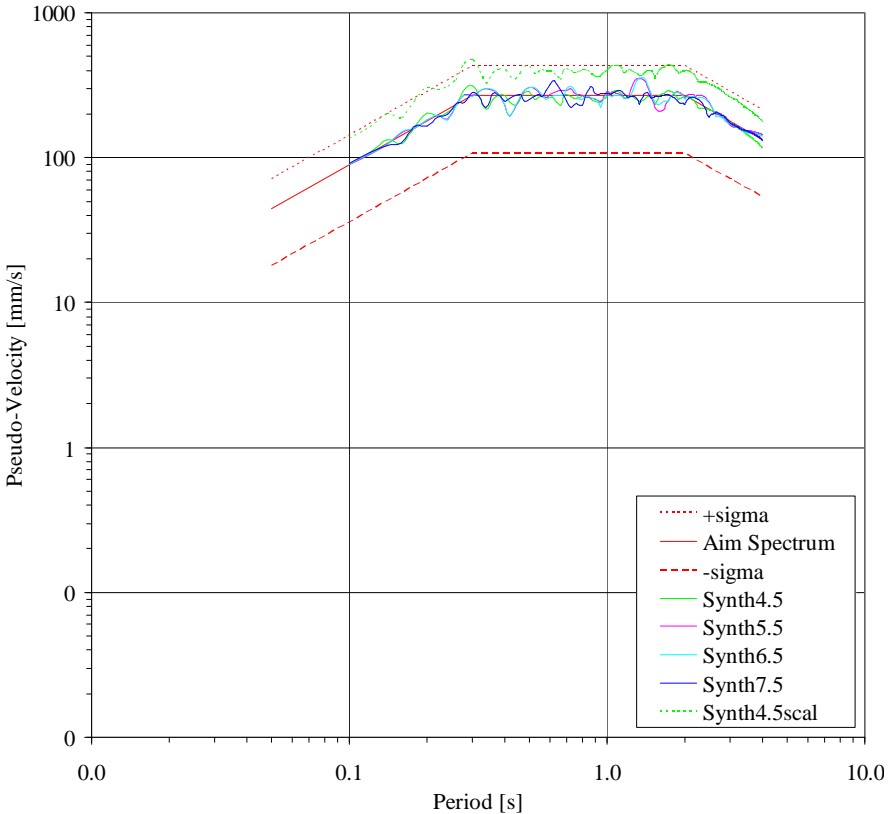


Fig. B-11: Pseudo-velocity diagram, return period of 10000 years

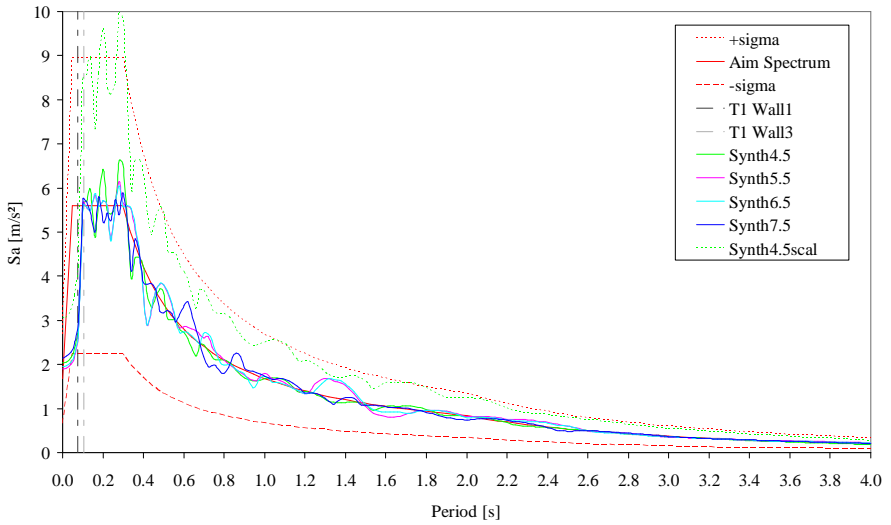


Fig. B-12: Spectral acceleration diagram, return period of 10000 years

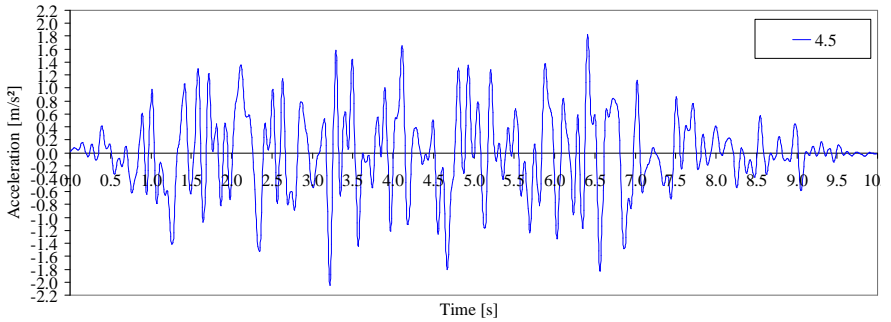


Fig. B-13: Accelerogram No. 1 for a steady state phase of 4.5 s

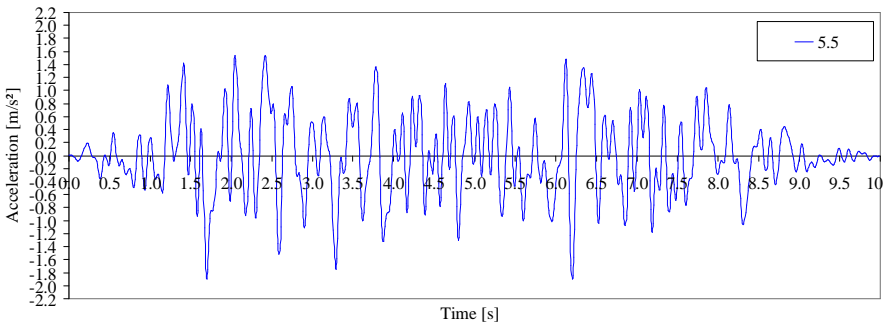


Fig. B-14: Accelerogram No. 2 for a steady state phase of 5.5 s

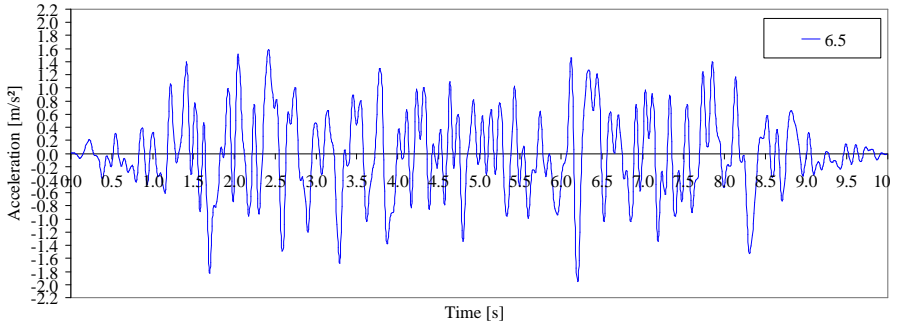


Fig. B-15: Accelerogram No. 3 for a steady state phase of 6.5 s

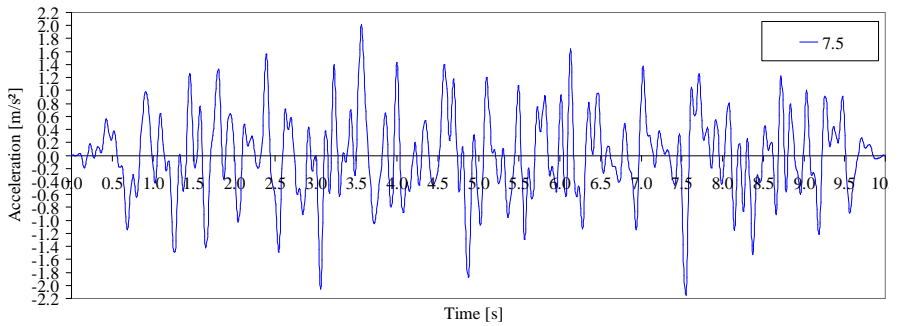


Fig. B-16: Accelerogram No. 4 for a steady state phase of 7.5 s

**Appendix C: Data of artificial generated strong motion earthquake**

No.	Over-all time	Increasing time	Start of decreasing	Steady phase	Simulation stop	Uniform Duration $D_{0.15}$	Significant Duration $D_{95}$	Arias Intensity AI	PGA
	[s]	[s]	[s]	[s]	[s]	[s]	[s]	[m/s <sup>2</sup> ]	[m/s <sup>2</sup> ]
1	10	1.5	3	2.5	5.5	8.29	5.91	1.94	4.31
2	10	1.5	5	3.5	6.5	8.25	5.86	2.27	3.76
3	10	1.5	6	4.5	7.5	8.89	6.90	2.45	3.50
4	10	1.5	7	5.5	8.5	8.41	6.85	2.38	3.95
5	10	1.5	8	6.5	9	8.7	6.92	2.21	4.40
6	10	1.5	9	7.5	10	8.82	7.62	2.58	4.17
7	10	1	9.5	8.5	10	8.61	8.12	2.44	4.50

Tab. C-1: Durations and Intensities of the generated accelerograms

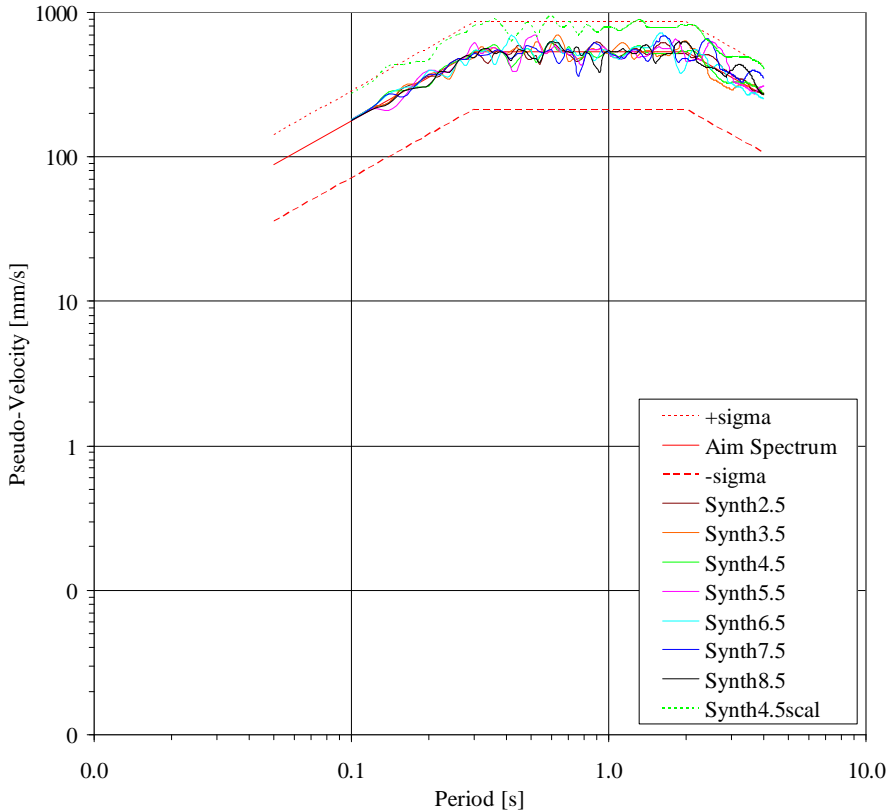


Fig. C-1: Pseudo-velocity diagram

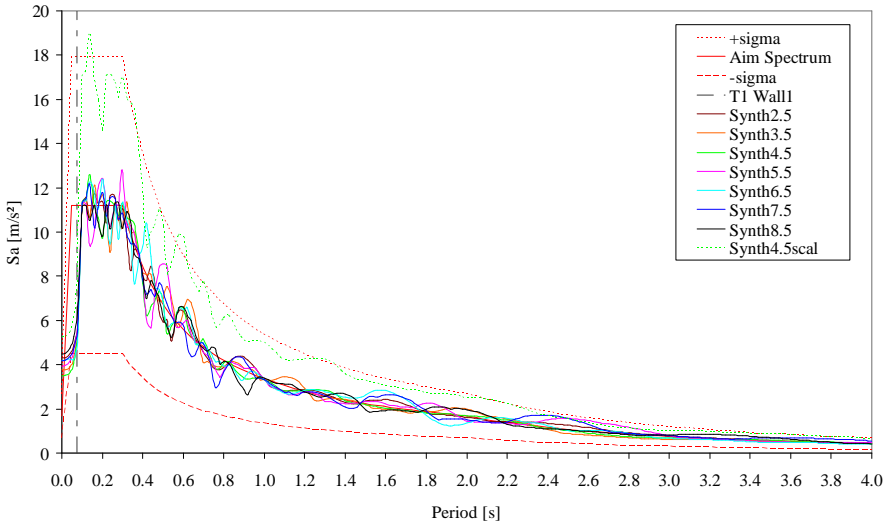


Fig. C-2: Spectral acceleration diagram

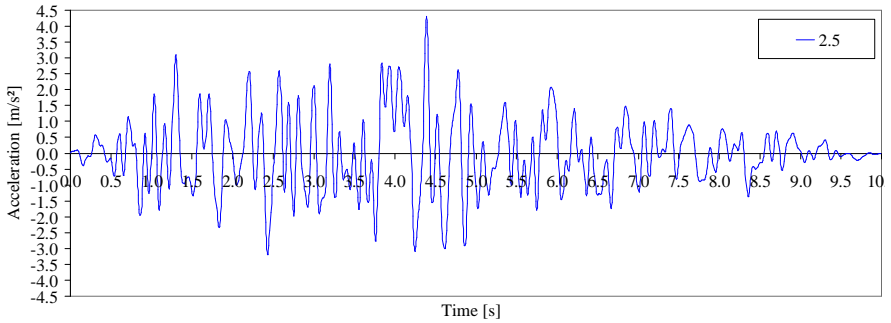


Fig. C-3: Accelerogram No. 1 for a steady state phase of 2.5 s

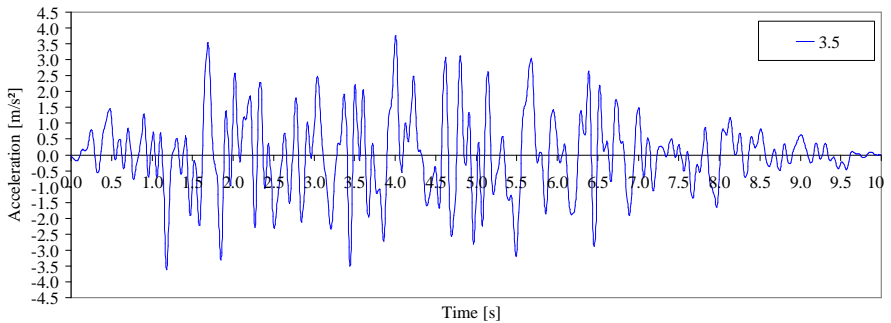


Fig. C-4: Accelerogram No. 2 for a steady state phase of 3.5 s

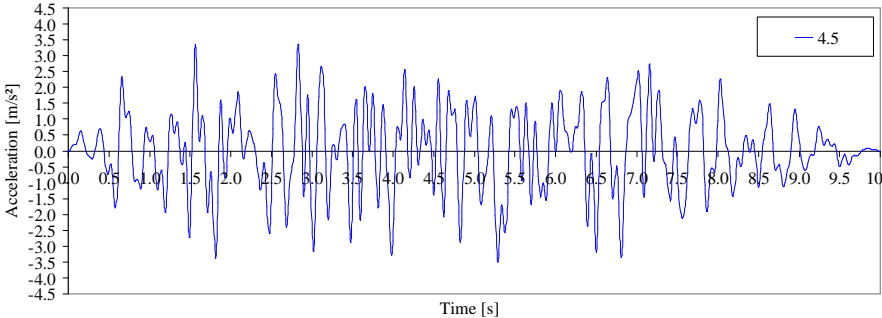


Fig. C-5: Accelerogram No. 3 for a steady state phase of 4.5 s

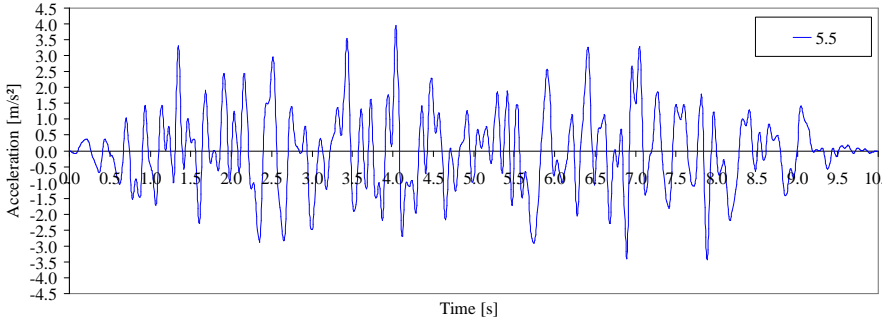


Fig. C-6: Accelerogram No. 4 for a steady state phase of 5.5 s

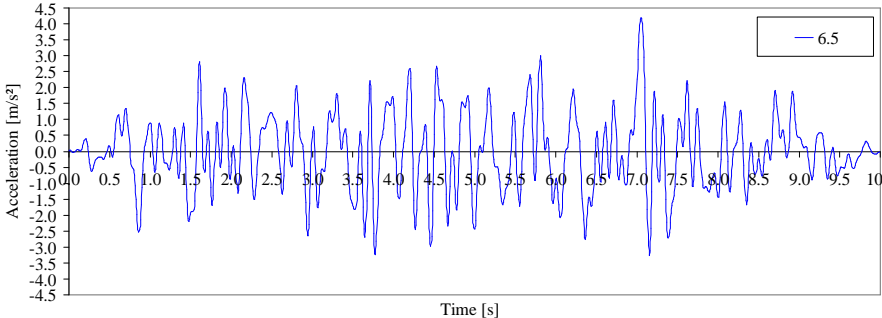


Fig. C-7: Accelerogram No. 5 for a steady state phase of 6.5 s

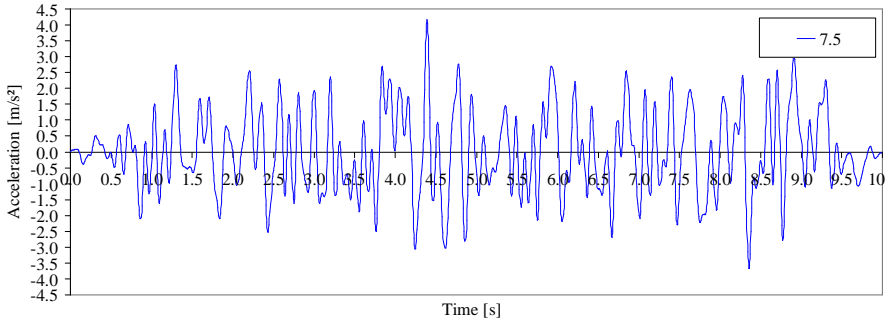


Fig. C-8: Accelerogram No. 6 for a steady state phase of 7.5 s

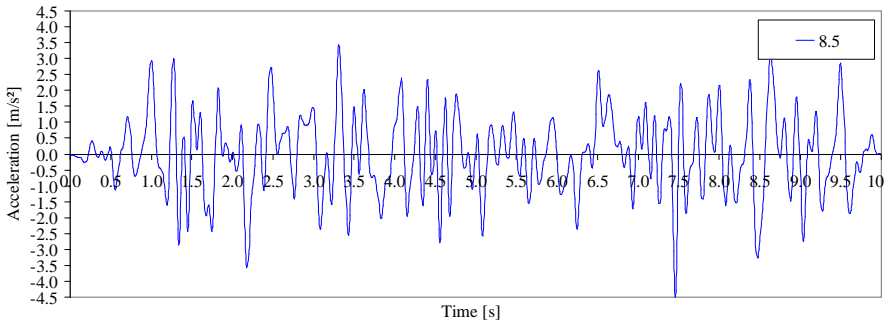


Fig. C-9: Accelerogram No. 7 for a steady state phase of 8.5 s

## Appendix D: Rotation of the wall for SC 2 in dependency on tendon position and slenderness

SC 2					SC2 and tendons in the middle						
Tendons		External forces			Tendons Middle		Forces Middle				
<b>S0.5</b>					<b>S0.5</b>						
h [mm]	h node right	h node left		h node right	h node left	h [mm]	h node right	h node left		h node right	h node left
Δh [mm]	-0.072776	-2.979960		0.192405	-3.712220	h [mm]	0.209925	-3.418090		0.192126	-3.713960
rot [%]	2.907184			3.904625		Δh [mm]	3.628015			3.906086	
Δrot [%]	0.116287			0.156185		rot [%]	0.145121			0.156243	
0.040					0.011						
<b>S1</b>					<b>S1</b>						
h [mm]	h node right	h node left		h node right	h node left	h [mm]	h node right	h node left		h node right	h node left
Δh [mm]	-0.269724	-4.040520		-0.018485	-4.317910	h [mm]	-0.037234	-4.269150		-0.020290	-4.317890
rot [%]	3.770796			4.299425		Δh [mm]	4.231916			4.297600	
Δrot [%]	0.150832			0.171977		rot [%]	0.169277			0.171904	
0.021					0.003						
<b>S2</b>					<b>S2</b>						
h [mm]	h node right	h node left		h node right	h node left	h [mm]	h node right	h node left		h node right	h node left
Δh [mm]	-2.545420	-5.531540		-2.458800	-5.650470	h [mm]	-2.447090	-5.636400		-2.458340	-5.650480
rot [%]	2.986120			3.191670		Δh [mm]	3.189310			3.192140	
Δrot [%]	0.119445			0.127667		rot [%]	0.127572			0.127686	
0.008					0.000						
<b>S3</b>					<b>S3</b>						
h [mm]	h node right	h node left		h node right	h node left	h [mm]	h node right	h node left		h node right	h node left
Δh [mm]	-5.000200	-7.185380		-4.948090	-7.259480	h [mm]	-4.940460	-7.249420		-4.940460	-7.259840
rot [%]	2.185180			2.311390		Δh [mm]	2.308960			2.319380	
Δrot [%]	0.087407			0.092456		rot [%]	0.092358			0.092775	
0.005					0.000						

Tab. D-1: Rotation of the top of the wall for SC 2 in dependency on tendon position and slenderness, determined on  $u_x = 5$  mm



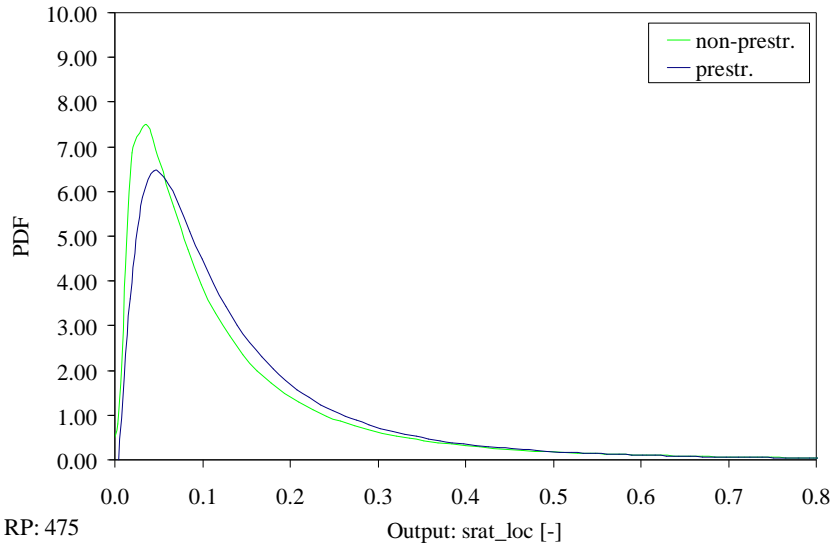
**Appendix E: Probabilistic results for wall 1 and wall 3****Wall 1:**

Fig. E-1: Probability density function of local unit damage of wall 1, Green line: For the non-prestressed wall, Blue line: For the prestressed wall

Further PDFs are displayed in Chap. 6.

**Wall 3:**

a) Return period of 475 years

The bar charts are displayed in Chap. 6.

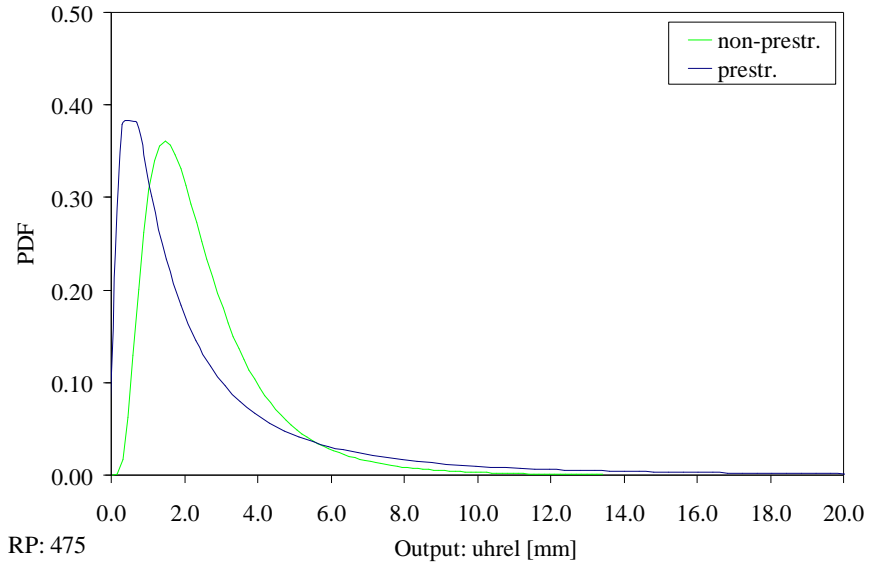


Fig. E-2: Probability density function of storey drift of wall 3, Green line: For the non-prestressed wall, Blue line: For the prestressed wall

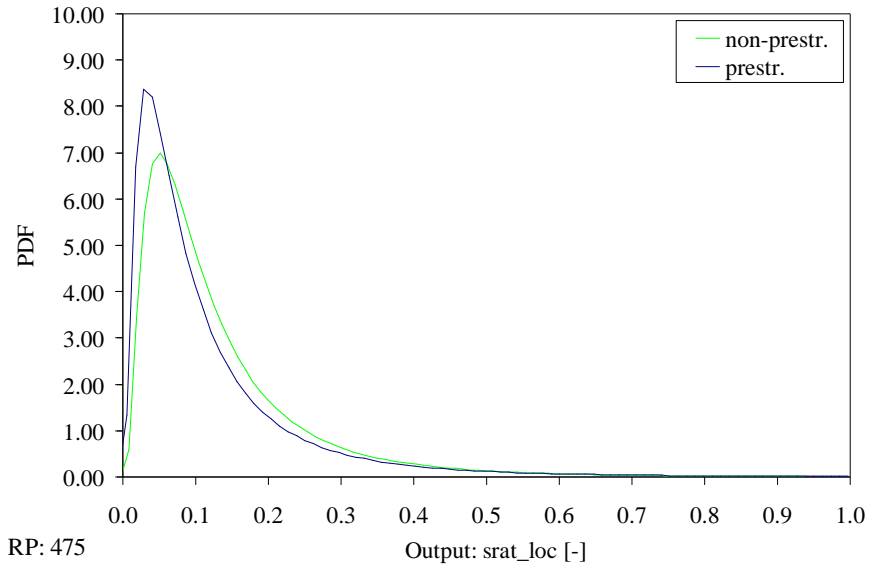


Fig. E-3: Probability density function of local unit damage of wall 3, Green line: For the non-prestressed wall, Blue line: For the prestressed wall

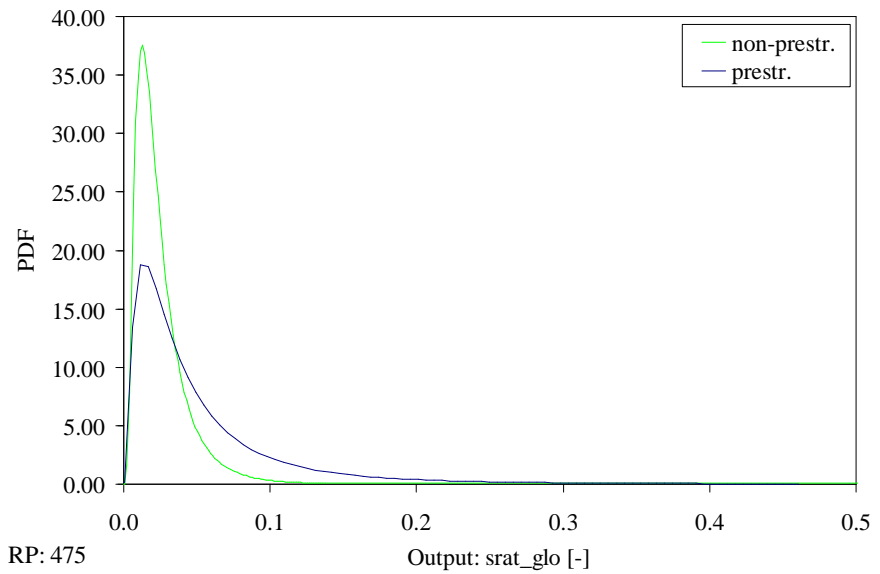


Fig. E-4: Probability density function of global unit damage of wall 3, Green line: For the non-prestressed wall, Blue line: For the prestressed wall

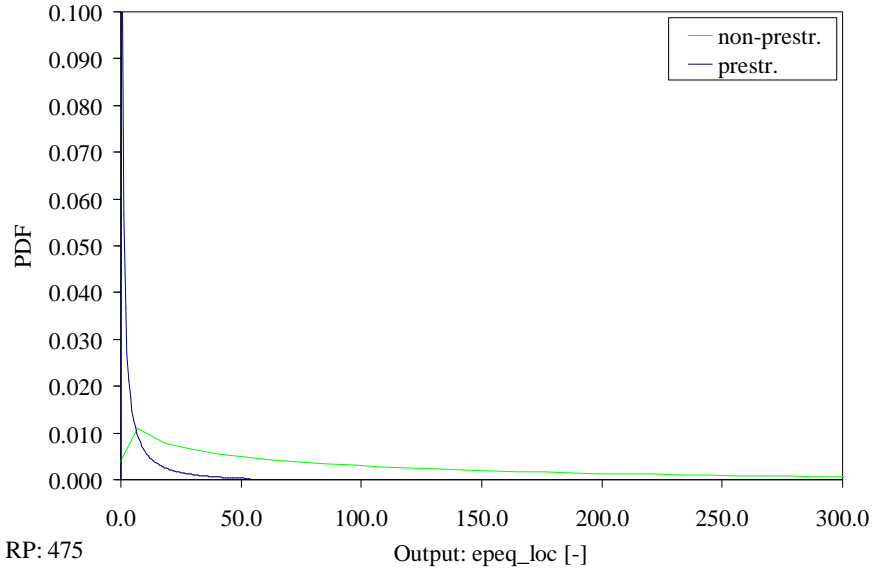


Fig. E-5: Probability density function of local mortar damage of wall 3, Green line: For the non-prestressed wall, Blue line: For the prestressed wall

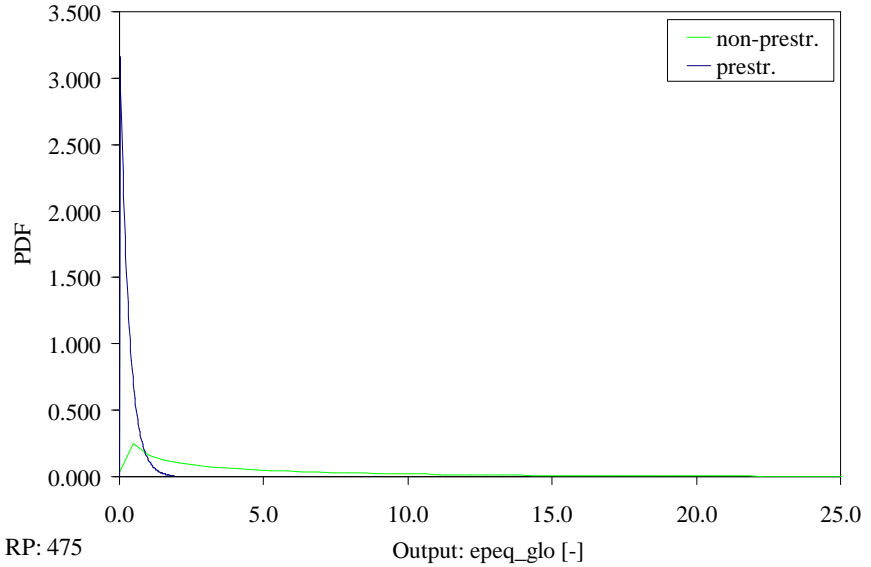


Fig. E-6: Probability density function of global mortar damage of wall 3, Green line: For the non-prestressed wall, Blue line: For the prestressed wall

b) Return period of 2000 years

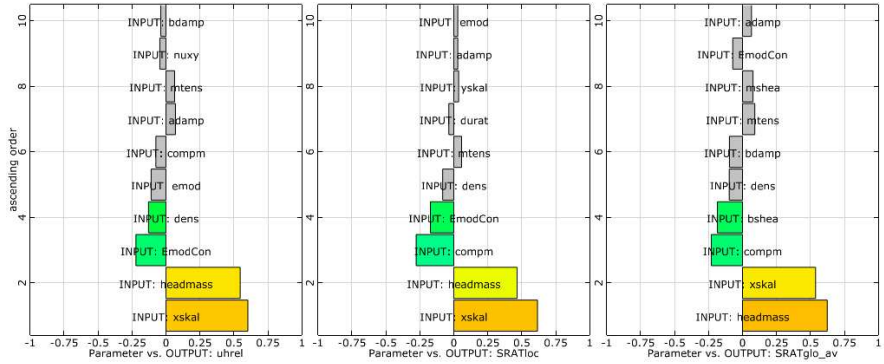


Fig. E-7: Linear correlation coefficients of the non-prestressed wall, Left: For storey drift, Middle: For local unit damage, Right: For global unit damage

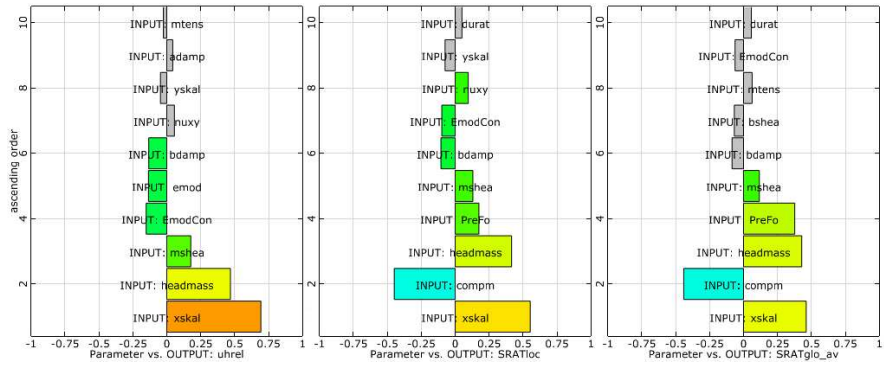


Fig. E-8: Linear correlation coefficients of the prestressed wall, Left: For storey drift, Middle: For local unit damage, Right: For global unit damage

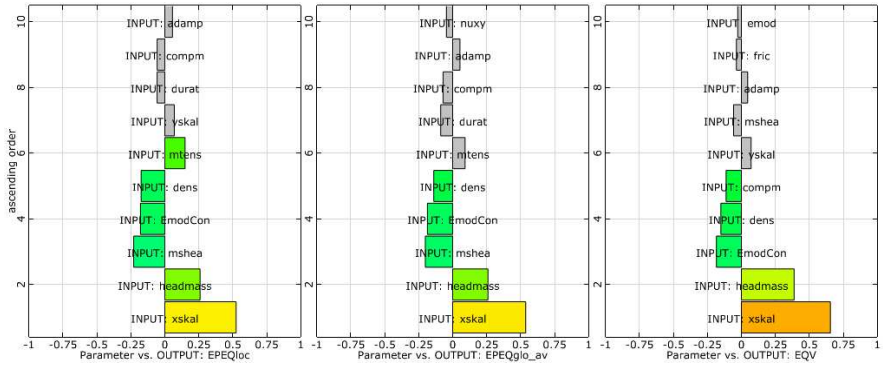


Fig. E9: Linear correlation coefficients of the non-prestressed wall, Left: For local mortar damage, Middle: For mortar global damage, Right: For equivalent plastic strain

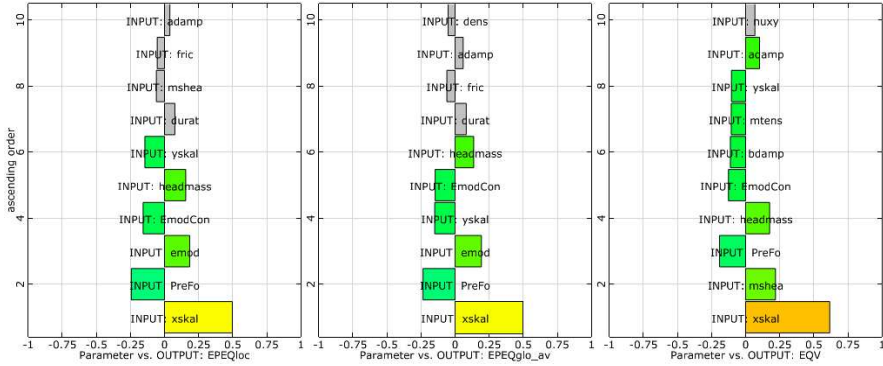


Fig. E-10: Linear correlation coefficients of the prestressed wall, Left: For local mortar damage, Middle: For mortar global damage, Right: For equivalent plastic strain

c) Return period of 10000 years

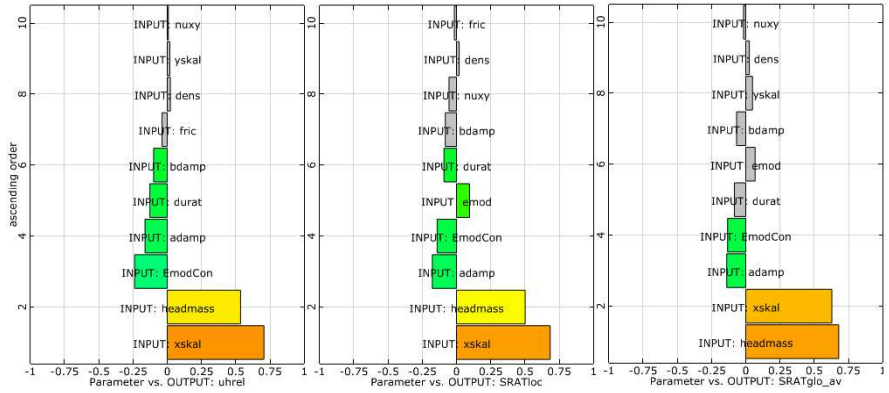


Fig. E-11: Linear correlation coefficients of the non-prestressed wall, Left: For storey drift, Middle: For local unit damage, Right: For global unit damage

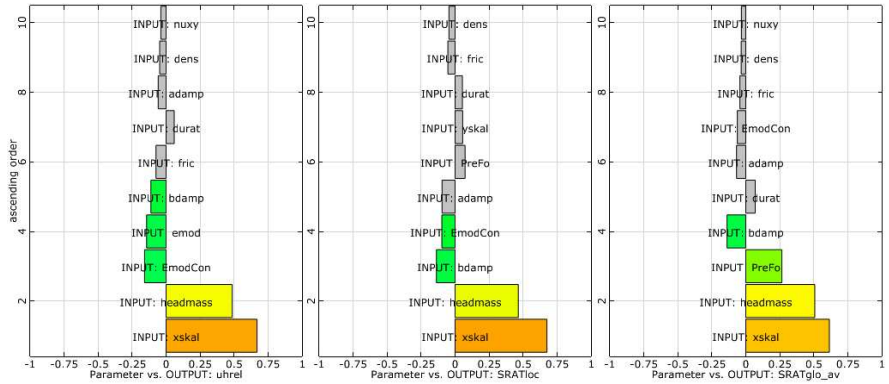


Fig. E-12: Linear correlation coefficients of the prestressed wall, Left: For storey drift, Middle: For local unit damage, Right: For global unit damage

Further bar charts are displayed in Chap. 6.

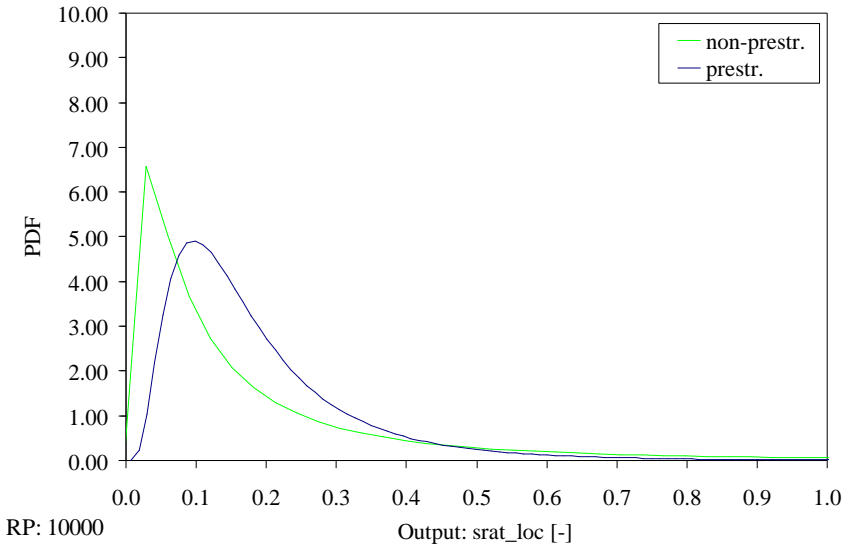


Fig. E-13: Probability density function of local unit damage of wall 3, Green line: For the non-prestressed wall, Blue line: For the prestressed wall

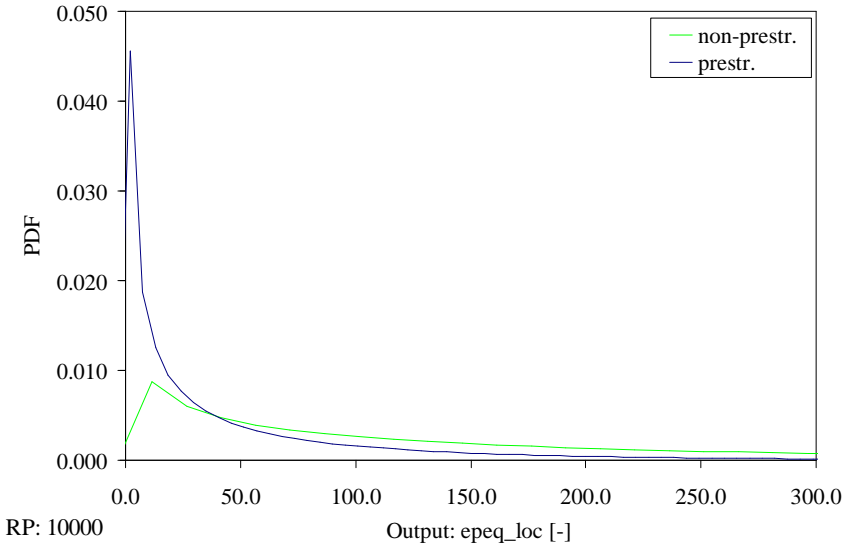


Fig. E-14: Probability density function of local mortar damage of wall 3, Green line: For the non-prestressed wall, Blue line: For the prestressed wall

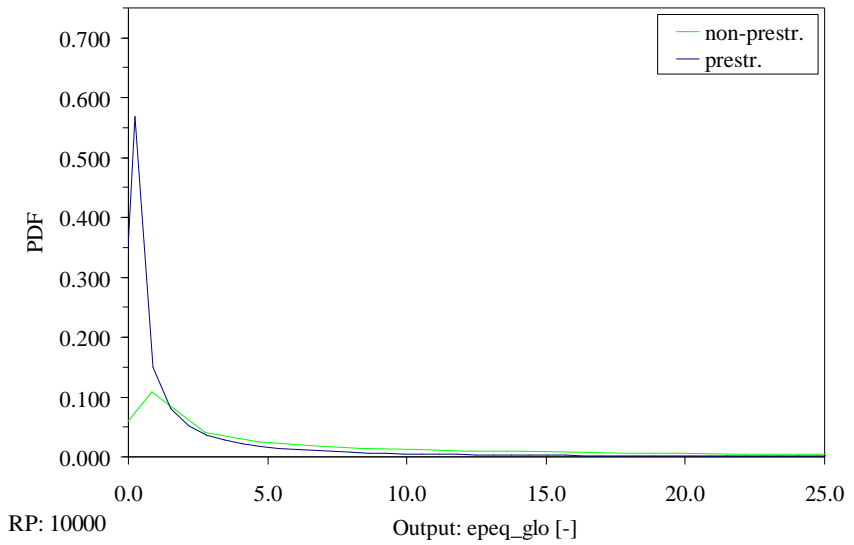


Fig. E-15: Probability density function of global mortar damage of wall 3, Green line: For the non-prestressed wall, Blue line: For the prestressed wall

Further PDFs are displayed in Chap. 8.



## Appendix F: Description of the Northridge earthquake

Note, that for all subsequent information of the Northridge earthquake a scaling factor of two is already included, as it is applied in the numerical simulations.

### Parameter for the horizontal excitation:

Maximum Acceleration: 1.49368g  
 at time t=0.69sec  
 Maximum Velocity: 310.9823955mm/sec  
 at time t=0.665sec  
 Maximum Displacement: 186.47032019mm  
 at time t=9.55sec  
 Vmax / Amax: 208.19880798sec  
 Acceleration RMS: 0.15970125g  
 Velocity RMS: 42.66384422mm/sec  
 Displacement RMS: 95.98099515mm  
 Arias Intensity: 3.75522266m/sec  
 Characteristic Intensity (Ic): 0.19727761  
 Specific Energy Density: 17392.04543362mm<sup>2</sup>/sec  
 Cumulative Absolute Velocity (CAV): 0.6873982mm/sec  
 Acceleration Spectrum Intensity (ASI): 0.55966288g\*sec  
 Velocity Spectrum Intensity (VSI): 912.5725031mm  
 Sustained Maximum Acceleration (SMA): 0.71868g  
 Sustained Maximum Velocity (SMV): 126.599031mm/sec  
 Effective Design Acceleration (EDA): 1.10018673g  
 A95 parameter: 1.48994112g  
 Predominant Period (Tp): 0.14sec  
 Mean Period (Tm): 0.15175475sec

### Parameter for the vertical excitation:

Maximum Acceleration: 0.76g  
 at time t=0.29sec  
 Maximum Velocity: 99.873648mm/sec  
 at time t=0.66sec  
 Maximum Displacement: 28.50754754mm  
 at time t=9.55sec  
 Vmax / Amax: 131.41269474sec  
 Acceleration RMS: 0.10070283g  
 Velocity RMS: 18.33186848mm/sec  
 Displacement RMS: 17.00118502mm  
 Arias Intensity: 1.49314806m/sec  
 Characteristic Intensity (Ic): 0.09878202  
 Specific Energy Density: 3211.02847596mm<sup>2</sup>/sec  
 Cumulative Absolute Velocity (CAV): 0.45758194mm/sec  
 Acceleration Spectrum Intensity (ASI): 0.14567055g\*sec  
 Velocity Spectrum Intensity (VSI): 310.34349462mm  
 Sustained Maximum Acceleration (SMA): 0.62g  
 Sustained Maximum Velocity (SMV): 71.506071mm/sec  
 Effective Design Acceleration (EDA): 0.22704249g  
 A95 parameter: 0.75809762g  
 Predominant Period (Tp): 0.02sec  
 Mean Period (Tm): 0.12830579sec

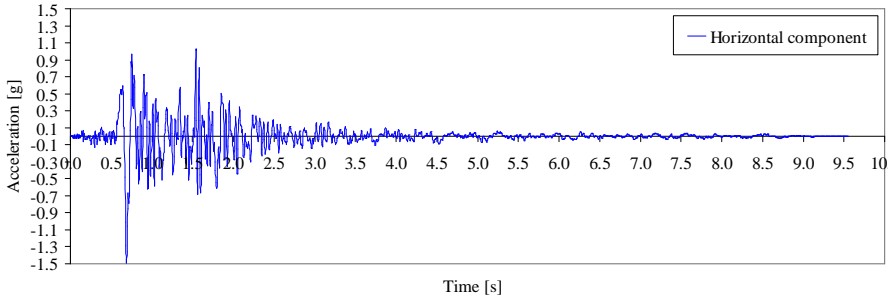


Fig. F-1: Accelerogram, horizontal excitation

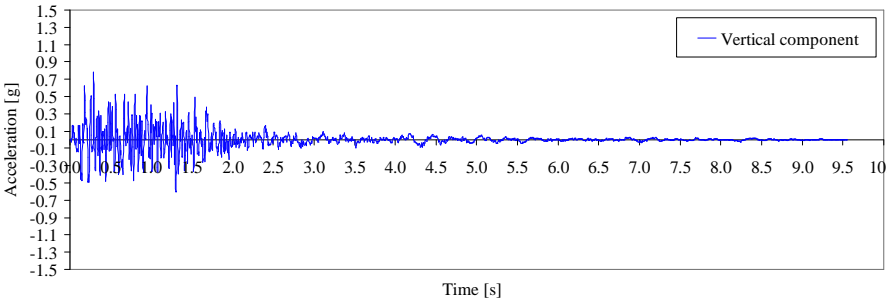


Fig. F-2: Accelerogram, vertical excitation

## Appendix G: Risk estimation

In this appendix some risk distributions are presented. For the different return periods, additional diagrams may be found in Chap. 8.

a) Return period of 475 years:

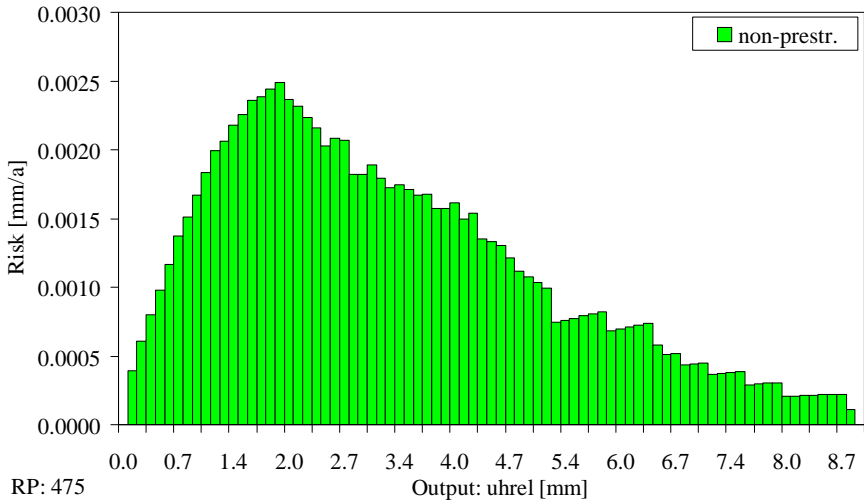


Fig. G-1: Risk distribution of the storey drift for a return period of 475 years without prestressing

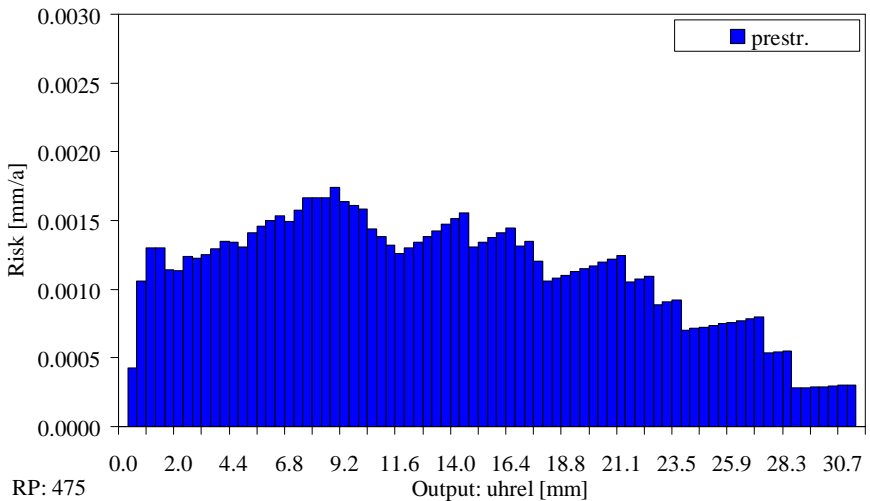


Fig. G-2: Risk distribution of the storey drift for a return period of 475 years with prestressing

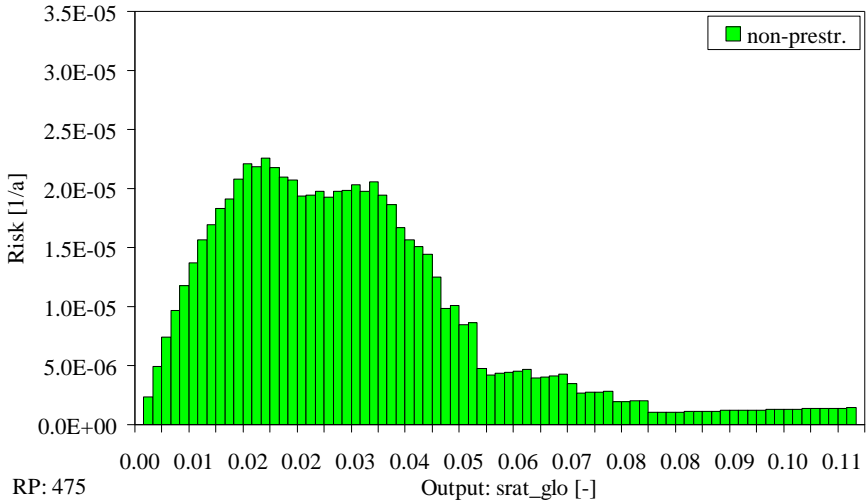


Fig. G-3: Risk distribution of the global unit damage for a return period of 475 years without prestressing

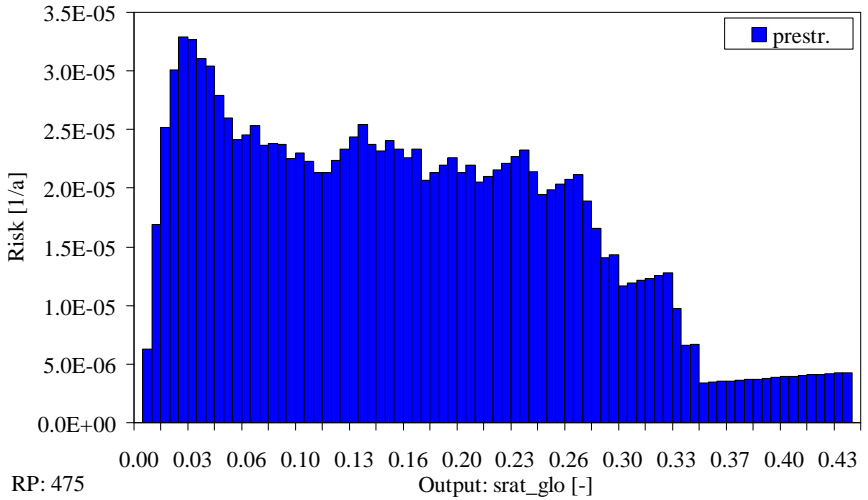


Fig. G-4: Risk distribution of the global unit damage for a return period of 475 years with prestressing

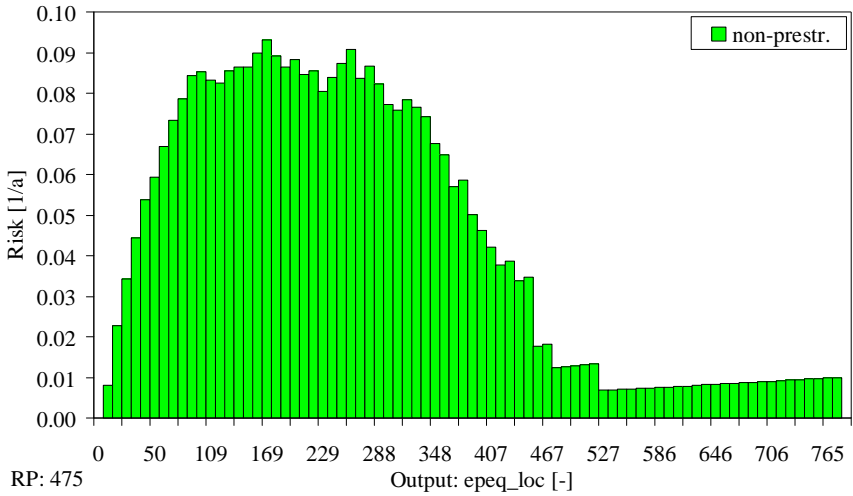


Fig. G-5: Risk distribution of the local mortar damage for a return period of 475 years without prestressing

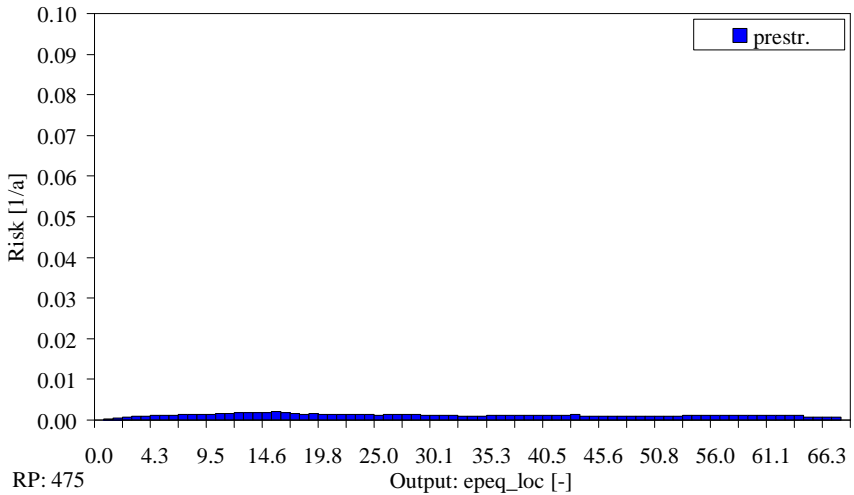


Fig. G-6: Risk distribution of the local mortar damage for a return period of 475 years with prestressing

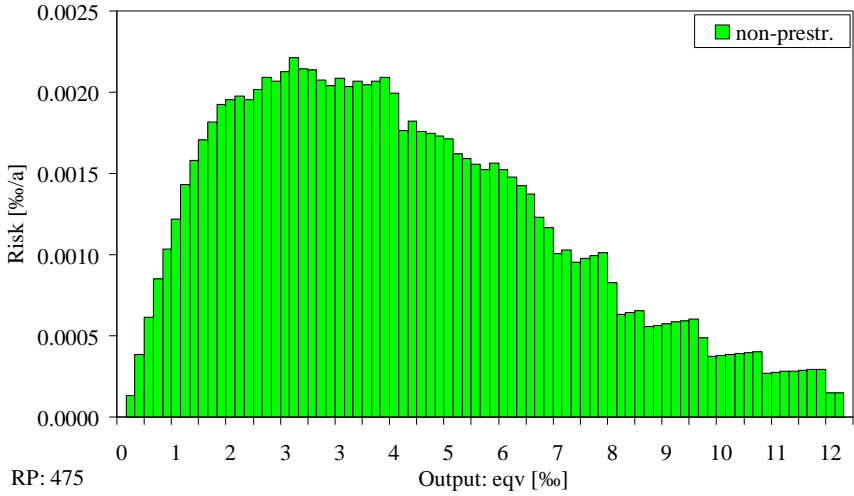


Fig. G-7: Risk distribution of the equivalent plastic strain for a return period of 475 years without prestressing

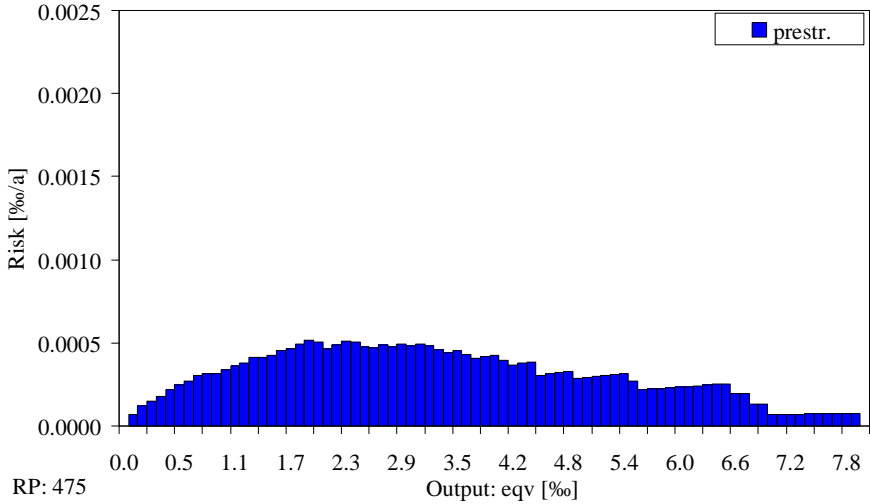


Fig. G-8: Risk distribution of the equivalent plastic strain for a return period of 475 years with prestressing

b) Return period of 10000 years

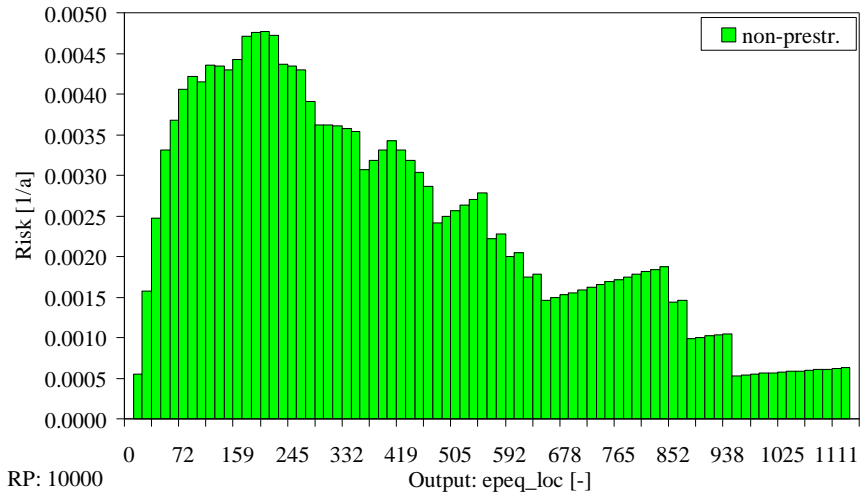


Fig. G-9: Risk distribution of the local mortar damage for a return period of 10000 years without prestressing

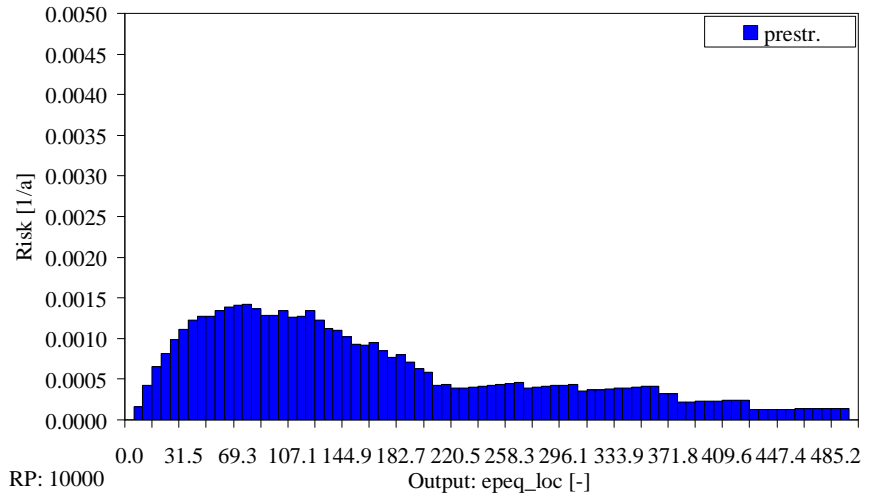


Fig. G-10: Risk distribution of the local mortar damage for a return period of 10000 years with prestressing

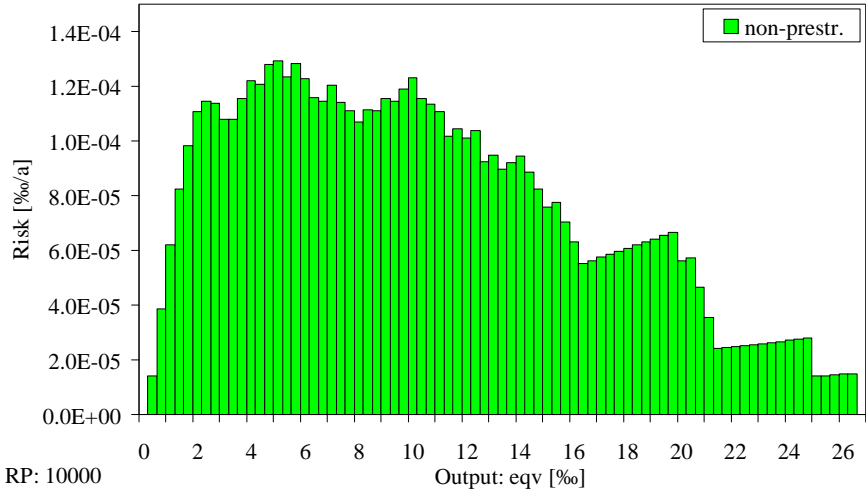


Fig. G-11: Risk distribution of the equivalent plastic strain for a return period of 10000 years without prestressing

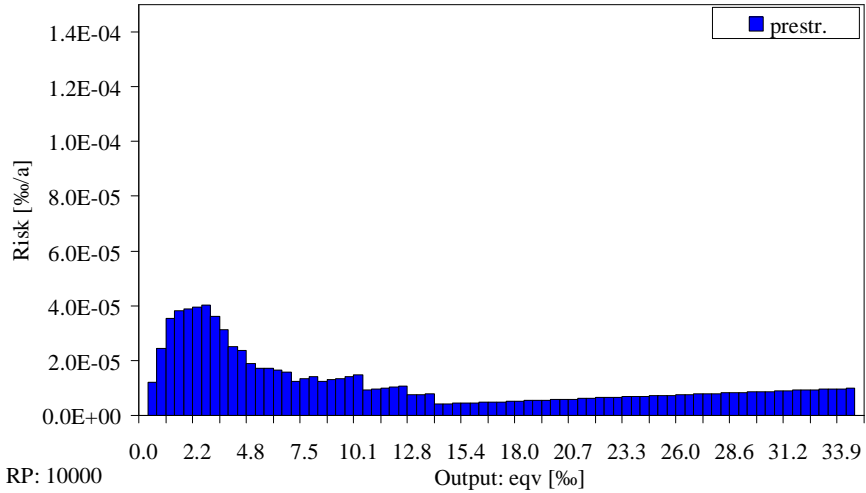


Fig. G-12: Risk distribution of the equivalent plastic strain for a return period of 10000 years with prestressing

## Appendix H: Material parameters

a) Material parameters for the Eindhoven walls J4D and J5D

	Prameter	Sym.	Value	Unit
Bricks	Young's modulus	E	16700	N/mm <sup>2</sup>
	Poisson's ratio	$\eta$	0.15	-
	Tensile strength	$f_t$	1.50	N/mm <sup>2</sup>
	Ultimate strain	$\varepsilon_u$	0.013	N/mm <sup>2</sup>
	shear retention factor	$\beta$	0.001	-
Joints	Linear normal stiffness	$D_{11}$	82	N/mm <sup>3</sup>
	Linear tangential stiffness	$D_{22}$	36	N/mm <sup>3</sup>
	Tensile strength	$f_t$	0.16	N/mm <sup>2</sup>
	Fracture energy I	$G_{\bar{n}}$	0.012	Nmm/mm <sup>2</sup>
	Cohesion	c	0.224	N/mm <sup>2</sup>
	Friction coefficient / angle	$\tan \varphi / \varphi$	0.75/36.6	- / °
	Dilatancy coefficient / angle	$\tan \psi / \psi$	0.55/28.8	- / °
	Residual friction coefficient / angle	$\tan \Phi / \Phi$	0.4/21.8	- / °
	Confining normal stress for psi0	$\sigma_u$	-0.50	N/mm <sup>2</sup>
	Exponential degradation coefficient	$\delta$	4.50	-
	Cap critical compressive strength	$f_c$	8.80	N/mm <sup>2</sup>
	Shear traction control factor	$C_s$	9.00	-
	Compressive fracture energy	$G_{fc}$	2.00	Nmm/mm <sup>2</sup>
	Equivalent plastic relative displacement	$\kappa_p$	0.093	N/mm <sup>2</sup>
	Fracture energy factor	b	0.05	-

Tab. H-1: Material parameters of the meso-model for the Eindhoven walls J4D and J5D

Parameter	Sym.	Value	Unit
Young's modulus of masonry	E	3000	N/mm <sup>2</sup>
Poisson's ratio	$\eta$	0.15	-
Friction coefficient	$\mu = \tan \varphi$	0.75	-
Tensile strength mortar	$\sigma_{bm}$	0.25	N/mm <sup>2</sup>
Shear strength of the mortar joints	$\tau_{mr}$	0.57	N/mm <sup>2</sup>
Inelastic deformation parameter for mortar	$c_{mi}$	1.0	-
Softening coefficient mortar	$\beta_m$	0.4	-
Compressive strength of masonry	$\sigma_{br}$	9.0	N/mm <sup>2</sup>
Shear strength of bricks	$\tau_{br}$	3.0	N/mm <sup>2</sup>
Inelastic deformation parameter for brick	$c_{bi}$	1.0	-
Softening coefficient of the masonry	$\beta_b$	0.4	-

Tab. H-2: Material parameters of the Lagomarsino model for the Eindhoven walls J4D and J5D

Parameter	Sym.	Value	Unit
Young's modulus vertical	$E_x$	2960	N/mm <sup>2</sup>
Young's modulus horizontal	$E_y$	2300	N/mm <sup>2</sup>
Poisson's ratio	$\eta$	0.15	-
Shear modulus	$G_{xy}$	1700	N/mm <sup>2</sup>
Shear modulus	$G_{yz}$	1000	N/mm <sup>2</sup>
Compressive strength masonry vertical	$f_{mx}$	8.8	N/mm <sup>2</sup>
Compressive strength masonry horizontal	$f_{my}$	3.0	N/mm <sup>2</sup>
Tensile strength masonry vertical	$f_{ix}$	0.16	N/mm <sup>2</sup>
Tensile strength masonry horizontal	$f_{iy}$	0.5*1.5	N/mm <sup>2</sup>
Friction angle / coefficient	$\varphi / \tan \varphi$	36.9	° / -
Cohesion	c	0.224	N/mm <sup>2</sup>
Residual friction angle / coefficient	$\varphi_r / \tan \varphi_r$	12/0.21	° / -
Dilatancy angle / coefficient	$\psi / \tan \psi$	28.8/0.55	° / -
Fracture energy MODE I vertical (joint)	$G_{I\,fj}$	0.012	Nmm/mm <sup>2</sup>
Fracture energy MODE I horizontal (unit)	$G_{I\,fb}$	0.08	Nmm/mm <sup>2</sup>
Fracture energy MODE II	$G_{II\,fj}$	0.075	Nmm/mm <sup>2</sup>
Fracture energy compression	$G_m$	2.0	Nmm/mm <sup>2</sup>
Equivalent length	h	0.08	m
Residual Cohesion	$c_r$	0.05	N/mm <sup>2</sup>
Residual tensile strength	$f_{ir}$	0.05	N/mm <sup>2</sup>
Residual dilatancy angle / coefficient	$\psi_r$	9/0.158	° / -

Tab. H-3: Material parameters of the Schlegel model for the Eindhoven walls J4D and J5D

## b) Material parameters for the Eindhoven walls J6D

	<b>Prameter</b>	<b>Sym.</b>	<b>Value</b>	<b>Unit</b>
Bricks	Young's modulus	E	16700	N/mm <sup>2</sup>
	Poisson's ratio	$\eta$	0.15	-
	Tensile strength	$f_t$	1.50	N/mm <sup>2</sup>
	Ultimate strain	$\varepsilon_u$	0.013	N/mm <sup>2</sup>
	shear retention factor	$\beta$	0.001	-
Joints	Linear normal stiffness	D <sub>11</sub>	110	N/mm <sup>3</sup>
	Linear tangential stiffness	D <sub>22</sub>	50	N/mm <sup>3</sup>
	Tensile strength	$f_t$	0.16	N/mm <sup>2</sup>
	Fracture energy I	G <sub>fl</sub>	0.012	Nmm/mm <sup>2</sup>
	Cohesion	c	0.224	N/mm <sup>2</sup>
	Friction coefficient / angle	$\tan \varphi / \varphi$	0.75/36.6	- / °
	Dilatancy coefficient / angle	$\tan \psi / \psi$	0.55/28.8	- / °
	Residual friction coefficient / angle	$\tan \Phi / \Phi$	0.25/14	- / °
	Confining normal stress for psi0	$\sigma_u$	-1.20	N/mm <sup>2</sup>
	Exponential degradation coefficient	$\delta$	4.50	-
	Cap critical compressive strength	$f_c$	8.80	N/mm <sup>2</sup>
	Shear traction control factor	C <sub>s</sub>	9.00	-
	Compressive fracture energy	G <sub>fc</sub>	2.00	Nmm/mm <sup>2</sup>
	Equivalent plastic relative displacement	$\kappa_p$	0.093	N/mm <sup>2</sup>
	Fracture energy factor	b	0.05	-

Tab. H-4: Material parameters of the meso-model for Eindhoven wall J6D

Parameter	Sym.	Value	Unit
Young's modulus vertical	$E_x$	2960	N/mm <sup>2</sup>
Young's modulus horizontal	$E_y$	3500	N/mm <sup>2</sup>
Poisson's ratio	$\eta$	0.15	-
Shear modulus	$G_{xy}$	2000	N/mm <sup>2</sup>
Shear modulus	$G_{yz}$	1233	N/mm <sup>2</sup>
Compressive strength masonry vertical	$f_{mx}$	8.8	N/mm <sup>2</sup>
Compressive strength masonry horizontal	$f_{my}$	3.0	N/mm <sup>2</sup>
Tensile strength masonry vertical	$f_{ix}$	0.16	N/mm <sup>2</sup>
Tensile strength masonry horizontal	$f_{iy}$	0.5*1.5	N/mm <sup>2</sup>
Friction angle / coefficient	$\varphi / \tan \varphi$	36.9	° / -
Cohesion	c	0.224	N/mm <sup>2</sup>
Residual friction angle / coefficient	$\varphi_r / \tan \varphi_r$	12/0.21	° / -
Dilatancy angle / coefficient	$\psi / \tan \psi$	28.8/0.55	° / -
Fracture energy MODE I vertical (joint)	$G_{I\,fj}$	0.012	Nmm/mm <sup>2</sup>
Fracture energy MODE I horizontal (unit)	$G_{I\,fb}$	0.08	Nmm/mm <sup>2</sup>
Fracture energy MODE II	$G_{II\,fj}$	0.05	Nmm/mm <sup>2</sup>
Fracture energy compression	$G_m$	2.0	Nmm/mm <sup>2</sup>
Equivalent length	h	0.08	m
Residual Cohesion	$c_r$	0.05	N/mm <sup>2</sup>
Residual tensile strength	$f_{ir}$	0.05	N/mm <sup>2</sup>
Residual dilatancy angle / coefficient	$\psi_r$	9/0.158	° / -

Tab. H-5: Material parameters of the Schlegel model for Eindhoven wall J6D

## **Appendix I: Suggestions for the practical application of prestressing on masonry**

In the following some important facts and suggestions are briefly summarised, which should be noticed regarding the practical application of vertical prestressing on masonry structures.

### a) Unreasonable and dangerous application of prestressing

External prestressing, especially in case of high prestressing degrees, leads usually to brittle failure, if high earthquake intensities exceed the shear capacity. This is very dangerous. In order to avoid this harm a high ductility of the masonry structures has to be ensured or sufficient safety distance to the shear capacity. In particular for long large-sized units, much unit damage is to expect, since this do not allow a stone rotation.

### b) Reasonable application of prestressing

In case of slender structures (e.g. towers) which behave like cantilevers, vertical local prestressing may reduce the horizontal displacement and so the resulting damages. The bending behaviour of such structures can be improved by external and internal prestressing, if the strands are placed near the edges. Thus, in the bending zone a reinforcement effect works as well know for reinforced and prestressed concrete cantilevers. A good example is the bell tower of Trignano (see Section 4.2.6.6), where the prestressing rehabilitation is combined with shape memory alloys.

### c) Suggestions for the practical execution

The author suggests an internal prestressing with bond or 'sufficient contact' between masonry and strand to achieve a wall-tendon interaction in order to increase the ductility considerable. Moreover, toe crushing is to avoid. Especially, slender walls are endangered, since rocking occurs mainly. This harm may be reduced due to elastomers under the lower corners.

In conjunction with vertical prestressing, high compression and tensile strength of the units are recommended to avoid stone cracking.

### d) Stability

An increase of normal forces, can led to stability problems. Especially in case of slender structures, this buckling is to take care in the design calculation. Note, that bond or 'sufficient contact' between strand and wall reduces stability problems. Consequently, an external prestressing or internal prestressing without any contact influences buckling negatively.

### e) Time-dependent phenomena

Time-dependent phenomena such as creep, shrinkage, moisture expansion, and relaxation have to be in mind, since they decrease the applied prestressing forces. A sufficient vertical prestress level is to ensure over the whole design life.



**List of abbreviations**Abbreviations

ADRS - Acceleration displacement response spectra

AI - Areas intensity

ALARP - As low as reasonably practicable

bn - Billion

CFRP - Carbon-fibre-reinforced plastic

Chap. - Chapter

CSH - Cultural social historical

Def. - Definition

DG - Damage grade

DR - Damage ratio

e.g. - Exempli gratia (Latin: For example)

EaNR - Elements at non risk

EaR - Elements at Risk

Earthq. - Earthquake

EMPA - Swiss federal laboratories for material testing and research

EMS - European Macroseismic Scale

Est. - Estimated

etc. - Et cetera (Latin: And so forth)

Extr. temp. - Extreme temperature

FAR - Fatal accident rate

FEM - Finite element method

Fig. - Figure

F-N - Frequency-number

i.e. - Id est (Latin: That is)

iBMB - Institute of Building Materials, Concrete Construction and Fire Protection

ID - Interstorey drift

JMA - Japanese meteorological agency scale

LLE - Lost life expectancy

LQI - Life quality index

LR - Loss ratio

MDR - Mean damage ratio

Mio. - Million  
MMI - Modified Mercalli Intensity scale  
MPA - Material testing institute  
MSK - Medvedev Sponheuer Karnik scale  
Nb - Number  
No. - Number  
non-prestr. - Non-prestressed  
Num. - Numerical  
P-D - Probability-Damage  
p-waves - Body waves  
PDF - Probability density function  
PGA - Peak ground acceleration  
PGD - Peak ground deformation  
PGV - Peak ground velocity  
Pos. - Position  
prestr. - Prestressed  
PSHA - Probabilistic seismic hazard analysis  
PL - Probable loss  
R.C. - Reinforced concrete  
RF - Rossi Forel scale  
rot - Rotation  
s-waves - Surface waves  
SC - Support condition  
SD - Storey drift  
SDOF - Single degree of freedom  
SH - Surface horizontal wave  
SL - Scenario loss  
SMA - Shape memory alloy  
SV - Surface vertical wave  
SW - Shear Wall  
Tab. - Table  
Tot. - Totally  
VSL - Vorspann System Losinger

Latin symbols

- $2xP_0$  - Sum of prestressing forces of two strands
- $(2xP_0)_u$  - Ultimate loading point
- $a$  - Seismic constant
- $A$  - Maximum recorded amplitude
- $A_0$  - Standard value of maximum recorded amplitude
- $A_f$  - Rupture area
- $a_g$  - Design ground acceleration
- $a_{rms}$  - Root mean square
- $A_s$  - Shear surface
- $b$  - Seismic constant
- $c$  - Cohesion
- $C_c$  - Replacement construction costs
- $c_{bn}$  - Compressive compliance parameter
- $c_{bt}$  - Tangential compliance parameter
- $c_d$  - Damping coefficient
- $c_{mn}$  - Extensional inelastic compliance parameter
- $c_{mt}$  - Tangential inelastic compliance parameter
- $cr$  - Occurrence of cracks
- $C_r$  - Repairing costs
- $d$  - Thickness
- $d\epsilon$  - Elastic strain rate
- $d\epsilon_{eps}$  - Equivalent plastic strain rate
- $d\sigma$  - Stress rate
- $d\lambda$  - Plastic multiplier rate
- $d\kappa$  - Scalar parameter adequate to the equivalent plastic strain rate
- $D$  - Damage
- $D_{b0,05}$  - Bracketed duration
- $D_{mw}$  - Internal compression force
- $D_s$  - Average amount of slip over the fault plane
- $D_{s75}$  - Significant duration (5% - 75%)
- $D_{s95}$  - Significant duration (5% - 95%)
- $D_u$  - Uniform distribution

- $e$  - Mean life expectancy
- $E$  - Young's modulus
- $E_c$  - Young's modulus for concrete
- $EI$  - Flexural stiffness
- $F$  - Force
- $f$  - Arc rise
- $f_c$  - Compressive strength
- $f_i$  - Interface
- $F_i$  - Composite yield surface (failure criteria)
- $F_M(m)$  - Probability of occurrence for magnitude  $m$
- $f_{my}$  - Compressive strength in y-direction
- $f_t$  - Tensile strength
- $g$  - Gravitational acceleration
- $G$  - Shear modulus
- $G+F$  - Dead loads and traffic loads
- $GA_s$  - Shear stiffness
- $G_c$  - Fracture energy for compression failure
- $G^I$  - Fracture energy
- $G_f^{II}$  - Fracture energy Mode II (shear)
- $G$  - Plastic potential
- $G_s$  - Associated plastic potential
- $H$  - Hazard
- $h$  - Height
- $h_0$  - Height
- $I$  - Moment of inertia
- $I_c$  - Characteristic intensity
- $I_E$  - Earthquake intensity
- $k$  - Constant for inverse Weibull distribution
- $K$  - Elastic stiffness matrix
- $K_M$  - Elastic compliance matrix
- $k_s$  - Stiffness of spring
- $L$  - Losses
- $l_0$  - Length

$\Delta m_u$  - Normalised out-of-plane bending capacity  
 $m$  - Mass  
 $M(\Delta P)$  - Restoring moment  
 $M_0$  - Seismic moment  
 $m_b$  - Body wave magnitude  
 $M_E$  - Energy magnitude  
 $M_L$  - Local/Richter magnitude  
 $M_{max}$  - Upper magnitude  
 $M_{min}$  - Lowest magnitude  
 $M_R$  - Resistance moment  
 $M_s$  - Surface wave magnitude  
 $m_u$  - Normalised bending capacity  
 $M_u$  - Ultimate moment  
 $M_w$  - Moment magnitude  
 $N$  - Normal forces  
 $n_u$  - Normalised normal forces  
 $p$  - Vertical compression / initial loads  
 $P$  - Vertical prestressing forces  
 $p$  - Probability  
 $p_{ex}(H)$  - Probability of exceedance of hazard  
 $R$  - Risk  
 $R(\alpha)$  - Toughness function  
 $R_D$  - Structural risk  
 $R_L$  - Total risk  
 $\Delta s$  - Shear capacity  
 $S$  - Lateral forces  
 $S_a$  - Pseudospectral acceleration  
 $S_d$  - Spectral displacement  
 $s_u$  - normalised shear capacity  
 $S_v$  - Pseudospectral velocity  
 $T_0$  - Total duration of the record  
 $T_d$  - Duration  
 $T_L$  - Design working life

$T_R$  - Return period of event

$u$  - Displacement

$u_{abs}$  - Absolute displacement

$u_g$  - Ground displacement

$u_{h,rel}$  - Storey drift

$u_{rel}$  - Relative displacement

$V$  - Vulnerability

$w$  - Constant for inverse Weibull distribution

$w$  - Crack width

$W$  - Wall

$X_{skal}$  - Scaling factor for horizontal acceleration

$Y_m$  - Damage energy release rate

$Y_{skal}$  - Scaling factor for vertical acceleration

### Greek symbols

$\alpha$  - Mass damping coefficient

$\alpha_b$  - Brick damage variable / unit damage

$\alpha_{b,loc}$  - Local unit damage

$\alpha_L$  - Distance of bed joints

$\alpha_m$  - Mortar damage variable

$\alpha_{Sy}$  - Distance of head joints

$\beta$  - Stiffness damping coefficient

$\beta$  - Softening Parameter

$\beta_{d,mw}$  - Masonry compressive strength

$\gamma$  - Sliding

$\Delta$  - Epicentral distance of seismometer

$\varepsilon$  - Strain, extension

$\varepsilon^{el}$  - Elastic strain

$\varepsilon^{pl}$  - Plastic strain

$\varepsilon_{eq}^{pl}$  - Equivalent plastic strain

$\varepsilon_{y,t}^{pl}$  - Vertical plastic tensile strain

$\theta$  - Wall end rotation

$\kappa$  - Hardening or softening scalar

$\lambda_m$  - Annual rate of exceedance

$\zeta$  - Modal damping

$\eta$  - Poisson's ratio

$\mu$  - Friction coefficient

$\rho$  - Density

$\rho_M$  - Head mass

$\sigma$  - Stress

$\sigma_{br}$  - Compressive strength

$\tau$  - Shear stress

$\tau_{br}$  - Shear strength

$\varphi$  - Friction angle

$\Psi$  - Dilatancy angle

$\omega$  - Natural frequency

$\omega_i$  - Natural frequency for vibration mode i

$\omega_{my}$  - Abbreviation in hardening/softening function

$\Omega$  - Hardening/softening function



## References

- Ahrens, H.; Dinkler, D. (1994): Finite-Element-Methode Teil 1. Institut für Baustatik der Technischen Universität Braunschweig, Germany.
- Alexander, D. (No Date): Theoretical Aspects of Risk Estimation. Analysis and Management.
- ASTM E 2026-99 (1999): Standard Guide for the Estimation of Building Damageability in Earthquakes.
- Australian and New Zealand Standard (1999): AS/NZS 4360, Risk Management.
- Bachmann, H. (2007): Erdbeben im «Glattalgraben»? - Ertüchtigung von Empa-Gebäuden mit moderner Technologie. In: Heimatbuch Dübendorf, Dübendorf, Switzerland, pp. 83-94.
- Baker, J.W.; Cornell, C.A. (2003): Uncertainty Specification and Propagation for Loss Estimation Using FOSM Methods. In: PEER Report 2003/07, Pacific Earthquake Engineering Research Center, College of Engineering, University of California, Berkeley.
- Bazrafshan, E. (2008): Untersuchung vorgespannter Mauerwerkswände bei dynamischer Schubbelastung mithilfe numerischer Simulationen und Bemessung. Studienarbeit, University Braunschweig, Germany, Unpublished.
- Bommer, J.J.; Magenes, G.; Hancock, J.; Penazzo, P. (2004a): The influence of strong motion duration on the seismic response of masonry structures. In: Bulletin of Earthquake Engineering, pp. 1-26.
- Bommer, J.J.; Abrahamson, N.A.; Strasser, F.O.; Pecker, A.; Bard, P.-Y.; Bungum, H.; Cotton, F.; Fäh, D.; Sabetta, F.; Scherbaum, F.; Studer, J.; (2004b): The challenge of defining upper bounds on Earthquake Ground Motions. In: Seismological Research Letters, January/February, pp. 82-95.
- Budelmann, H.; Gunkler, E.; Husemann, U.; Becke, A. (2004): Rationell hergestellte Wände aus vorgespanntem großformatigem MW mit hohem Erdbebenwiderstand, Abschlussbericht, iBMB der Technischen Universität Braunschweig, Germany.
- Budelmann, H.; Gunkler, E.; Wichmann, H.J.; Husemann, U. (2006): Gebäudeaussteifung mittels vorgespannter Dünn- und ‚Normalbett‘-Mauertafeln. In: Mauerwerk 10 , H.1, pp. 2-7.
- Budelmann, H.; Gunkler, E.; Wigger, H. (2003): Untersuchungen zum Biegedrucktragverhalten von vorgespanntem Kalksandstein-Planstein-Mauerwerk. In: Das Mauerwerk, Heft 5, pp. 150-157.
- Calderini, C. (2004): Un modello costitutivo per la muratura: formulazione ed implementazione per l'analisi di strutture complesse, Doctoral thesis, University of Genoa, Italy.
- Castellano, M. G. (2001): Innovative Technologies for Earthquake Protection of Architectural Heritage. In: Proceedings of International Millennium Congress, More than Two Thousand Years in the History of Architecture, UNESCO-ICOMOS, Paris, 10-12 September 2001.
- Chen, W.F. (1982): Plasticity in Reinforced Concrete. New York: McGraw-Hill Book Company.
- Chen, W.F.; HAN, D.J. (1988): Plasticity for structural engineers. Springer-Verlag, New York, New York, USA.
- Cohen, B.L. (1991): Catalogue of Risks extended and updated. In: Health Physics. September, Volume 61, Number 3, pp. 317-334.

- Cohen, B.L. (2003): Risks in Perspective. In: Journal of American Physicians and Surgeons, Volume 8, Number 2, pp. 50-53.
- Cornell, C. (1968): Engineering Seismic Risk Analysis. In: BSSA, 5, pp. 1583-1606.
- Desroches, R.; Smith, B. (2002): Shape Memory Alloys in Seismic Resistant Design and Retrofit: A Critical Review of the state of the art, potential, and limitations: School of Civil & Environmental Engineering, Georgia Institute of Technology, Atlanta, USA.
- DIN 4149: 2005-04, 2005. Bauten in deutschen Erdbebengebieten - Lastannahmen, Bemessung und Ausführung üblicher Hochbauten, Germany.
- Einstein, H.H. (1988): Landslide Risk Assessment Procedure. In: Proceedings Fifth International Symposium On Landslides, Lausanne, Switzerland.
- EM-DAT (2008): The OFDA/CRED International Disaster Database. [www.emdat.be](http://www.emdat.be) - Université catholique de Louvain, Brussels, Belgium, last access 08.09.2008.
- Empelmann, M. (2006): Sonderprobleme im Massivbau - Erdbebenbemessung. Lecture notes, Technische Universität Braunschweig, Germany.
- Eurocode 6: Design of masonry structures. General rules for reinforced and unreinforced masonry structures. British-Adopted European Standard. December 2005.
- Eurocode 8: Design of structures for earthquake resistance - Part 1: General rules, seismic actions and rules for buildings. Final Draft, December 2003.
- European Spatial Planning Observation Network (2003): Glossary of Terms, <http://www.gsf.fi/projects/espon/glossary.htm>, last access 01.10.2008.
- Falkner, H.; Gunkler, E. (1994): Vorgespanntes Mauerwerk. In: Bauingenieur Heft Nr. 69, pp. 431-437.
- FEMA 306 (1998): Evaluation of earthquake damaged concrete and masonry wall buildings - Basic Procedures Manual. Applied Technology Council (ATC).
- FEMA 308 (1998): Repair of earthquake damaged concrete and masonry wall buildings. Applied Technology Council (ATC).
- FEMA 356 (2000): Prestandard and Commentary for the seismic rehabilitation of buildings. American Society of Civil Engineers (ASCE), Reston, VA., USA.
- Floodrisknet (2008): Glossary. Pub. by School of Civil Engineering and Geosciences at the University of Newcastle. <http://www.floodrisknet.org.uk/glossary>, last access 08.09.2008.
- Fugazza, D. (2003): Shape-memory alloy devices in earthquake engineering: Mechanical properties, constitutive modelling and numerical simulations. Doctoral thesis, University Pavia, Italy.
- Gambarotta, L.; Lagomarsino, S. (1997a): Damage models for the seismic response of brick masonry shear walls. Part I: the mortar joint model and its applications. Earth. Eng. Struct. Dyn. 26, pp. 423-439.
- Gambarotta, L.; Lagomarsino, S. (1997b): Damage models for the seismic response of brick masonry shear walls. Part II: the continuum model and its applications. Earth. Eng. Struct. Dyn. 26, pp. 441-462.
- Ganz, H.R. (1985): Mauerwerkscheiben unter Normalkraft und Schub. ETH Zürich, Institut für Baustatik und Konstruktion. Birkhäuser Verlag, Basel.

- Ganz, H.R. (1990a): Post-tensioned masonry structures - Properties of Masonry Design Considerations Post-Tensioning System for Masonry Structures Applications. VSL Report Series No. 2, VSL International Ltd, Berne, Switzerland.
- Ganz, H.R. (1990b): Vorgespanntes Mauerwerk. In: Schweizer Ingenieur und Architekt, Heft Nr. 8, pp. 177-182.
- Ganz, H.R. (2003): Post-Tensioned Masonry around the World. In: Concrete International, Heft 1 Januar 2003.
- Gisin, W.; Bachmann, H. (1985): Versuche zum dynamischen Verhalten teilweise vorgespannter Leichtbeton- und Betonbalken. Bericht-Nr. 7501-2, Institut für Baustatik und Konstruktion ETH Zürich, Birkhäuser Verlag Basel; Boston; Stuttgart, Germany, ISBN 3-7643-1758-2.
- Grossi, P.; Kunreuther, H. (2005): Catastrophe Modeling: A New Approach to Managing Risk. Springer Science Business and Media Inc.
- Grünthal, G. (ed.) (1998): European Macroseismic Scale 1998. Centre Européen de Géodynamique et de Séismologie, Luxembourg, Volume 15.
- Gunkler, E. (1993): Zur nachträglichen Erhöhung der Biegetragfähigkeit von Mauerwerkswänden durch bewehrte Ergänzungsschichten. Doctoral thesis, Heft 98 der Schriftenreihe des Instituts für Baustoffe, Massivbau und Brandschutz, Technische Universität Braunschweig, Germany.
- Gunkler, E. (1999): Vorgespanntes Mauerwerk. In: Mauerwerk-Kalender 2000, Ernst & Sohn, Berlin, pp. 333-359.
- Gunkler, E.; Budelmann, H. (2007): Mauerwerk kompakt - Für Studium und Praxis. Pub. by Werner Verlag, Neuwied, Germany, ISBN-13: 978-3804118256.
- Hagerty, M.R.; Cummins, R.A.; Ferriss, A.L.; Land, K.; Michalos, A.C.; Peterson, M.; Sharpe, A.; Sirgy, J.; Vogel, J. (2001): Quality of Life Indexes for National Policy: Review and Agenda for Research. Social Indicators Research, Volume 55, pp. 1-96.
- Hammer, W. (1972): Handbook of System and Product Safety. In: Englewood Cliffs, NJ: Prentice-Hall, Inc.
- Helm, P. (1996): Integrated Risk Management for Natural and Technological Disasters. Tephra, June 1996, Vol. 15, No. 1, New Zealand Ministry of Civil Defense, pp. 4-13
- Hori, T.; Zhang, J.; Tatano, H.; Okada, N.; Likebuchi, S. (2002): Micro-zonationbased Flood Risk Assessment in Urbanized Floodplain. In: Second Annual IIASA-DPRI Meeting Integrated Disaster Risk Management Megacity Vulnerability and Resilience, Laxenburg, Austria.
- Hilsdorf, H. (1965): Untersuchungen über die Grundlagen der Mauerwerksfestigkeit. Materialprüfungsamt für das Bauwesen, Technische Universität München, Munich, Germany, Bericht No. 40.
- Hofstetter, G.; Mang, H.A. (1995): Computational Mechanics of Reinforced Concrete Structure. Wien: Vieweg.
- Hosser, D. et al. (1986): Realistische seismische Lastannahmen für Bauwerke. Abschlußbericht zu einem gemeinsamen IfBt-Forschungsvorhaben von König und Heunisch, Frankfurt, Erdbebenstation Bensberg der Universität Köln und Institut für Geophysik der Universität Stuttgart, Germany, October 1986.
- Hubbard, D. (2007): How to Measure Anything: Finding the Value of Intangibles in Business. Pub. by John Wiley & Sons.

- Huster, U. (2000): Tragverhalten von einschaligem Natursteinmauerwerk unter zentrischer Druckbeanspruchung - Entwicklung und Anwendung eines Finiten-Elemente-Programmes. Doctoral thesis, Universität Gesamthochschule Kassel, Germany.
- Indirli, M.; Castellano, M. G.; Clemente, P.; Martelli, A. (2001): Demo-Application of Shape Memory Alloy Devices: The Rehabilitation of the S. Giorgio Church Bell--Tower. In: Proceedings of SPIE, Smart Structures and Materials.
- ISDR (2007): Disaster Risk Reduction: 2007 Global Review. consultation edition prepared for the Global Platform for Disaster Risk Reduction, First session, Geneva, Switzerland, 5-7 June 2007, ISDR/GP/2007/3.
- Jäger, W.; Schöps, P. (2006): Shear Stress Distribution of Stiffening Walls. Proc. 7<sup>th</sup> International Masonry Conference London, UK, 30<sup>th</sup> October until 1<sup>st</sup> November, 2006.
- Knight, F.H. (1921): Risk, Uncertainty and Profit. Hart, Schaffner & Marx, Houghton Mifflin Company, Boston or <http://www.econlib.org/library/Knight/knRUP.html>, last access 06.09.2008.
- Kramer, S.L. (1996): Geotechnical Earthquake Engineering. In: Prentice-Hall International Series, Upper Saddle River, New Jersey, USA.
- Lang, K. (2002): Seismic vulnerability of existing buildings. Zürich: vdf, Hochschulverlag an der ETH.
- Link, M. (2002): Finite Elemente in der Statik und Dynamik. 3. Auflage, Teubner Verlag, Karlsruhe, Germany.
- Lourenço, P.B. (1994): Analysis of masonry structures with interface elements. Theory and applications. Report N° 03.21.22.0.01, Delft University of Technology, Delft, Netherlands.
- Lourenço, P.B. (1996): Computational strategies for masonry structures. Doctoral thesis, Delft University of Technology, Netherlands.
- Lourenço, P.B.; Rots, J.G. (1997): A multi-surface interface model for the analysis of masonry structures. In: J. Eng. Mech., ASCE, 123(7), pp. 660-668.
- Mann, W.; Müller, H. (1978): Schubtragfähigkeit von Mauerwerk. In: Mauerwerk-Kalender 1978, Ernst & Sohn, Berlin, Germany, pp. 35-65.
- Mann, W.; Müller, H. (1982): Failure of shear-stressed masonry - an enlarged theory, tests and application to shear walls. Proc. British Ceramic Society, Vol. 30, pp. 223-235.
- Magenes, G.; Calvi, G.M. (1995): Shaking table tests on brick masonry walls. In: Proc. 10<sup>th</sup> European Conference on Earthquake Engineering, Vienna, Austria, 1995, pp. 2491-2424.
- Merritt, F.S.; Ricketts, J.T. (2001): Building Design and Construction Handbook. In: 6<sup>th</sup> ed. New York, USA, McGraw-Hill Professional.
- Meskouris, K.; Hinzen, K.G. (2003): Bauwerke und Erdbeben. Pub. by Vieweg & Sohn Verlag, Wiesbaden, Germany.
- Mistler, M. (2006): Verformungsbasiertes seismisches Bemessungskonzept für Mauerwerksbauten, Doctoral thesis, Aachen, Germany.
- Mistler, M.; Butenweg, C.; Fehling, E.; Stürz, J. (2007): Verformungsbasierte seismische Bemessung von Mauerwerksbauten auf Grundlage zyklischer Schubwandversuche. D-A-CH-Mitteilungsblatt, Band 82, März 2007.
- Munich Re (2007): Topics Geo: Natural Catastrophes 2007 - Analyses, assessments, positions. Available online: <http://www.munichre.com/en/publications/default.aspx>, last access 07.09.2008.

- Müller, G.; Groth, C. (2001): FEM für Praktiker. Bd. 1: Grundlagen. 11. Aufl. Renningen-Malmsheim : expert.
- Nathwani, J.S.; Lin, N.C.; Pandey, M.D. (1997): Affordable Safety by Choice: The Life quality Method. University of Waterloo, Waterloo, Ontario, ISBN 0-9696747-9-1
- NOAA; USGS (1996): Seismicity Catalogs. Volume 2: Global and Regional, 2150 BC-1996 AD (CD ROM). National Oceanic and Atmospheric Administration (NOAA), National Geophysical Data Center, Boulder, Colorado; and U.S. Geological Survey (USGS), National Earthquake Information Center, Denver, Colorado, USA.
- NRC (1983): Risk Assessment in the Federal Government: Managing the Process. National Research Council (NRC), National Academy Press, Washington, DC.
- Oliveira, D.V. (2003): Experimental and numerical analysis of blocky masonry structures under cyclic loading. Doctoral thesis, University of Minho, Portugal.
- Ötes, A.; Löring, S.; Elsch, B. (2002): Erhöhung der Schubtragfähigkeit von KS-Wänden unter Erdbebenlasten durch schlaf bewehrte Betonstützen in Formsteinen bzw. durch Vorspannung der Wand. Forschungsbericht Nr. 94, Forschungsvereinigung Kalk-Sand e.V., Germany.
- Ötes, A.; Löring, S. (2006): Zum Tragverhalten von Mauerwerksbauten unter Erdbebenbelastung. In: Bautechnik 83, 2006, Heft 2.
- Owen, D.R.J.; Hinton, E. (1980): Finite Elements in Plasticity: Theory and Practice. Swansea: Pineridge Press Ltd.
- Page, A.W., Samarasinghe, W.; Hendry, A.W. (1980): The failure of masonry shear walls. In: Int. J. Masonry Constr., 1(2), pp. 52-57.
- Park, R.; Paulay, T. (1976): Reinforced Concrete Structures. In: John Wiley and Sons, New York, USA.
- Park, Y.J.; Ang, A.H.S. (1985): Mechanistic seismic damage model for reinforced concrete. In: Journal of Structural Engineering, ASCE 111, pp. 722-739.
- Pieper, K. (1983): Sicherung historischer Bauten. Pub. by Ernst & Sohn, Berlin, München, Germany, ISBN 3-433-00967-8.
- Pijaudier-Cabot, G., Borderie, C.L.A and Fichant, S. (1994): Damage mechanics for concrete modeling: Applications and comparisons with plasticity and fracture mechanics, in: Computational modeling of concrete structures, eds. H. Mang et al., Pineridge Press, Swansea, UK, pp. 17-36.
- Pliefke, T.; Sperbeck, S.T.; Urban, M. (2006): The Probabilistic Risk Management Chain - General Concept and Definitions. Internal Discussion Paper, International Research Training Group 802, <http://www.grk802.tu-braunschweig.de/Links/>
- Pliefke, T.; Sperbeck, S.T.; Urban, M.; Peil, U.; Budelmann, H. (2007): A standardized methodology for managing disaster risk – An attempt to remove ambiguity. In: Luc Taerwe & Dirk Proske (Eds.), Proceedings of the 5th International Probabilistic Workshop, Ghent, Belgium.
- Pliefke, T.; Peil, U. (2007): On the integration of equality considerations into the life quality index concept for managing disaster risk. Luc Taerwe & Dirk Proske (Eds.), Proceedings of the 5th International Probabilistic Workshop, Ghent, Belgium.
- Pliefke, T.; Peil, U. (2008): Public investments into disaster risk reduction - the role of the LQI in social CBA. Proceedings of the 6th International Probabilistic Workshop, Darmstadt, Germany.

- Pliefke, T. (2010): The life quality index as a risk management tool - An economic analysis. Doctoral thesis, Technische Universität Braunschweig, Germany.
- Pocanschi, A.; Phocas, M.C. (2003): Kräfte in Bewegung – Die Techniken des erdbebensicheren Bauens. Pub. by B.G. Teubner Verlag, Wiesbaden, ISBN: 978-3-519-00429-1.
- Porter, K.A. (2003): An Overview of PEER's Performance-Based Earthquake Engineering Methodology. In: Conference on Applications of Statistics and Probability in Civil Engineering (ICASP9), San Francisco, CA.
- Prestressing method Macalloy Bar System (1993): McCalls Special Products. Sheffield, England.
- Priestley, N. (2007): The Need for Displacement-Based Design and Analysis. In: Advanced Earthquake Engineering Analysis, CISM International Centre for Mechanical Sciences, Volume 494, Springer Vienna, pp. 121-132.
- Proske, D. (2004): Katalog der Risiken – Risiken und ihre Darstellung. In: Eigenverlag Dresden, ISBN 3-00-014396-3.
- Rackwitz, R. (2004): Optimal and Acceptable Technical Facilities involving Risks. Risk Analysis, Vol. 24, No. 3, pp. 675-695.
- Rackwitz, R. (2006): Zuverlässigkeit und Lasten im konstruktiven Ingenieurbau. Lecture, Technische Universität München, Munich, Germany.
- Rots, J.G. (1997): Structural Masonry: An Experimental/Numerical Basis for Practical Design Rules. Pub. by Balkema, Rotterdam, Netherlands, ISBN 90 5410 680 8.
- Sánchez-Silva, M.; Rackwitz, R. (2004): Socioeconomic Implications of Life Quality Index in Design of Optimum Structures to Withstand Earthquakes. In: Journal of Structural Engineering, Volume 130, pp. 969-977.
- Schmitt, T. (2004): Erdbebenparameter, Erschütterungswirkung und Antwortspektren, Erdbebengefährdungsanalyse. Pub. by Institute for Geosciences and Natural Resources, Hannover, Germany.
- Schmitt, T. (2005): Grundlagen der Ingenieurseismologie und Erdbebengefährdungsanalyse. Pub. by Institute for Geosciences and Natural Resources, Hannover, Germany.
- Schermer, D. (2004): Verhalten von unbewehrtem Mauerwerk unter Erdbebenbeanspruchung. Doctoral thesis, Lehrstuhl für Massivbau Institut für Baustoffe und Konstruktion, Technische Universität München, Munich, Germany.
- Schlegel, R. (2004): Numerische Berechnung von Mauerwerkstrukturen in homogenen und diskreten Modellierungsstrategien. Doctoral thesis, Universität Weimar, Germany.
- Simeonova1, S.D.; Solakov1, D.E.; Leydecker, G.; Busche, H.; Schmitt, T.; Kaiser, D. (2006): Probabilistic seismic hazard map for Bulgaria as a basis for a new building code. In: Natural Hazards and Earth System Sciences, pub. by Copernicus GmbH on behalf of the European Geosciences Union, pp. 881-887.
- Sperbeck, S.T.; Budelmann, H. (2007): Prestressed Masonry in Case of Earthquake Loading – Numerical Investigations and Influences on Simulation Results. In: ANSYS Conference & 25<sup>th</sup> CADFEM Users' Meeting 2007, November 21-23, 2007, Dresden, Germany.
- Sperbeck, S.T.; Budelmann, H. (2008): Experimental and Numerical Investigation of Prestressed Masonry Structures under Earthquake Loading – Influences on Simulation Results. In: 14<sup>th</sup> International Brick & Block Masonry Conference, 17-20 February, 2008, Sydney, Australia.

- Thywissen, K. (2006): Components of Risk - A Comparative Glossary. In: Publication Series of United Nations University-EHS, No. 2.
- Twelmeier, H.; Sperbeck, S.T.; Budelmann, H. (2008): Restoration mortar for historical masonry durability prediction by means of numerical and engineering models. In: 14<sup>th</sup> International Brick & Block Masonry Conference, 17-20 February, 2008, Sydney, Australia.
- UNDP (United Nations Development Programme) Bureau for Crisis Prevention and Recovery (2004): Reduced Disaster Risk: A Challenge for Development. A Global Report.
- USGS (2008): U.S. Geological Survey,  
[http://neic.usgs.gov/neis/eq\\_depot/2008/eq\\_080512\\_ryan/neic\\_ryan\\_1.html](http://neic.usgs.gov/neis/eq_depot/2008/eq_080512_ryan/neic_ryan_1.html), last access 12.10.2008.
- Urban, M.; Sperbeck, S.T.; Peil, U. (2006): Approach to assess the seismic risk of historical churches. In: 5<sup>th</sup> International Conference on Structural Analysis of Historical Constructions SAHC 2006, 6-8 November 2006, New Delhi, India, pp. 1595-1602.
- Urban, M. (2007): Earthquake Risk Assessment of Historical Structures. Doctoral thesis, Technische Universität Braunschweig, Germany.
- Van der Pluijm, R. (1993): Shear behavior of bed joints. In: Proc. 6<sup>th</sup> North American Masonry Conf., eds. A.A. Hamid and H.G. Harris, Drexel University, Philadelphia, Pennsylvania, USA, pp. 125-136.
- Van Zijl, G.P.A.G. (2000): Computational Modelling of Masonry Creep and Shrinkage. Doctoral thesis, Delft University of Technology, Netherlands, Pub. by Meinema BV, ISBN 90-9013475-1.
- Vermeltfoort, A.Th.; Raijmakers, T.M.J. (1993): Deformation controlled meso shear tests on masonry piers. Part 2, Draft report, TU Eindhoven, dept. BKO, Eindhoven, Netherlands.
- Wang, E.Z.; Shrive, N.G. (1993): Numerical simulation of initial cracking process in a masonry prism in a compression test. In: Proc. 2<sup>nd</sup> Int. Symposium on Computer Methods in Structural Masonry, Swansea, pp. 27-37.
- WiCo (2008): Wikimedia Commons, Category:2008 Sichuan earthquake,  
[http://commons.wikimedia.org/wiki/Category:2008\\_Sichuan\\_earthquake?uselang=de](http://commons.wikimedia.org/wiki/Category:2008_Sichuan_earthquake?uselang=de), last access 12.10.2008.
- Wood, H.O.; Neumann, F. (1931): Modified Mercalli Intensity Scale of 1931. In: Bulletin of the Seismological Society of America, 21, pp. 277-283.
- Zimmerli, B.; Schwartz, J.; Schwegler, G. (1999): Mauerwerk: Bemessung und Konstruktion. Birkhäuser, Basel.